Interplay of Anderson Localization and Strong Interactions in Disordered Systems

Dissertation
zur
Erlangung des Doktorgrades (Dr. rer. nat.)
der
Mathematisch-Naturwissenschaftlichen Fakultät
der
Rheinischen Friedrich-Wilhelms-Universität
zu Bonn

vorgelegt von
Peter Henseler
aus
Melle

Bonn 2009

Angefertigt mit Genehmigung der Mathematisch-Naturwissenschaftlichen Fakultät der Rheinischen Friedrich-Wilhelms-Universität Bonn

Referent:	Prof. Dr. J. Kroha
Korreferent:	Prof. Dr. R. Flume
Tag der Promotion:	03.02.2010
Tag der Abgabe:	30.09.2009
Erscheinungsjahr:	2010

Ich versichere, dass ich die Arbeit selbstständig verfasst und keine anderen als die angegebenen Quellen und Hilfsmittel benutzt sowie die Zitate kenntlich gemacht habe.

Abstract

We study the interplay of disorder localization and strong local interactions within the Anderson-Hubbard model. Taking into account local Mott-Hubbard physics and static screening of the disorder potential, the system is mapped onto an effective single-particle Anderson model, which is studied within the self-consistent theory of electron localization. For fermions, we find rich nonmonotonic behavior of the localization length ξ, particularly in two-dimensional systems, including an interaction-induced exponential enhancement of ξ for small and intermediate disorders and a strong reduction of ξ due to hopping suppression by strong interactions. In three dimensions, we identify for half filling a Mott-Hubbard-assisted Anderson localized phase existing between the metallic and the Mott-Hubbard-gapped phases. For small U there is re-entrant behavior from the Anderson localized phase to the metallic phase. For bosons, the unrestricted particle occupation number per lattice site yields a monotonic enhancement of ξ as a function of decreasing interaction, which we assume to persist until the superfluid Bose-Einstein condensate phase is entered.
Besides, we study cold atomic gases expanding, by a diffusion process, in a weak random potential. We show that the density-density correlation function of the expanding gas is strongly affected by disorder and we estimate the typical size of a speckle spot, i.e., a region of enhanced or depleted density. Both a Fermi gas and a Bose-Einstein condensate (in a mean-field approach) are considered.

Contents

Chapter 1

Introduction

The question of why some materials are conductors while others are not, has been and is still one of the major topics of condensed matter physics. In many experiments, a slight variation of an external parameter like temperature, pressure, chemical composition etc. can induce a metal-insulator transition (MIT), turning a highly conducting metal into a highly resistive insulator and vice versa. The range in which the conductivity of a material can change thereby is one of the largest of all laboratory-measurable physical quantities [ER95]. Every progress in our understanding of the underlying physical mechanisms yields automatically a deeper insight into the fundamental properties of many-body systems and solids, and is, of course, also of great importance for commercial applications and technology.

The development of the quantum theory of solids during the last century led to the detection of different mechanisms being able to cause a MIT [ER95]. The most important of them are, by far, the band structure of solids [AM76, Hoc92], strong interactions among electrons (particles) [Mot61] and the presence of disorder [And58]. Although not all details could be clarified by now, either of these effects, on its own, has become basically understood during the last decades and a generally well-accepted theoretical description emerged. However, in many real situations not only one single mechanism is relevant for the MIT, but an interplay of different effects takes place [Tho76, ER95, IFT98]. In many cases, this interplay is only poorly understood and remains one of the great challenges of modern condensed matter theory.

30 years ago, the scaling theory of Anderson localization was developed [AALR79]. It describes the scaling-dependence of the conductance of real, disordered materials and is the basis of our today's understanding of (noninteracting) disordered systems. In particular, it predicts the absence of (macroscopic) metals in less than three space dimensions. Parallel to the formulation of this standard theory of disordered single-particle systems, the question, how the presence of interac-

tions might modify these fundamental findings has been pushed into the focus of research [Tho76, FAL78, EP85]. At least since the surprising discovery of experimental evidence for a two-dimensional metal-insulator transition [KKF$^+$94], the quest for a better understanding of the interplay of strong interactions and disorder has been one of the most important challenges of modern condensed matter theory. Despite the intensive research throughout the last three decades no generally accepted and conclusive theory has been established yet.

In recent years, the enormous experimental progress in quantum optics opened up a new possibility to examine the physics of interacting many-body systems [LSA$^+$07, BDZ08]. Particularly, the evaporative laser cooling of atomic gases to ultra low temperatures and the production of very precisely controllable optical potentials allow for an experimental realization of lattice systems, originally developed for the theoretical description of solids. It seems very likely that these experiments will help to resolve important theoretical puzzles on the interplay of interactions and disorder in the near future.

In this thesis, we will investigate the Anderson-Hubbard model, as one example for a lattice system containing both, strong disorder and strong local interactions. Many numerical studies on the Anderson-Hubbard model have observed a strong nonmonotonic influence of the interaction on the transport properties of this model, e.g., [SBS03, HT04, BHV05, CDS07]. In particular, it has been observed that the presence of weak interactions might induce a significant enhancement of transport, while strong interactions contrarily tend to strongly suppress it. Therefore, we will focus on the question whether we can find a conclusive, physical explanation of these results. Special attention will be payed to a possible MIT in two dimensions, reported by some of the numerical studies on the Anderson-Hubbard model [HT04, CDS07]. For that purpose, we will formulate a technically simple, but physically non-trivial approximation to the Anderson-Hubbard model, which is based on an expansion around the strongly localized atomic-limit of that model. As we will argue, our approach allows a systematic analysis of the static interplay of interaction and disorder, reproducing quite well the nonmonotonic interaction-dependence of transport properties of the Anderson-Hubbard model, found within most of the numerical results. In this way, we will be able to provide a simple and conclusive explanation of the physical mechanism underlying these results. Furthermore, we will show that, under certain conditions, interactions can indeed yield an (exponentially) large enhancement of the relevant transport length scale, and, hence, induce a tremendous delocalization of the system. However, we will also give strong arguments that the numerically observed metal-insulator transition in two dimensions is most likely a numerical artefact due to finite-size effects, which can be uncovered by our infinite-size approach.

The thesis is organized as follows: In Ch. 2, we will briefly summarize the main mechanisms of metal-insulator transitions. As the Anderson transition in disordered systems is the central subject of this thesis, in Ch. 3, we will present a more detailed overview of its physics and introduce the relevant objects and quantities needed within the subsequent parts of this thesis. A general discussion of interacting, disordered systems and an overview of some important results will be the subject of Ch. 4. In Ch. 5, we will turn to the specific example of the Anderson-Hubbard model and its physical motivation. Also a brief overview of the physics of the non-disordered, usual Hubbard model will be given there. The atomic-limit approximation of the Anderson-Hubbard model will be presented in Ch. 6. After its detailed derivation and a discussion of the regime of validity of this approach, we will evaluate it in the limit of very strong disorder and low dimensions, respectively, which allows for an analytical treatment. Afterwards, a quantitative analysis will be done by applying the self-consistent theory of Anderson localization, which is the subject of Ch. 7. The interaction and disorder-dependence of the localization length, which defines the relevant transport length scale, will be studied in one and two dimensions, and the three-dimensional phase diagram of the Anderson-Hubbard model within the atomic-limit approximation will be calculated. Additionally, a detailed comparison with and discussion of known numerical results from the literature will be presented. In Ch. 8, we turn our attention to experiments on cold atomic gases. Measurements on these gases are often done by using the time-of-flight technique. Therefore, we discuss the noninteracting, diffusive expansion of an atomic gas in a disordered environment. Since by now most experiments on cold gases have been done with Bose gases, in Ch. 9, we will discuss our atomic-limit approximation for the disordered Bose-Hubbard model. At the end of this thesis, we offer a conclusion and a brief discussion of possible further research.

Chapter 2

Metal-insulator transitions

In this first chapter, we will give a very brief overview of the three main mechanisms responsible for metal-insulator transitions in many-body systems.

2.1 Ideal solids: single particle in a periodic potential

The most basic description of solids is based on the assumption of freely moving, noninteracting electrons in a static, periodic potential, which is caused by ions [AM76]. In this idealized picture, the electron wavefunctions are solutions of the stationary single-particle Schrödinger equation[1]

$$\hat{H}\psi(r) \equiv \left(-\frac{\Delta}{2m} + U(r)\right)\psi(r) = E\psi(r). \tag{2.1}$$

Here, m denotes the particle mass and $U(r)$ is the periodic potential with $U(r + a) = U(r)$ for each lattice vector a. The solutions of Eq. (2.1), the *Bloch states*, are known to be lattice-periodic, extended wave functions. The spectrum of $\hat{H}$ is absolutely continuous and consists of bands [AM76, MW04]. Therefore, despite its simplicity, the model of an ideal crystal already provides an important possible mechanism for a metal-insulator transition, because systems described by Eq. (2.1), are either perfect conductors or insulators [AM76]. The former happens if the Fermi energy ε_{F} lies within one of the energy bands, while the latter happens if ε_{F} lies within a gap of the spectrum. Insulators of this kind, e.g., diamond, are called *band insulators*.

[1] Throughout this thesis we use units in which $\hbar = k_B = 1$.

2.2 Disorder-induced metal-insulator transition

The assumption of a perfect periodic potential in the previous section is, of course, an idealization. Every real solid contains inevitably lattice imperfections and all other kinds of disorder [Zim79, LGP88] and, thus, differs significantly from the ideal model. To account for the effect of disorder we are therefore forced to extend our single-particle Schrödinger equation, Eq. (2.1), by adding a disorder potential $V(r)$,

$$\hat{H}\psi(r) \equiv \left(-\frac{\Delta}{2m} + U(r) + V(r)\right)\psi(r) = E\psi(r). \tag{2.2}$$

The presence of disorder can strongly alter the results of the previous section. While the Bloch states were always extended and the spectrum of the periodic Hamiltonian, Eq. (2.1), was purely continuous, the disordered model always contains bound states and a point spectrum [LGP88, PF92, Sto01, Lan91]. As it was first noticed by P. W. Anderson in his seminal paper [And58], disorder can even induce a metal-insulator transition, at which all wave functions become localized and bounded. This *Anderson transition* will be subject of Ch. 3 and discussed in detail there. At this point, we only want to emphasize that the nature of the Anderson transition is quite different from the metal-insulator transition in a periodic system. The latter is caused by a gap in the spectrum, i.e., by the fact that only partially filled bands can carry an electrical current [AM76], even if all states are extended. Contrarily, at the Anderson transition the spectrum typically can remain gapless,[2] but the states become localized and cannot propagate through the medium. Examples of an Anderson insulator are heavily doped semiconductors like Si:P and Si:B, where a disorder driven MIT has been observed experimentally [RMP$^+$83, Sar95, Löh98].

2.3 Interaction-induced metal-insulator transition

So far, only single-particle mechanisms for a MIT have been presented. Mott [Mot61, Mot90] was one of the first who pointed out that also the interactions between the electrons of a solid can give rise to a MIT. For that purpose, he considered a crystal, where the number of atoms equals exactly the number of electrons, i.e., a crystal with, on average, one valence electron per atom [Mot61]. Mott noticed that the competition between the activation energy to create an electron-hole pair, due to the Coulomb interaction, and the kinetic energy gained by the delocalization of the electron yields a MIT. Thus, a system which should be a metal, according to its single-particle band structure, can become insulating because of the electrostatic interparticle interaction. Typical examples for these

[2] Hence, the density of states behaves uncritical at the Anderson transition [LGP88], see Ch. 3.

Mott insulators are NiO and VO_2 [ER95, IFT98]. Besides the high-T_c cuprate superconductors are believed to be underdoped Mott insulators. Therefore this kind of metal-insulator transition plays also a crucial role in the search for a theory of high-T_c superconductivity [And97, LNW06].
Shortly after Mott's discovery, Hubbard introduced a simplified lattice model [Hub63, Hub64a, Hub64b] which contains the essential features of the electrostatic interaction. This model and its *Mott-Hubbard transition* will be discussed in more detail in Sec. 5.1.

Chapter 3

Anderson localization

In this chapter, we give a more detailed overview of the Anderson transition (see Sec. 2.2) and its fundamental properties. The research on this disorder-induced metal-insulator transition has been started in 1958 by the publication of P. W. Anderson's seminal article [And58] and is still a very active field of both physics and mathematics. For reviews on many aspects of this subject see, e.g., [Tho74, LR85, BZ92, KM93, BK93, Jan98, EM08] and [LGP88, CL90, PF92, Sto01], respectively.

3.1 Locator expansion

In his original article [And58], Anderson studied a tight-binding lattice version of Eq. (2.2), i.e., the Hamiltonian

$$\hat{H}_A \equiv \hat{H}_{dis} + \hat{H}_{kin} = \sum_{i\sigma} \varepsilon_i c^\dagger_{i\sigma} c_{i\sigma} - t \sum_{<i,j>,\sigma} c^\dagger_{i\sigma} c_{j\sigma}. \tag{3.1}$$

The first term, $\hat{H}_{dis}$, describes the disordered potential. The on-site energies $\{\varepsilon_i\}$ are assumed to be independent and identically-distributed (i.i.d.) random variables with a distribution function $p(\varepsilon) = 1/\Delta \cdot \Theta(\Delta/2 - |\varepsilon|)$, where $\Theta(x)$ denotes the Heaviside step function. $c^\dagger_{i\sigma}(c_{i\sigma})$ is the creation(annihilation) operator of a particle at site i with spin[1] σ. The second term, $\hat{H}_{kin}$, accounts for the kinetic energy, where $< i, j >$ denotes the sum over all nearest-neighbor lattice sites. t is the nearest-neighbor hopping amplitude arising from the discrete (tight-binding) Laplace operator on a d-dimensional lattice,

$$(\Delta f)(x) := \sum_{y\in\mathbb{Z}^d, |y|=1} (f(x+y) - f(x)). \tag{3.2}$$

Throughout this thesis, we will assume all lattices being simple cubic ones with lattice constant $a = 1$. Then we can always set $t \geq 0$ without loss of generality,

[1] The explicit spin index σ was suppressed in [And58].

because for bipartite lattices unitary transformations exist mapping $\hat{H}_{kin}$ onto $-\hat{H}_{kin}$ while leaving $\hat{H}_{dis}$ invariant [LW03].

Anderson considered the question, whether (spin) transport in such a system can occur. For that purpose, starting from the unperturbed local Green's function, also called *locator*,

$$G^0_{ij\sigma\sigma'}(E) \;=\; \langle i\sigma|(E-\hat{H}_{dis})^{-1}|j\sigma'\rangle \;=\; \frac{\delta_{ij}\,\delta_{\sigma\sigma'}}{E-\varepsilon_i}, \tag{3.3}$$

a perturbation expansion in the hopping amplitude was used. Doing so it was shown in [And58] that above a certain critical disorder strength, $(\Delta/t)_{crit.}$, the self-energy $\Sigma_i(E)$ of the full local Green's function,

$$G_{i\sigma}(E) \;\equiv\; G_{ii\sigma\sigma}(E) \;=\; \langle i\sigma|(E-\hat{H}_A)^{-1}|i\sigma\rangle \;=\; \frac{1}{E-\varepsilon_i-\Sigma_i(E)}, \tag{3.4}$$

almost surely remains real (see also [SI95]). From this result it was concluded that for disorder strengths $(\Delta/t) > (\Delta/t)_{crit.}$ a particle, initially occupying any given lattice site i, does not spread infinitely, but stays in a finite region around site i, i.e., it gets *localized*. As a direct consequence [And58, SI95, Eco06], transport becomes impossible, and, hence, the disorder yields an "absence of diffusion" [And58].

The statement of complete localization for strong disorder strengths was later made rigorous in [FS83] by use of a multi-scaling analysis (see also [Sto01]) as well as in [DK89] and [AM93]. For the special case of one dimension (1D) it was shown [GMP77] that the spectrum of $\hat{H}_A$ is purely point-like, independent of the strength of disorder. That means a one-dimensional system, described by a single-particle Anderson model, gets completely localized and, hence, insulating, as soon as an arbitrary amount of disorder is present. This strong implication was conjectured already in [MT61] and further supported by [Tho72] and [Ish73] and is in perfect accordance with the predictions of the scaling theory of Anderson localization (see Sec. 3.4, below).

3.2 Characteristics of Anderson localized systems

Next, we summarize some characteristics of Anderson localized systems, which we will refer to in the subsequent parts of this thesis.

3.2.1 Wavefunctions' asymptotics

In general, the wavefunctions of eigenstates of the Anderson Hamiltonian $\hat{H}_A$, Eq. (3.1), have a very complex, multifractal structure with large amplitude variations in space [EM08]. However, the common characteristic feature of all localized

states is, that they fall off exponentially at large distances. More precisely, for any given eigenstate $|\psi_\alpha\rangle$ of $\hat{H}_A$, $\hat{H}_A|\psi_\alpha\rangle = E_\alpha|\psi_\alpha\rangle$, the corresponding wavefunction $\psi_\alpha(x)$ obeys [LGP88]

$$\left|\psi_\alpha(x)\right| \;\leq\; C_\alpha \cdot e^{-|x-x_0^{(\alpha)}|/\xi}. \tag{3.5}$$

$x_0^{(\alpha)}$ is the center of localization of state $|\psi_\alpha\rangle$ and C_α is some constant, independent of x. The characteristic length scale $\xi \equiv \xi(E_\alpha)$ is called *localization length* and determines the asymptotic behavior of $\psi_\alpha(x)$, when $|x| \to \infty$.

Denoting the average over the disorder realizations of any (random) physical quantity A by an overbar, $\overline{A}$, one can find an alternative definition of the localization length [LGP88],

$$-\frac{1}{\xi(E)} \;=\; \lim_{|x_i - x_j|\to\infty} \frac{\log\left(\overline{\left|G_{ij\sigma}(E)\right|^2}\right)}{2|x_i - x_j|}, \tag{3.6}$$

which remains meaningful even in an interacting system, where no single-particle eigenstates exist (see Sec. 6.4).
More precisely, Eq. (3.6) corresponds to the definition of dynamical localization, i.e., the property that a particle stays in a finite volume of space ("absence of diffusion"). Contrarily, Eq. (3.5) describes an exponential localization of wave functions. From a rigorous point of view, these two cases are not equivalent [RJLS95, GK04]. While dynamical localization implies exponential localization [CFKS87, GK04], the converse is generally not true, but some stronger conditions on the coefficients in Eq. (3.5) must hold [RJLS95, GK04]. However, as for the Anderson model always both criteria, if any, were proven to be fulfilled [GK04], we will not differentiate explicitely between these two definitions in the following.

3.2.2 Inverse participation ratio

A further characteristic quantity of disordered (localized) systems is the *inverse participation ratio* (IPR) [Tho74, Weg80, KM93, Eco06],

$$\text{IPR} \;\equiv\; \text{IPR}(E_\alpha) \;=\; \sum_x \left|\psi_\alpha(x)\right|^4 \;\simeq\; \int_V dx\, \left|\psi_\alpha(x)\right|^4. \tag{3.7}$$

In the last equation, the sum runs over all lattice sites x and V denotes the volume of the system. The IPR measures the extension of the wave function and is therefore a suitable measure for localization [Tho74, KM93]. To see this we will consider first the case of an extended, periodic Bloch state. From the periodicity

of the wave function we easily deduce

$$\int_V dx \left|\psi_\alpha(x)\right|^4 = N \int_\Omega dx \left|\psi_\alpha(x)\right|^4 \leq N \left(\int_\Omega dx \left|\psi_\alpha(x)\right|^2\right)^2 \tag{3.8}$$

$$= N \cdot \frac{1}{N^2} \overset{N\to\infty}{\longrightarrow} 0, \tag{3.9}$$

where Ω is the volume of the unit cell. The last equality follows from the normalization of the wavefunction. Thus, in the thermodynamic limit, the IPR of a Bloch state vanishes and so it does for a general extended wave [Tho74]. In contrast, the IPR of a localized wave function remains finite. Assuming the wave function to be an s-wave,

$$\psi_\alpha(x) = C_\alpha \cdot e^{-|x-x_0^{(\alpha)}|/\xi}, \quad C_\alpha = \frac{1}{\sqrt{(\xi/2)^d (d-1)! A_d}}, \tag{3.10}$$

where d is the dimension of the system and A_d the surface area of the d-dimensional unit sphere, we get

$$\int_V dx \left|\psi_\alpha(x)\right|^4 \overset{V\to\infty}{=} C_\alpha^4 A_d \int_0^\infty dx\, x^{d-1}\, e^{-4x/\xi} = \frac{1}{\xi^d A_d (d-1)!}. \tag{3.11}$$

Comparison of Eqs. (3.7) and (3.11) shows that a disordered single-particle system is an insulator if its IPR at the Fermi level is finite. Furthermore, from Eq. (3.11), it follows that the larger the IPR of a wave function the stronger it is localized.
Although the simple proportionality IPR $\sim \xi^{-d}$ does not generally hold [KM93], both quantities are closely related and, hence, both notions are often used synonymously in the literature (cf. Sec.7.6).

3.2.3 Mobility edge

In Sec. 3.1, we discussed the possibility of a metal-insulator transition by increasing the strength of the disorder potential. As it was described, all single-particle eigenstates of $\hat{H}_A$ become exponentially localized above a certain critical value of Δ. In addition, it was shown [FS83, AM93, Sto01] that the states at the bottom of the spectrum are always localized, even for $0 < \Delta < \Delta_{crit.}$. On the other hand every day experience tells that metals exist, at least in dimension $d = 3$ (see discussion in 3.4 below). Therefore, it is commonly accepted that, for weak enough disorder, extended solutions exist for the Anderson model in $d \geq 3$, although no rigorous proof has been found yet [GK04] (see also, e.g., [Elg09] for a recent reference on that question). As Mott argued [Mot67, MD79], in this case localized and extended states should be separated by a sharp energy E_c, called

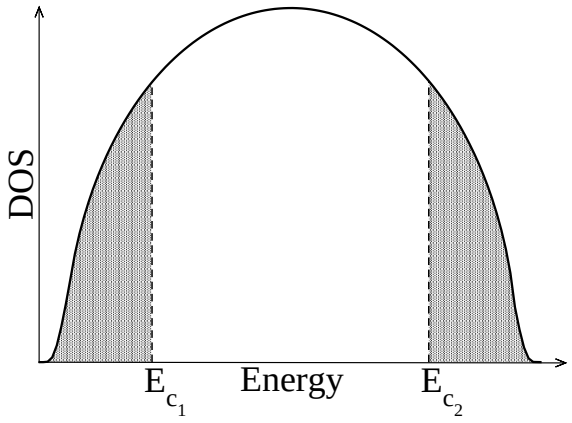

Figure 3.1: Sketch of the density of states (DOS) of the Anderson model. The shaded regions of localized states are separated by the mobility edges E_{c_1} and E_{c_2} from the region of extended states in the center of the band. The DOS is a smooth function decaying exponentially at its boundaries corresponding to Eq. (3.12). (Plot reconstructed from [KM93].)

mobility edge [CFO69] (see also Fig. 3.1). According to Mott's argument, the coexistence of extended and localized states at the same energy would yield a mixture of these states under any arbitrary small perturbation and, hence, destroy the localized states. Although no rigorous proof has been found yet, the existence of such a mobility edge was confirmed numerically as well as experimentally [KM93]. Therefore, not only the variation of the disorder strength, but also the variation of the Fermi energy (across the mobility edge) can induce the Anderson metal-insulator transition.

3.2.4 Lifshitz tails

Some physical properties of disordered systems originate from the appearance of rare configurations of on-site energies. One of them is the existence of *Lifshitz states* with eigenenergies close to the boundary of the spectrum [Lif64, LGP88, Sto01]. As Lifshitz pointed out [Lif64, LGP88], the eigenstates of $\hat{H}_A$ with eigenenergies $E \approx E_0^{\pm}$, with $E_0^{\pm} = \pm(\Delta/2 + 2td)$ being the upper (lower) boundary of the spectrum of $\hat{H}_A$,[2] can only exist in large regions of space, where all on-site energies ε_i are lying in a small interval very close to the boundary of the energy distribution, i.e., $|\varepsilon_i| \approx \Delta/2$. The existence of arbitrarily large but finite regions with on-site energies $\varepsilon_i \in [\pm\Delta/2, \pm\Delta/2 \mp \delta]$ is guaranteed for any $\delta > 0$ by the independence of the disorder potential at different lattice sites. States with eigenenergies close to the boundary are strongly localized within

[2] The argument holds for more general Anderson Hamiltonians as well [CL90, PF92, Sto01].

those regions and arise, hence, as a consequence of strong potential fluctuations. The probability p to find such a rare configuration of N adjacent lattice sites within a finite part of the lattice is exponentially low. It can be estimated by $p \sim \exp(-N \cdot const.) \sim \exp(-V \cdot const.)$, V being the volume enclosing the N sites. From the dispersion relation $(E - E_0^{\pm}) \sim k^2 \sim V^{-2/d}$, k being the wave vector of the wavefunction, we see that the density of states of a disordered system decays exponentially as $E \to E_0^{\pm}$ (cf. Fig. 3.1),

$$N(E) \;\sim\; \exp\left(-c \cdot |E - E_0^{\pm}|^{-d/2}\right) \quad \text{for } E \to E_0^{\pm}. \tag{3.12}$$

3.3 Weak localization

At the beginning, research on Anderson localization of quantum particles in a random potential was mostly concentrated on the regime of strong disorder. In particular, Anderson considered this regime when proving the complete localization of all wave functions above a critical disorder strength [And58]. Also the existence of Lifshitz states is the result of strong disorder: particles with extremely low(high) energies compared to the average disorder potential are bound within the valleys(hills) of the energy landscape. Although this observation is already highly non-trivial - one might expect every quantum particle could at least slowly diffuse by tunneling - the physically more relevant mechanism for localization is the coherent superposition of waves. This can be best visualized heuristically by use of Feynman paths [AA85, SA01]: The probability that a particle propagates from a point A to a point B within some time t is given by the sum of all paths connecting A and B (see Fig. 3.2), i.e.,

$$P_{A\to B} \;=\; \left|\sum_i A_i\right|^2 \;=\; \sum_i \left|A_i\right|^2 + \sum_{i\neq j} A_i A_j^*. \tag{3.13}$$

A_i is the probability amplitude of the Feynman path i and the sum runs over all possible paths. The right hand side of Eq. (3.13) was split into its classical contribution, $\sum_i |A_i|^2$, and the quantum correction due to the superposition of different paths. Every amplitude is a complex number and can be decomposed into its modulus $|A_i|$ and its phase φ_i,

$$P_{A\to B} \;=\; \sum_i \left|A_i\right|^2 + \sum_{i\neq j} \left|A_i\right| \left|A_j\right| e^{\mathrm{i}(\varphi_i - \varphi_j)}. \tag{3.14}$$

In general, different paths will develop different phases such that the phase difference in Eq. (3.14) will become a random number. Therefore, almost all contributions due to superposition of different paths will cancel and only the classical (diffusive) contribution will survive. However, if the system is symmetric under

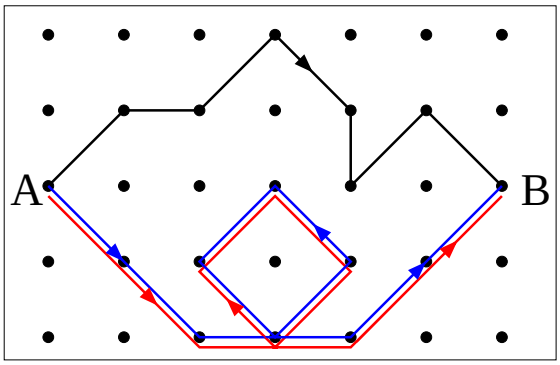

Figure 3.2: Different Feynman paths connecting points A and B. The blue and the red one contain each a loop which are identical under time-reversal.

time-reversal, there is an important exception. Let's assume the two points A and B are very close to each other or even the same. Then for each path A_i there exists exactly one path A_j which is the time-reversed copy of A_i (see Fig. 3.2). Since the system is supposed to be symmetric under time-reversal, the phases φ_i and φ_j must equal and cancel each other in Eq. (3.14). Thus, the return probability is twice as large as that of a classical particle,

$$P_{A\to B\approx A} \;=\; 2\sum_i \left|A_i\right|^2 . \tag{3.15}$$

As the total probability is normalized,

$$\sum_B P_{A\to B} \;=\; 1, \tag{3.16}$$

the quantum mechanical correction to the classical result by coherent superpositions of different paths yields a reduction of the particle's probability to propagate through the system [AA85, AM07].

Consequently, the enhanced return probability corresponds to a reduction of the conductivity of the system. To see this we must consider the two-particle Green's function of $\hat{H}_A$. In the presence of a static external field $E = -\partial_t A(x,t)$, the Hamiltonian $\hat{H}_A$ becomes

$$\hat{H} \;=\; \frac{(\mathrm{i}\nabla + eA(r,t))^2}{2m} + U(r) + V(r). \tag{3.17}$$

Within linear response theory, the *Kubo formula* for the conductivity tensor $(\sigma^{ij})_{ij}$ in energy-momentum representation yields [AA85, AM07, Ram98]

$$\sigma^{ij}(q,\omega) \;=\; \frac{V}{\pi}\left(\frac{e}{m}\right)^2 \int \frac{dk}{(2\pi)^d}\int \frac{dk'}{(2\pi)^d}\, k_i\, k'_j\, \overline{G^A(k'_-,k_-,\varepsilon_\mathrm{F})\, G^R(k'_+,k_+,\varepsilon_\mathrm{F}+\omega)}. \tag{3.18}$$

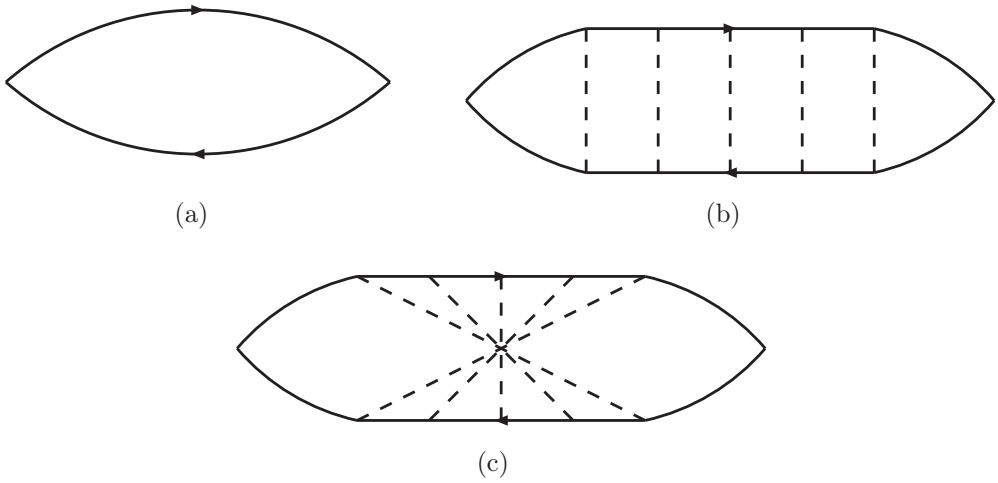

Figure 3.3: Contributions to the perturbation series of the conductivity: (a) bare two-particle propagator, (b) diffuson, (c) cooperon. The solid lines represents the disorder-averaged, retarded (advanced) single-particle propagator, the dashed lines represent the scattering off the disorder potential.

The overbar in Eq. (3.18) denotes again the average over disorder realizations. G^A (G^R) is the advanced (retarded) Green's function (in momentum representation), ε_{F} is the Fermi energy, and $k_\pm \equiv k \pm q/2$.
Treating the disorder potential as a perturbation (cf. Appendix A), the leading order contribution is the bare product of the disorder-averaged single-particle Green's functions, $\overline{G^A}\,\overline{G^R}$, see Fig. 3.3(a) [AM07, Ram98]. The next-leading order contribution arises from the *ladder diagrams*, also called *diffuson*, Fig. 3.3(b). Denoting by $\epsilon_k = \langle k|\hat{H}_{kin}|k\rangle$ the Fourier transform of the periodic, kinetic term[3] of Eqs. (2.2) and (3.1), respectively, and assuming the imaginary part of G to be small and slowly varying (weak disorder), i.e., (see Appendix A)

$$\overline{G_k^{R,A}}(E) \;=\; \frac{1}{E - \epsilon_k \pm \mathrm{i}/2\tau}, \tag{3.19}$$

the leading order contributions yield the Drude result for the DC conductivity [AM76, Ram98]

$$\sigma^{ij} \;\equiv\; \lim_{\omega\to 0}\lim_{p\to 0}\sigma^{ij}(q,\omega) \;=\; \frac{ne^2\tau}{m}\cdot\delta_{ij}. \tag{3.20}$$

Here n denotes the average particle density, e is the elementary electric charge and τ is the *elastic collision time* [AM07].

[3]To distinguish the kinetic energy from the random on-site potential, the former is always denoted by ϵ, while the latter is denoted by ε.

Fig. 3.3(c) shows the *cooperon* contribution, which is the class of diagrams containing the time-reversed counterparts of the leading order ladder diagrams (see Appendix A). They are also called *maximally crossed diagrams* and *Langer-Neal diagrams* [LN66], respectively. In the absence of time-reversal symmetry breaking terms like magnetic impurities, spin-orbit-coupling etc., the calculation of the cooperon yields a correction to the (classical) conductivity by [GLK79, AM07, Ram98]

$$\Delta\sigma^{ij}(q=0,\omega) \;=\; -\frac{2e^2}{\pi}A_d\int\limits_0^{k_0}\frac{dk}{(2\pi)^d}\frac{k^{d-1}}{-\mathrm{i}\omega/D_0+k^2}, \tag{3.21}$$

D_0 being the (bare) diffusion constant. The upper integration limit, $k_0 < \infty$, was needed to account for the limits of the applicability of the diffusion approximation used in the derivation of Eq. (3.21).
The cooperon contribution is negative, corresponding to the reduction of transport in a disordered quantum mechanical system by the *weak localization* corrections. The prefactor of Eq. (3.21) is one order of $(1/k_F l)$ smaller than the classical term, Eq. (3.20), where k_F denotes the Fermi momentum and the Fermi wave vector, respectively, and $l = k_\mathrm{F}\tau/m$ is the *elastic mean free path* [AM07]. Thus, one could think it would only lead to a minor correction, as long as $k_\mathrm{F} l \gg 1$. However, in the static limit, $\omega \to 0$, the integral is divergent in low dimensions, $d < 3$, and can become arbitrarily large in $d = 3$, depending on the disorder strength. In particular, it can become as large as the classical contribution, Eq. (3.20), indicating the possibility of an Anderson metal-insulator transition due to coherent backscattering of the electron waves and, thus, marking the definitive breakdown of simple perturbation theory.

3.4 Scaling theory

A milestone in understanding single-particle localization was achieved by the development of the scaling theory of Anderson localization [AALR79]. It started with the observation [Lan70] that, in the localized regime, transport in finite systems is not well described by the conductivity σ, but rather by the conductance

$$G \;=\; \sigma L^{d-2}. \tag{3.22}$$

Thouless and co-workers [ET72, Tho74, LT75a, LT75b] then noted two important facts. First, the conductance G of a finite sample is determined by the ratio of two microscopic energy scales: ΔE, the averaged energy spacing of two neighboring eigenenergies in the volume, and the *Thouless energy* E_th, i.e., the energy related to the average diffusion time a particle needs to propagate through the volume

$V = L^d$,

$$E_{\text{th}} := \frac{h}{\tau_{\text{th}}}, \tag{3.23}$$

with

$$\tau_{\text{th}} := \frac{L^2}{D}, \tag{3.24}$$

being the *Thouless time* and D being the diffusion constant.
Namely, from the *Einstein relation*

$$\sigma = e^2 N(\varepsilon_{\text{F}}) D, \tag{3.25}$$

where $N(\varepsilon_{\text{F}})$ denotes the density of states at the Fermi level [AM07], we get by combining Eqs. (3.22) - (3.25)

$$G = e^2 N(\varepsilon_{\text{F}}) D L^{d-2} = e^2 N(\varepsilon_{\text{F}}) \frac{1}{\tau_{\text{th}}} L^d = \frac{e^2}{h} \frac{dN}{dE}(\varepsilon_{\text{F}}) E_{\text{th}} = \frac{e^2}{h} \frac{E_{\text{th}}}{\Delta E}. \tag{3.26}$$

For convenience, instead of G one usually uses the *dimensionless conductance*

$$g \equiv \frac{h}{e^2} G = \frac{E_{\text{th}}}{\Delta E} \tag{3.27}$$

to describe the conductance of a given finite sample.
Second, it was observed in the numerical analysis of disordered two-dimensional systems [LT75a, LT75b] that the variation of the conductance, when scaling the system to a larger size, depends only on the conductance of the smaller system and the scaling factor. Moreover, the observed metal-insulator transition in two dimensions was determined by a universal minimal conductance and, in particular, was independent of the lattice structure and other microscopic details. Thus, the results indicated the existence of *one single relevant scaling parameter*, the dimensionless conductance g. This observation is supported by Eq. (3.27), where only the ratio of the two microscopic energy scales ΔE and E_{th} enters.
Based on this (numerical) scaling results, Wegner developed a renormalization group analysis to describe the scaling near the mobility edge [Weg76, Weg79]. His results predicted the complete localization for any amount of disorder not only in one but also in two dimensions. Furthermore, contrarily to Mott's assumption of a minimal conductivity [Mot61, ER95] the MIT in $d > 2$ was predicted to be continuous,

$$\sigma \sim \left| E - E_c \right|^{\nu}, \tag{3.28}$$

where ν denotes the critical exponent of the conductivity [LR85].
Finally, Abrahams, Anderson, Licciardello, and Ramakrishnan formulated *the*

scaling theory for disordered systems [AALR79], which is sometimes also called the *standard model* of disordered systems. For that purpose, the conjecture [ET72, Tho74, LT75a, LT75b] was used that the conductance of a cube of size $n \cdot L$ is solely determined by the conductance $g(L)$ and the scaling factor n, i.e.,

$$g(n \cdot L) \quad = \quad f(n, g(L)). \tag{3.29}$$

Using the empirically known limits of Ohm's law for an almost pure metal with a large conductance, $g \sim L^{d-2}$, and of the strongly Anderson localized regime, $g \sim e^{-L/\xi}$, the *β-function* was calculated by smoothly interpolating these two limits,

$$\beta(g) \quad = \quad \frac{d \log g}{d \log L} \quad = \quad \begin{cases} d-2 & , \quad g \gg 1 \\ \log g & , \quad g \ll 1 \end{cases} . \tag{3.30}$$

While in 1D the β-function is always negative, and, thus, the system always scales towards the insulating, Anderson localized regime in the thermodynamic limit, in $d > 2$ dimensions a *critical value* g_c exists, where $\beta(g_c) = 0$ and the Anderson transition takes place. From Eq. (3.27), one can estimate [ET72, Jan98] that the transition takes place when $g = \mathcal{O}(1)$, i.e., the averaged level spacing becomes of the order of the Thouless energy. This estimate could also be motivated by considering the Landauer formula for transport through mesoscopic systems [Lan57, Dat95, Jan98]

$$g \quad = \quad \sum_{n=1}^{M} T_n, \tag{3.31}$$

where M is the total number of conductance channels and T_n the transmission probability of channel n.
Moreover, the critical exponent s of the localization length, defined via

$$\xi(E) \quad \sim \quad \left| E - E_c \right|^{-s}, \tag{3.32}$$

can be calculated to equal the critical exponent of the conductivity, $s = \nu$ [LR85, Jan98, Imr02].

In 2D, the situation is special, because the leading order contribution to the β-function vanishes in the ohmic regime. In the presence of time-reversal symmetry, we get from the perturbation theory calculation, Eq. (3.21), a negative correction, $\beta(g) \sim -1/g$. Thus, as in 1D, in the limit $L \to \infty$ the system tends necessarily towards the insulating, Anderson localized regime. However, in the presence of time-reversal symmetry breaking terms like spin-orbit coupling (or, more precisely, if one considers a different universality class [AZ97, EM08]), the sign of the correction can change and therefore, also in 2D a phase transition

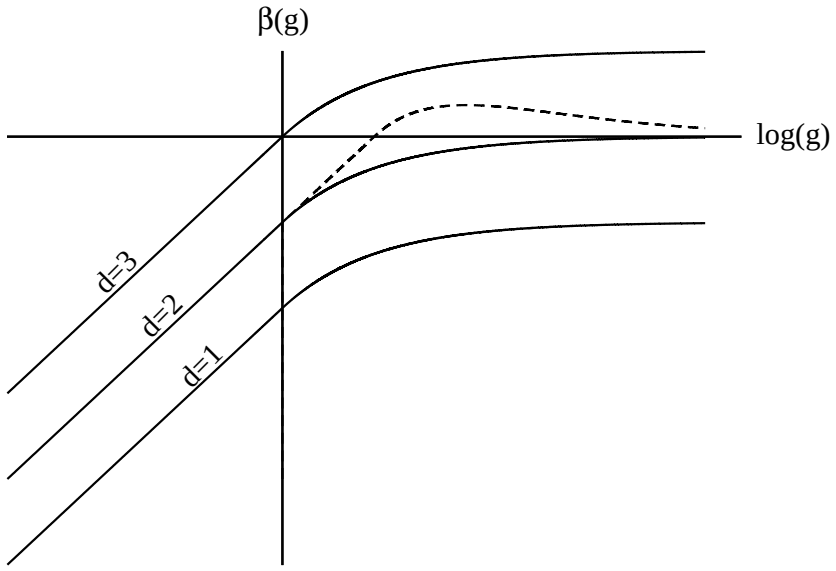

Figure 3.4: Qualitative plot of the β-function of Anderson localization in dimensions $d = 1, 2, 3$. The solid lines show the result for a system with time-reversal symmetry, the dotted line indicates the 2D result in the presence of spin-orbit coupling. (Reconstructed from [Jan98].)

can occur [HLN80, Ber84, Jan98, EM08]. A qualitative plot of the complete β-function is shown in Fig. 3.4.

Eq. (3.30) also allows to derive qualitatively the disorder-dependence of the localization length. On length scales $L < \xi$, where the system size is smaller than the localization length, transport may be well described by Ohm's law. Integrating Eq. (3.30) yields for the ohmic regime in one dimension ($\beta(g) = -1$)

$$g(L) \sim g_0 \frac{L_0}{L}. \tag{3.33}$$

g_0 and L_0 denote the conductance and the corresponding system size, respectively, within the ohmic regime, where g_0 is given by the Drude result, Eq. (3.20). As soon as the system size exceeds the localization length, transport should change from the ohmic regime to the localized regime. From the discussion above, one expects that this happens, when $g = \mathcal{O}(1)$. Thus, one can estimate

$$\begin{aligned} 1 &\simeq g(\xi) = g_0 \frac{L_0}{\xi} \\ \Rightarrow \quad \xi &\sim g_0 \sim k_{\mathrm{F}} l. \end{aligned} \tag{3.34}$$

In two dimensions (in the presence of time-reversal symmetry), the analogous

calculation yields ($\beta(g) = -c/g$)

$$\xi \sim \exp(g_0) \sim \exp(k_F l). \tag{3.35}$$

While in 1D the localization length depends only linearly on the (inverse) disorder strength ($l \sim 1/\Delta^2$ in Born approximation, see Appendix A), in 2D it grows exponentially fast with decreasing disorder.

The predictions of the scaling theory of localization were supported by further theoretical and numerical studies [KM93, Jan98, Phi93]. However, from time to time its correctness was called into question. The first serious doubt resulted from the usage of g as the relevant scaling parameter. For a specific, finite system, the conductance depends obviously on the microscopic details and the disorder realization. In particular, the conductance can strongly fluctuate from sample to sample [PSO09] (cf. Sec. 3.2.4) and its mean value may even diverge [Lan70, Sha86a]. Therefore, the scaling theory has to be interpreted in a probabilistic sense [Sha86a, Jan98]. Not the flow of the averaged conductance, but rather its distribution should be determined by a single parameter, uniquely defining the final thermodynamic state. The conductance g in Eq. (3.30) may then denote a typical value of the conductance rather than its mean value [Sha86a, Jan98].
Some numerical results also seemed to indicate deviations from the predictions of the scaling theory, for instance by yielding different critical exponents for different disorder distributions [KBMS90, Phi93]. However, these deviations seem to originate from numerical finite size effects, and recent calculations for the Anderson model agree within the errors bars with the predictions of the scaling theory [EFR08]. Therefore, the scaling theory of single-particle localization became widely accepted and its predictions are assumed to describe correctly the physics at the Anderson transition.
However, as discussed previously (cf. Sec. 2.3), in many real experiments the influence of interactions cannot be neglected a priori, and it has remained an open question to what extent the predictions of the scaling theory remain valid in the presence of interactions (see discussion below).

3.5 Self-consistent transport theory of Anderson localization

In Sec. 3.3, the weak localization corrections to the classical Drude conductivity, Eq. (3.20), were discussed. As we pointed out, perturbation theory fails in $d \leq 2$ dimensions, because the corrections arising from the maximally crossed diagrams, Eq. (3.21), yield a diverging contribution. Also when approaching the mobility edge and the localized regime, in $d > 2$ dimensions bare perturbation theory

becomes invalid. However, as the diffusion constant and the conductivity are related to each other via the Einstein relation, Eq. (3.25), one can overcome these limitations and derive a self-consistent equation for the dynamical diffusion constant $D(\omega)$ by replacing the bare diffusion constant D_0 by the dynamical one on the right hand side of Eq. (3.21),

$$D(\omega) \;=\; D_0 \,-\, \frac{1}{\pi N(\varepsilon_{\mathrm{F}})} \int \frac{d^d p}{(2\pi)^d} \, \frac{1}{-\mathrm{i}\omega/D(\omega) + p^2}. \tag{3.36}$$

The validity of this heuristic replacement could be proven more rigorously by using a systematic resummation of the most divergent (Cooperon) contributions to the particle-hole vertex [VW80a, VW80b, VW82, VW92]. In this way, it was possible to establish a systematic, self-consistent diagrammatic theory which allows to go beyond the limits of bare perturbation theory.
The first formulation of the self-consistent transport theory, Eq. (3.36), was based on the assumption of weak disorder. Later on, based on a locator expansion the theory was extended to general disorder strengths [Kop84a, Kop84b, KKW90] (see Appendix F). In Ch. 7, the self-consistent transport theory will be used extensively to analyze the interplay of disorder and local interactions within an effective single-particle Anderson model.
The development of the self-consistent theory gave additional support to the scaling theory of Anderson localization. The self-consistent equation for the conductivity yields the same critical behavior as the single-parameter scaling theory [Sha82, VW82]. Moreover, the critical exponents of the localization length and the conductivity in three dimensions were predicted to be $s = \nu = 1$. However, exact numerical studies of the Anderson tight-binding model indicate that the correct critical exponents are $s = \nu \simeq 1.5$ [EFR08], indicating that the critical regime is not correctly captured by the self-consistent theory (see also Appendix F.3.2). But apart from the critical regime, the self-consistent theory has been proven to yield even quantitatively suitable results [Kro90].

3.6 Experimental observations on the Anderson transition

The earliest experiments on Anderson localization measured the temperature dependence of the conductivity of amorphous semiconductors in the localized regime. As Mott proposed [Mot69, MD79], at finite temperatures the electron-phonon coupling of localized electrons can yield a thermally activated conductivity (*variable range hopping*)

$$\sigma(T) \;\sim\; \exp\left(-(T_0/T)^{\frac{1}{d+1}}\right), \tag{3.37}$$

which was confirmed in several experiments [Cla67, MW71, KM93], proving the existence of a localized phase.
Later on, experiments on thin films and mesoscopic Aharonov-Bohm experiments on disordered rings verified the validity of the coherent backscattering effects and the resulting weak localization corrections in two dimensions [SS82, Ber84, AA85].

Also the predictions of the one-parameter scaling theory were tested experimentally. In particular, the critical exponents at the MIT in three dimensions have been and are still a subject of intensive research. Here, the situation is less clear, because different critical exponents, $\nu \simeq 1$ and $\nu \simeq 0.5$, have been observed for samples which are believed to belong to the same universality class [Löh98, WPL99, EM08]. While the observation of two different values might be explained by a misleading analysis of the experimental data (see discussion in [WPL99, EM08]), still a strong discrepancy remains between the experimentally observed values and the numerical ones. As discussed in the previous chapter, electron-electron interaction may play an important role and, hence, these deviations from the theory were interpreted as a consequence of the presence of interaction [BK93, EM08]. Thus, the experiments seemed to indicate that the inclusion of interactions into the theory may cause deviations from the predictions of the single-particle scaling theory.

In the mid 1990's, resistivity measurements on two-dimensional semiconductor heterostructures indicated an even more dramatic change of the hitherto well accepted picture of the physics of disordered systems [KKF$^+$94, AKS01, KS04]. The experimental data from the original publication [KKF$^+$94] are shown in Fig. 3.5. As one observes, for low electron densities the resistivity curves have a negative slope, i.e., they increase with decreasing temperature, and seem to tend to an insulating ground state at zero temperature. In contrast, for electron densities above a certain threshold (indicated the dashed lines in the plots of Fig. 3.5) the slope changes its sign and the curves seem to decrease monotonously with decreasing temperature, indicating a metallic ground state. Obviously, if the interpolation of the data towards zero temperature is correct, it would prove a metal-insulator transition in two dimensions, in contrast to the predictions of the single-parameter scaling theory.[4] In the following years, the measurements could be confirmed by different groups, and also further semiconductor samples (for a review, see, e.g., [KS04]) showing the same behavior, have been found. Two remarkable facts were noted by analyzing the materials. The first one was that the electron-electron interaction of the charge carriers exceeded the Fermi energy of the material by an order of magnitude [AKS01]. Second, the conducting phase could be destroyed (or at least significantly suppressed) by applying in-

[4]Time-reversal symmetry breaking due to, e.g., spin-orbit coupling as the origin of the experimental data could be excluded.

plane magnetic fields [PBPB97, SKSP97]. As parallel magnetic fields only couple to the spin of the electrons, it again indicated that electron-electron interactions were important for an understanding of this effect.

Since its first publication, a plethora of possible explanations and interpretations of the experimental data was presented and discussed very controversially. One point under debate is, for instance, the relevant temperature scale in the experiments. Since the measurements were done at very low charge carrier densities, the Fermi temperature of these probes is rather low. Therefore, some authors claimed that the metallic behavior would be due to finite temperature effects only and, most probably, the resistivity of the 'metallic curves' would turn towards an insulating ground state at much lower temperatures [AMM$^+$nt, HXT$^+$07, FW08a, FW08b, FWnt]. Others claimed that in the experiments a real transition was found, and suggested an extension of the single-parameter scaling theory to a two-parameter scaling theory, which allows, within a certain parameter regime, for metallic solutions even in two dimensions [Fin83, Fin84, PF02, PF05]. Many more suggestions were also debated (see, e.g., [AKS01]), but after 15 years of intense research still no generally accepted theory has emerged. Anyhow, whatever will turn out at the end to be the correct explanation, the experiments clearly showed once again that a better understanding of the interplay of disorder and interactions is needed.

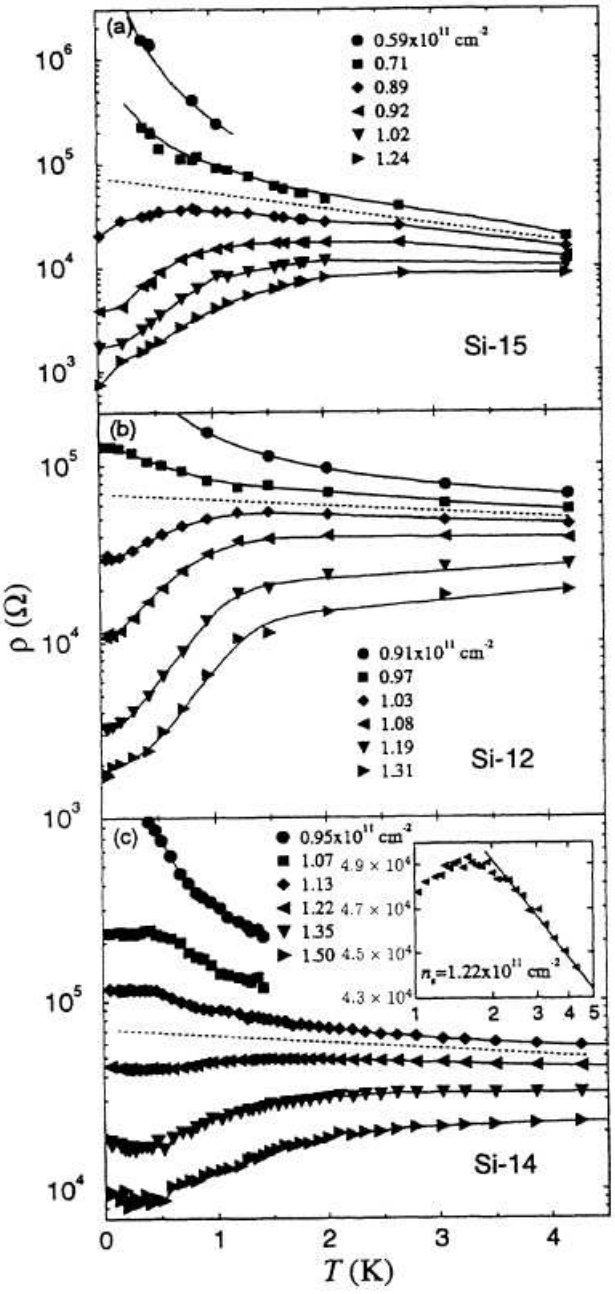

Figure 3.5: Resistivity of different two-dimensional silicon samples for different electron densities as a function of temperature. Varying the electron density the slope of the resistivity seems to indicate a metal-insulator transition in two dimensions, which is marked by the dashed line. The plot was taken from [KKF$^+$94].

Chapter 4

Interacting disordered systems

In the second half of the 1970's, the physics of single-particle Anderson localization became better understood, and a generally accepted picture of the basic behavior of disordered systems emerged [Tho74, AALR79]. At the same time, the question of possible qualitative modifications of the single-particle results, due to interactions, got into the focus of research [Tho76, FAL78, FA80].
One of the questions asked in this context is, whether in the presence of interactions (a continuum of) extended states can appear, although the noninteracting problem may be known to be completely localized. In particular, can the interacting problem become conducting, if the noninteracting one is not (and vice versa)? And, assuming a metal-insulator transition might happen, which kind of interaction (long-ranged, short-ranged etc.) is needed for that?

A related question is, whether the mobility edge in $d > 2$ dimensions can get renormalized, such that the Fermi level and the mobility edge cross each other. In that case, also a metal-insulator transition could occur. But even if the system remains localized, one can wonder, how the localization properties, like low-temperature transport (Eq. (3.37)) or the characteristic localization length (Eq. (3.6)), may be altered.
Obviously, the list of interesting questions might be greatly extended and some of them will be addressed in the following. By now, only few of these questions, if any, could be answered satisfactorily, and nearly no rigorous statement could be proven, despite intense research during the last three decades.

4.1 Interactions and the Anderson transition

In this section, we will consider the question, of whether a completely localized single-particle system can become delocalized in the presence of a (repulsive) interaction. Special attention will be paid to the role of the (effective) range of the interaction. That problem was first considered in [FAL78, FA80].

We assume the noninteracting system to be completely localized and denote the basis of localized eigenstates of $\hat{H}_A$ by $\{|\alpha\rangle\}$ (cf. Sec. 3.2.1). Furthermore, the matrix element of the repulsive two-particle interaction $\hat{U}$ shall be denoted by $\langle\alpha_1\alpha_2|\hat{U}|\alpha_4\alpha_3\rangle \equiv U_{\alpha_1\alpha_2\alpha_3\alpha_4}$. Then the interacting Anderson Hamiltonian becomes

$$\begin{aligned} \hat{H} &\equiv \hat{H}_A + \hat{H}_I \\ &= \sum_{\alpha} \varepsilon_\alpha c_\alpha^\dagger c_\alpha + \frac{1}{2} \sum_{\alpha_1,\alpha_2,\alpha_3,\alpha_4} U_{\alpha_1\alpha_2\alpha_3\alpha_4}\, c_{\alpha_1}^\dagger c_{\alpha_2}^\dagger c_{\alpha_4} c_{\alpha_3}. \end{aligned} \tag{4.1}$$

As it was emphasized in [FAL78, FA80], $\hat{H}_A$ and $\hat{H}_I$ do not posses the same symmetry groups. While $\hat{H}_I$ is generally translation invariant, $\hat{H}_A$ is not. Consequently, no conservation law, like the momentum conservation in the periodic problem, occurs. Therefore, the full Green's function and the self-energy are non-diagonal in the basis $\{|\alpha\rangle\}$,

$$G_{\alpha\alpha'}(E) = \langle\alpha|(E-\hat{H})^{-1}|\alpha'\rangle = \frac{1}{(E-\varepsilon_\alpha)\delta_{\alpha,\alpha'} - \Sigma_{\alpha\alpha'}(E)} \nsim \delta_{\alpha,\alpha'}. \tag{4.2}$$

The lack of 'momentum' conservation allows for two different ways, a single-particle excitation near the Fermi surface can decay: By a many-body decay of a cascade of particle-hole excitations, like in the interacting periodic problem, and by a single-particle decay. The former is known from Landau's Fermi liquid theory [Lan56, Lan59, PN66, AGD77]. The estimate on the available phase-space for such many-body processes yields that its contribution to the imaginary part of the self-energy vanishes like $(E-\varepsilon_{\mathrm{F}})^2$ [FA80]. The situation for the single-particle decay processes is less well known. As it was estimated in [FA80], a short-ranged interaction, i.e., an interaction decaying not slower than $1/r^d$ for $r \to \infty$, should not be able to destroy the localized nature of the states and cannot drive the system into the conducting state. For long-ranged interactions, it was concluded that a temperature dependent transport similar to the phonon assisted variable range hopping, Eq. (3.37), may occur. Of course, this analysis was not rigorous, but it was stated that "the persistence of the Anderson transition in the presence of interactions is at least plausible" [FA80].
Moreover, the following relevant and subtle effects were identified: First, the presence of a (spin) degeneracy of the eigenstates, i.e., $E_\alpha = E_{\alpha'}$ for $|\alpha\rangle \neq |\alpha'\rangle$, may yield a screening of the disorder potential due to the interaction between the states $|\alpha\rangle$ and $|\alpha'\rangle$ (cf. Ch. 6). Second, in the presence of a mobility edge (cf. Sec. 3.2.3), the interactions may renormalize the mobility edge. Thus, even if the noninteracting system is localized and the Fermi level lies inside the localized part of the spectrum (cf. Fig. 3.1), the interaction may turn the system conducting, if the mobility edge and the Fermi level cross (cf. Sec. 7.4). Third, the (virtual) scattering of localized states below the Fermi level into extended

states above the mobility edge (and above the Fermi level), may become relevant, if both energy scales come close to each other. Last, the question of the effective range of the two-particle interaction was introduced. The bare Coulomb interaction in 3D between two charged particles is $U(r) \sim 1/r$. Thus, it would be long-ranged according to the criterion from [FAL78, FA80]. However, as it is well known, in metals the Coulomb interaction between the conduction electrons gets strongly screened, yielding $U(r) \sim 1/r^3$ [FW71], which is at the border between long-ranged and short-ranged interactions. Thus, one could assume that it is just short-ranged. However, within the (Anderson) insulating phase, the electrons are less mobile and, most probably, cannot screen the potential as efficiently as in the metallic phase. Therefore, by now it is unknown what the effective range of the interaction is.

In subsequent years, the interacting Anderson model could be mapped onto an effective field theory, a non-linear sigma model, which allowed the development of a scaling theory for the interacting problem starting from the disordered Fermi liquid fixed point [Fin83, Fin84]. In two dimensions, for weak disorder the scaling equations seemed to allow for a metallic solution [Fin84, CCLM84, CCL$^+$84], in contrast to the noninteracting problem, where all systems (of the orthogonal ensemble) are believed to have an insulating ground state only (cf. Sec. 3.4). After the experimental discovery of the possible metal-insulator transition in two dimensions (cf. Sec. 3.6) the predictions of this two-parameter scaling theory received renewed interest [CCL98, PF02, PF05]. However, the solutions of the scaling equations start to diverge at a certain length scale of the system [CCL98, CLN99], indicating a possible breakdown of the perturbative ansatz. Therefore, the predictions are at least inconclusive and the theory has generally not become accepted yet.

In recent years, the ideas of the early works of [FAL78, FA80] were picked up again and the problem of delocalization by interactions were again addressed [GMP05, BAA06, BAA08]. In [GMP05] a (quasi) one-dimensional system of localized states in the presence of a short-ranged interaction was considered. The many-body problem was mapped onto a Caylee tree, where the nodes represented many-body states of the Fock space, and the edges connected states which can be transformed into each other by a single decay process. The result of this calculation was that a delocalization transition could only occur above a finite, critical temperature T_c. Below T_c all states remained localized in the Fock space. It was argued, the same result would be also valid in two dimensions, and, hence, an interaction driven MIT of the disordered system in $d < 3$ dimensions, at zero temperature, would not be possible, in contrast to the predictions of the two-parameter scaling theory. However, also this result has been remained inconclusive. The mapping onto the Caylee tree was a strong approximation, which could not be convincingly justified. In particular, it seems to completely neglect

the possibility of single-particle decays, which were identified to be relevant in [FAL78, FA80].
In [BAA06, BAA08], the possibility of a localization-delocalization transition in Fock space due to the presence of a short-ranged interaction was studied, as well. Again the original model was mapped from Fock space onto a graph, similar but less restrictive than in [GMP05]. The analysis was then done by using nonequilibrium perturbation theory. The result was similar to the one in [GMP05]. Below some finite critical temperature T_c the system remains localized and insulating. Above T_c, a many-body delocalization may occur and transport due to electron-electron interaction assisted variable range hopping may take place. By construction, the validity of the analysis is restricted to the perturbative regime of weak and short-ranged interactions. Additionally, it did not become clear, whether all relevant processes (see discussion above) were included carefully enough. Recent numerical studies on that topic [OH07, OPH09] could not confirm the existence of a many-body localization transition at finite temperature. An experimental setup to search for such a transition was recently suggested [BAA07], but till now no reports on experimental evidence of manifestations of many-body localization have been presented.

In summary, no rigorous statements, and almost no generally accepted, conclusive results on the problem of Anderson localization in interacting systems have been presented yet. Much effort has been made via numerical studies to get a deeper insight into that problem. But also here, the situation is far from being clear and many contradictory results have been obtained. Some of these will be subject of subsequent chapters and discussed in detail there. But before, we want to present some important results on the behavior of the disorder-averaged density of states in an interacting system.

4.2 Zero bias anomalies of the density of states

As we mentioned in Secs. 3.2.3 and 3.2.4, the disorder-averaged density of states of a noninteracting system is a smooth and uncritical quantity, even at and in the vicinity of the Anderson transition. However, in the presence of (long-ranged) interactions the situation can change. Here, the DOS can develop pseudogaps at the Fermi level, both in the strongly and the weakly localized regime of a diffusive metal.

4.2.1 Efros-Shklovskii anomaly

First, we will discuss the case of long-ranged interactions in a perfectly localized insulator, i.e., an insulator with immobile charge carriers. As it was first shown in [ES75], in this situation, a long-ranged Coulomb interaction, $U(r) \sim 1/r$, leads

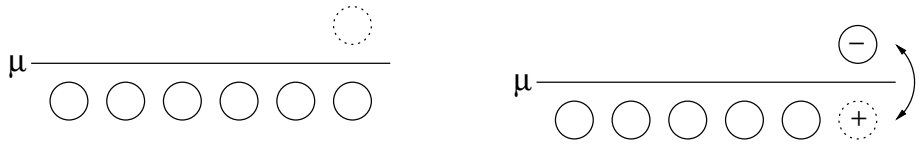

(a) (b)

Figure 4.1: Sketch of the low energy excitation discussed in the proof of the Efros-Shklovskii anomaly (see text). Solid circles denote occupied lattice sites, the dashed ones correspond to an unoccupied one. μ is the chemical potential.

to a complete depletion of states at the Fermi level and, hence, the density of states develops a pseudogap.
For the derivation of this statement, we consider a simple static model of localized charges, e.g., in a doped semiconducting material [ES75, ES85]. Then the system consists of N negatively charged electrons, N positively charged ions, and M neutral atoms. Ions and atoms form a lattice, where the electrons are placed onto. Then the total energy of the system is given by

$$E \;=\; \sum_i \varepsilon_i n_i \;+\; e^2 \sum_i \sum_{j>i} \frac{q_i\, q_j}{r_{ij}}, \tag{4.3}$$

where the first term arises from the energies of the single-particle states, and the second one is the static Coulomb energy of the system. Here, n_i denotes the electron occupation number of lattice site (= single-particle state) i, q_i is its total charge (measured in units of the elementary charge e) and r_{ij} denotes the distance between lattice sites i and j. The lattice sites $i = 1, ..., N$ shall correspond to the positions of the ions, while the remaining sites with $i > N$ shall denote the positions of the neutral atoms. For simplicity, we assume that in the ground state all electrons are occupying a lattice site of an ion, i.e.,

$$n_i \;=\; \begin{cases} 1 & , \quad i \le N \\ 0 & , \quad i > N \end{cases} \qquad , \qquad q_i \;\equiv\; 0. \tag{4.4}$$

An energetically low lying excitation will then correspond to the creation of a particle-hole pair, where an electron moves from a lattice site of one of the ions, i. e., $i \le N$, to a lattice site of one of the neutral atoms, $j > N$ (see Fig. 4.1). By this process, both the local occupation numbers ($n_i \mapsto 0$, $n_j \mapsto 1$) and the local charges ($q_i \mapsto 1$, $q_j \mapsto -1$) are changed. Thus, the energy difference between these two configurations is

$$\Delta E \;=\; \varepsilon_j \,-\, \varepsilon_i \,-\, \frac{e^2}{r_{ij}} \;\ge\; 0. \tag{4.5}$$

Thus, for an excitation from a state at the Fermi level ($\varepsilon_i = 0$) with an excitation energy

$$\varepsilon \equiv \varepsilon_j - \frac{e^2}{r_{ij}} \geq 0, \tag{4.6}$$

a particle-hole pair must be created, which is at least separated by a minimal distance $r_\varepsilon = e^2/\varepsilon$. Hence, within a finite volume V, the number of low lying excitations can be estimated by

$$\#N(E < \varepsilon + \varepsilon_\mathrm{F}) - \#N(E < \varepsilon_\mathrm{F}) \sim V/r_\varepsilon^d. \tag{4.7}$$

Since $\#N(E < \varepsilon)$, the number of states with energy $E \leq \varepsilon$, is given by

$$\#N(E < \varepsilon) = V \int_{-\infty}^{\varepsilon} N(\varepsilon')\, d\varepsilon', \tag{4.8}$$

we can estimate the density of states in the vicinity of the Fermi level by

$$N(\varepsilon) = \frac{1}{V}\frac{d}{d\varepsilon}\#N(E < \varepsilon) \sim \frac{d}{d\varepsilon}\frac{1}{r_\varepsilon^d} \sim \left|\varepsilon - \varepsilon_\mathrm{F}\right|^{d-1}. \tag{4.9}$$

The pseudogap of the DOS at the Fermi level, described by Eq. (4.9), is called *Efros-Shklovskii anomaly* [ES75, ES85]. The physical origin of this anomaly is the long-ranged nature of the effective Coulomb interaction. Since the charge carriers were assumed to be completely localized, e.g., due to the presence of strong disorder, they were not able to screen efficiently the bare Coulomb interaction. In contrast, mobile charge carriers, like in metals, could rearrange. This would lower the charging energy of the particle-hole pair and result in a short-ranged effective interaction [FW71].

4.2.2 Altshuler-Aronov anomaly

Not only for the strongly localized regime it is known that the interplay of disorder and interaction can induce a zero bias anomaly of the density of states. Also in the opposite regime, i.e., that of a diffusive metal, such an effect is known [AA79, AAL80, AA85]. For weakly interacting, disordered metals, a perturbation theory calculation of first order in the interaction strength shows that the disorder-averaged density of states at the Fermi level gets strongly suppressed, because of the presence of the repulsive interaction. An evaluation of the corresponding diagrams (see Fig. 4.2) yields at zero temperature a correction to the density of states of [AA85, AM07]

$$\frac{\delta N(\varepsilon)}{N(\varepsilon)} \sim -\frac{U_0}{D}\left(1 - \frac{c_\mathrm{H}}{c_\mathrm{F}}\right)\begin{cases} 1/\sqrt{|\varepsilon - \varepsilon_\mathrm{F}|} & , \quad d = 1 \\ -\log|\varepsilon - \varepsilon_\mathrm{F}| & , \quad d = 2 \\ C - \sqrt{|\varepsilon - \varepsilon_\mathrm{F}|} & , \quad d = 3 \end{cases}. \tag{4.10}$$

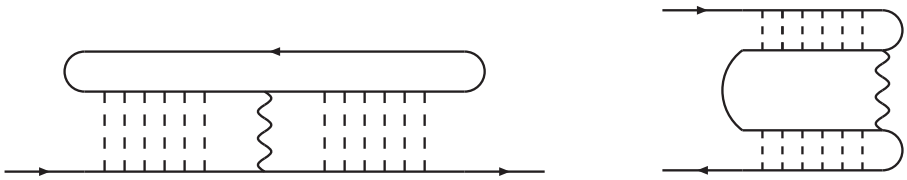

Figure 4.2: First order perturbation theory corrections to the single-particle self-energy and the density of states, respectively. a) Hartree diagram b) Fock diagram. Solid lines represent the disorder-averaged single-particle propagators, dashed lines denote the diffusion vertex, and wavy lines denote the effective two-particle (Coulomb) interaction [AA85, AM07].

Here, $U_0 \geq 0$ parametrizes the interaction strength, D is the diffusion coefficient and C is a constant, independent of ε. The coefficients c_{H} and c_{F} are weights of the Hartree and the Fock diagrams, respectively. Their ratio depends on the range of the effective, repulsive interaction. For an extended interaction, i.e., $U(x) \nsim \delta(x)$, $c_{\mathrm{H}} < c_{\mathrm{F}}$ yields a negative contribution, and, thus, a reduction of the density of states at the Fermi level, called *Altshuler-Aronov anomaly*. This anomaly remains also valid, if one takes into account contributions from the cooperon vertex and higher order corrections [AA85]. The divergency at $\varepsilon \to 0$ is an artefact of the finite order perturbation theory calculation and can be corrected by a resummation of the leading order self-energy contributions [SCK09].

The existence of the Altshuler-Aronov anomaly could be observed experimentally by tunnel conductance measurements. For instance, the voltage dependence of the tunnel conductance of, e.g., two disordered metals separated by an oxide film is directly proportional to the single-particle density of states of the two metals and perfectly displays the Altshuler-Aronov anomaly at zero bias voltage [AA85, PPJ$^+$01, AM07]. Also measuring the temperature dependence of the conductivity of disordered metals could confirm the prediction of the Altshuler-Aronov anomaly [AA85, AM07].

Chapter 5

Anderson-Hubbard model

So far, the discussion of disordered, interacting system has been based on rather general interaction potentials. In the following, we will restrict our studies to a specific, local interaction potential. Before we start the discussion of the full problem, we first give a very brief introduction to the corresponding nondisordered *Hubbard model*.

5.1 Hubbard model

The Hubbard model [Hub63, Hub64a, Hub64b] is a paradigm of condensed matter theory. Generally, it is too simple to model any real material. However, it is at least believed to grasp the salient features of strongly correlated systems and its rich physical properties, e.g., Mott metal-insulator transitions (cf. Sec. 2.3), (anti-)ferromagnetism, superconductivity etc. [GKKR96, LNW06]. Therefore, it is one of the most studied models in current research, and a large literature about its physics exist. In the following, we will only briefly summarize the most important aspects needed in the subsequent parts of this thesis. For a more detailed discussion and reviews on different aspects of the Hubbard model, we refer to, e.g., [Lie95, GKKR96, Geb97, IFT98, EFG+05] and references therein.

The Hubbard model (for spin-1/2 fermions) is defined by the Hamiltonian

$$\hat{H}_H \;=\; -t \sum_{<i,j>,\sigma} c^\dagger_{i\sigma} c_{j\sigma} \;+\; \frac{U}{2} \sum_{i\sigma} \hat{n}_{i,\sigma} \hat{n}_{i,-\sigma} \;-\; \mu \sum_{i\sigma} \hat{n}_{i,\sigma}, \tag{5.1}$$

where $U > 0$ denotes the repulsive Hubbard interaction strength ($U < 0$ is not considered in this thesis). μ is the chemical potential and $\hat{n}_{i,\sigma} = c^\dagger_{i\sigma} c_{i\sigma}$ is the occupation number operator of site i.
The Hubbard Hamiltonian describes a strongly simplified many-body (many-electron) system. As in the Anderson model, the conduction band is assumed to

be narrow and is approximated by the tight-binding Laplacian. The effective, repulsive interaction is treated as purely local. Therefore, the simplified effective interaction mimics a strongly screened metal (cf. discussion in Ch. 4), which in continuous systems would correspond to a pointlike interaction, $U(r-r') \sim \delta(r-r')$. This ansatz is motivated by the observation that in strongly correlated materials, like the transition metal compounds, the intraorbital interaction of electrons of the same atom is much larger than the interorbital interaction between electrons of neighboring atoms.

The Hubbard model is the minimal lattice model containing the physics of electron-electron correlations. Nevertheless, its theoretical understanding is still far from being complete. The only exact solution has been found for the ground state of the one-dimensional system. Here, the model is known to be integrable [Sha88, Lie95] and the exact ground state could be constructed by using Bethe ansatz [LW68, LW03, Lie95]. From this solution, it could be proven that in 1D, for any $U > 0$, the Hubbard model has an insulating ground state at half-filling, which corresponds to $\mu = U/2$ in Eq. 5.1. As described in Sec. 2.3, the insulating state is a Mott insulator with a Mott-Hubbard gap in the density of states around μ. Moreover, the ground state is a spin singlet with antiferromagnetic order [LM62, LW68]. Away from half-filling, the DOS of the one-dimensional system remains gapless for all values of U and the system is in a metallic state.

In dimensions $d > 1$, no exact solution exists at the moment and only numerical results are obtainable. However, already the numerical treatment of the Hubbard model is complicated and still a non-trivial challenge. Due to limitations of computer time and memory, non-approximative methods like exact diagonalization (ED) and quantum Monte Carlo (QMC) are strongly restricted to small system sizes and low dimensions ($d \leq 2$) [Hir85, Dag94, CA09]. On the other hand, approximate solutions often suffer from the problem that relevant physical properties, e.g., antiferromagnetic ordering, charge fluctuations etc. are missed. However, during the last two decades much progress has been made by the development of dynamical mean field theory (DMFT) [MV89, GK92, GKKR96]. DMFT is based on a self-consistent mean-field approximation mapping the original Hubbard model onto an effective single-impurity problem. In its basic formulation, dynamical (temporal) charge fluctuations are exactly included, which is essential for including real many-body effects, while, in contrast, spatial correlations are only treated within a mean-field approximation, assuming the self-energy to be local. Thus, DMFT becomes exact only in the limit of infinite dimensions and infinite lattice coordination number, respectively. However, it turned out that the approximation of large coordination numbers is a good approach to the Hubbard model in higher dimensions, while it is less accurate in low dimensions ($d \lesssim 2$). Its prediction for (and slightly away from) half filling is that the system undergoes a first order (Mott) phase transition from a metal to a Mott insula-

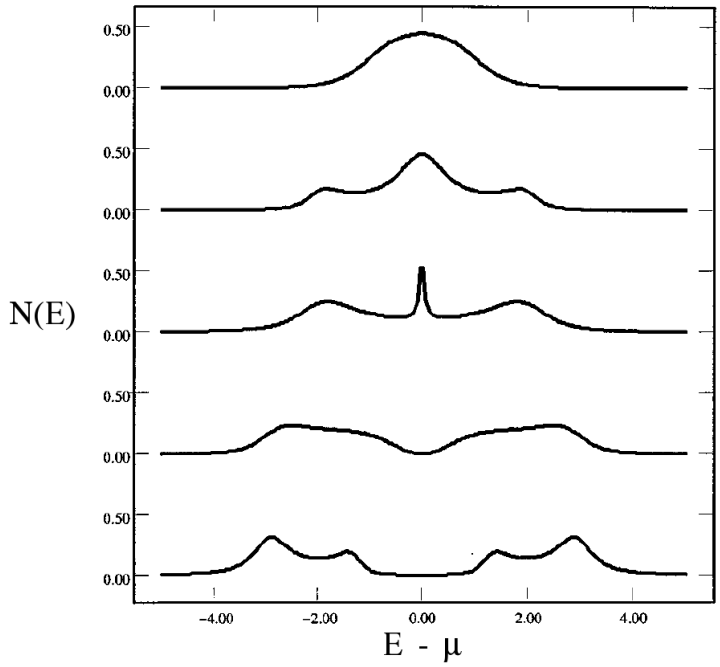

Figure 5.1: Density of states of the Hubbard model at low temperatures and at half-filling as a function of energy. From top to bottom the interaction strength increases. For low interactions (topmost curve) the Hubbard model is metallic. Close to the critical interaction strength (second and third curve from the top) the formation of a pronounced many-body resonance at the Fermi level ('Kondo peak') takes place. It indicates the formation of local magnetic moments and the corresponding long-ranged antiferromagnetic order. For strong interactions (two curves at the bottom) the DOS becomes gapped and two Mott-Hubbard bands exist. (Plot taken from [GKKR96].)

tor. The transition takes place at some critical interaction strength U_c, which is of the order of the band width of the noninteracting ($U = 0$) electron gas, i.e., $U_c/(2td) \approx 1..2$ [GKKR96, KV04] (see Fig. 5.1). Furthermore, with increasing interaction strength local magnetic moments are formed and a long-ranged antiferromagnetic order arises [GKKR96, KV04].

The formation of an insulating, antiferromagnetic ground state at half filling can be best understood from the limit $U/t \to \infty$. At half filling, all sites will then be occupied by exactly one electron. Charge fluctuations will be energetically disfavored. However, virtual hopping processes, where an electron hops to a neighboring site and afterwards returns to its original site, can lower the ground state energy and are of the order t^2/U. These processes can only occur if

the electrons' spins are opposite at neighboring sites. Thus, an antiferromagnetic ground state will be favorable. Formally, this means the Hubbard model becomes equivalent to the *t-J model* [Vol94]

$$\hat{H}_{t-J} \;=\; -t \sum_{<i,j>\sigma} (1-\hat{n}_{i,-\sigma}) c^{\dagger}_{i\sigma} c_{j\sigma} (1-\hat{n}_{j,-\sigma}) \;+\; J \sum_{<i,j>} \left(\hat{S}_i \cdot \hat{S}_j - \frac{1}{4} \hat{n}_i \hat{n}_j \right), \tag{5.2}$$

where $J = 4t^2/U$ and $\hat{S}_i$ is the spin operator at site i. At half filling, in the limit $U/t \to \infty$ the model reduces to the antiferromagnetic ($J > 0$) Heisenberg model

$$\hat{H} \;=\; J \sum_{<i,j>} \hat{S}_i \cdot \hat{S}_j. \tag{5.3}$$

5.2 Anderson-Hubbard model

In the previous section, the Hubbard model was introduced as the minimal lattice model of strongly correlated systems. If one is interested in the interplay of disorder and interactions, one needs to treat both potentials on the same level. Therefore, it is a natural and convenient choice to extend the disordered single-particle Anderson model by including the local Hubbard interaction term to obtain an interacting, disordered many-body system.[1] The result is known as the *Anderson-Hubbard model*, which is sometimes also called *disordered Hubbard model (for fermions)*. With the same notations as before, the Hamiltonian of the Anderson-Hubbard model reads

$$\begin{aligned} \hat{H}_{AH} \;&\equiv\; \hat{H}_{loc} + \hat{H}_{kin} \;\equiv\; \hat{H}_{dis} + \hat{H}_U + \hat{H}_{kin} \\ &=\; \sum_{i\sigma} (\varepsilon_i - \mu) c^{\dagger}_{i\sigma} c_{i\sigma} \;+\; \frac{U}{2} \sum_{i\sigma} \hat{n}_{i,\sigma} \hat{n}_{i,-\sigma} \;-\; t \sum_{<i,j>,\sigma} c^{\dagger}_{i\sigma} c_{j\sigma}, \end{aligned} \tag{5.4}$$

where the on-site energies $\{\varepsilon_i\}$ are again assumed to be i.i.d. with an uniform box distribution of width $\Delta \geq 0$ (see Sec. 3.1).

In the discussion of the Hubbard model, Sec. 5.1, we explained that the model was originally motivated by the assumption of a strong screening of the bare Coulomb interaction. Therefore the effective interaction was reduced to a purely local one. However, as we discussed in Ch. 4, the effective range of the Coulomb interaction in disordered materials might be significantly larger. In particular, localized electrons are much less mobile than the conduction electrons of a nearly

[1] Again, we only consider the case of a repulsive interaction and will always assume $U \geq 0$. The case of an attractive interaction, $U < 0$, is studied intensively in the context of disordered superconductors, see, e.g., [DMA07].

free electron gas in an almost pure conductor. Thus, the applicability of the Anderson-Hubbard model to real materials is less clear. A more realistic description would probably require, e.g., a self-consistent inclusion of an effective screening length. However, the Anderson-Hubbard model, as the simplest non-trivial lattice model for interacting particles in a disordered environment, is nevertheless a good starting point to try getting a basic understanding of strongly interacting, disordered systems. And, as we will discuss below, it is already the origin of rather rich and complex physics. Besides, in recent years a new field of physics, the research on cold atomic gases in optical potentials, came into close contact with condensed matter theory. While the Anderson-Hubbard model can only mimic, if at all, the relevant physical processes of real materials, it can provide a very good description of many experiments on cold atomic gases (see Ch. 8).

As we discussed above, the physics of the Hubbard model strongly depends on the filling factor of the lattice. At least in the strong coupling limit, where $U \gg \Delta$, this also holds for the disordered case. Therefore it is useful to denote this important quantity in the following by ρ. ρ is defined as the average site occupation number, or as the ratio of the total particle number and the total number of lattice sites, respectively,

$$\rho \;=\; \lim_{N\to\infty} \frac{1}{N} \sum_{i=1}^{N} \sum_{\sigma} \langle \hat{n}_{i\sigma} \rangle \;=\; \overline{\langle \hat{n}_{i\sigma} \rangle}. \tag{5.5}$$

For spin-1/2 particles (electrons), $0 \leq \rho \leq 2$. In particular, $\rho = 1$ corresponds to the important case of half-filling, where the number of particles equals the number of lattice sites.

5.3 Numerical observations on the Anderson-Hubbard model

Although the Anderson-Hubbard model is in some sense the simplest interacting, disordered model, almost no analytical results have been obtained yet. Therefore, one has to rely on numerical results to get some insight into the physical behavior of the Anderson-Hubbard model, and the interplay of the two competing potentials.

In particular, after the experimental discovery of the possible two-dimensional metal-insulator transition [KKF$^+$94, AKS01, KS04] (see Sec. 3.6), the Anderson-Hubbard model gained much interest and many numerical calculations were performed. The reason is that the presence of a Hubbard-like interaction would explain the experimentally observed magnetoresistance, and the strong influence

of an external, in-plane magnetic field. Supposing, that the presence of the Hubbard interaction implies the strong suppression of electron localization by disorder, one expects that this effect would easily get destroyed by spin-polarization induced by an external magnetic field [Her01]. Moreover, the screening of the disorder potential by the local Hubbard interaction was suggested as a possible mechanism, how interactions could induce a delocalization of the system. However, the numerical analysis of the Anderson-Hubbard model (references will be given in Sec. 7.6) showed that the interplay of disorder and interaction is rather complex. Generally, it was observed that weak interactions indeed yield a delocalizing effect. Sometimes even signatures of an intermediate extended, metallic state in two dimensions were found. In contrast, a strong interaction even seems to support the localizing nature of the disorder potential. However, a conclusive explanation of the observed results could not be given, and the origin of the non-monotonic interaction-dependence remained unclear.
In the following, we will therefore try to present a simple physical approximation, which allows for an explanation of most of the observed features and their physical origin. Moreover, we will critically re-address the question of a possible metal-insulator transition in two dimensions within the Anderson-Hubbard model.

Chapter 6

Atomic-limit approximation of the Anderson-Hubbard model

In the last chapter, we mentioned that a large number of numerical studies on the Anderson-Hubbard model observed a nonmonotonic, (de-)localizing effect due to the presence of the interaction. In the following, we will work out the physical origin of this observation and present a qualitative and quantitative analysis of its influence. For that purpose, we will use an analytically simple, but by no means trivial, single-particle approximation to the Anderson-Hubbard model.

6.1 Physical motivation of the atomic-limit approximation

We start our consideration for the case of strong disorder, i.e., $\frac{\Delta}{t}, \frac{\Delta}{U} \gg 1$ (or $\rho \ll 1$ [TL93]). In this limit, in any dimension the system is strongly believed to become insulating because of the disorder. To understand the physical properties of this (insulating) system, we have to consider the propagation (and the lifetime) of a single-particle excitation at the Fermi level, which is accessible, e.g., via the retarded zero-temperature Green's function [AGD77]

$$\mathcal{G}^R_{ij\sigma}(t) \;=\; -\mathrm{i}\Theta(t)\langle[c_{i\sigma}(t), c^\dagger_{j\sigma}(0)]_+\rangle. \tag{6.1}$$

Here, $[\cdot,\cdot]_+$ denotes the anticommutator of two (fermion) operators. Furthermore, to avoid any confusion, we will always denote the propagator of the interacting Anderson-Hubbard model by $\mathcal{G}$, while the propagator of the noninteracting (effective) single-particle Anderson model will be denoted by G.
An exact calculation of $\mathcal{G}^R_{ij\sigma}(t)$ is generally impossible. However, as in the noninteracting case, we could principally use a locator expansion in powers of the hopping amplitude t [FWGF89], which could be principally done, e.g., by use of the auxiliary-particle representation (see Appendix B). Nevertheless, any explicit

calculation remains technically challenging and, in practice, is restricted to low orders of perturbation theory. But the formal analogy of the interacting locator expansion to the noninteracting one allows us to adopt results from the noninteracting Anderson model to our case of the Anderson-Hubbard model.
From the noninteracting problem [And58], it is known that an electron, which is initially located at any lattice site i, will stay at that site with high probability. More precisely, the change of the occupation number of site i is

$$\delta\langle n_i\rangle \;\equiv\; \langle\hat{n}_i\rangle \,-\, \langle\hat{n}_i\rangle_0 \;=\; \mathcal{O}((t/\Delta)^2), \tag{6.2}$$

where

$$\langle\hat{n}_i\rangle_0 \;=\; \frac{\mathrm{tr}\{e^{-\beta\hat{H}_{dis}}\,\hat{n}_i\}}{\mathrm{tr}\{e^{-\beta\hat{H}_{dis}}\}} \tag{6.3}$$

is the occupation number of site i in the atomic limit, where $t = 0$.
Assuming validity and convergence of the interacting locator expansion, the results of Eqs. (6.2) and (6.3) remain formally the same. The only thing that changes is that we have to replace $\hat{H}_{dis}$ by $\hat{H}_{loc} \equiv \hat{H}_{dis} + \hat{H}_U$ in Eq. (6.3), and, in Eq. (6.2), the disorder strength has to be interpreted as an effective one, $\Delta \mapsto \Delta_{eff}$, whose value generally depends on the interaction strength U and the lattice filling ρ. The origin of this disorder renormalization can be understood by considering again the propagation of a single-particle excitation at the Fermi level, on top of the interacting Fermi sea. When propagating through the lattice, the quasiparticle is affected by the local potential of each lattice site. For each site i, the total potential is not determined solely by the disorder potential ε_i, but also by the interaction potential, which can yield an additive contribution. From Eq. (6.2), we are motivated to approximately describe the propagation of a quasiparticle at the Fermi sea by treating the interaction term as a static background potential, created by the charge density of the Anderson-Hubbard model in the atomic limit. By doing so, we arrive at an effective noninteracting single-particle Anderson Hamiltonian

$$\hat{H}_A \;=\; \sum_{i\sigma}\varepsilon_i c^\dagger_{i\sigma}c_{i\sigma} \,-\, t\sum_{<i,j>,\sigma} c^\dagger_{i\sigma}c_{j\sigma}, \tag{6.4}$$

where the on-site energies are now distributed according to a renormalized probability function, denoted by $p_{\mathrm{A}}(\varepsilon)$. Thereby, the original Hubbard interaction strength U enters only as a parameter of $p_{\mathrm{A}}(\varepsilon)$.

Before we start to determine the effective probability distribution and to analyze the Hamiltonian (6.4), we have to discuss the range of validity of our ansatz. Our derivation of the effective single-particle model was based on the assumption that, at all times, the average occupation number of the lattice sites does

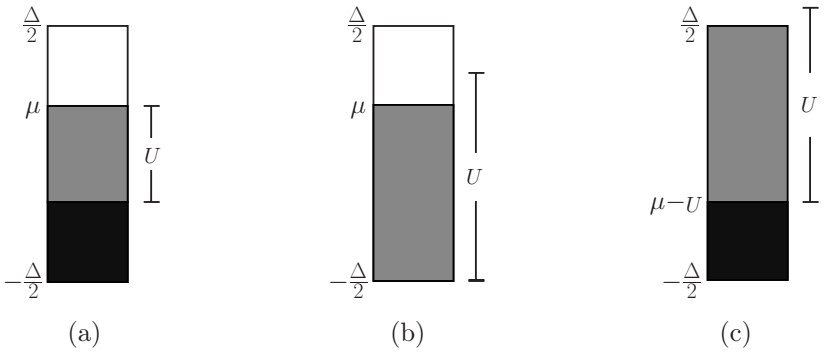

Figure 6.1: Ground state configuration of the atomic limit for a) weak interaction b) strong interaction and $\rho \leq 1$ c) strong interaction and $\rho > 1$.

not significantly deviate from its value in the atomic limit. Surely this means that we have to restrict to the regime of strong disorder, $\Delta_{eff} \gg t$. One might be tempted to expect that this also means that each particle has to be closely localized around a certain lattice site. That would correspond to the condition that the localization length of the particles has to be of the order of the lattice spacing, i.e., $\xi = \mathcal{O}(1)$, or, at least, $\xi \lesssim \mathcal{O}(\bar{l})$, where $\bar{l} = (1-|1-\rho|)^{-1}$ is the mean interparticle distance. However, it is important to note that our argumentation was based on the value of the *total average charge density*. Even if the single-particle localization lengths' become significantly larger than $\mathcal{O}(1)$, the charge density may still vary on the scale of the lattice spacing. Thus, a priori we can allow for large localization lengths without contradicting the applicability of the atomic-limit approximation.[1] However, we have to emphasize that the atomic-limit ansatz can only capture the *static* physics of the Anderson-Hubbard model. In contrast, any physical effect determined mainly by the *dynamics* of the system can be captured only by chance, if at all.

6.2 Ground state of the atomic limit

The effective disorder potential depends on the ground state occupation numbers of the atomic limit. Therefore, we have to start our approximative treatment of the Anderson-Hubbard model by calculating these occupation numbers. For that purpose, we will first concentrate on the most relevant case of spin-1/2 particles (electrons), postponing the discussion of a general spin system to Sec. 7.5.

At first, we note that in the ground state of the atomic limit the occupation

[1] See also Appendix F.3.2, as well as [CG09], for a discussion of the question, when disorder becomes already strong enough for calling it "strong disorder".

number of any given lattice site i takes one of the values $0, 1, 2$. Moreover, three different cases have to be distinguished (see Fig. 6.1). a) The interaction strength is relatively weak. Therefore, some sites with low local potentials will be doubly occupied, some sites with intermediate local potentials are singly occupied, and the sites with a very high local potential will be empty. b) The interaction is relatively strong, and the lattice filling is $\rho \leq 1$. In this case, all sites are at most singly occupied, because double occupancy is energetically disfavored. c) The interaction is strong, and $\rho > 1$.[2] In that case, all sites have to be occupied at least by one electron, because of the high lattice filling. The sites with a low local potential are even doubly occupied.

Let's consider first case a): From Fig. 6.1(a) we can determine the chemical potential μ by counting states,

$$\rho \stackrel{!}{=} 2\,\frac{\mu - U + \Delta/2}{\Delta} + \frac{\mu - (\mu - U)}{\Delta} \tag{6.5}$$

$$\Leftrightarrow \quad \mu = \frac{1}{2}(\Delta\rho - \Delta + U). \tag{6.6}$$

From Fig. 6.1 and from the discussion above we see that this ground state configuration only occurs for relatively low interaction strengths. More precisely, the ground state configuration changes to case b) (Fig. 6.1(b)), if the energy, needed to occupy the site with the lowest possible local potential, $-\Delta/2$, is higher than the chemical potential. Therefore, we immediately get the restriction

$$-\frac{\Delta}{2} + U \stackrel{!}{\leq} \mu \tag{6.7}$$

$$\Leftrightarrow \qquad U \stackrel{!}{\leq} \Delta\rho. \tag{6.8}$$

On the other hand, case a) only occurs if the chemical potential lies within the interval $[-\Delta, 2, \Delta/2]$. Otherwise case c) becomes the correct ground state configuration. Hence, we obtain a second condition on U,

$$\mu \stackrel{!}{\leq} \Delta/2 \tag{6.9}$$

$$\Leftrightarrow \quad U \stackrel{!}{\leq} \Delta(2 - \rho). \tag{6.10}$$

We easily read off, that Eq. (6.8) is the relevant condition if $\rho \leq 1$, while Eq. (6.10) is the relevant one if $\rho \geq 1$.

Now, we can continue with case b), i.e., $U > \Delta\rho$ and $\rho \leq 1$. Again counting states yields immediately the result for the chemical potential,

$$\rho \stackrel{!}{=} \frac{\mu + \Delta/2}{\Delta} \tag{6.11}$$

$$\Leftrightarrow \quad \mu = \Delta(\rho - \frac{1}{2}). \tag{6.12}$$

[2] In principal, we could restrict to $\rho \leq 1$, because of particle-hole symmetry. Nevertheless, for completeness, we will explicitly determine the ground state for $\rho > 1$, as well.

Finally, we have to determine the ground state of case c) where $U > \Delta(2-\rho)$ and $\rho \geq 1$. As before, we can read off

$$\rho \stackrel{!}{=} 2\,\frac{\mu - U + \Delta/2}{\Delta} + \frac{\Delta/2 - (\mu - U)}{\Delta} \tag{6.13}$$

$$\Leftrightarrow \quad \mu = \Delta(\rho - \frac{3}{2}) + U. \tag{6.14}$$

In summary, we find the following ground state configuration within the atomic limit:

$$\langle n_i \rangle_0 = \begin{cases} 2 & , \quad \varepsilon_i \leq \mu - U \\ 1 & , \quad \mu - U < \varepsilon_i \leq \mu \\ 0 & , \quad \varepsilon_i > \mu \end{cases}, \tag{6.15}$$

$$\mu = \begin{cases} \frac{1}{2}(\Delta\rho - \Delta + U) & , \quad \rho < 1\,,\, U < \Delta\rho \\ \Delta(\rho - \frac{1}{2}) & , \quad \rho < 1\,,\, U \geq \Delta\rho \\ \frac{1}{2}(\Delta\rho - \Delta + U) & , \quad \rho \geq 1\,,\, U < 2\Delta - \Delta\rho \\ \Delta(\rho - \frac{3}{2}) + U & , \quad \rho \geq 1\,,\, U \geq 2\Delta - \Delta\rho \end{cases}. \tag{6.16}$$

6.3 Effective probability distribution

Having calculated the ground state configuration, we are able to derive the effective probability distribution of the atomic-limit approximation, $p_{\mathrm{A}}(\varepsilon)$. For that we notice first, that the effective probability distribution function $p_{\mathrm{A}}(\varepsilon)$ is directly related to the disorder-averaged local density of states of the Hamiltonian (6.4) in the atomic limit ($t = 0$) by

$$N(E) = \int d\varepsilon_i\, p_{\mathrm{A}}(\varepsilon_i)\, N_i\,(E) \tag{6.17}$$

$$= -\frac{1}{\pi} \int d\varepsilon_i\, p_{\mathrm{A}}(\varepsilon_i)\, \mathrm{Im} G_i^R(E) \tag{6.18}$$

$$= -\frac{1}{\pi} \int d\varepsilon_i\, p_{\mathrm{A}}(\varepsilon_i)\, \mathrm{Im} \frac{1}{E - (\varepsilon_i - \mu) + \mathrm{i}0^+} \tag{6.19}$$

$$= p_{\mathrm{A}}(E + \mu) \tag{6.20}$$

$$\Leftrightarrow \quad p_{\mathrm{A}}(E) = N(E - \mu). \tag{6.21}$$

As discussed above, the effective disorder distribution shall take into account the effective shift of the local potential in the Anderson-Hubbard model according to its ground state configuration. Thus, we can see from Eq. (6.21) that we can directly obtain it from the single-particle excitation spectrum and the disorder-averaged density of states, respectively, of the Anderson-Hubbard model in the

atomic limit. The excitation spectrum is given by the imaginary part of the retarded Green's function of the Anderson-Hubbard model. Therefore, we can determine the effective distribution function via

$$p_{\mathrm{A}}(E) \;=\; \int d\varepsilon_i \, p(\varepsilon_i) \, \mathrm{Im}\mathcal{G}^{R,0}_{i\sigma}(E-\mu), \tag{6.22}$$

where

$$\mathcal{G}^{R,0}_{i\sigma}(E) \;=\; \langle i|(E+\mathrm{i}0^+ - \hat{H}_{loc})^{-1}|i\rangle \tag{6.23}$$

$$\;=\; \int dt \, e^{\mathrm{i}Et} \, \mathcal{G}^{R,0}_{i\sigma}(t) \tag{6.24}$$

is the Green's function of the Anderson-Hubbard model in the atomic limit, i.e., the Fourier transform of Eq. (6.1) (for hopping amplitude $t = 0$).
The time-evolution of the creation and annihilation operators is readily obtained from the Heisenberg equation of motion yielding

$$c_{i\sigma}(t) \;=\; e^{-\mathrm{i}(\varepsilon_i - \mu + U\hat{n}_{i,-\sigma})t} \, c_{i\sigma} \tag{6.25}$$

$$c^\dagger_{i\sigma}(t) \;=\; e^{\mathrm{i}(\varepsilon_i - \mu + U\hat{n}_{i,-\sigma})t} \, c^\dagger_{i\sigma}. \tag{6.26}$$

From Eqs. (6.1), (6.24), and (6.25), we finally get

$$\mathcal{G}^{R,0}_{i\sigma}(E) \;=\; \frac{\langle \hat{n}_{i,-\sigma}\rangle_0}{E-(\varepsilon_i-\mu+U)+\mathrm{i}0^+} + \frac{1-\langle \hat{n}_{i,-\sigma}\rangle_0}{E-(\varepsilon_i-\mu)+\mathrm{i}0^+}. \tag{6.27}$$

Eqs. (6.22) and (6.27) now enable us to determine the effective probability distribution function $p_{\mathrm{A}}(\varepsilon)$ describing the propagation of an excitation of spin σ. As we can read off from the poles of the Green's function, Eq. (6.27), the general rule is that the local potential ε_i of sites which are *occupied by an electron of opposite spin* is shifted by U. In contrast, the local potential ε_i of all sites which are *not occupied by an electron of opposite spin* remains unshifted.[3]
To decide whether a site is occupied by an electron with an opposite spin, we can use the ground state configuration of the atomic limit, Eq. (6.15). As we calculated, all sites which fulfill $\varepsilon_i < \mu - U$ are doubly occupied and, hence, these on-site energies have to be shifted by U. All sites with $\varepsilon_i > \mu$ are empty. Consequently, these on-site energies remain unchanged. In case of $\mu - U < \varepsilon_i < \mu$, the site is singly occupied. Here, we assume that half of the singly occupied sites are occupied by electrons with spin σ, while the second half is occupied by electrons with spin $-\sigma$. Furthermore, we assume the distribution of spins among the singly occupied sites to be completely random and uncorrelated,

$$\langle \hat{n}_{i\sigma}\rangle \;=\; \langle \hat{n}_{i,-\sigma}\rangle \;=\; \frac{1}{2}, \tag{6.28}$$

$$\langle \hat{n}_{i\sigma}\hat{n}_{j\sigma'}\rangle \;\overset{(i\neq j)}{=}\; \langle \hat{n}_{i\sigma}\rangle\langle \hat{n}_{j\sigma'}\rangle, \tag{6.29}$$

[3]The rule is similar, but not identical to a Hartree-Fock approach, where one would use $\varepsilon_i \mapsto \varepsilon_i + \frac{U}{2}\langle \hat{n}_i\rangle$.

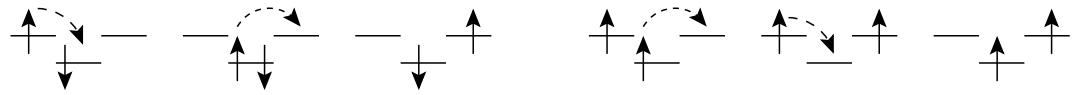

(a) (b)

Figure 6.2: Hopping transport of a quasiparticle with spin σ across a singly occupied site. Hopping processes are indicated by dashed arrows. a) Particle-like transport. The intermediate state is doubly occupied yielding a shift of the local potential according to $\varepsilon_i \mapsto \varepsilon_i + U$. b) Hole-like transport. The intermediate state is singly occupied and the local potential remains unchanged.

i.e., we neglect spin ordering effects. Then, we have to shift half of these sites by U, while the rest remains unchanged.

The physical reason for the spin-dependency of the shift of the local potential can be understood from Fig. (6.2). The hopping process of an electron from the lattice site $i-1$ to the lattice site $i+1$ across the lattice site i, which is not occupied by an electron with the same spin, is particle-like (Fig. 6.2(a)). In contrast, it is hole-like if site i is originally already occupied by an electron of the same spin (Fig. 6.2(b)). Thus, in the latter process no (intermediate) doubly occupied state occurs at this site, and the local potential equals ε_i. In contrast, in the former case, the intermediate state is doubly occupied, and, therefore, the effective local potential equals $\varepsilon_i + U$.

In summary, the rule to determine the effective on-site energy is

$$\varepsilon_i \;\mapsto\; \begin{cases} \varepsilon_i + U & , \quad \varepsilon_i \leq \mu - U \\ \varepsilon_i + U \\ \qquad \varepsilon_i & , \quad \mu - U < \varepsilon_i \leq \mu \left(\begin{array}{c} \text{each with} \\ \text{prob. of } \frac{1}{2} \end{array} \right) \\ \qquad \varepsilon_i & , \quad \varepsilon_i > \mu \end{cases} . \tag{6.30}$$

As for the ground state, the actual calculation of $p_{\mathrm{A}}(\varepsilon)$ acquires a distinction between different parameter regimes. Since the total number of these regimes is 16, we will only present the concrete calculation for one single case here. The list of all possible cases can be found in Appendix C.1.
Let us assume

$$\rho \;\leq\; 1, \qquad\qquad U \;\leq\; \tfrac{1}{3}\Delta\rho, \tag{6.31}$$

which corresponds to an energy hierarchy (cf. Eq. (6.16))

$$-\frac{\Delta}{2} + U \;\leq\; \mu - U \;\leq\; \mu \;\leq\; \mu + U \;\leq\; \frac{\Delta}{2}. \tag{6.32}$$

Then, from Eqs. (6.22) and (6.27), we can deduce

$$
\begin{aligned}
p_{\mathrm{A}}(E) &= \int d\varepsilon\, p(\varepsilon)\, \langle \hat{n}_{i,-\sigma} \rangle\, \delta(E-\varepsilon-U) \qquad (6.33)\\
&\quad + \int d\varepsilon\, p(\varepsilon)\, (1-\langle \hat{n}_{i,-\sigma} \rangle)\, \delta(E-\varepsilon)\\
&= \frac{1}{\Delta} \int\limits_{-\frac{\Delta}{2}}^{\mu-U} d\varepsilon\, \delta(E-\varepsilon-U) \,+\, \frac{1}{2\Delta} \int\limits_{\mu-U}^{\mu} d\varepsilon\, \delta(E-\varepsilon-U) \qquad (6.34)\\
&\quad + \frac{1}{2\Delta} \int\limits_{\mu-U}^{\mu} d\varepsilon\, \delta(E-\varepsilon) \,+\, \frac{1}{\Delta} \int\limits_{\mu}^{\frac{\Delta}{2}} d\varepsilon\, \delta(E-\varepsilon)\\
&= \frac{1}{\Delta} \int\limits_{-\frac{\Delta}{2}+U}^{\mu-U} d\varepsilon\, \delta(E-\varepsilon) \,+\, \frac{3}{2\Delta} \int\limits_{\mu-U}^{\mu+U} d\varepsilon\, \delta(E-\varepsilon) \qquad (6.35)\\
&\quad + \frac{1}{\Delta} \int\limits_{\mu+U}^{\frac{\Delta}{2}} d\varepsilon\, \delta(E-\varepsilon)\\
\Rightarrow \quad p_{\mathrm{A}}(\varepsilon) &= \frac{1}{\Delta} \cdot \begin{cases} 1 & , \; -\Delta/2+U \le \varepsilon \le \mu-U \\ 3/2 & , \; \mu-U \le \varepsilon \le \mu+U \\ 1 & , \; \mu+U \le \varepsilon \le \Delta/2 \\ 0 & , \; \text{elsewhere} \end{cases} . \qquad (6.36)
\end{aligned}
$$

In Fig. 6.3, the effective distribution function $p_{\mathrm{A}}(\varepsilon)$ is plotted for different interaction strengths for a fixed disorder strength and filling factor. The values of U range thereby from very weak to strong interaction. From this figure, we notice that increasing the interaction yields an asymmetric probability function through the mapping of the energetically lower part onto and above the energetically higher part of the original distribution $p(\varepsilon)$. This is a direct consequence of the site-occupation dependent renormalization of the local potential. Sites with a lower on-site energy ε_i generally have a higher occupation number than sites with a higher on-site energy. Hence, only the sites from the lower part of the probability spectrum are shifted by U. This leads to a further and very important observation. The effect of the repulsive interaction is expected to be different for weak and strong interactions. In the former case, corresponding to Fig. 6.3(b) and Fig. 6.3(c), the width of the effective distribution, $\tilde{\Delta}$, is smaller than the original one, Fig. 6.3(a). Furthermore, the probability to find sites with energies narrowly distributed around the Fermi level is strongly enhanced. In contrast, for strong interactions, Fig. 6.3(d) and especially Fig. 6.3(e), the width is larger than the original one. In addition, the probability to find a site with an effective

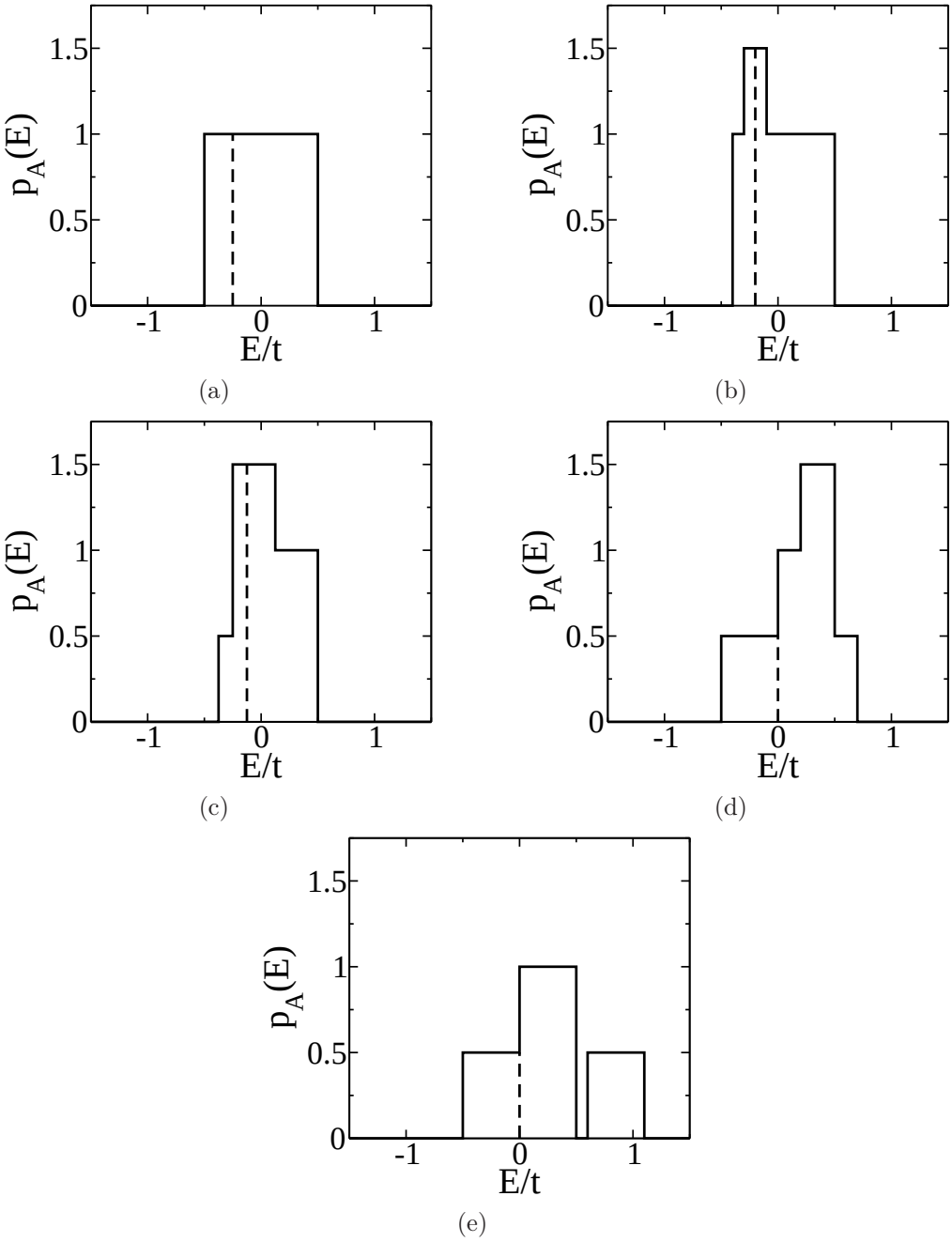

Figure 6.3: Probability distribution function $p_{\mathrm{A}}(\varepsilon)$ for $\Delta/t = 1$, $\rho = 0.5$ and (a)-(e) U/t =0.0, 0.1, 0.25, 0.7, 1.1. The dashed line marks the position of the chemical potential μ/t.

on-site energy narrowly distributed around the Fermi level is strongly reduced. The reason for this is that the presence of a weak interaction leads to a small or moderate shift of all energetically low-lying sites. Therefore, the effective on-site energy of an occupied site equals that of an energetically higher lying unoccupied site. As a consequence, the resulting effective distribution is narrower than the original one, and the disorder potential gets *screened* by the interaction. In contrast, strong interactions strongly shifts the occupied sites and even above the unoccupied sites. For a propagating single-particle excitation these occupied sites act like extremely high potential barriers. Effectively, the disorder strength gets then even larger than in the noninteracting regime. Both cases are visualized in Fig. 6.4.

The effective disorder distribution is not as simple as the original box distribution, which could be characterized by a single parameter, Δ. Therefore, we cannot expect to find a simple relation between the transport properties of the Hamiltonian (6.4) and the probability distribution. However, from the above considerations we can already predict the overall behavior in the limit of weak and strong interactions. In the former case, the transport should be enhanced by the interaction due to the screening of the disorder potential. In contrast, strong interactions should not be able to screen the disorder potential, but we expect it to reduce the mobility even beyond the noninteracting value.

Although the complexity of the effective, atomic-limit Hamiltonian is drastically reduced compared to the original many-body Anderson-Hubbard model, Eq. (5.4), the analysis of the Hamiltonian (6.4) is still highly non-trivial. Exact, analytical methods do not exist to quantitatively evaluate the single-particle Anderson model. Therefore, we have to use numerical methods instead. The most accurate ones are based on a transfer matrix method and finite-size scaling techniques [KM93, EFR08]. However, these methods are numerically very challenging and can easily suffer from finite-size effects [EFR08] (see also discussion in Sec. (3.4)). In addition, the required computing time is rather large, in particular in dimensions $d > 1$ [EMM$^+$99]. For that reason, we will use approximate methods, which are known to yield reasonable quantitative results in all dimensions and a large parameter range, and which allow for a systematic and thorough study of our effective single-particle Anderson model.

According to the single-parameter scaling theory (Sec. 3.4), the only relevant length scale, within the effective single-particle Anderson model, is the localization length of a particle at the Fermi level, $\xi \equiv \xi(E = 0)$. In particular, all zero temperature transport properties are determined by the value of ξ. In the context of the original many-body Anderson-Hubbard model, this meaning of ξ will still be valid, although single-particle eigenstates do not exist any longer (cf. Eq. (3.6)). Therefore, our analysis in the following sections will concentrate

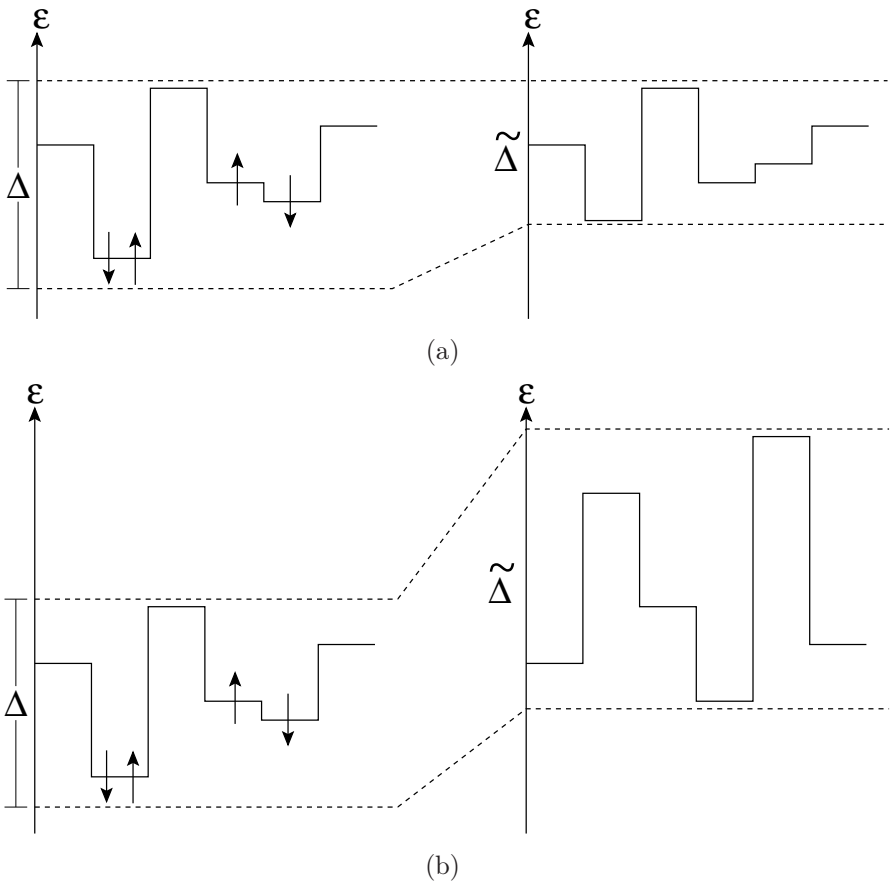

Figure 6.4: Graphical sketch of the effective distribution in comparison to the original one for (a) weak interaction (b) strong interaction.

on a careful determination of the dependence of ξ on the parameters (Δ, U, ρ).

6.4 Strong disorder approximation

In this section, we will give a first qualitative estimate on the behavior of ξ within a strong disorder approximation, where the localization length can be directly related to the (effective) disorder distribution $p_{\mathrm{A}}(\varepsilon)$,

$$\frac{1}{\xi} \approx \int d\varepsilon\, p_{\mathrm{A}}(\varepsilon)\, \log|\varepsilon - \varepsilon_{\mathrm{F}}|. \tag{6.37}$$

(Since $\varepsilon_{\mathrm{F}} = \mu$ at zero temperature, we use both terms synonymously.)

In one dimension, Eq. (6.37) follows immediately from the Herbert-Jones-Thouless formula, Eq. (D.26), in the limit $t/\Delta \to 0$ (cf. Eq.(6.21)),

$$\frac{1}{\xi} = \int d\varepsilon\, N(\varepsilon)\, \log|\varepsilon| \tag{6.38}$$

$$\approx \int d\varepsilon\, p_{\mathrm{A}}(\varepsilon)\, \log|\varepsilon - \varepsilon_{\mathrm{F}}|. \tag{6.39}$$

In dimensions $d > 1$, we can derive Eq. (6.37) from the Anderson-Hubbard model by evaluating (cf. Eq. (3.6))

$$-\frac{1}{\xi} = \lim_{|i-j|\to\infty} \frac{\log\left(\overline{\left|\mathcal{G}^R_{ij\sigma}(E=0)\right|^2}\right)}{2|i-j|}. \tag{6.40}$$

in lowest order perturbation theory. In this case, as we show in detail in Appendix B.3, Eq. (6.40) reduces to

$$-\frac{1}{\xi} = \lim_{|i-j|\to\infty} \frac{\log\left(\overline{\left|G^R_{ij\sigma}(E=0)\right|^2}\right)}{2|i-j|}. \tag{6.41}$$

While in Eq. (6.40) the disorder average has to be taken w.r.t. the original box distribution, $p(\varepsilon)$, in Eq. (6.41) the overbar denotes the average w.r.t. the effective distribution, $p_{\mathrm{A}}(\varepsilon)$.

Eq. (6.41) is equivalent to the statement [MK92] that, for very strong disorder, only the direct path between site i and j enters in Eq. (6.40). Thus, for very strong disorder, the dimensionality of the system no longer plays a relevant role, and Eq. (6.37) becomes generally valid in that limit.

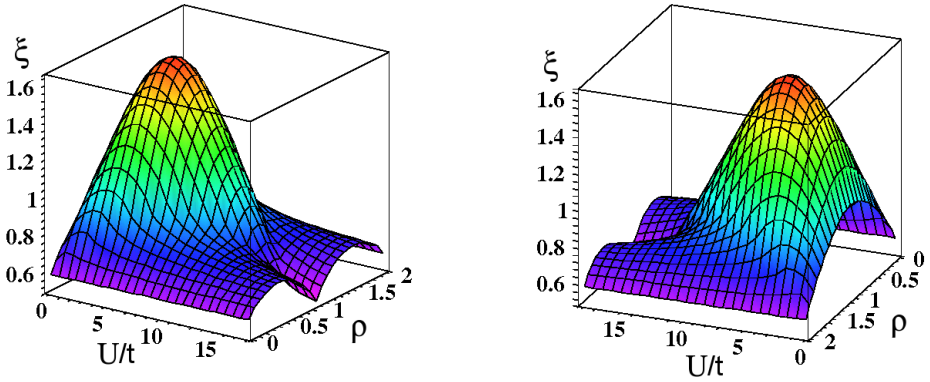

(a) (b)

Figure 6.5: Localization length ξ as a function of the interaction strength U and the lattice filling ρ for fixed disorder strength $\Delta/t = 15$.

In Fig. 6.5, the localization length, calculated via Eq. (6.37), is plotted as a function of the interaction strength and the lattice filling, while the disorder strength has been fixed. As one can clearly see, for each lattice filling, the localization length depends nonmonotonically on U. As expected from the discussion of the previous section, the presence of a weak interaction induces a screening of the bare disorder potential yielding a reduced effective disorder strength. Correspondingly, the localization length gets enlarged, indicating a higher mobility of the interacting system. For strong interactions, the behavior completely changes. Now, an increasing interaction effectively yields an enhancement of the disorder potential. Consequently, the localization length decreases with increasing interaction strength, and the mobility gets reduced. In particular, the effective disorder strength is not bounded by the noninteracting one, as $U \to \infty$, but monotonically increases with the interaction. Hence, the localization length can become significantly shorter than the noninteracting one, $\xi(U \gg 1) \ll \xi(U = 0)$, reaching a maximum at some intermediate value of U.

The interaction dependence of ξ can also be observed in Fig. 6.6, where the localization length is plotted as a function of U, for the same disorder strength as in Fig. 6.5 and two different values of the lattice filling ρ. As one can see, the value of the interaction strength, where the localization length becomes maximal, depends not only on the bare disorder strength, but also on the lattice filling. In addition, the relative enhancement factor, i.e., the ratio between the noninteracting localization length $\xi(U = 0)$ and the maximal localization length, $\xi_{\max}$, depends on both, Δ and ρ.

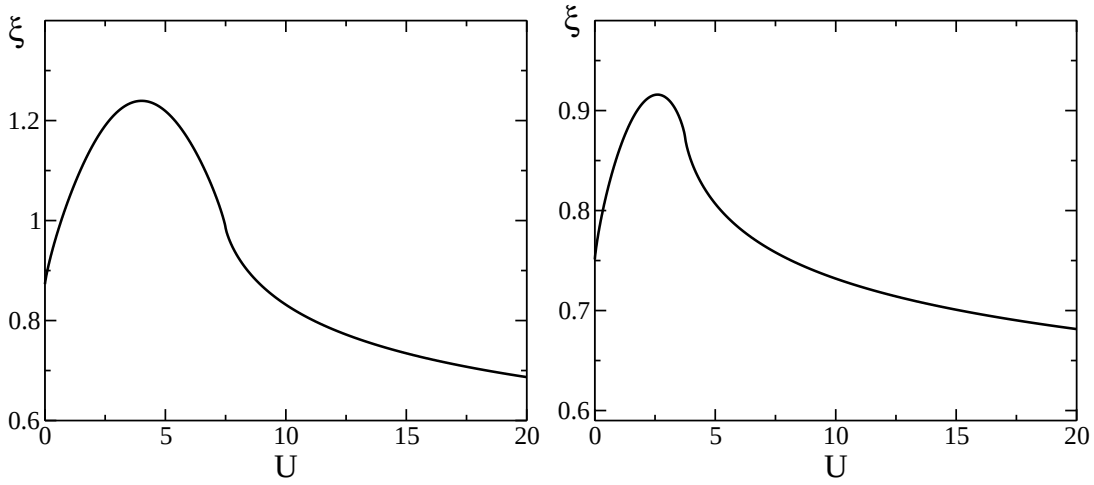

Figure 6.6: Localization length ξ as a function of the interaction strength U for fixed disorder strength $\Delta = 15$ and fixed lattice filling a) $\rho = 0.5$ b) $\rho = 0.25$.

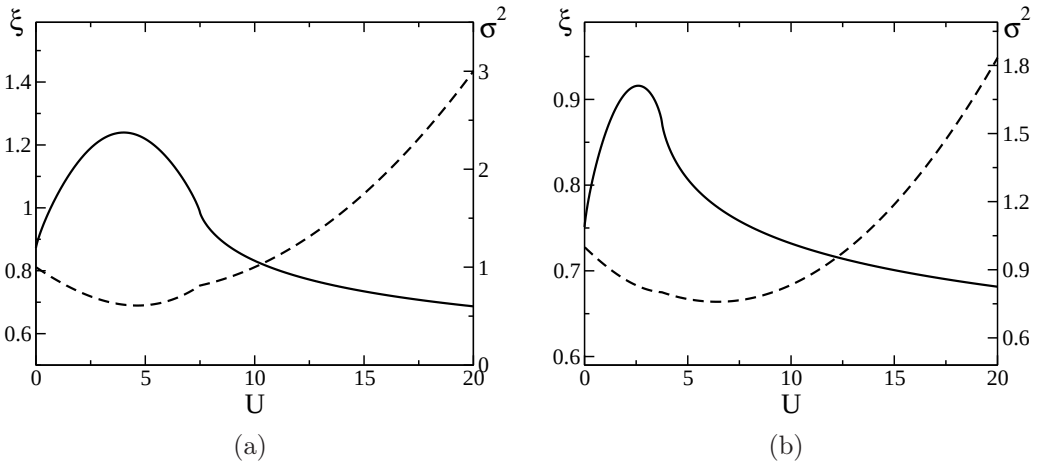

Figure 6.7: Comparison of the localization length ξ (solid line) and the variance σ^2 (dashed line) of the effective distribution function $p_{\mathrm{A}}(\varepsilon)$, normalized to its noninteracting value $\Delta^2/12$, for $\Delta = 15$ and a) $\rho = 0.5$ b) $\rho = 0.25$.

The main advantage of the strong disorder approximation, Eq. (6.37), is that it allows for an exact analytical calculation. Thus, by using the explicit expressions for the effective disorder distribution, Appendix C.1, we can exactly determine the value of the interaction strength U_ξ where the localization length becomes maximal. A straightforward calculation yields

$$U_\xi \;=\; \frac{\Delta}{3}\left(\sqrt{1+3\rho(2-\rho)}-1\right). \tag{6.42}$$

From weak disorder perturbation theory, one is used to deduce physical (transport) properties of a disordered system from the variance of the disorder potential (cf. Appendix A). However, for strong disorder not only the second moment of the disorder distribution enters, but also higher moments must be taken into account. Besides, $p_{\mathrm{A}}(\varepsilon)$ is more complex than the original box distribution $p(\varepsilon)$, which is uniquely characterized by a single parameter, its width Δ and its variance, $\sigma^2 = \Delta^2/12$, respectively. Therefore, we cannot easily deduce the localization of the Anderson-Hubbard model (Eq. (5.4)) and the effective Anderson model (Eq. (6.4)), respectively, from a simple statistical analysis of the on-site energy distribution. Actually, as Fig. 6.7 shows, the values of the interaction strength corresponding to the maximal localization length, U_ξ, and to the minimal variance, U_σ, are not simply related to each other. This statement can be made precise by calculating U_σ from the effective distribution (Appendix C.1),

$$U_\sigma \;=\; \begin{cases} \frac{\Delta}{9}\left(\sqrt{\hat{\rho}^2+9\hat{\rho}}-\hat{\rho}\right) & , \;\; \frac{1}{3} \lesssim \rho \lesssim \frac{5}{3} \\ \Delta\frac{|1-\rho|}{1+|1-\rho|} & , \;\; \text{otherwise,} \end{cases}, \tag{6.43}$$

where $\hat{\rho} = 3\rho(2-\rho)$. Unless $\rho = 1$, these two interaction values differ, $U_\xi \neq U_\sigma$, particularly if $|\rho - 1| \to 1$.

As a side remark, we want to emphasize that Eqs. (6.42) and (6.43), as well as Fig. 6.5, clearly express the particle-hole symmetry of the Anderson-Hubbard model, i.e., the symmetry under the transformation $\rho \leftrightarrow 2-\rho$.

The plots in Figs. 6.6 and 6.7 show a pronounced kink at some intermediate value of U. Its origin is the crossover from the regime where an increase of U yields a change in the ground state occupation numbers (Fig. 6.1(a)), to the regime where the ground state configuration has been saturated (Fig. 6.1(b) and Fig. 6.1(c), respectively). However, its magnitude is an artefact of the atomic-limit approximation. Obviously, an efficient screening of the disorder potential corresponds to an optimal adaption of the ground state occupation numbers to the external potentials. Therefore, the kink always happens for values of $U > U_\xi$, see Figs. 6.6 and 6.7.

Chapter 7

Self-consistent analysis of the atomic-limit approximation

In the previous chapter, the localization length was roughly estimated under the assumption of a very strong disorder strength. This approximation was sufficient to get a qualitative impression of the (de-)localizing effect of the Hubbard interaction. Besides, it allowed for an analytical analysis, e.g., of the interaction dependence of the localization length. To obtain also quantitatively reliable results, in particular for weaker disorder strengths, we have to go beyond this crude approximation. Therefore, we have to use a quantitatively reliable numerical method which allows for an efficient and systematic scan of a large parameter regime of (Δ, U, ρ) in dimensions $d = 1, 2, 3$. As we mentioned above, the most precise numerical methods need substantial computing time, especially in dimensions $d > 1$. Moreover, in higher dimensions they are often restricted by finite-size effects. However, we want to analyze the screening effect also in the regime where the disorder is not very strong anymore. As we can expect the localization length to become substantially large, we need a method which additionally is able to yield, at least principally, infinite-size results. For these reasons, we will use the self-consistent transport theory of Anderson localization, which is the best known method fulfilling all these requirements to a sufficient level.

7.1 Self-consistent transport theory for the atomic-limit approximation

The self-consistent transport theory of Anderson localization constitutes a resummation of the most divergent (cooperon) contributions to the irreducible particle-hole vertex, leading to a self-consistent equation for the dynamical diffusion coefficient (cf. Sec. 3.5 and Appendix F). In its most general formulation [KKW90, Kro90, VW92], which allows for both strong and weak disorder, this

self-consistent equation is given by

$$\begin{aligned} D(E,\omega) &= D_0(E) + \frac{2\mathrm{Im}\Sigma^R(E)}{[\mathrm{Im}\overline{G_0^R}(E)]^2 D_0(E)} \int_\Omega \frac{dk}{(2\pi)^d} \\ &\quad \times \int_\Omega \frac{dk'}{(2\pi)^d} (v_k \cdot \hat{q}) \frac{\mathrm{Im}\overline{G_k^R}(E)[\mathrm{Im}\overline{G_{k'}^R}(E)]^2}{(k+k')_{2\pi}^2 - \mathrm{i}\omega/D(\omega,E)} (v_{k'} \cdot \hat{q}). \end{aligned} \tag{7.1}$$

Here,

$$D_0(E) = -\frac{1}{\mathrm{Im}\overline{G_0^R}(E)} \int_\Omega \frac{dk}{(2\pi)^d} (v_k \cdot \hat{q})^2 [\mathrm{Im}\overline{G_k^R}(E)]^2 \tag{7.2}$$

is the bare diffusion constant.

$$\overline{G_k^R}(E) = \frac{1}{E - (\epsilon_k - \mu) - \Sigma^R(E)} \tag{7.3}$$

is the disorder-averaged, retarded Green's function of the single-particle Anderson Hamiltonian, Eq. (6.4), and $\Sigma^R(E)$ is the corresponding self-energy, which is assumed to be purely local, i.e., momentum independent (cf. Appendix E).

$$\overline{G_0^R}(E) = \int_\Omega \frac{dk}{(2\pi)^d} \overline{G_k^R}(E) \tag{7.4}$$

is the local (= momentum integrated) Green's function. $v_k = \nabla_k \epsilon_k$. $\hat{q}$ is a unit vector pointing in the direction of the transport, which we can set to $\hat{q} = \hat{e}_1$, where $\hat{e}_1$ denotes the first basis vector of $\mathbb{R}^d$, because we are always dealing with an isotropic lattice, where the transport does not depend on its direction. All momentum integrations are restricted to the first Brillouin zone, which in our case of a square lattice of unit length is given by $\Omega = \otimes_{i=1}^d [-\pi, \pi]$ [AM76].

In Appendix A, we derive the expression for the cooperon propagator in the limit of weak disorder, Eq. (A.22),

$$C(\omega, k, k') = \frac{1}{-\mathrm{i}\omega + D_0(k+k')^2}. \tag{7.5}$$

There, its derivation is based on an expansion of small momentum transfer of the diffuson vertex, Eq. (A.14). The reason is that the most relevant contribution to the ladder diagrams arise from the case $\epsilon_{k+q} \approx \epsilon_k$. For the dispersion relation of a free electron gas, $\epsilon_k = k^2/(2m)$, this yields $q \approx 0$. However, we are considering a lattice system with a periodic dispersion relation, $\epsilon_k = \epsilon_{k+2\pi}$. Therefore, the condition on the momentum transfer q has to be replaced by

$$q \approx 0 \bmod 2\pi, \tag{7.6}$$

and the expansion has to be done with respect to the closest lattice vector of the reciprocal lattice. Taking this aspect into account, the cooperon propagator becomes

$$C(\omega, k, k') \;=\; \frac{1}{-\mathrm{i}\omega + D_0 (k+k')^2_{2\pi}}, \tag{7.7}$$

where the subscript 2π, appearing also in Eq. (7.1), refers to the condition

$$(k+k')_{2\pi} \;\equiv\; (k+k') \bmod 2\pi \quad \wedge \quad (k+k')_{2\pi} \in [-\pi, \pi], \tag{7.8}$$

and denotes a possible shift of the vector $k + k'$ by 2π within the first Brillouin zone. As we will discuss below, this periodicity of the cooperon propagator strongly simplifies the numerical evaluation of the self-consistent equation of the dynamical diffusion coefficient. Furthermore, it is necessary to ensure particle-hole symmetry (see Appendix F.2)).

To evaluate the self-consistent transport theory of Anderson localization, we have to first determine the single-particle self-energy. In [Kro90], it was shown that one can use the coherent potential approximation (CPA) (see Appendix E) to yield results within the self-consistent approach, which are in a good qualitative and quantitative agreement with the numerically exact ones obtained by a transfer matrix calculation. Therefore, we will also use the CPA to calculate the disorder-averaged single-particle propagator and self-energy, respectively. In our case, the self-consistent equation of the CPA reads (cf. Eq. (E.17))

$$0 \;=\; \int d\varepsilon \, p_{\mathrm{A}}(\varepsilon) \, \frac{\varepsilon - \Sigma^R(E)}{1 - \overline{G_0^R}(E)(\varepsilon - \Sigma^R(E))}. \tag{7.9}$$

We can rewrite Eq. (7.9) in a second way to emphasize once again the underlying physical assumptions of our approach. For that purpose, let us define the spin-occupation distribution function

$$p_\sigma(s) \;=\; \frac{1}{2}\left(\delta(s - 1/2) \,+\, \delta(s + 1/2)\right). \tag{7.10}$$

Furthermore, we define a functional $F(s, \varepsilon)$, which maps each local function $g(\varepsilon_i)$, that depends on the value of the on-site energy ε_i, according to

$$F(s,\varepsilon)[g] \;=\; \begin{cases} g(\varepsilon) & , \quad \langle n_i \rangle_0 = 0 \\ g(\varepsilon) & , \quad \langle n_i \rangle_0 = 1, \quad s = \frac{1}{2} \\ g(\varepsilon + U) & , \quad \langle n_i \rangle_0 = 1, \quad s = -\frac{1}{2} \\ g(\varepsilon + U) & , \quad \langle n_i \rangle_0 = 2 \end{cases} . \tag{7.11}$$

Then, from the discussion above, or by inserting the corresponding expressions, we get

$$\int d\varepsilon\, p_{\mathrm{A}}(\varepsilon)\, g(\varepsilon) \;=\; \int ds\, p_\sigma(s) \int d\varepsilon\, p(\varepsilon)\, F(s,\varepsilon)[g]. \tag{7.12}$$

It is useful to apply the identity Eq. (7.12) to the CPA equation, Eq. (7.9), in the limit of vanishing disorder, $\Delta \to 0$, i.e., $p(\varepsilon) = \delta(\varepsilon)$ within appropriate energy units. In this case, Eq. (7.9) is known as the Hubbard-III approximation for the Hubbard model [Hub64b, VKE68], which is sometimes also called random, binary alloy approximation. Assuming that essentially no spin-spin correlations exist and, thus, the spin of any chosen electron of the system takes the values $\frac{1}{2}$ and $-\frac{1}{2}$ with equal probability (cf. Eq. (7.10)), within the Hubbard-III approximation the physics are determined by the two-pole structure of the local Hubbard propagator, Eq. (6.27), neglecting dynamical effects, which are known to become important at and close to the Mott-Hubbard transition (see Sec. 5.1).

7.2 CPA self-energy and disorder-averaged density of states

As the first step of the self-consistent analysis of the atomic-limit approximation, we have to obtain the disorder-averaged single-particle propagator. This means, we have to calculate the single-particle self-energy from the CPA equation, Eq. (7.9). In the CPA equation, the momentum-integrated single-particle propagator enters. For a fixed value of the self-energy, it can be calculated via (see Eq. (7.4))

$$\overline{G_0^R}(E) \;=\; \int_\Omega \frac{dk}{(2\pi)^d}\, \overline{G_k^R}(E) \;=\; \int d\epsilon\, N_0(\epsilon)\, \frac{1}{E - (\epsilon - \mu) - \Sigma^R(E)}, \tag{7.13}$$

where $N_0(\epsilon)$ is the bare density of states.

Bare density of states

From the dispersion relation of the d-dimensional square lattice,

$$\begin{aligned} \epsilon_k \;&=\; \langle k|\hat{H}_{kin}|k\rangle \;=\; \sum_{i,j} \langle k|i\rangle\langle i|\hat{H}_{kin}|j\rangle\langle j|k\rangle \;=\; \frac{1}{N} \sum_{<i,j>} (-t) e^{\mathrm{i}k\cdot(i-j)} \\ &=\; -t \sum_{i=1}^{d} (e^{\mathrm{i}k_i} + e^{-\mathrm{i}k_i}) \;=\; -2t \sum_{i=1}^{d} \cos(k_i), \end{aligned} \tag{7.14}$$

the bare density of states is calculated via

$$N_0(\epsilon) \;=\; \int_\Omega \frac{dk}{(2\pi)^d}\, \delta(\epsilon - \epsilon_k). \tag{7.15}$$

An analytic solution for Eq. (7.15) exists only in one dimension. Here, a short calculation yields

$$N_0^{(1D)}(\epsilon) = \frac{1}{2\pi t}\frac{1}{\sqrt{1-(\epsilon/2t)^2}}. \tag{7.16}$$

In $d = 2, 3$ dimensions, no closed form exists and $N_0(\epsilon)$ is defined by the integral equations,

$$N_0^{(2D)}(\epsilon) = \frac{1}{2\pi^2 t}\int_{-1}^{1}\frac{dx}{\sqrt{1-x^2}}\frac{\Theta(1+(\epsilon/2t)+x)\,\Theta(1-(\epsilon/2t)-x)}{\sqrt{1-((\epsilon/2t)+x)^2}} \tag{7.17}$$

$$N_0^{(3D)}(\epsilon) = \frac{1}{2\pi^3 t}\int_{-1}^{1}\frac{dx}{\sqrt{1-x^2}}\int_{-1}^{1}\frac{dy}{\sqrt{1-y^2}} \times \frac{\Theta(1+(\epsilon/2t)+x+y)\,\Theta(1-(\epsilon/2t)-x-y)}{\sqrt{1-((\epsilon/2t)-x)^2}}, \tag{7.18}$$

which must be calculated numerically. For that purpose, we used an adaptive Gauss-Kronrod integration routine, provided by the GNU scientific library [GSL]. Plots of the bare density of states in dimensions $d = 1, 2, 3$ are shown in Fig. 7.1.

CPA self-energy

Knowing the bare density of states, the CPA self-energy can be numerically determined from Eqs. (7.9) and (7.13). The numerical integrations are again done by using an adaptive Gauss-Kronrod integration routine [GSL]. The real and imaginary part of $\Sigma(E)$ are determined from Eq. (7.9) by using a two-dimensional Newtonian root finder, also provided by [GSL].

Fig. 7.2 shows the three-dimensional, noninteracting self-energy and the corresponding disorder-averaged density of states for different values of the disorder strength Δ, at half filling. One clearly sees how the self-energy evolves from the weak localization result, Fig. 7.2(a), which is almost identical to the Born approximation, Eq. (A.6), to the strong localization result, Fig. 7.2(c). Correspondingly, the disorder-averaged density of states evolves from the almost unperturbed shape, $N(E) \approx N_0^{(3d)}(E)$, towards the strong disorder limit, $N(E) \approx p_{\mathrm{A}}(E+\mu)$, Fig. 7.2(d) (cf. Eq. (6.21)).
The same behavior is also found in dimensions $d < 3$, which is not plotted explicitly here.

In Figs. 7.3 and 7.4, we plotted the disorder-averaged density of states, for fixed (Δ, ρ) and different interaction strengths, ranging from noninteracting to the

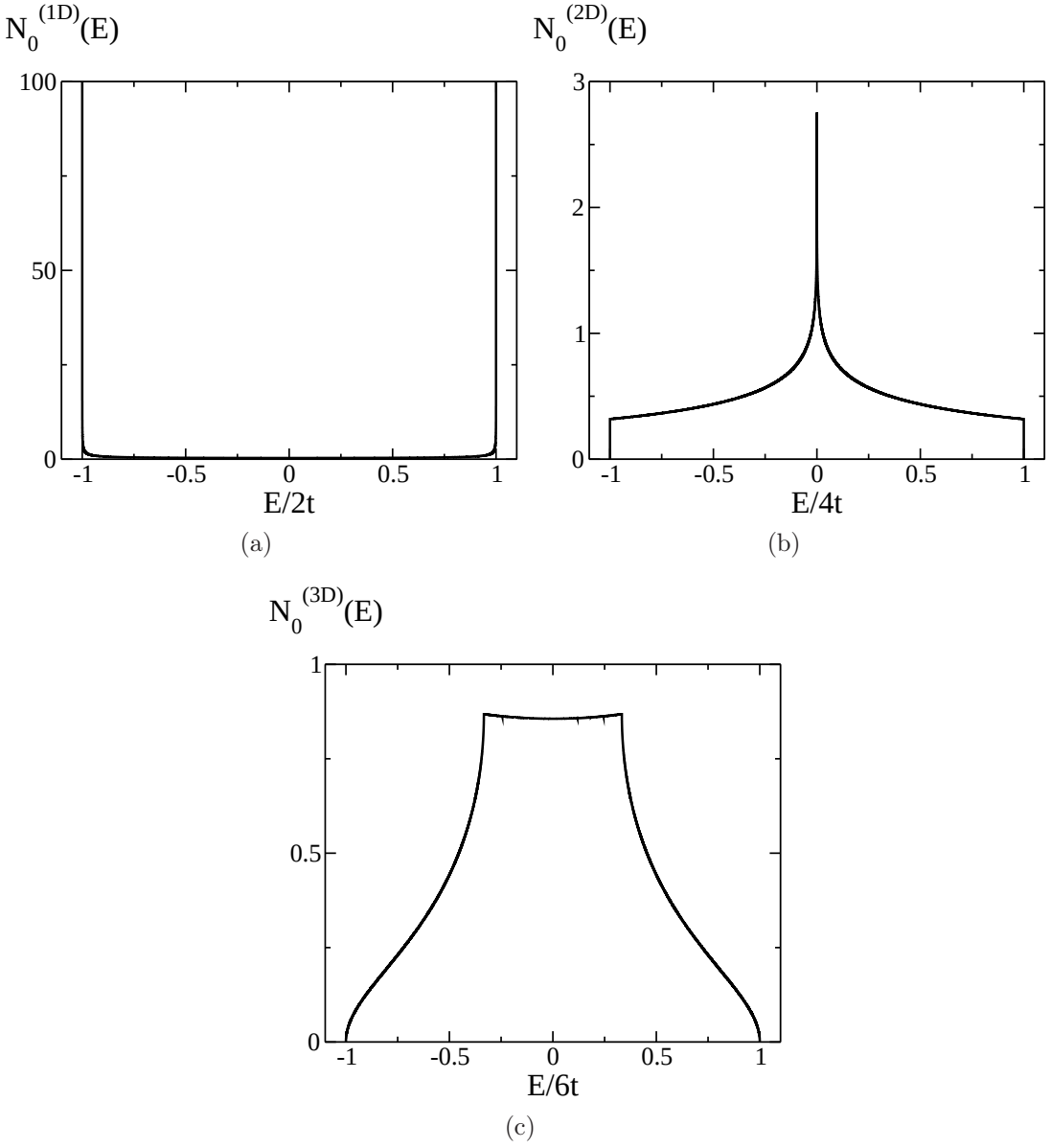

Figure 7.1: Bare density of states of the d-dimensional hypercubic lattice.

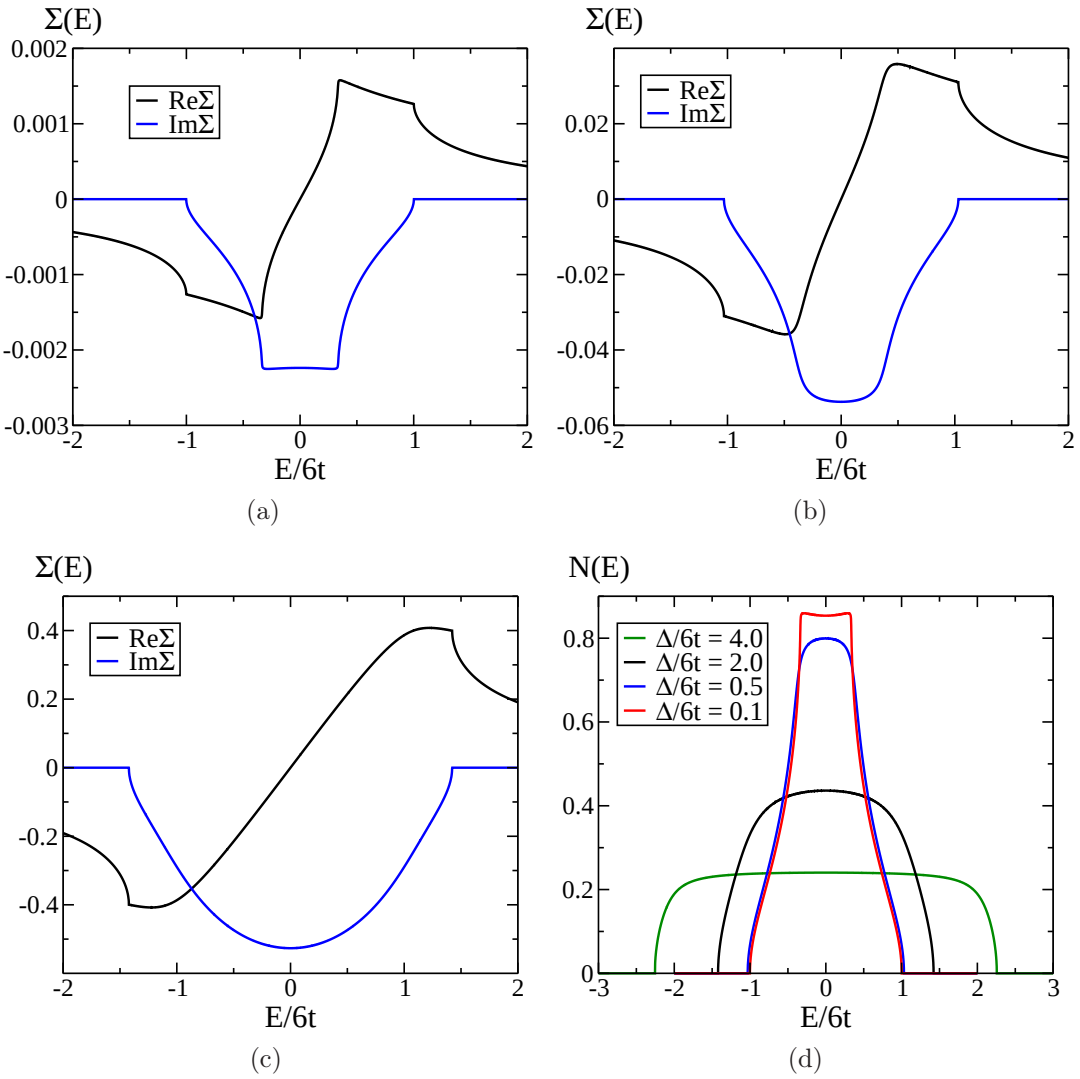

Figure 7.2: a)-c) Noninteracting ($U = 0$) CPA self-energy in $d = 3$ dimensions at half filling for disorder strengths $\Delta/6t = 0.1,\ 0.5,\ 2.0$ (increasing from a) - c)). d) Disorder-averaged density of states in $d = 3$ dimensions at half filling.

strongly interacting regime. As expected, the density of states displays the evolution of the underlying effective probability distribution, derived in Sec. 6.3 (cf. Fig. 6.3). First, the increase of the interaction yields a reduced disorder strength with a smaller width of the spectrum and an enhanced value at the chemical potential ($E = 0$). For strong interactions, the spectrum gets broadened, the density of states gets suppressed at $E = 0$, and finally the spectrum becomes gapped with two disorder-broadened Mott-Hubbard bands. At half filling, Fig. 7.3, the system becomes a Mott-Hubbard insulator, where the chemical potential lies within the gap. As we already mentioned in the beginning of this chapter, the atomic-limit approximation includes only static effects. Thus, the many-body resonance, present in high dimensions in the non-disordered case at the chemical potential (see Fig. 5.1), is not expected to be observed. However, by now, it is unknown, whether this resonance will survive in the presence of disorder at all .

Away from half filling, Fig. 7.4, the chemical potential lies within the lower Hubbard band. Thus, we can expect that at half filling, the transition from the weakly interacting, disorder reduced regime to the strongly interacting one might be most pronounced.

7.3 Localization length in $d \leq 2$ dimensions

In dimension $d = 1$, all single-particle states of the effective Anderson model get localized by disorder for any finite disorder strength. According to the scaling theory of Anderson localization the same holds also in $d = 2$ dimensions (see Secs. 3.1 and 3.4). In the localized regime, diffusive transport cannot take place and, therefore, the dynamical diffusion coefficient $D(E, \omega)$ vanishes in the static limit $\omega \to 0$. Thus, the self-consistent equation transforms into (see Appendix F.1)

$$\begin{aligned} 0 \stackrel{!}{=} D_0(E) + \frac{2\mathrm{Im}\Sigma^R(E)}{[\mathrm{Im}\overline{G_0^R}(E)]^2 D_0(E)} \int \frac{dk}{(2\pi)^d} \int \frac{dk'}{(2\pi)^d} (v_k \cdot \hat{q}) \\ \times \frac{\mathrm{Im}\overline{G_k^R}(E)[\mathrm{Im}\overline{G_{k'}^R}(E)]^2}{(k+k')_{2\pi}^2 + 4/\xi^2(E)} (v_{k'} \cdot \hat{q}), \end{aligned} \tag{7.19}$$

from which we can calculate $\xi(E)$ by determining numerically the root of the right hand side of Eq. (7.19).

However, the numerical calculation of the double integral in Eq. (7.19) needs a large computing time, in particular in dimension $d > 1$. But we can use the 2π-periodicity of the integrands to transform the $2d$-dimensional integral into a d-dimensional sum by Fourier transformation. (Furthermore, we set $E = 0$ from

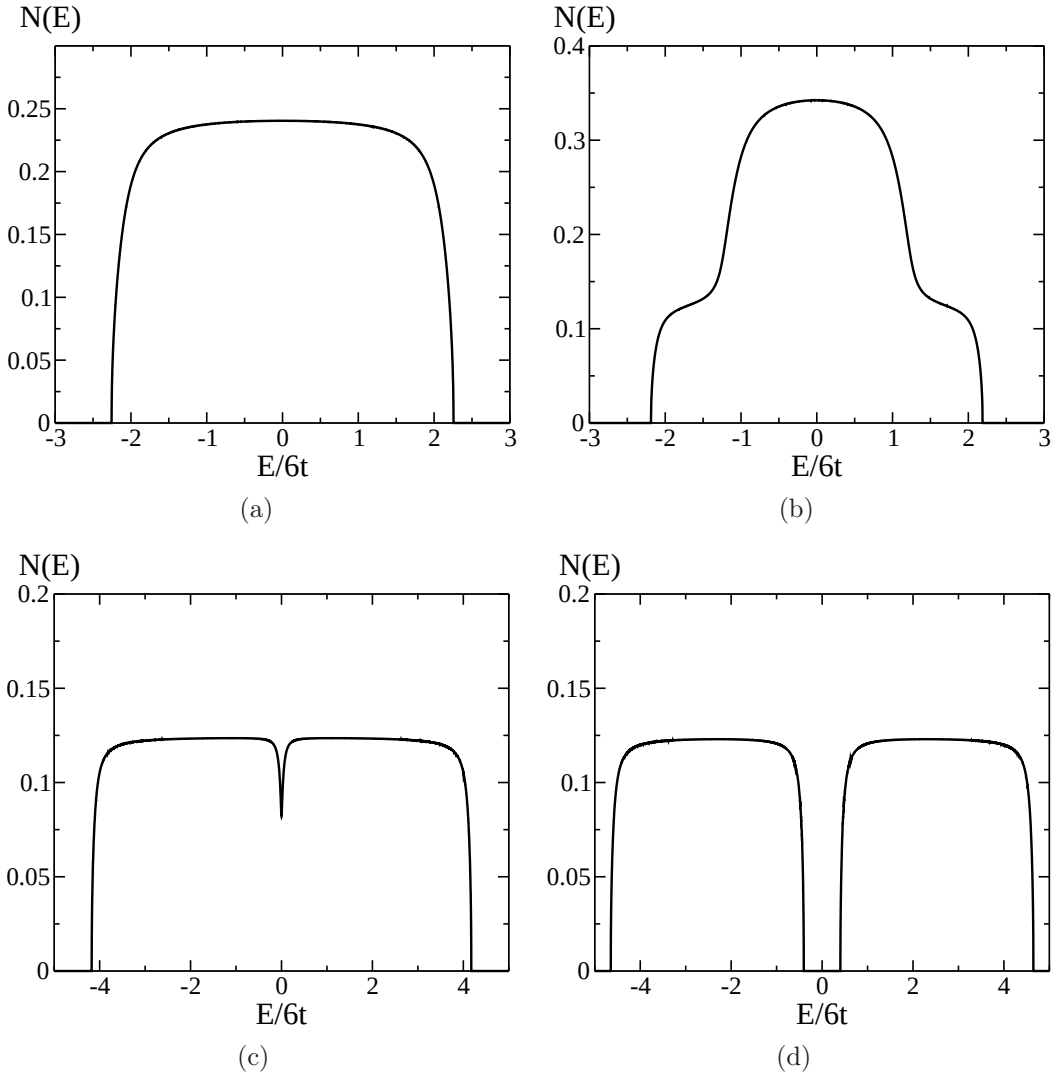

Figure 7.3: Disorder-averaged density of states in $d = 3$ dimensions at half-filling for fixed disorder strength, $\Delta/6t = 4$, and different interaction strengths a) $U/6t = 0.00$ b) $U/6t = 2.00$ c) $U/6t = 4.05$ d) $U/6t = 5.00$.

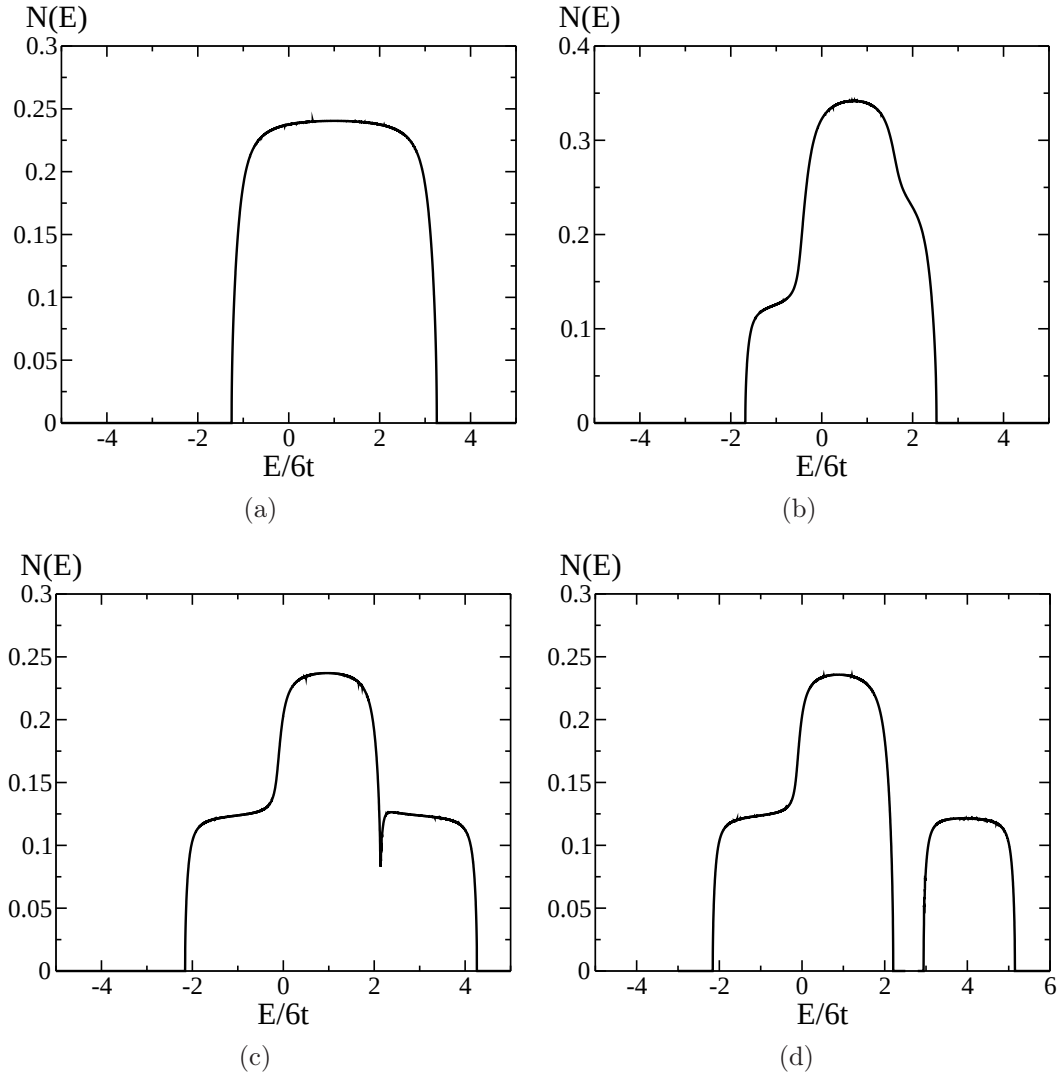

Figure 7.4: Disorder-averaged density of states in $d = 3$ dimensions for fixed disorder strength, $\Delta/6t = 4$, and at quarter filling, $\rho = 0.5$, for different interaction strengths a) $U/6t = 0.0$ b) $U/6t = 1.5$ c) $U/6t = 4.1$ d) $U/6t = 5.0$.

now on and drop the explicit energy dependence, as we are only interested in the localization length of a particle at the Fermi level.)

In 1D, the Fourier transforms of the integrands read

$$\begin{aligned}
\hat{v}(x) &= \int_{-\pi}^{\pi} \frac{dk}{2\pi}\, v_k\, e^{-\mathrm{i}kx} \;=\; 2\mathrm{i}t \int_{-\pi}^{\pi} \frac{dk}{2\pi} \sin(k)\, \sin(kx) \\
&= \mathrm{i}t(\delta(1-x) \,-\, \delta(1+x)) \qquad (7.20)\\
\hat{g}(x) &= \int_{-\pi}^{\pi} \frac{dk}{2\pi}\, \mathrm{Im}\overline{G_k^R}\, e^{-\mathrm{i}kx} \;=\; \int_{-\pi}^{\pi} \frac{dk}{2\pi}\, \mathrm{Im}\overline{G_k^R}\, \cos(kx) \qquad (7.21)\\
\hat{g}_2(x) &= \int_{-\pi}^{\pi} \frac{dk}{2\pi}\, (\mathrm{Im}\overline{G_k^R})^2\, e^{-\mathrm{i}kx} \;=\; \int_{-\pi}^{\pi} \frac{dk}{2\pi}\, (\mathrm{Im}\overline{G_k^R})^2\, \cos(kx) \qquad (7.22)\\
\hat{C}(x) &= \int_{-\pi}^{\pi} \frac{dk}{2\pi}\, \frac{e^{-\mathrm{i}kx}}{k^2 + 4/\xi^2} \;=\; \int_{-\pi}^{\pi} \frac{dk}{2\pi}\, \frac{\cos(kx)}{k^2 + 4/\xi^2} \qquad (7.23)
\end{aligned}$$

Inserting these functions into Eq. (7.19), we get after a short and straightforward calculation

$$\begin{aligned}
&\int_{-\pi}^{\pi} \frac{dk}{2\pi} \int_{-\pi}^{\pi} \frac{dk'}{2\pi} (v_k \cdot \hat{q}) \frac{\mathrm{Im}\overline{G_k^R}[\mathrm{Im}\overline{G_{k'}^R}]^2}{(k+k')_{2\pi}^2 + 4/\xi^2} (v_{k'} \cdot \hat{q})\\
&= -t^2 \sum_{x=-\infty}^{\infty} \hat{C}(x)[\hat{g}(-1-x) \,-\, \hat{g}(1-x)]\,[\hat{g}_2(-1-x) \,-\, \hat{g}_2(1-x)] \qquad (7.24)\\
&= -2t^2 \sum_{x=1}^{\infty} \hat{C}(x)[\hat{g}(1+x) \,-\, \hat{g}(1-x)]\,[\hat{g}_2(1+x) \,-\, \hat{g}_2(1-x)], \qquad (7.25)
\end{aligned}$$

where in the last line we used the symmetry of the propagators and the cooperon under the parity transformation $x \mapsto -x$. Thus, in one dimension the self-consistent equation becomes

$$0 \;\stackrel{!}{=}\; D_0 \,-\, \frac{4t^2\, \mathrm{Im}\Sigma^R}{[\mathrm{Im}\overline{G_0^R}]^2\, D_0} \sum_{x=1}^{\infty} \hat{C}(x)[\hat{g}(1+x) \,-\, \hat{g}(1-x)]\,[\hat{g}_2(1+x) \,-\, \hat{g}_2(1-x)]. \qquad (7.26)$$

With the same nomenclature, the corresponding equation in two dimensions reads

$$\begin{aligned}
0 \;\stackrel{!}{=}\; D_0 \,-\, \frac{8t^2\, \mathrm{Im}\Sigma^R}{[\mathrm{Im}\overline{G_0^R}]^2\, D_0} &\sum_{x=1}^{\infty} \sum_{y=0}^{\infty} \hat{C}(x,y)[\hat{g}(1+x,y) \,-\, \hat{g}(1-x,y)]\\
&\times [\hat{g}_2(1+x,y) \,-\, \hat{g}_2(1-x,y)]\,(1 - \frac{1}{2}\delta(y)), \qquad (7.27)
\end{aligned}$$

where we used the additional symmetry of all summands under the transformation $x \leftrightarrow y$.

The localization length can then be calculated numerically by finding the root of the functions

$$F_{1D}(\xi) \equiv D_0 - \frac{4t^2 \mathrm{Im}\Sigma^R}{[\mathrm{Im}\overline{G_0^R}]^2 D_0} \sum_{x=1}^{\infty} \hat{C}(x)[\hat{g}(1+x) - \hat{g}(1-x)] \times [\hat{g}_2(1+x) - \hat{g}_2(1-x)], \quad (7.28)$$

and

$$F_{2D}(\xi) \equiv D_0 - \frac{8t^2 \mathrm{Im}\Sigma^R}{[\mathrm{Im}\overline{G_0^R}]^2 D_0} \sum_{x=1}^{\infty}\sum_{y=0}^{\infty} \hat{C}(x,y)[\hat{g}(1+x,y) - \hat{g}(1-x,y)] \times [\hat{g}_2(1+x,y) - \hat{g}_2(1-x,y)]\,(1-\frac{1}{2}\delta(y)), \quad (7.29)$$

respectively.

If the disorder is strong enough ($\Delta \gtrsim 2dt$), $\mathrm{Im}\Sigma^R$ and $1/\xi^2$ become large, such that the momentum-dependence of the single-particle propagators and the cooperon propagator becomes strongly weakened. Consequently, their Fourier transforms are strongly peaked and only the very first ($\sim \mathcal{O}(10)$) summands significantly contribute to the sums of Eq. (7.26) - (7.29). Thus, the convergence is quite fast and Eqs. (7.26) and (7.27) provide an efficient way to determine the single-particle localization length ξ.

The roots of Eqs. (7.28) and (7.29) were numerically determined by again using a routine provided by [GSL], the Brent-Dekker algorithm, which is based on a combination of an interpolation and a bisection algorithm. Integrations were done by using the same routines as in the previous section.

Fig. 7.5 shows the localization length as a function of the interaction strength and the lattice filling, for fixed disorder strength, in one dimension, calculated by using the self-consistent approach. As in the strong disorder approximation, Fig. 6.5, the localization length nonmonotonically depends on U with a pronounced maximum at some intermediate value U_ξ. Furthermore, we see that the general behavior is close to the one observed within the strong disorder approximation. In particular, the delocalizing effect, i.e., the ratio $\xi(U_\xi)/\xi(U=0)$ (for a fixed lattice filling) is quite similar in both approximations. For instance, for $\rho = 1$ we obtain in both cases (Fig. 6.5 and Fig. 7.5), the value $\xi(U_\xi)/\xi(U=0) \approx 3$. In contrast, the absolute values of ξ strongly differ in both figures due to the much weaker disorder strength used in Fig. 7.5.

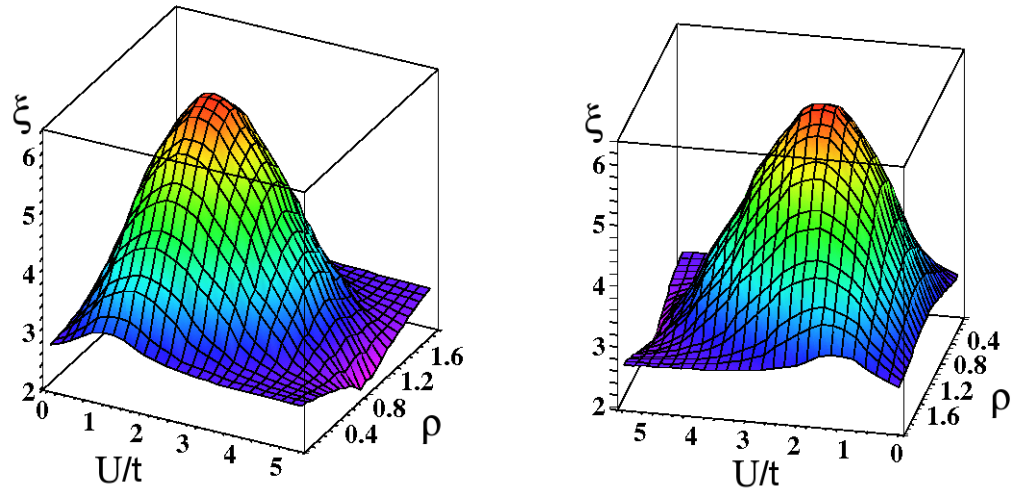

(a) (b)

Figure 7.5: Localization length ξ in one dimension for fixed disorder strength $\Delta/t = 6$ as a function of the interaction strength U and filling factor ρ.

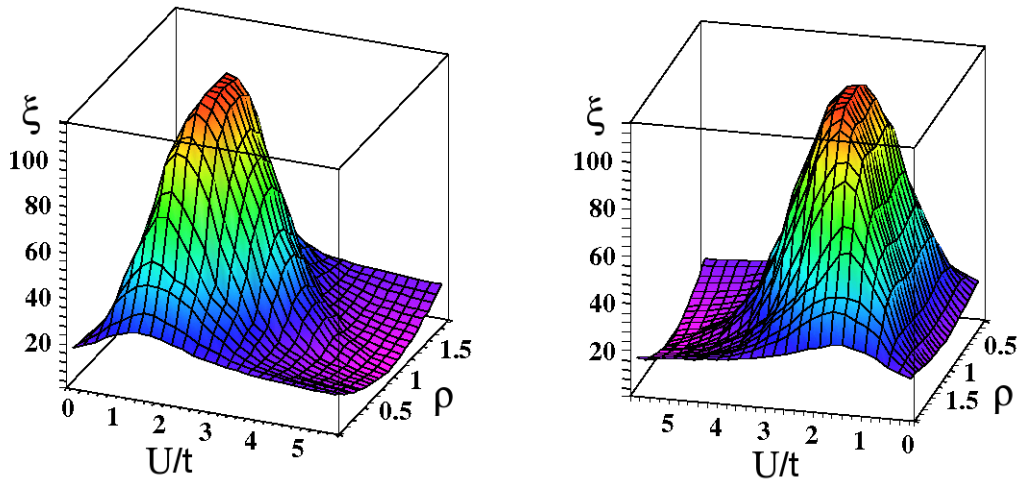

(a) (b)

Figure 7.6: Localization length ξ in two dimensions for fixed disorder strength $\Delta/t = 6$ as a function of the interaction strength U and filling factor ρ.

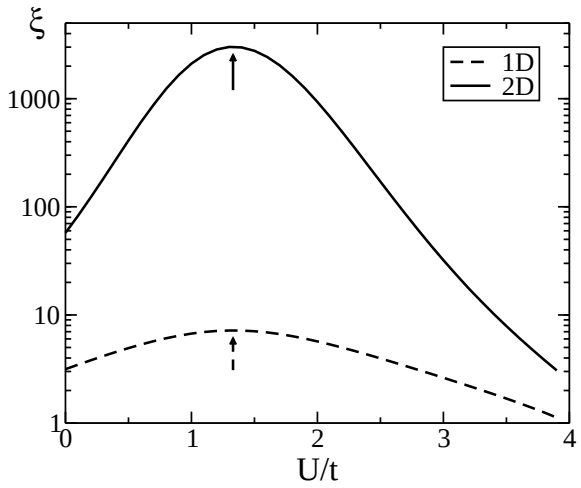

Figure 7.7: Localization length as a function of the interaction strength U for fixed disorder strength $\Delta/t = 4$ at half-filling ($\rho = 1$) in one and two dimensions. The arrows indicate the position of the maximum ξ as obtained from the strong disorder approximation.

Fig. 7.6 shows the corresponding result for the two-dimensional case. Here, two rather interesting points have to be noted. First, the delocalizing effect is significantly stronger than in one dimension and in the strong disorder approximation. Second, the qualitative behavior is nevertheless similar. In particular, the value of the interaction strength, where the localization length reaches its maximum (for a fixed lattice filling), is almost the same as in one dimension, and as in the strong disorder approximation. Both aspects can be observed even more clearly in Fig. 7.7. While the position of the maximum of ξ in both dimensions almost perfectly agrees with the strong disorder prediction, Eq. (6.42), in two dimensions the delocalizing effect is dramatically stronger with a ratio $\xi(U_\xi)/\xi(U=0) \approx 50$.

As we discussed before, and in Appendix F as well, for very strong disorder the dimensionality of the system becomes unimportant. However, for weak and, as we see from Fig. 7.7, moderately strong disorder, the effect of the interplay of disorder and interaction crucially depends on the dimension. We can understand this from the predictions of the scaling theory of Anderson localization. In Sec. 3.4, we derived the dependence of the localization length on the transport mean free path (Eqs. (3.34) and (3.35)),

$$\xi \sim \begin{cases} k_{\mathrm{F}} l & , \quad d = 1 \\ \exp\left(k_{\mathrm{F}} l\right) & , \quad d = 2 \end{cases} , \tag{7.30}$$

which with the results from Appendix A becomes

$$\xi \;\sim\; \begin{cases} 1/\tilde{\Delta}^2 & , \quad d=1 \\ \exp\left(1/\tilde{\Delta}^2\right) & , \quad d=2 \end{cases} . \tag{7.31}$$

Here, $\tilde{\Delta}$ denotes the effective disorder strength resulting from the interplay of Δ and U within the atomic-limit approximation. Although the exact value of $\tilde{\Delta}$ is hard to obtain (see discussion in Sec. 6.4), we can estimate it from the variance of the effective probability distribution, $p_{\rm A}(\varepsilon)$, which was calculated in Appendix C, Eq. (C.18). As we can see, the interaction strength U enters the variance only via the ratio U/Δ. Since the ratio U_ξ/Δ depends on the lattice filling only (see Eq. (6.42)), we find for the effective disorder strength the relation

$$\frac{\tilde{\Delta}^2}{12} \;\equiv\; \mathrm{var}[\varepsilon](U=U_\xi) \;=\; \alpha_\rho^2\,\mathrm{var}[\varepsilon](U=0) \;=\; \alpha_\rho^2\frac{\Delta^2}{12} \tag{7.32}$$

$$\Leftrightarrow \quad \tilde{\Delta} \;=\; \alpha_\rho\,\Delta, \tag{7.33}$$

where $\alpha_\rho < 1$ depends on ρ only. Combining Eqs. (7.31) and (7.33) we can therefore estimate the disorder dependence of the interaction enhancement of ξ by

$$\frac{\xi(U_\xi)}{\xi(U=0)} \;=\; \begin{cases} 1/\alpha_\rho^2 & , \quad d=1 \\ \exp\left(\beta_\rho^2/\Delta^2\right) & , \quad d=2 \end{cases} , \tag{7.34}$$

with

$$\beta_\rho^2 \;=\; \frac{1}{\alpha_\rho^2} - 1 \;>\; 0. \tag{7.35}$$

Thus, from Eq. (7.34) we predict that in 1D the optimal screening of the disorder by the interaction yields an almost constant effect, not significantly varying for different disorder strengths. In contrast, in 2D we expect that the screening effect will exponentially increase with decreasing Δ, due to the exponential dependence of the localization length on the disorder strength. Indeed, Fig. 7.8, where the ratio $\xi(U_\xi)/\xi(U=0)$ is plotted as a function of the bare disorder strength, supports our argumentation. For weak and moderate disorder strengths, we find an exponential enhancement of the localization length by the screening effect in two dimensions. In one dimension, however, the enhancement stays almost the same for all disorder strengths.

Fig. 7.9 shows the localization length ξ as a function of U for a fixed disorder strength, in $d = 2$ dimensions, for $\rho = 1$ and $\rho = 0.5$. We see that both, the disorder screening and the disorder enhancement by weak and strong interactions, respectively, are more pronounced at half filling. The former arises from the fact

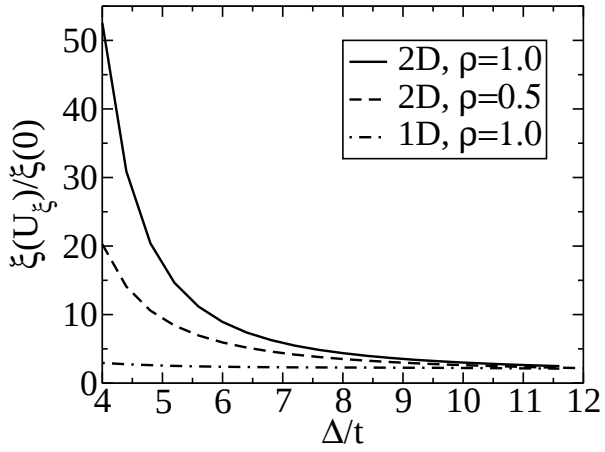

Figure 7.8: Magnitude of the delocalizing effect as a function of disorder strength in $d = 1$ and 2 dimensions.

that a larger number of charge carriers can be redistributed to optimally adopt the charge density to the total, local potential, which means that a larger portion of the spectrum is effectively shifted towards the Fermi energy. Generally, this effect is the larger, the closer the lattice filling is to half filling. The strong suppression at half filling for large values of U can be explained by the formation of the Mott-Hubbard gap (see inset of Fig. 7.9). At some critical interaction strength $U > \Delta$, the density of states at the Fermi level, $N(0)$, vanishes. From Eqs. (3.21) and (F.21), respectively, and the fact that

$$N(0) \int dk \, \frac{k}{a + k^2} \quad = \quad \frac{1}{2} N(0) \, \log (k^2 + a), \tag{7.36}$$

we can deduce that, simultaneously to the density of states at the Fermi level, $\xi(U)$ vanishes as

$$\log (\xi(U)) \sim -\frac{1}{N(0)}. \tag{7.37}$$

Till now, we have concentrated on the interaction dependence of the localization length. However, the disorder dependence is also important and yields complex physics. While the interaction dependence could be understood on the level of disorder screening and hopping suppression, varying the disorder strength has a further consequence. Besides the interplay of U and Δ, competition between disorder and kinetic energy, determined by the ratio Δ/t, also influences the localization of the system. In the absence of interactions ($U = 0$), a reduction of Δ necessarily yields a monotonic delocalization and an enhancement of the localization length with $\xi \to \infty$ for $\Delta \to 0$. In the presence of interactions, the situation changes. For a fixed interaction strength and very strong disorder, $\Delta \gg t$ and

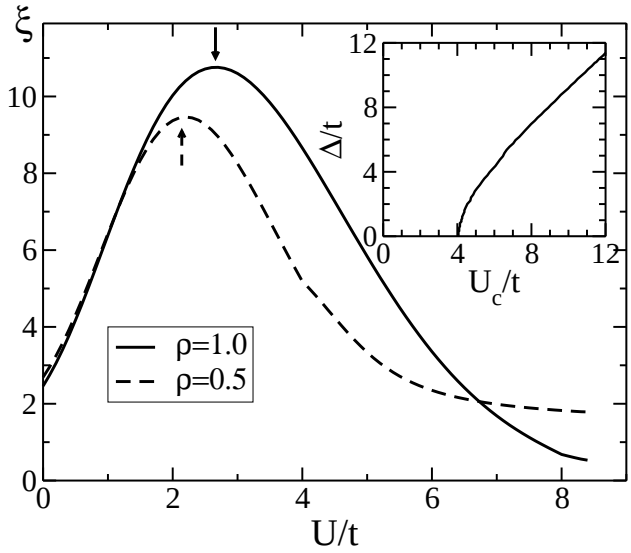

Figure 7.9: Localization length in two dimensions as a function of the interaction strength for different filling factors and fixed disorder strength $\Delta/t = 8$. The arrows again indicate the position of the maximum of ξ as predicted by Eq. (6.42). The inset shows the Mott-Hubbard transition line, where the density of states becomes gapped at half filling.

$\Delta \gg U$, a reduction of the disorder should also induce a delocalization of the system. The disorder screening effect becomes more efficient and the competition of disorder and kinetic energy also favors a delocalization. However, when the disorder becomes weaker, $\Delta \approx U$, the point of optimal screening gets reached. A further reduction of the disorder strength then yields successively worse screening effects, and the regime of hopping suppression by interaction, which corresponds to an effective disorder enhancement, takes over. On the other hand, the kinetic term still favors a delocalization of the system, because this process monotonically depends on the ratio Δ/t. Thus, we have a superposition of, on the one hand, the nonmonotonic interplay of interaction and disorder, and, on the other hand, the monotonic interplay of disorder and kinetics. Fig. 7.10 shows the result of this two competing tendencies. Here, the inverse localization length ξ^{-2}, which corresponds to the inverse participation ratio (see Sec. 3.2.2), is plotted as a function of the disorder strength at half filling in two dimensions. As expected, the noninteracting curve monotonically decreases with decreasing disorder strength. The interacting one also decreases in the strong disorder regime, where both interplays, interaction-disorder and kinetic energy-disorder, tends towards a more delocalized system. Then, at $\Delta \approx U$, the nonmonotonic effect, caused by the interplay of interaction and disorder, dominates and the IPR starts to increase again. At low disorder strengths, the kinetic delocalization effect becomes stronger, such

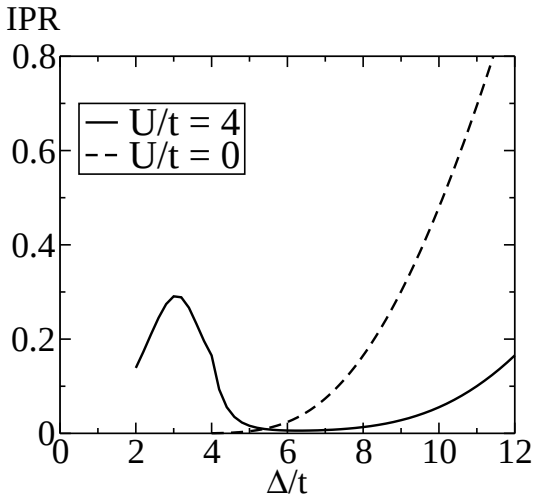

Figure 7.10: Inverse participation ratio ξ^{-2} as a function of the disorder strength in two dimensions at half filling ($\rho = 1$) in the noninteracting ($U/t = 0$) and in the interacting ($U/t = 4$) case.

that finally the IPR decreases again, and, in the limit $\Delta \to 0$, the localization length diverges, $\xi \to \infty$.

7.4 Anderson-Hubbard transition in three dimensions

In one and two dimensions, we found a rich and complex interplay of disorder and interactions yielding a nonmonotonic (de-)localization. However, in the presence of any finite disorder potential, our (static) single-particle approximation allowed only for localized solutions, according to the scaling theory of Anderson localization. In three dimensions, the situation is different. Here, as we discussed in Ch. 3, a real metal-insulator transition exists. For very strong disorder, $\Delta \gg \Delta_c$, Δ_c being the critical disorder strength at which the metal-insulator transition occurs in the noninteracting Anderson model, the dimensionality is again unimportant. There we can find the same qualitative and quantitative behavior as in $d = 1, 2$ dimensions. Therefore, we will concentrate our discussion on the regime close to the critical disorder strength where the renormalization of the effective disorder by the interaction gets most relevant and interesting, and, in particular, on the interaction dependence of $\Delta_c \equiv \Delta_c(U)$ for different lattice fillings ρ.

The critical disorder strength $\Delta_c(U, \rho)$, at which the transition takes place, can

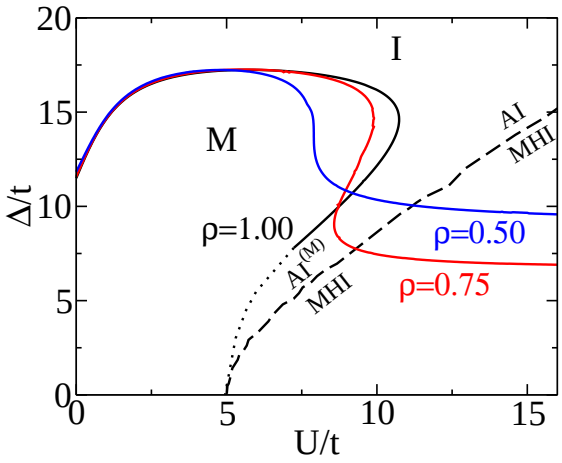

Figure 7.11: Phase diagram of localization in three dimensions in the (U, Δ)-plane within the atomic-limit approximation. The metallic phase (M) is to the lower left, the insulating phase (I) to the upper right of the phase boundary (solid lines). Shown are the curves for $\rho = 0.5$, 0.75 and 1.0, respectively. The dotted line is an extrapolation of the phase boundary at $\rho = 1$ toward small disorder, where the evaluation of the self-consistent equation, Eq. (7.38), becomes numerically costly. The dashed line denotes the crossover from the Anderson insulating (AI) phase, and the Mott-Hubbard assisted Anderson insulating phase, respectively, to the Mott-Hubbard insulating (MHI) phase at half filling (see explanation in the text).

be obtained from the self-consistent equation, which reads in three dimensions

$$\begin{aligned} 0 \stackrel{!}{=} D_0 - \frac{32t^2\,\mathrm{Im}\Sigma^R}{[\mathrm{Im}\overline{G_0^R}]^2 D_0} \sum_{x=1}^{\infty}\sum_{y=0}^{\infty}\sum_{z=y}^{\infty} \hat{C}(x,y,z)[\hat{g}(1+x,y,z) - \hat{g}(1-x,y,z)] \\ \times [\hat{g}_2(1+x,y,z) - \hat{g}_2(1-x,y,z)]\,(1-\frac{1}{2}\delta(y))\,(1-\frac{1}{2}\delta(z)) \\ \times (1-\frac{1}{2}\delta(y-z)). \end{aligned} \tag{7.38}$$

For its derivation we used the same notations for the Fourier transforms as in the previous section. Therefore, its derivation is completely analogously to Eqs. (7.26) and (7.27).

The Anderson metal-insulator transition is marked by the divergence of the localization length, $\xi \to \infty$ at Δ_c. Thus, defining

$$\begin{aligned} \hat{C}_\infty(x,y,z) &\equiv \lim_{\xi\to\infty} \hat{C}(x,y,z) \\ &= \int_{-\pi}^{\pi}\frac{dk_x}{2\pi}\int_{-\pi}^{\pi}\frac{dk_y}{2\pi}\int_{-\pi}^{\pi}\frac{dk_z}{2\pi}\,\frac{\cos(k_x x)\,\cos(k_y y)\,\cos(k_z z)}{k_x^2+k_y^2+k_z^2}, \end{aligned} \tag{7.39}$$

the critical disorder strength is defined as the root of the function

$$\begin{aligned} F(\Delta) = D_0 - \frac{32t^2\,\mathrm{Im}\Sigma^R}{[\mathrm{Im}\overline{G_0^R}]^2 D_0} \sum_{x=1}^{\infty}\sum_{y=0}^{\infty}\sum_{z=y}^{\infty} \hat{C}_\infty(x,y,z)[\hat{g}(1+x,y,z) - \hat{g}(1-x,y,z)] \\ \times [\hat{g}_2(1+x,y,z) - \hat{g}_2(1-x,y,z)]\,(1-\frac{1}{2}\delta(y))\,(1-\frac{1}{2}\delta(z)) \\ \times (1-\frac{1}{2}\delta(y-z)), \end{aligned} \tag{7.40}$$

which we numerically determined by using the same routines as before.

In Fig. 7.11, we plotted the phase diagram of localization, obtained from Eq. (7.40). In the noninteracting limit ($U = 0$), we found an Anderson transition at a critical disorder strength $\Delta_c/t \approx 11.7$, which is slightly smaller than the correct value of $\Delta_c/t \approx 16.5$ [EFR08] (cf. Sec. F.3.2). In [Kro90] the self-consistent equation was solved under the additional approximation of an isotropic dispersion relation, neglecting the lattice periodicity of the system. Therefore, the critical disorder strength obtained therein deviates from our result, being somewhat closer to the correct one.

For weak interactions, we found for all lattice fillings an increase of the critical disorder strength, i.e., a positive slope of the phase boundary as a function

of U (see Fig. 7.11). This is a direct consequence of the disorder screening by weak to intermediate interactions. Here, it is interesting to note that the phase boundary in this part of the phase diagram is almost universal for all lattice fillings. By further increase of the interaction strength, at some intermediate value of U, which now depends on the lattice filling, the point of optimal screening is reached, i.e., the slope of the phase boundary changes its sign. At this point, the crossover from disorder screening to the effective disorder enhancement by hopping suppression due to the interaction takes place. Correspondingly, for disorder strengths slightly larger than the noninteracting, critical one, $\Delta \gtrsim \Delta_c$, e.g., $\Delta/t = 15$, we find a re-entrance behavior by increasing U from weak to strong interactions. While weak interactions causes an insulator-to-metal transition, strong interactions induces a second transition, from the metallic phase back to the Anderson-insulating phase.
A similar effect exists also as a function of the disorder strength for lattice fillings $|1 - \rho| < 0.5$ when fixing U at a rather large value. Remarkably, the phase boundary in the strongly interacting part of the phase diagram is S-shaped, and therefore even a (double) re-entrance behavior is predicted by our results. For instance, let's concentrate on the curve of the phase boundary for $\rho = 0.75$ and fix the interaction strength at $U/t \approx 8.5$. Now by decreasing the disorder strength, starting from $\Delta/t > 18$, we first observe an insulator-to-metal transition at $\Delta/t \approx 16$. Next, a re-entrance from the metallic to the insulating phase can be found at $\Delta/t \approx 13$, and, finally, the system re-enters the metallic phase again at $\Delta/t \approx 8$.
Again it is important to note that the effective disorder strength is not bounded by the noninteracting one, but can exceed it, i.e., $\Delta_c(U/t > 15) < \Delta_c(U = 0)$.

At half filling, the situation is different, because of the presence of the Mott-Hubbard metal-insulator transition (see Secs. 2.3 and 5.1, respectively). Here, for strong interactions, the system becomes gapped around the Fermi level. Therefore, even at $\Delta = 0$ the system is an insulator for strong enough interaction strengths. Furthermore, two different kinds of insulators can be distinguished. A compressible ($d\rho/d\mu > 0$) Anderson insulator, whose spectrum is not gapped around the Fermi level, and an incompressible ($d\rho/d\mu = 0$) Mott-Hubbard insulator, whose spectrum is gapped at ε_{F}. In particular, in the context of the disordered Bose-Hubbard model [GS87, FWGF89, BPVB07, PPST09] (see Ch. 9), but also for Fermions [BHV05, SI09a], it is a longstanding and open question, whether a direct transition from a metal (superfluid) to a Mott-Hubbard insulator can exist, or whether these two phases are always separated by an Anderson-type insulator (also called Bose glass phase in the Bose-Hubbard model).
By construction, we find in our model at half filling an Anderson insulator sandwiched between the metallic phase and the Mott-Hubbard insulator (see Fig. 7.11). Moreover, we observe a gradual vanishing of the density of states at the Fermi level. Correspondingly, when the density of states at the Fermi level

falls below some critical value, the system gets completely localized by disorder. The Mott-Hubbard insulating region is entered only at a higher interaction strength, where the density of states then completely vanishes. In Fig. 7.11, in addition to the phase boundary between the metallic and the insulating phase, we marked the crossover line between the two types of insulators, at which the density of states at the Fermi level vanishes. At low disorder strengths, the Anderson insulating phase only exists because of the reduction of the density of states due to the interaction potential. Therefore, we called this a 'Mott-Hubbard assisted' Anderson insulator ($\mathrm{AI}^{(\mathrm{M})}$) to distinguish it from the usual Anderson insulator (AI).

7.5 Spin-3/2 particles

In the following, we will shortly discuss the atomic-limit approximation for fermions with total spin $S > 1/2$. Qualitatively, the behavior is, of course, the same as before. However, quantitatively, we expect the screening effect to be more efficient, because now up to $2S + 1$ particles can occupy each lattice site. Our discussion is motivated by the experiments on two-dimensional semiconductor heterostructures [KKF$^+$94, AKS01, KS04] which seem to indicate a possible metal-insulator transition in two dimensions, the results of which were already presented in Sec. 3.6. In these materials, among other important properties, the band structure possesses a two-fold valley degeneracy [AKS01, PF02, FW08b], which can be modeled as an effective spin-3/2 system [FW08b].

As in the case of spin-1/2 particles, we can analyze the spin-3/2 system with the same strategy. This means, we first obtain the ground state configuration and afterwards calculate the effective probability distribution from it. To keep the discussion simple, we will not present all the details here. Furthermore, we will restrict to the case of $\rho < 0.5$, which is the relevant regime, because all of the experiments are done at extremely low charge carrier densities (see Sec. 3.6).

The Anderson-Hubbard Hamiltonian for a general spin system reads

$$\hat{H}_{AH} = \sum_{i\sigma}(\varepsilon_i - \mu)c^\dagger_{i\sigma}c_{i\sigma} + \frac{U}{2}\sum_{i,\sigma\neq\sigma'}\hat{n}_{i,\sigma}\hat{n}_{i,\sigma'} - t\sum_{<i,j>,\sigma}c^\dagger_{i\sigma}c_{j\sigma}, \quad (7.41)$$

where the spin indices run from $-S, \ldots, S$.

Concentrating on the case of $S = 3/2$ ($n = 4$), the site occupation numbers

are straightforwardly calculated,

$$\langle n_i \rangle_0 \;=\; \begin{cases} 4 & , \quad \varepsilon_i \leq \mu - 3U \\ 3 & , \quad \mu - 3U < \varepsilon_i \leq \mu - 2U \\ 2 & , \quad \mu - 2U < \varepsilon_i \leq \mu - U \\ 1 & , \quad \mu - U < \varepsilon_i \leq \mu \\ 0 & , \quad \varepsilon_i > \mu \end{cases} . \tag{7.42}$$

The chemical potential for $\rho < 1$ is also easily deduced and becomes

$$\mu \;=\; \begin{cases} \frac{1}{4}(\Delta\rho - 2\Delta + 6U) & , \quad 0 < U \leq \frac{1}{6}\Delta\rho \\ \frac{1}{3}(\Delta\rho - \frac{3}{2}\Delta + 3U) & , \quad \frac{1}{6}\Delta\rho < U \leq \frac{1}{3}\Delta\rho \\ \frac{1}{2}(\Delta\rho - \Delta + U) & , \quad \frac{1}{3}\Delta\rho < U \leq \Delta\rho \\ \Delta(\rho - \frac{1}{2}) & , \quad U \geq \Delta\rho \end{cases} . \tag{7.43}$$

Solving the corresponding Heisenberg equation of motion for the fermion creation and annihilation operators, and following the analogous calculation as in Sec. 6.2, the retarded, local Green's function becomes

$$\begin{aligned} \mathcal{G}^{R,0}_{i\sigma_1}(E) \;=\; & \frac{(1 - \langle \hat{n}_{i,\sigma_2} \rangle_0)\,(1 - \langle \hat{n}_{i,\sigma_3} \rangle_0)\,(1 - \langle \hat{n}_{i,\sigma_4} \rangle_0)}{E - (\varepsilon_i - \mu) + \mathrm{i}0^+} \\ & + 3\,\frac{\langle \hat{n}_{i,\sigma_2} \rangle_0\,(1 - \langle \hat{n}_{i,\sigma_3} \rangle_0)\,(1 - \langle \hat{n}_{i,\sigma_4} \rangle_0)}{E - (\varepsilon_i - \mu + U) + \mathrm{i}0^+} \\ & + 3\,\frac{\langle \hat{n}_{i,\sigma_2} \rangle_0\,\langle \hat{n}_{i,\sigma_3} \rangle_0\,(1 - \langle \hat{n}_{i,\sigma_4} \rangle_0)}{E - (\varepsilon_i - \mu + 2U) + \mathrm{i}0^+} \\ & + \frac{\langle \hat{n}_{i,\sigma_2} \rangle_0\,\langle \hat{n}_{i,\sigma_3} \rangle_0\,\langle \hat{n}_{i,\sigma_4} \rangle_0}{E - (\varepsilon_i - \mu + 3U) + \mathrm{i}0^+}, \end{aligned} \tag{7.44}$$

where we denoted the four different spin states by $\{\sigma_1, \sigma_2, \sigma_3, \sigma_4\}$ and assumed $\langle n_{i\sigma_i} \rangle_0 = \langle n_{i\sigma_j} \rangle_0 \; \forall i, j$ (cf. Eq. (6.28)).

From Eq. (7.44), we can read off again, how the effective probability distribution can be constructed: All sites with occupation number $\langle n_i \rangle_0 = 4$ (which corresponds to the last line of Eq. (7.44)) are shifted by $3U$, all sites with $\langle n_i \rangle_0 = 3$ (last two lines of Eq. (7.44)) are shifted either by $3U$ or by $2U$. The probability that the latter case (hole-like propagation) occurs is $3/4$, while the probability for a particle-like propagation is $1/4$, as follows from the prefactors in Eq. (7.44).

All other cases follow analogously, and we end up with the rule

$$\varepsilon_i \;\mapsto\; \begin{cases} \varepsilon_i + 3U & , \quad \varepsilon_i \leq \mu - 3U \\ \varepsilon_i + 3U \\ \varepsilon_i + 2U & , \quad \mu - 3U < \varepsilon_i \leq \mu - 2U \left(\begin{array}{l} \text{prob. of } 1/4 \\ \text{prob. of } 3/4 \end{array} \right) \\ \varepsilon_i + 2U \\ \varepsilon_i + U & , \quad \mu - 2U < \varepsilon_i \leq \mu - U \left(\begin{array}{l} \text{each with} \\ \text{prob. of } 1/2 \end{array} \right) \\ \varepsilon_i + U \\ \varepsilon_i & , \quad \mu - U < \varepsilon_i \leq \mu \left(\begin{array}{l} \text{prob. of } 3/4 \\ \text{prob. of } 1/4 \end{array} \right) \\ \varepsilon_i & , \quad \varepsilon_i > \mu \end{cases} \quad . \tag{7.45}$$

The resulting expressions for the probability function can be found in Appendix C.2. Having calculated the effective probability distribution, the remaining analysis of the atomic-limit approximation is the same as for the spin-1/2 system.

In Fig. 7.12, we plotted the localization length for the spin $S = 3/2$-system in one and two dimensions. The comparison with the curve for $S = 1/2$ confirms that qualitatively the behavior is the same in both cases. However, quantitatively, as expected, the screening is much more efficient for a higher spin degeneracy, yielding an enhancement of the localization length in two dimensions, which is significantly larger than the one for $S = 1/2$.

Eq. (7.45) can easily be generalized to the case of an arbitrary spin system with $n = 2S + 1$ spin states per lattice site. For that purpose, we consider a lattice site with occupation number $\langle n_i \rangle_0 \equiv m \leq n$. Then the effective shift of the local potential for a particle-like propagation of a quasiparticle at the Fermi level is $\varepsilon_i + mU$. The probability that a particle-like propagation takes place is given by $\frac{\#\text{ free states at site } i}{\#\text{ states at site } i} = \frac{n-m}{n}$. A hole-like process yields a shift of $(m-1)U$, which takes place with probability $\frac{m}{n}$. Thus, we get the general rule,

$$\varepsilon_i \;\mapsto\; \left\{ \begin{array}{r} \varepsilon_i + mU \\ \varepsilon_i + (m-1)U \end{array} \right. \quad , \quad \mu - mU < \varepsilon_i \leq \mu - (m-1)U \left(\begin{array}{l} \text{prob. of } \frac{n-m}{n} \\ \text{prob. of } \frac{m}{n} \end{array} \right). \tag{7.46}$$

While the explicit calculation of the probability function $p_{\mathrm{A}}(\varepsilon)$ has the advantage that one can analyze the interplay of disorder and interaction analytically, it requires the fixing of the spin degeneracy factor and is quite involved for $S > 1/2$, because many different parameter regimes have to be distinguished. Therefore, for a general treatment it is more efficient to determine the localization length

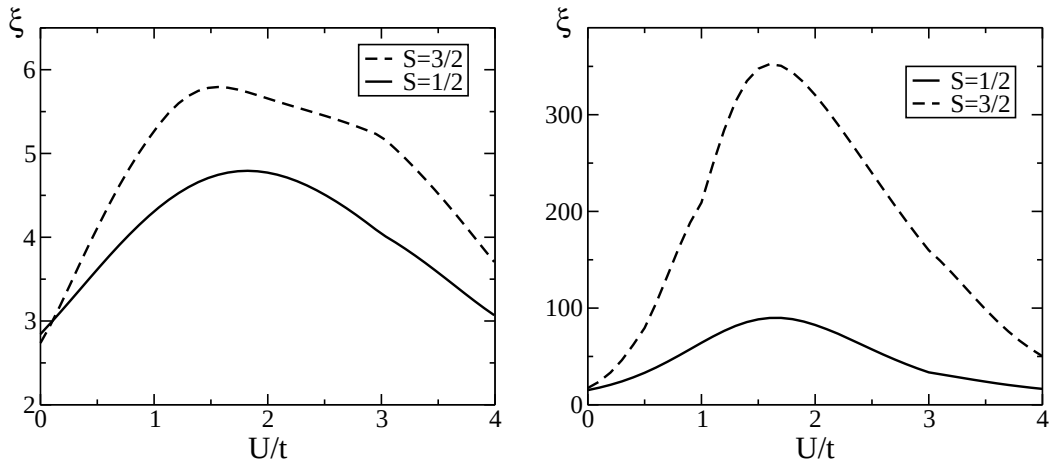

Figure 7.12: Comparison of the localization length as a function of U for fixed disorder strength $\Delta/t = 6$ and lattice filling $\rho = 0.5$ for spin $S = 1/2$ and $S = 3/2$. a) $d = 1$ b) $d = 2$.

without a preceding calculation of the probability function. For this purpose, we use the identity

$$
\begin{aligned}
& \int d\varepsilon\, p_{\mathrm{A}}(\varepsilon)\, g(\varepsilon) \\
= & \int d\varepsilon\, p(\varepsilon) \left(\frac{\langle n_i \rangle_0}{n} g(\varepsilon + (\langle n_i \rangle_0 - 1)U) \; + \; \frac{n - \langle n_i \rangle_0}{n} g(\varepsilon + \langle n_i \rangle_0 U) \right) \\
= & \int\limits_{-\infty}^{\mu-(n-1)U} d\varepsilon\, p(\varepsilon)\, g(\varepsilon + nU) \; + \; \int\limits_{\mu}^{\infty} d\varepsilon\, p(\varepsilon)\, g(\varepsilon) \\
& + \sum_{k=1}^{n-1} \int\limits_{\mu-kU}^{\mu-(k-1)U} d\varepsilon\, p(\varepsilon) \left(\frac{n-k}{n}\, g(\varepsilon + kU) \; + \; \frac{k}{n}\, g(\varepsilon + (k-1)U) \right) \\
= & \int\limits_{-\infty}^{\mu+U} d\varepsilon\, p(\varepsilon - nU)\, g(\varepsilon) \; + \; \int\limits_{\mu}^{\infty} d\varepsilon\, p(\varepsilon)\, g(\varepsilon) \\
& + \sum_{k=1}^{n-1} \left(\frac{n-k}{n} \int\limits_{\mu}^{\mu+U} d\varepsilon\, p(\varepsilon - kU)\, g(\varepsilon) \; + \; \frac{k}{n} \int\limits_{\mu-U}^{\mu} d\varepsilon\, p(\varepsilon - (k-1)U)\, g(\varepsilon) \right),
\end{aligned}
\tag{7.47}
$$

which follows directly from Eq. (7.46) (cf. Eq. (7.12)), and which is valid for each

(local) function $g(\varepsilon)$, in particular for the CPA functional

$$F(\Sigma(E),\varepsilon) \;=\; \frac{\varepsilon-\Sigma^R(E)}{1-\overline{G_0^R}(E)(\varepsilon-\Sigma^R(E))}. \tag{7.48}$$

(A similar approach will be used in Ch. 9, when we discuss the atomic-limit approximation for the disordered Bose-Hubbard model.)

7.6 Comparison with known numerical results for the Anderson-Hubbard model

Our motivation for the applicability of the atomic-limit approximation for strong disorder was based on a heuristic argumentation. Therefore, in this section, we will give further support to the validity of our ansatz by comparing our observations with known numerical results from the literature (cf. Sec. 5.3).

In [OYTM08, OYTM09], a density matrix renormalization group (DMRG) study on the one-dimensional Anderson-Hubbard model was published. Here, the charge density profile had been obtained, whose results showed strong (hole) localization for $\Delta > t$ for strong and weak interactions. Furthermore, it was shown that the charge density rapidly varies from lattice site to lattice site. Thus, it confirms our main assumption of a strong charge density localization by disorder and supports the validity of the atomic-limit approximation.

In [SBS03], the Anderson-Hubbard model was studied at half filling in $d = 1, 2$ dimensions by using a quantum Monte Carlo (QMC) method. Here, the localization length and the inverse participation ratio, respectively, was extracted from the charge density and calculated as a function of the interaction strength. In qualitative agreement with our results, a nonmonotonic evolution was found, with a maximum of the localization length at an intermediate interaction strength, Fig. 7.13. However, our calculation predicts a much stronger enhancement of ξ in 2D than it was observed in [SBS03]. As has been stressed by the authors of [SBS03], the localization length was calculated by averaging over all energies. Since states at low energies are generally much stronger localized than particles at the Fermi level (compare to our prediction for the ρ-dependence of $\xi(U)$), a much weaker enhancement of ξ must be expected and is not in contradiction to our results.

In [SWA08], the two-dimensional Anderson-Hubbard model was analyzed by using a statistical DMFT method, where a Hubbard-I approximation was used as the impurity solver. The inverse participation ratio at the Fermi level was extracted from the local charge density and used to define the localization length

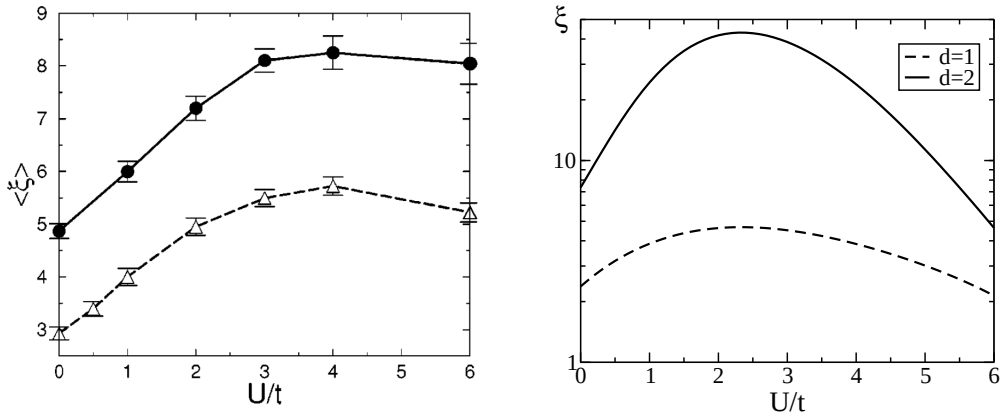

(a) (b)

Figure 7.13: Localization length as a function of the interaction strength for $\Delta/t = 7$ at half filling in $d = 1$ (dashed lines) and $d = 2$ (solid lines) dimensions. a) Plot taken from [SBS03] b) Result obtained by the self-consistent analysis of the atomic-limit approximation (logarithmic scale).

via

$$\xi \;=\; (\mathrm{IPR})^{-1/d}\,. \tag{7.49}$$

Fig. 7.14 shows their and our result for the same set of parameters. Apart from an overall factor of unity, which most probably arises from the different definitions of the localization length (see discussion in Sec. 3.2.2), both plots almost perfectly agree, qualitatively as well as quantitatively. The same holds for the case $\rho = 0.5$, which is not shown in the figure. Moreover, in [SWA08], also the disorder-averaged density of states was determined, which completely agrees with our CPA prediction for the atomic-limit approximation (Figs. 7.3 and 7.4).

In [DST99, DS03, CDS07] a quantum Monte Carlo simulation was used to obtain the finite-temperature dc conductivity in two dimensions. As we argued above, in the interacting many-body problem of the Anderson-Hubbard model, the localization length should be understood as the relevant scale of the system, which determines the transport properties of the model. Therefore, we can compare the nonmonotonic interaction dependence of the dc conductivity with the interaction dependence of the localization length for the same parameters of Δ and ρ, Fig. 7.15. Here, the nonmonotonicity of our zero-temperature localization length is more pronounced than the finite-temperature conductivity, which is acceptable, because physical quantities are generally more smooth at finite temperatures than at zero temperature. The qualitative agreement is nevertheless surprisingly good. In particular, the position of the maximum of the conductivity agrees quite well

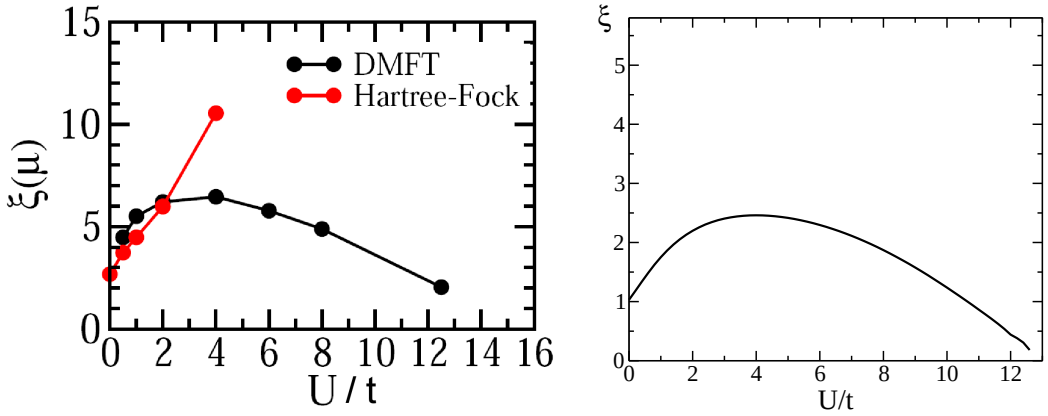

(a) (b)

Figure 7.14: Localization length as a function of the interaction strength for $\Delta/t = 12$ at half filling in $d = 2$ dimensions. a) Plot taken from [SWA08] b) Result obtained by the self-consistent analysis of the atomic-limit approximation.

with the prediction of the atomic-limit approximation, $U_\xi \approx 2.14$.

The authors of [HT04] used an unrestricted Hartree-Fock approximation to calculate the IPR as a function of the disorder strength for a fixed interaction strength. Comparison of their result and ours, Fig. 7.16 shows a nearly perfect agreement over the complete parameter range. In particular, the position of the local minimum and maximum, as well as the competition of the nonmonotonic interplay of disorder and interaction and the monotonic tendency of delocalization due to the interplay of kinetic energy and disorder, are clearly seen in both plots of Fig. 7.16.

The extrapolation of the finite-size data of [DST99, DS03, CDS07, HT04] indicated the existence of a metallic ground state in $d = 2$ dimensions within an intermediate parameter regime of the interaction strength [DST99, DS03, CDS07] and the disorder strength [HT04], respectively. Of course, the existence of such a metallic state would be beyond our effective single-particle approach. However, as we showed, the results of our approach, which by construction yields only localized solutions in $d \leq 2$ according to the predictions of the scaling theory of Anderson localization, were in very good agreement with the finite-size results of [DST99, DS03, CDS07, HT04]. Furthermore, we explained in Sec. 7.3, that the screening of the disorder potential by the interaction can lead to an exponentially enhanced localization length in 2D. In particular, in the parameter regime where the metallic ground state was observed in [HT04], the localization length was enhanced by almost two orders of magnitude (cf. Fig. 7.8). Thus, the largest system size used for the numerics of [DST99, DS03, CDS07, HT04] was at least

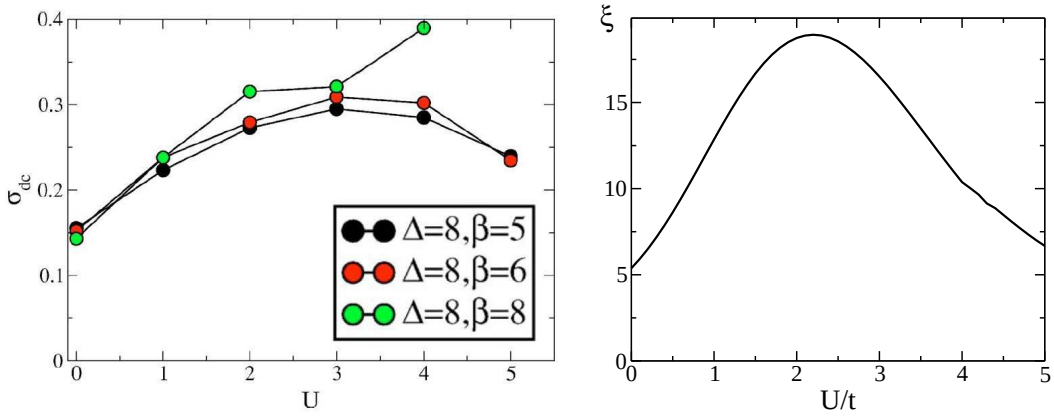

(a) (b)

Figure 7.15: a) Finite-temperature ($\beta = 1/T$) dc conductivity as a function of the interaction strength ($U \equiv U/t$) for $\Delta/t = 8$ and $\rho = 0.5$. Plot taken from [CDS07] b) Localization length as a function of the interaction strength for the same disorder strength and lattice filling as in a). Result obtained by the self-consistent analysis of the atomic-limit approximation.

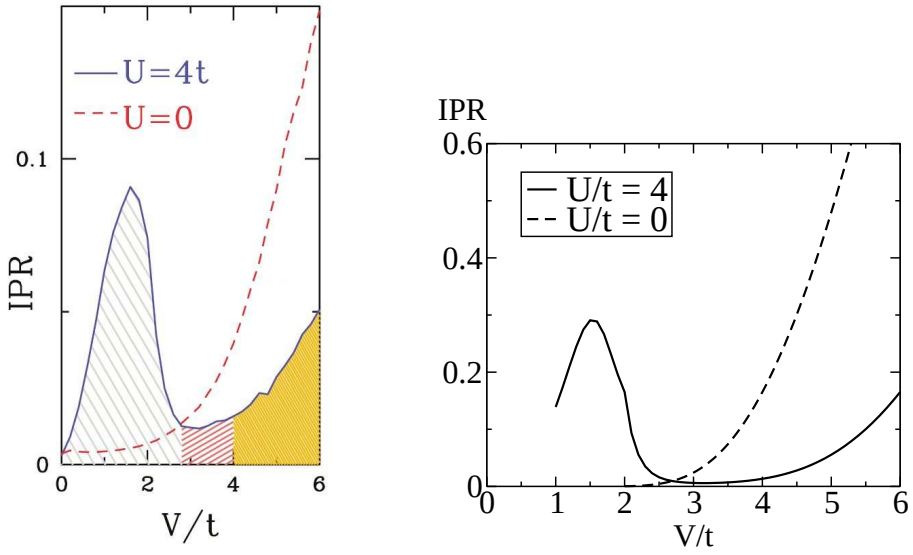

(a) (b)

Figure 7.16: a) Inverse participation ratio as a function of the disorder strength ($V = \Delta/2$) at half filling in $d = 2$ dimensions. Plot taken from [HT04]. b) Result obtained by our self-consistent analysis of the atomic-limit approximation (cf. Fig. 7.10.

an order of magnitude smaller than the interaction-enhanced localization length. Therefore, we strongly believe that the infinite-size extrapolation erroneously indicate a metallic solution.

In this context, it is also interesting to note the results of [FW08a, FW08b]. Here, motivated by the experiments on semiconductor heterostructures (see Sec. 3.6), a QMC simulation for an interacting Anderson model with extended interactions was considered. Additionally, two different spin values, $S = 1/2$ and $S = 3/2$, were considered to account for the valley degeneracy of the materials (see Sec. 7.5). Again the interaction and disorder dependence of the localization length, here extracted from the Thouless conductance g (Eq. (3.27)), was analyzed at low particle densities. Within an appropriate parameter regime, the results showed a tremendous enlargement of ξ exceeding by far the system size of their numerical simulation. However, as was stressed, a scaling analysis of the localization length showed a perfect agreement with the prediction from single-parameter scaling theory. Therefore, it was concluded that the system remains insulating in the thermodynamic limit of infinite system size, but behaves 'metallic' on small systems. Although both models cannot be expected to behave completely the same, it nevertheless gives further support to our argumentation. Furthermore, as both models show the same general nonmonotonic behavior, also for an extended interaction the screening of the disorder potential might be a dominant effect [Fle].

In [BHV05], the three-dimensional phase diagram of the Anderson-Hubbard model was calculated within a statistical DMFT approach, Fig. 7.17. As the DMFT only provides results for local, single-particle quantities, within this method the phase diagram is obtained from the density of states by calculating its geometrical average over disorder realizations. Comparing the phase diagram of [BHV05] with our result, Fig. 7.11, we find agreement in that, for weak interactions, the metallic phase is extended from the noninteracting value to larger disorder strengths. However, in [BHV05] this effect is more pronounced than in our approach. Also the re-entrance behavior as a function of Δ for large U is similarly predicted in their and our work. The same was observed in [TL93], where the 3D phase diagram at half filling was calculated for a Gaussian disorder distribution by using an unrestricted Hartree-Fock approximation.
For weak disorder, in [BHV05] a direct first order phase transition from the metallic phase to the Mott insulator was found, in contrast to our prediction of the existence of an intermediate Mott-Hubbard assisted Anderson insulating phase. While our static approach neglects dynamical effects, and, therefore cannot correctly reproduce the Mott-Hubbard transition at $\Delta = 0$, the DMFT is based on a mapping onto a single-particle quantum impurity problem, which yields the formation of a Kondo resonance at the Fermi level (see Sec. 5.1). Therefore, within DMFT a concatenated unitary sum rule for the density of states at the Fermi

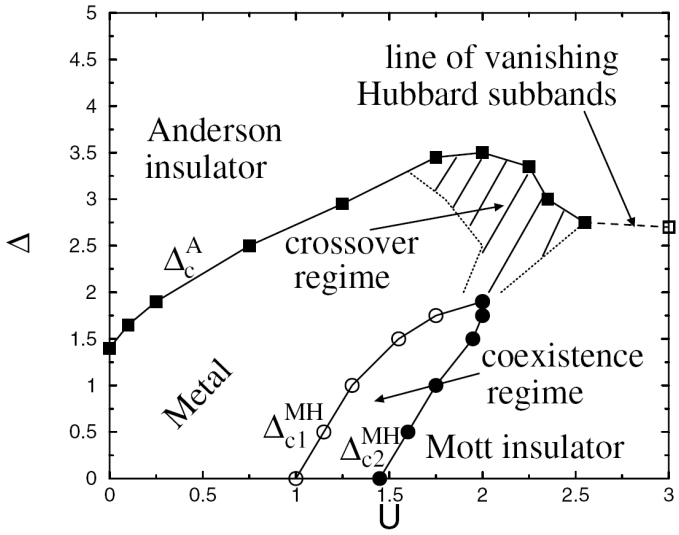

Figure 7.17: 3D phase diagram of the Anderson-Hubbard model at half filling obtained within a statistical DMFT calculation. Plot taken from [BHV05]. (Energies measured in units of the bare bandwidth.)

level, $N(0)$, prevents by construction the gradual suppression of $N(0)$, as it was observed in our approach. The question of whether the survival of the Kondo resonance, which is the origin of the first order phase transition, is still correct in the presence of disorder, is still an open one. Therefore, it remains an open issue to see which one of the two scenarios, if any, predicts the correct physical behavior.

A 3D phase diagram for the Anderson-Hubbard model at half filling was also presented in [KNS08]. Again a DMFT approach was used. However, in contrast to [BHV05], the self energy was not obtained by (geometrically) averaging over different disorder realizations, but the self energy was split into two additive parts. The first one was the local, interacting self energy of the usual DMFT approximation. The second one was the disorder contribution obtained within a self-consistent Born approximation (cf. Appendix A.1). The MIT was then determined by analyzing the optical conductivity, where the DMFT single-particle propagators were used to evaluate the transport equations. Effectively, this method yields a disorder-averaged self-energy contribution, which completely misses correlations between disorder and interaction contributions. In particular, the screening effect, which we identify as a physically relevant contribution, was not included. Consequently, varying the interaction strength had almost no influence on the upper phase boundary of the phase diagram in [KNS08], and the critical disorder strength was constant, $\Delta_c(U) \equiv \Delta_c(0)$. In subsequent work [KKNSnt], the same method was used to study the 2D localization length. Again

ξ was a constant of the interaction strength and depended only on the disorder strength. Both observations are the direct consequence of the construction of the self energy contributions, where interaction and disorder effects were treated independently from each other.

In [CG09] the 3D phase transition for $\rho = 0.5$ was considered within an unrestricted Hartree-Fock approximation. Due to the long computing time needed for their algorithm to achieve convergence, only a few selected data points could be evaluated. The results of [CG09] agree with our phase diagram, Fig. 7.11, in the general observation, that for weak disorder ($\Delta/t = 2$) only a metallic phase exists for $\rho = 0.5$, while for stronger disorder a metal-insulator transition occurs. However, the actual numbers differ from our prediction. While the authors of [CG09] found for $\Delta/t = 6$ a metal-insulator transition at a critical interaction strength $U/t \approx 9$, in our calculation the transition takes place only for $\Delta/t \gtrsim 9$. However, as we mentioned before, the critical disorder strengths for the Anderson transition, obtained within the self-consistent transport theory, are not very accurately determined (cf. Appendix F.3.2) and should be handled with care. Thus, we find, at least, a qualitative agreement with the results of [CG09].
For strong interaction, the authors of [CG09] additionally observed the gradual development of a pseudogap of the density of states at the Fermi level, which does not occur in our approach (see also discussion below). As it was emphasized in [CG09], the pseudogap could only be observed by allowing for the formation of local magnetic moments and was absent when applying a paramagnetic Hartree-Fock approximation. The importance of the formation of local magnetic moments for a complete understanding of the Anderson-Mott transition was also emphasized in [MSB89], as well as in [TDAK03], where the correlated, weakly disordered metallic phase was studied. Therefore, we want to emphasize again that our approach does not completely ignore the formation of local magnetic moments, i.e., lattice sites occupied by a single spin, but effectively includes it via the two-pole structure of the local Hubbard Green's function, Eq. (6.27). However, as we mentioned in Sec. 6.3, effects arising from dynamics and magnetic ordering (cf. Eqs. (6.28) and (6.29)) were not captured by our ansatz.

Summarizing the comparisons, we found good qualitative and quantitative agreement with many numerical studies. As we could show, the disorder screening by weak interactions and the hopping suppression by strong interactions, which corresponds to an effective disorder enhancement, could very well explain most of the features observed in these studies. Therefore, an understanding on the basis of a single-particle description is possible, which was strongly doubted in some works [HT04, CDS07]. But this should not be confused with the statement that one could easily read off the physical behavior from the shape of the effective disorder distribution [CDS07, CG09]. Particularly, the identification of the interaction parameter yielding the largest localization length in 1D and 2D, Eq. (6.42), and

the determination of the exact position of the phase transition line in 3D needs a more careful analysis of the effective disorder potential, as we explained. In particular, a simple statistical analysis of the effective on-site energy distribution, as it was done in [CDS07], is not sufficient.

Before we finish this section, we want to mention some recent results [CCPS08, SI09a, SI09b, SInt] on the disorder-averaged density of states. As reported, the analysis of the Anderson-Hubbard model by a recent QMC simulation [CCPS08] and an unrestricted Hartree-Fock calculation [SI09a, SI09b, SInt] showed a strong suppression [CCPS08] or even the existence of a pseudogap [SI09a, SI09b, SInt] of the density of states at the Fermi level for all values of $\Delta, U, t > 0$. If this turns out to be true, it will be quite remarkable. At first, one could be tempted to believe that such a suppression/pseudogap has to be expected, because of our discussion of the Altshuler-Aronov anomaly (Sec. 4.2.2). However, the Altshuler-Aronov anomaly in disordered metals was caused by the interplay of the Hartree and the Fock contribution in first order perturbation theory. As the (Anderson-)Hubbard model only contains a purely local interaction, the Fock contribution exactly vanishes. Recalling the discussion of Sec. 4.2.2, in this case one would expect an enhancement of $N(0)$ for weak interactions, as we observed in our atomic-limit approach. Supposing that the calculation of Altshuler-Aronov could be extended to the insulating phase, a suppression of $N(0)$ should arise only for a non-vanishing Fock contribution. Indeed, in [SBWA09] such an effect was observed when including an additional *nearest-neighbor interaction*. However, the existence of a pseudogap for arbitrarily weak interaction and without a nearest-neighbor interaction would be of different nature. In particular, it should not be confused with the findings of [CG09] where the pseudogap formation for $\rho = 0.5$ was reported for strong interactions only, while for weak interactions an effective enhancement of $N(0)$ was observed. (For a discussion of a possible mechanism for the pseudogap formation see [SI09b].)
Moreover, as we showed, our approach yields good agreement with the non-monotonic behavior of the localization and the transport properties of the system, which can be traced back to the enhancement of the DOS for weak interactions and a suppression for strong interactions. However, it seems less understandable, how the same behavior can arise for a system with an immediate formation of a pseudogap in the DOS at the Fermi level. While preliminary results shall agree with the known works [SI], it remains to be seen what the final results for the localization length will be, and how this puzzle can be solved.

7.7 Summary of the results of the atomic-limit approximation

We close the self-consistent analysis of the atomic-limit approximation by briefly summarizing our main results. As we have shown, we observed the following characteristic properties:

- The interplay of disorder and interaction causes a nonmonotonic behavior of all physical (transport) quantities, as can be read off from the localization length.
- Weak interaction strengths yield an enhancement of the localization length by screening of disorder.
- In contrast, strong interactions yield an effective amplification of the disorder potential, which results from the hopping suppression by interactions, and which causes a reduction of the localization length. In particular, in the strongly interacting regime ($U \to \infty$) the localization length becomes significantly shorter than the noninteracting one.
- While for strong disorder the screening effect is universal for all dimensions, for weak disorder it differs. In one dimension, the maximal enlargement of the localization length is almost constant for all disorder strengths. However, in two dimensions it exponentially increases with decreasing disorder strength.
- In three dimensions, the interplay of disorder and interaction generates a rich and complex phase diagram, with (depending on the parameters) a re-entrance behavior when varying either the interaction strength or the disorder potential. At half filling, the Mott-Hubbard insulating phase is always separated from the metallic phase by an intermediate (Mott-Hubbard assisted) Anderson insulating phase.
- A comparison with other numerical studies on the Anderson-Hubbard model shows a good agreement, qualitatively and, in many cases, even quantitatively, proving the validity of our approach in the regime of strong disorder, $\Delta \gg t$.

Chapter 8

Cold atomic gases in random potentials

Having so far focused our discussion on electrons in disordered materials, we will now turn to a different physical system, where interactions and, particularly, transport in a disordered environment also play an important role.

During the last 10-15 years, the originally distinct fields of condensed matter physics and many-body physics, respectively, and atomic physics came successively closer into contact. In particular, the discovery of Bose-Einstein condensation (BEC) [AEM+95, BSTH95, DMA+95], and the use of optical lattices [DJ98, GWO99], made ultracold gases a new laboratory for quantum many-body physics. For instance, the Hubbard model can be simulated by experiments on ultracold, neutral atoms in an optical lattice [JBC+98] (cf. Ch. 9). Generally, the main advantage of optical setups over conventional materials is the high tunability of almost all parameters, be it the lattice depth by varying the field strength or the interaction potential by using Feshbach resonances [TVS93, CGJTnt]. Also tunable non-periodic, random potentials can be created, e.g., by using laser speckles [LFM+05] or bichromatic lattices [FLG+07]. For recent reviews on the very rapidly developing field of probing many-body physics by ultracold gases, we refer to, e.g., [LSA+07, BDZ08, KZ08, GPS08].

8.1 Typical experimental setup

Most experiments on cold atomic gases are done by using the time-of-flight technique, all of them principally following a very similar scheme [BDZ08]. A dilute gas of atoms is confined by an optical trapping potential, which is built-up by crossing laser beams, and cooled down to ultralow temperatures. Depending on the experimental issue, the gas is then transferred into an optical (lattice) potential. After having switched off the optical potential, the gas expands either

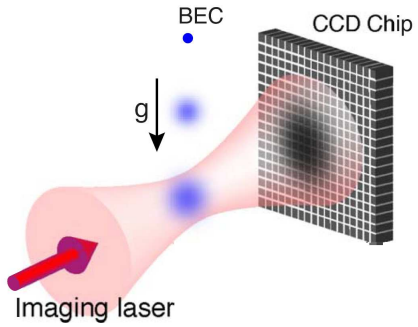

Figure 8.1: Sketch of the experimental setup for a time-of-flight measurement on an expanding BEC. Picture taken from [BDZ08].

ballistically or within a further external optical potential, e.g., a disordered potential. After a certain time of flight, an image of the gas cloud is taken by using an absorption imaging method (for a sketch of the experimental setup see Fig. 8.1). Repeating the experiment under the same conditions many times allows for a statistical analysis of the absorption pictures. In that way, information is obtained about the density and momentum distribution of the gas cloud, respectively, which allows for conclusions regarding the quantum state of the gas *before* the release from the trap.

Among the spectacular measurements by time-of-flight experiments were the first detection of Anderson localization of matter waves [BJZ+08, RDF+08], the superfluid-Mott insulator transition within the Bose-Hubbard model [GME+02] (cf. Ch. 9), and the direct observation of the statistics of fermions [RBO+07] and bosons [FGW+05].

Although experiments on ultracold gases offer a fantastic opportunity to examine important problems of many-body and condensed matter physics, they also differ in some important aspects from 'usual' condensed matter systems. Considering the (transport) properties of solids, the number of conduction electrons is typically large enough to assume the system being in the thermodynamic limit. In contrast, the number of atoms within an atomic gas cloud is typically of the order of $10^4 - 10^6$ (see, e.g., [FGW+05, BJZ+08]). Furthermore, in time-of-flight experiments, all particles contribute to the absorption image of the density distribution, even for gases of fermionic atoms. However, in solids, at least in bulk systems, most often only conduction electrons at the Fermi level, or within a small energy interval around the Fermi level, contribute.

Within this chapter, we will concentrate on the concrete example of a diffusively expanding gas cloud in a random potential, in two and three dimensions.

Here, we will assume that the particles' mean free paths are significantly larger than the trapping potential, which initially confines the gas cloud, i.e., we assume the trap to be free of disorder. Furthermore, we will assume that the gas is only weakly interacting, such that we can neglect interparticle interactions during the expansion process.
Besides the average density, we are particularly interested in the "atomic speckles": complicated, highly irregular, wave intensity patterns formed because of the scattering of the particles' wave functions off the inhomogeneities of the disorder potential. Speckles are also well known from optics, when light is propagating in a disordered dielectric medium, and from disordered electronic conductors, where, due to electron scattering on impurities, a random distribution of electron density and currents is established within the sample, manifesting themselves, e.g., in the sample-to-sample conductance fluctuations [AM07]. The speckles are characterized by higher correlation functions, such as the density-density correlation function [AM07].

8.2 Diffusing Fermi gas

8.2.1 Average particle density

We consider N fermions with spin S, initially occupying the N lowest energy eigenstates in a trap. Assuming zero temperature and neglecting interactions the quantum expectation value of the particle density is

$$\langle \hat{n}(r) \rangle_0 \;=\; g_s \sum_n \Theta(\varepsilon_{\rm F} - \varepsilon_n) \left|\phi_n(r)\right|^2 , \tag{8.1}$$

where $g_s = 2S+1$ is the spin-degeneracy factor, $\phi_n(r)$ is the orbital part of an eigenstate in the trap and ε_n the corresponding eigenenergy.
At time $t = 0$ the Fermi gas is released from the trap and the single-particle wave functions start to evolve according to the Schrödinger equation

$$\mathrm{i}\,\partial_t \psi_n(r,t) \;=\; -\frac{1}{2m}\triangle\psi_n(r,t) \,+\, V(r)\,\psi_n(r,t)\,, \tag{8.2}$$

where $V(r)$ is the external static random potential and $\psi_n(r,t)$ the single-particle wave function with $\psi_n(r,0) = \phi_n(r)$. Its time evolution can be expressed by using the retarded Green's function, $G^R(r,R,t)$, of the Hamiltonian $\hat{H}$ of Eq. (8.2) [Sha08],

$$\begin{aligned} \psi_n(r,t) \;&=\; \langle r|\psi_n(t)\rangle \;=\; \langle r|e^{-\mathrm{i}\hat{H}t}|\phi_n\rangle \;=\; \int dR\,\langle r|e^{-\mathrm{i}\hat{H}t}|R\rangle\,\phi_n(R) \\ &=\; \int dR\; G^R(r,R,t)\,\phi_n(R). \end{aligned} \tag{8.3}$$

Then, the quantum expectation value of the particle density, at time t, for a given realization of randomness is equal to

$$\begin{aligned}\langle \hat{n}(r,t)\rangle &= g_s \sum_n \Theta(\varepsilon_{\rm F}-\varepsilon_n)\left|\psi_n(r,t)\right|^2 \\ &= g_s \int dR \int dR'\, G^R(r,R,t)\, G^A(r,R',t) \sum_n \Theta(\varepsilon_{\rm F}-\varepsilon_n)\,\phi_n(R)\,\phi_n^*(R').\end{aligned} \tag{8.4}$$

At times $t<0$ the system is described by the Hamiltonian $\hat{H}_{trap}$, whose eigenfunctions are the $\phi_n(r)$. The corresponding retarded Green's function shall be denoted by $\mathcal{G}^R(r,R,t)$ and should not be confused with the function $G^R(r,R,t)$ which describes propagation from point R to an observation point r, upon the release of the gas from the trap. Using the resolvent representation of the Green's function (cf. Eq. D.2)

$$\mathcal{G}^R(R,R',\varepsilon) = \langle R|(\varepsilon-\hat{H}_{trap}+{\rm i}0^+)^{-1}|R'\rangle = \sum_n \frac{\phi_n(R)\phi_n^*(R')}{\varepsilon-\varepsilon_n+{\rm i}0^+}, \tag{8.5}$$

the sum in Eq.(8.4) can conveniently be written as

$$\begin{aligned}\sum_n \Theta(\varepsilon_{\rm F}-\varepsilon_n)\,\phi_n(R)\phi_n^*(R') &= \int_{-\infty}^{\varepsilon_{\rm F}} d\varepsilon \sum_n \phi_n(R)\phi_n^*(R')\,\delta(\varepsilon-\varepsilon_n) \\ &= -\frac{1}{\pi}\int_{-\infty}^{\varepsilon_{\rm F}} d\varepsilon\, {\rm Im}\mathcal{G}^R(R,R',\varepsilon).\end{aligned} \tag{8.6}$$

By averaging over disorder realizations, the density becomes

$$\overline{\langle \hat{n}(r,t)\rangle} = -\frac{g_s}{\pi}\int dR \int dR'\, \overline{G^R(r,R,t)\, G^A(r,R',t)} \int_{-\infty}^{\varepsilon_{\rm F}} d\varepsilon\, {\rm Im}\mathcal{G}^R(R,R',\varepsilon). \tag{8.7}$$

The last integral in Eq. (8.7) contains information about the initial state of the gas in the trap. The product of the two propagators, $\overline{G^R\,G^A}$, propagates this information in space and time.

In the diffusion regime, which is considered here, the average product of the two Green's functions can be evaluated as described in Appendix A.3, yielding

$$\begin{aligned}\overline{\langle \hat{n}(r,t)\rangle} &= \frac{g_s}{\pi^2}\int d\epsilon \int dR\; P_\epsilon(r-R,t) \int d\Delta R\; {\rm Im}\overline{G^R}(\Delta R,\epsilon) \\ &\quad \times \int_{-\infty}^{\varepsilon_{\rm F}} d\varepsilon\, {\rm Im}\mathcal{G}^R(R+\Delta R/2, R-\Delta R/2,\varepsilon),\end{aligned} \tag{8.8}$$

where (Eq. (A.28))

$$P_{\epsilon}(r,t) \;=\; \frac{e^{-r^2/4D_{\epsilon}t}}{(4\pi D_{\epsilon}t)^{d/2}} \tag{8.9}$$

is the diffusion propagator, in d dimensions ($d = 2, 3$) and D_{ϵ} is the diffusion coefficient for a particle at energy ϵ. The average Green's function is given by [AM07] (Eq. A.24)

$$\bar{G}(\Delta R,\epsilon) \;=\; G^{R,0}(\Delta R,\epsilon)\, e^{-\Delta R/2l_{\epsilon}}, \tag{8.10}$$

where $G^{R,0}$ is the free retarded Green's function and l_{ϵ} is the particle mean free path. Eqs. (8.9) and (8.10) for P and $\bar{G}$ are only valid for sufficiently large values of the energy parameter ε, namely if $k_{\epsilon}l_{\epsilon} \gg 1$, where $k_{\epsilon} = \sqrt{2m\epsilon}$. Therefore, $k_{\mathrm{F}}l_{\mathrm{F}}$ is the essential parameter which determines the overall behavior of the gas, after switching off the trap, where k_{F} and l_{F} denote the value of the Fermi momentum and of the mean free path at the Fermi energy ε_{F}, respectively. Only for $k_{\mathrm{F}}l_{\mathrm{F}} \gg 1$, which we assume here, most of the atomic cloud will diffuse away from the trap. (A similar condition, with the chemical potential μ replacing the Fermi energy, is required for the diffusive behavior of a BEC cloud [Sha07].)

To facilitate analytic treatment, we assume that the size of the trap is much smaller than its distance from the observation point r. Then, choosing the coordinate origin somewhere inside the trap, we can set $R = 0$ in the argument of the diffusion propagator, writing it simply as $P_{\epsilon}(r,t)$. Moreover, since upon release from the trap, each particle goes on its own (long) diffusive trajectory, the actual shape of the trap is of no importance. It is convenient to replace the actual harmonic trap by a cubic trap of size L, with periodic boundary conditions, which yields

$$\mathrm{Im}\mathcal{G}^R(R+\Delta R/2, R-\Delta R/2,\varepsilon) \;=\; \int \frac{dk}{(2\pi)^d}\, \mathrm{Im}\mathcal{G}^R(p,\varepsilon)\, e^{-\mathrm{i}k\Delta R}. \tag{8.11}$$

Thus, after inserting Eq. (8.11) into Eq. (8.8), we get

$$\overline{\langle\hat{n}(r,t)\rangle} \;=\; \frac{g_s}{\pi^2}\int d\epsilon\; P_{\epsilon}(r,t)\int dR\int\frac{dk}{(2\pi)^d}\,\mathrm{Im}\overline{G^R}(k,\epsilon)\int_{-\infty}^{\varepsilon_{\mathrm{F}}} d\varepsilon\,\mathrm{Im}\mathcal{G}^R(k,\varepsilon) \tag{8.12}$$

$$\;=\; \frac{g_s V_{trap}}{\pi^2}\int d\epsilon\; P_{\epsilon}(r,t)\int\frac{dk}{(2\pi)^d}\,\mathrm{Im}\overline{G^R}(k,\epsilon)\int_{-\infty}^{\varepsilon_{\mathrm{F}}} d\varepsilon\,\mathrm{Im}\mathcal{G}^R(k,\varepsilon), \tag{8.13}$$

with V_{trap} being the trap volume.
Since we assume no disorder in the trap, it follows that $\mathrm{Im}\mathcal{G}^R(k,\varepsilon) = -\pi\delta(\varepsilon-\varepsilon_k)$

and integration over ε results in a step function $\Theta(k_{\rm F}-k)$. Furthermore, since $k_{\rm F}l_{\rm F} \gg 1$, it follows that the weak disorder condition, $k_\epsilon l_\epsilon \gg 1$, is satisfied for the great majority of k's in Eq. (8.13). Therefore, $\mathrm{Im}\bar{G}(k,\epsilon)$ can be approximated by $\mathrm{Im}\bar{G}(k,\epsilon) \approx -\pi\delta(\epsilon-\epsilon_k)$ and integration over ϵ can be carried out,[1] resulting in the final expression for the average particle density

$$\overline{\langle\hat{n}(r,t)\rangle} \;=\; g_s V_{trap} \int\limits_{k<k_{\rm F}} \frac{dk}{(2\pi)^d}\; P_{\epsilon_k}(r,t)\,, \tag{8.14}$$

where $\epsilon_k = k^2/2m$.

Eq. (8.14) has a very simple interpretation: Particles, prior to their release from the trap, occupy all states up to $k_{\rm F}$, with $L^d dk/(2\pi)^d$ being the number of particles in the d-dimensional element dk. When the trap is switched off, particles start diffusing and $P_{\epsilon_k}(r,t)$ is the probability density that a particle with momentum k will reach point r in time t. Integration over k gives the average particle density $\overline{\langle\hat{n}(r,t)\rangle}$. An equation similar to (8.14) also exists for a BEC [Sha07].
As particles at low energies are always strongly localized by disorder (cf. Ch. 3) some fraction of the released particles will not propagate by diffusion but will remain localized near their original location [Sha07]. However, for $k_{\rm F}l_{\rm F} \gg 1$ the fraction of such particles and the corresponding correction to Eq. (8.14) are small and we can ignore this effect here.

The disorder-averaged particle density, Eq. (8.14), is a quite featureless, homogenous function. However, as has been particularly emphasized in [Leg01, ADL04], a single imaging experiment (with sufficient resolution) does not measure $\langle\hat{n}(r,t)\rangle$ but rather one particular event, i.e., some particular density pattern, $n(r,t)$, whose probability is dictated by the many-body wave function of the system. Thus, a single image contains much more information, which gets lost, if one simply averages over many experimental runs. To extract this information, one must instead consider higher correlations functions like the density-density correlation function, $\langle\hat{n}(r,t)\hat{n}(r',t)\rangle$, which is subject of the following section.

8.2.2 Density-density correlation function

We now turn to the calculation of the density-density correlation function, $\langle\hat{n}(r,t)\,\hat{n}(r',t)\rangle$. Experimentally, this correlation function can be measured from time-of-flight images by averaging the product $n(r)n(r')$ over many realizations, for fixed r, r' and t. It should be noted, however, that already a single image, although noisy and "grainy", contains information about the density-density correlation

[1] We numerically checked that for $N = 10^4 \ldots 10^5$ particles, the step functions are indeed excellent approximations (cf. discussion in Sec. 8.1).

function. This information will be revealed by taking the product $n(r)n(r+\Delta r)$ and averaging it over many points r, for fixed Δr (the equivalence of the two averaging procedures constitutes the "ergodic assumption" in mesoscopic physics [AM07]).

Let us first note that, already in the absence of disorder, a Fermi gas possesses some subtle density correlations of purely quantum nature, because of the Pauli exclusion principle [LL80, Cas08]. For fermions confined to a trap of size L, the density-density correlation function exhibits rapidly decaying oscillations with a characteristic period $\Delta x_0 \approx k_{\rm F}^{-1}$ [LL80]. For instance, considering fermions in a three-dimensional box of side length L, whose wave functions fulfill periodic boundary conditions, a short calculation yields the normalized correlation function [LL80]

$$\begin{aligned} I(r,r',t) &\equiv \frac{\langle\hat{n}(r,t)\hat{n}(r',t)\rangle - \langle\hat{n}(r,t)\rangle\langle\hat{n}(r',t)\rangle - \delta(r-r')\langle\hat{n}(r,t)\rangle}{\langle\hat{n}(r,t)\rangle\langle\hat{n}(r',t)\rangle} \\ &= -\frac{9}{g_s}\frac{[\sin(k_{\rm F}r) - (k_{\rm F}r)\cos(k_{\rm F}r)]^2}{(k_{\rm F}r)^6}. \end{aligned} \tag{8.15}$$

(For a harmonic trap the effective trap size is determined by $m\omega^2 L^2 \simeq \varepsilon_{\rm F}$, which gives $L \simeq N^{1/2d}/\sqrt{m\omega}$.)

When the gas is released from the trap it starts expanding. For the case of a ballistically (freely) expanding gas, and, for times $t > (L/v_{\rm F}) \equiv t_0$, the size of the cloud grows linearly with time and so does the correlation length $\Delta x(t) \approx \Delta x_0 \cdot t/t_0$ [NG07]. Thus, roughly speaking, the free, ballistic expansion amplifies the scale of correlations by the factor t/t_0 and keeps the correlation length on the scale of the mean interparticle distance. As we will see below, in the presence of a random potential, i.e., when the expansion is diffusive instead of ballistic, the picture is different: The size of the atomic cloud grows as $\sqrt{t}$ (cf. Eq. (8.14)) whereas the short-range correlations do not get amplified at all.

The density-density correlation function in the presence of disorder is defined as

$$C(r,r',t) = \overline{\langle\hat{n}(r,t)\hat{n}(r',t)\rangle} - \overline{\langle\hat{n}(r,t)\rangle}\,\overline{\langle\hat{n}(r',t)\rangle} - \delta(r-r')\overline{\langle\hat{n}(r,t)\rangle}. \tag{8.16}$$

The last term describes trivial correlations, which already exist in a classical ideal gas and which are commonly subtracted, in order to isolate the nontrivial correlations [LL80]. There are two kinds of averaging in (8.16): The quantum mechanical averaging, for a given realization of disorder, and averaging over the

ensemble of different realizations. The first averaging leads to [LL80]

$$\langle \hat{n}(r,t)\hat{n}(r',t)\rangle = \sum_{\sigma_1,\sigma_2}\sum_{n,m,k,l} \psi_n^*(r,t)\,\psi_k(r,t)\,\psi_m^*(r',t)\,\psi_l(r',t)\langle c_{n\sigma_1}^\dagger c_{k\sigma_1} c_{m\sigma_2}^\dagger c_{l\sigma_2}\rangle \tag{8.17}$$

$$= -\sum_{\sigma_1,\sigma_2}\sum_{n,m} \psi_n^*(r,t)\,\psi_k(r,t)\,\psi_m^*(r',t)\,\psi_l(r',t)\langle c_{n\sigma_1}^\dagger c_{m\sigma_2}^\dagger c_{k\sigma_1} c_{l\sigma_2}\rangle + \sum_{\sigma_1}\sum_{n,l} \psi_n^*(r,t)\,\psi_l(r,t)\langle c_{n\sigma_1}^\dagger c_{l\sigma_1}\rangle\,\delta(r-r') \tag{8.18}$$

$$= g_s^2 \sum_n \Theta(\varepsilon_{\rm F}-\varepsilon_n)\left|\psi_n(r,t)\right|^2 \sum_m \Theta(\varepsilon_{\rm F}-\varepsilon_m)\left|\psi_m(r',t)\right|^2 - g_s\left|\sum_n \Theta(\varepsilon_{\rm F}-\varepsilon_n)\psi_n^*(r,t)\psi_n(r',t)\right|^2 + g_s\delta(r-r')\sum_n \Theta(\varepsilon_{\rm F}-\varepsilon_n)\left|\psi_n(r,t)\right|^2, \tag{8.19}$$

where the absence of overbars indicates that this expression refers to a specific realization of the random potential.
Next, we must average Eq. (8.17) over the disorder. This involves averaging products of four single-particle wave functions. For short-range correlations, i.e., on a scale smaller than the mean free path ($|r-r'|<l_\varepsilon$), such averages decouple into products of pairwise averages [AM07]. For instance,

$$\overline{\psi_n^*(r,t)\psi_n(r',t)\psi_m^*(r',t)\psi_m(r,t)} \approx \overline{\psi_n^*(r,t)\psi_n(r',t)}\;\overline{\psi_m^*(r',t)\psi_m(r,t)} + \overline{\psi_n^*(r,t)\psi_m(r,t)}\;\overline{\psi_m^*(r',t)\psi_n(r',t)}. \tag{8.20}$$

Performing such decoupling in Eq. (8.17), Eq. (8.16) becomes

$$C(r,r',t) = \sum_{n,m}\Theta(\varepsilon_{\rm F}-\varepsilon_n)\Theta(\varepsilon_{\rm F}-\varepsilon_m)\left[-g_s A_{nn}(r,r',t)A_{mm}^*(r,r',t) - g_s A_{nm}(r,r,t)A_{nm}^*(r',r',t) + g_s^2\left|A_{nm}(r,r',t)\right|^2\right], \tag{8.21}$$

where

$$A_{nm}(r,r',t) \equiv \overline{\psi_n^*(r,t)\psi_m(r',t)}. \tag{8.22}$$

The first term in Eq. (8.21) describes quantum correlations, due to the Pauli exclusion principle. In particular, for $r'\to r$, it approaches the value $-g_s\overline{\langle\hat{n}(r,t)\rangle}^2$ and, thus, it is proportional to N^2. The third term is of "classical" origin, in the sense that it originates from the interference between multiply scattered waves. It contributes positive correlations, similarly to speckle pattern in optics. However,

in contrast to a single frequency laser speckle, here there are many waves with different frequencies. Since contributions from different frequencies should be added incoherently, i.e., intensities (rather than amplitudes) are summed up, the third term is proportional to N and will be neglected. The second term in Eq. (8.21) is a combination of quantum and classical correlations. Its sign and the factor g_s originate from the exclusion principle. However, since wave functions at different energies are essentially uncorrelated, this term is also proportional to N and can be neglected in the large-N limit. Thus, keeping only the first term in Eq. (8.21), we obtain

$$C(r,r',t) \;=\; -g_s \left| \sum_n \Theta(\varepsilon_{\rm F}-\varepsilon_n) A_{nn}(r,r',t) \right|^2 \;\equiv\; -g_s \left| F(r,r',t) \right|^2 . \quad (8.23)$$

The function

$$F(r,r',t) \;\equiv\; \sum_n \Theta(\varepsilon_{\rm F}-\varepsilon_n)\, \overline{\psi_n^*(r,t)\psi_n(r',t)} \quad (8.24)$$

can be expressed in terms of the Green's functions, in complete analogy with the earlier derivation of the average density (see Appendix A.3). The only difference is that now there are two "observation points", r and r'. The resulting expression for $F(r,r',t)$ (cf. Eq. (8.7)) is

$$F(r,r',t) \;=\; -\frac{1}{\pi}\int dR \int dR'\, \overline{G^R(r,R,t)\, G^A(r',R',t)} \int_{-\infty}^{\varepsilon_{\rm F}} d\varepsilon\, {\rm Im}\mathcal{G}(R',R,\varepsilon). \quad (8.25)$$

In order for the average product of Green's functions not to be exponentially small, the pair of points r, r' should not be separated by more than the mean free path. On the other hand, $|r-R|$ is much larger than $l_{\rm F}$. The computation of the average product in Eq. (8.25) is explained in detail in Appendix A.3 and yields

$$\overline{G^R(r,R,t)\, G^A(r',R',t)} \;=\; -\frac{1}{\pi}\int d\epsilon\, f(\Delta r,\epsilon)\, P_\epsilon\,(r,R,t) {\rm Im}\bar{G}(r-R',\epsilon), \quad (8.26)$$

where the extra factor $f(\Delta r,\varepsilon)$, as compared to Eq. (A.39), is given by

$$f(\Delta r,\epsilon) \;=\; -\frac{1}{\pi N_0(\epsilon)} {\rm Im}\bar{G}(\Delta r,\epsilon)\,, \quad \Delta r \;=\; |r-r'|\,. \quad (8.27)$$

Following the same line of derivation as for the average density, Eq. (8.14), we arrive at

$$F(r,r',t) \;=\; V_{trap} \int\limits_{k<k_{\rm F}} \frac{dk}{(2\pi)^d}\, P_{\epsilon_k}(r,t) f(\Delta r,\epsilon_k)\,. \quad (8.28)$$

For $d = 3$ (Eqs. (A.23) and (A.24)),

$$f(\Delta r, \epsilon_k) \;=\; \frac{\sin(k\Delta r)}{k\Delta r}\exp(-\Delta r/2l_{\epsilon_k}). \tag{8.29}$$

While the kernel P_{ϵ_k} and the mean free path l_{ϵ_k} are slowly varying with k, the function $f(\Delta r, \epsilon_k)$, for $\Delta r \gg k_{\rm F}^{-1}$, contains a rapidly oscillating factor within the integration region in Eq. (8.28). Taking the "slow" functions out of the integral and computing the remaining integral we obtain

$$C(r,r',t) \;=\; -g_s\, V_{trap}^2\, P_{\varepsilon_{\rm F}}(r,t)^2 e^{-\Delta r/l_{\rm F}} \frac{k_{\rm F}^6}{4\pi^4} \frac{\left[\sin(k_{\rm F}\Delta r) \;-\; \Big(k_{\rm F}\Delta r\Big)\cos(k_{\rm F}\Delta r)\right]^2}{\Big(k_{\rm F}\Delta r\Big)^6}, \tag{8.30}$$

where P_ϵ and l_ϵ are taken at $\epsilon = \varepsilon_{\rm F}$. It is convenient to normalize the correlation function by the average density which yields

$$\begin{aligned} I(r,r',t) \;&\equiv\; \frac{C(r,r',t)}{\overline{\langle\hat{n}(r,t)\rangle}\;\overline{\langle\hat{n}(r',t)\rangle}} \\ &=\; -\frac{9}{g_s} e^{-\Delta r/l_{\rm F}} \frac{\left[\sin(k_{\rm F}\Delta r) \;-\; \Big(k_{\rm F}\Delta r\Big)\cos(k_{\rm F}\Delta r)\right]^2}{\Big(k_{\rm F}\Delta r\Big)^6}\,. \end{aligned} \tag{8.31}$$

The analogous calculation for $d = 2$ yields

$$I(r,r',t) \;=\; -\frac{4}{g_s} e^{-\Delta r/l_{\rm F}} \frac{{\rm J}_1(k_{\rm F}\Delta r)^2}{\Big(k_{\rm F}\Delta r\Big)^2}\,, \tag{8.32}$$

where ${\rm J}_1(k_{\rm F}\Delta r)$ is the Bessel function of the first kind.

In Fig. 8.2, the normalized density-density correlation functions (Eqs. (8.31) and (8.32)) are plotted. The solid lines in this figure represent the corresponding functions obtained by computing the integral in Eq. (8.28) numerically, without taking the "slow" functions out of the integral. In this computation a white noise random potential has been used which yields $l_\epsilon = const$ in three dimensions and $l_\epsilon \sim \sqrt{\epsilon}$ in two dimensions (this implies that the diffusion coefficient is proportional to $\sqrt{\epsilon}$ and ϵ in three and two dimensions, respectively). Fig. 8.2 demonstrates that for the decaying envelope of $I(\Delta r)$ the agreement between the numerically exact results and the approximate expressions, Eqs. (8.31) and (8.32), is quite good. For the oscillations the agreement is only qualitative. Due to the rapid decay of the envelope function, the oscillations are rather small and

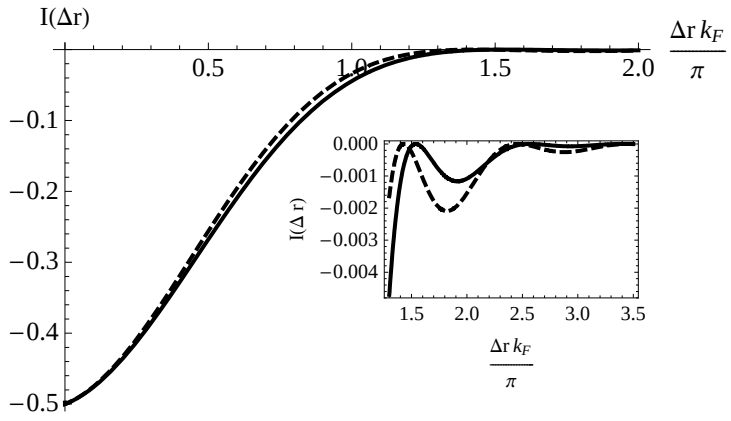

(a)

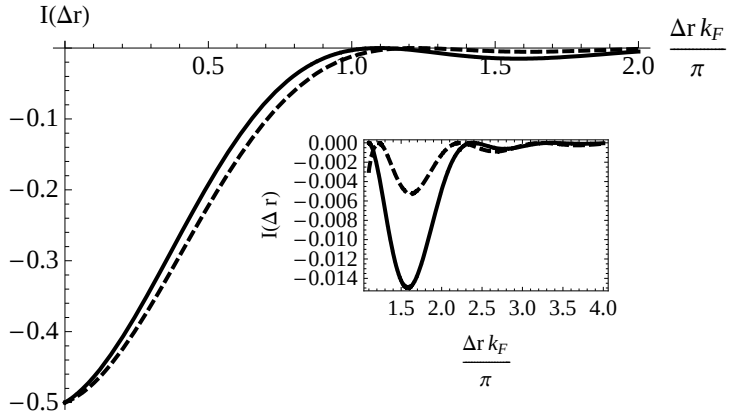

(b)

Figure 8.2: The normalized density-density correlation function $I(\Delta r, t)$ of a Fermi gas with $g_s = 2$, for $k_{\rm F} l_{\rm F} = 10$, $r = 50 l_{\rm F}$ and $t = 3r^2/(2dD_{\varepsilon_{\rm F}})$. (a) $d = 3$ (b) $d = 2$. The dashed curves in (a) and (b) correspond to Eqs. (8.31) and (8.32), respectively. The solid curves are the result of an exact numerical integration, as described in the text. The insets show the oscillating decay of $I(\Delta r, t)$ with increasing Δr.

clearly visible only on an amplified scale, as shown in the insets to the figure.

It is quite remarkable that, while the atomic cloud keeps expanding, the local normalized density correlations, Eqs. (8.31) and (8.32), do not depend on time. In particular, the characteristic length of oscillations, $\Delta r \sim k_{\rm F}^{-1}$, remains the same as for the gas in the trap, prior to its release (cf. Eq. 8.15)). This behavior is in sharp contrast to that for a free ballistic expansion, when the spatial oscillation period is growing linearly in time, just as the average interparticle distance [NG07]. The essential difference between the ballistic and diffusive cases can be traced to the evolution of the phase of a wave function. In the ballistic expansion the characteristic spatial period of a wave packet keeps increasing. (This statement can be easily verified by taking an initial wave packet of a Gaussian shape, $\phi(r) \sim \exp(-\frac{r^2}{a^2} + i\frac{r^2}{b^2})$, with $b \ll a$, whose time evolution is exactly soluble.) On the contrary, in the diffusive expansion the phase of a wave function gets randomized after few scattering events and no long-range order in the phase can be established.[2] An oscillating wave function with some period b, subjected to diffusive evolution, will locally look like a plane wave, with the same period, where "locally" means on a scale smaller than the mean free path. Thus, at any time t, the diffusing wave function can be viewed as made up of "patches" of plane waves, of size $l_{\rm F}$ each, but with no phase relation among different patches. This observation explains the somewhat counterintuitive behavior of the correlations, namely, that the correlation functions in Eqs. (8.31) and (8.32) remain stationary, while the interparticle distance increases under the expansion. This leads to an increase of the relative fluctuation of the particle number, in a given volume. For a homogeneous Fermi gas in equilibrium (in three dimensions) the particle number variance $\overline{\Delta N^2}$, in a certain volume, is not equal to the average number of particles $\overline{N}$ (in the same volume) but is proportional to $\overline{N}^{2/3} \log \overline{N}$ [ACP07, Cas08]. This means that, due to correlations, the Fermi gas possesses some kind of "rigidity". (The effect is particularly spectacular in 1D, where $\overline{\Delta N^2}$ grows only as $\log \overline{N}$). Free expansion of the gas, in the absence of disorder, does not affect this rigidity, because, as was already mentioned, the scale of correlations is amplified in exact proportion to the interparticle distance. The disorder disrupts this proportionality and leads to the destruction of rigidity and to the $\overline{\Delta N^2} = \overline{N}$ behavior (in the long time limit). Therefore, the image of a Fermi gas, expanding in the presence of disorder, should look more "grainy" than the image of a freely expanding gas. This effect might be observable experimentally.

[2] This is, of course, only approximatively correct. However, within the region of diffusion, where $r^2 \simeq dD_{\epsilon_{\rm F}} t$, next-to-leading-order corrections are negligible weak [CS08].

8.3 Diffusing Bose-Einstein condensate

So far, we have considered the dynamics of a degenerate Fermi gas. We finish this chapter by a brief discussion of the case of a Bose-Einstein condensate (BEC), expanding in the presence of a random potential. (For an introduction into the subject of Bose-Einstein condensation, see, e.g., [DGPS99, PS03].) Within the mean-field approach the BEC is described by a macroscopic wave function, $\Psi(\mathbf{r}, t)$, whose dynamics satisfies the Gross-Pitaevskii equation [DGPS99]

$$\begin{aligned} i\hbar\,\partial_t\,\Psi(r,t) &= -\frac{\hbar^2}{2m}\,\triangle\Psi(r,t) \,+\, V(\mathbf{r})\Psi(r,t) \\ &\quad + g|\Psi(r,t)|^2\Psi(r,t)\,, \end{aligned} \tag{8.33}$$

where g is the interaction parameter related to the scattering length (we again assume positive g, i.e., repulsive interactions). Eq. (8.33) describes the evolution of the condensate, in the random potential $V(r)$, upon its release from the trap. We assume an isotropic harmonic trap, characterized by a frequency ω. For weak randomness, we assume that the expansion can be separated into two distinct stages [SPCL$^+$07, Sha07, SMTS08]: a rapid ballistic "explosion", during the time of order $(1/\omega)$, followed by an essentially linear evolution. However, the influence of the nonlinearity is a subtle point and still an open question. In particular, this kind of argument would imply that in a one-dimensional system nonlinearity cannot destroy Anderson localization, which is heavily debated, see, e.g., [She93, FKS08, PS08, KKFA08, WZ09, FKS09a, FKS09b, VKF09] and references therein. However, in [CS09] it was at least shown that in first order perturbation theory in g, the interaction only induces a weak renormalization of the diffusion coefficient. Thus, we assume that the expansion process can at least approximately be described by this separation of time scales. The first stage then is dominated by the nonlinearity. At the second stage, however, most of the interaction energy has already been converted into the kinetic (flow) energy, so that the nonlinearity becomes weak and is neglected. Thus, below we consider the linear equation

$$i\hbar\,\partial_t\,\Psi(r,t) \;=\; -\frac{\hbar^2}{2m}\,\triangle\Psi(r,t) \,+\, V(r)\,\Psi(r,t). \tag{8.34}$$

The initial condition for this equation is supplied by the wave function $\Phi(r)$ at the end of the first stage of the expansion, i.e., at time of order $1/\omega$. Qualitatively, this wave function is of the form [Cas08, KSS96]

$$\Phi(r) \;=\; \mathcal{F}(r)\,\exp(ir^2/a_0^2), \tag{8.35}$$

where $a_0 = (\hbar/m\omega)^{1/2}$ is the oscillator size of the trap and $\mathcal{F}(r)$ is an envelope function which decays on the characteristic distance $R_0 \gg a_0$, where

R_0 is the initial size of the BEC in the trap. The envelope is often approximated by a Gaussian, $\mathcal{F}(r) = A\exp(-r^2/2R_0^2)$, or by the inverted parabola $\mathcal{F}(r) = A\sqrt{1-(r/R_0)^2}$, with A being the normalization constant.

The emerging linear problem, Eqs. (8.34) and (8.35), is considerably simpler than the fermionic problem treated above. This is because the BEC is described by a single coherent wave function which can be treated as a classical field. Within such mean-field description, there are no density fluctuations in the absence of disorder. The notion of density correlations, with their inherent statistical features, becomes meaningful only in the presence of an external random potential. Thus, the problem becomes similar to that considered in the theory of optical speckles, where a classical electromagnetic wave or a scalar wave propagates and gets scattered on a random potential [AM07]. The essential difference is that in the theory of optical speckles one usually assumes a monochromatic field, whereas the BEC wave function, Eq. (8.34), contains a broad spectrum of wave numbers. For a monochromatic field $\psi_\omega(r)$ with a wave number k_ω, the disorder-induced intensity-intensity correlation function,

$$C_\omega(r,r') = \overline{|\psi_\omega^*(r)\psi_\omega(r')|^2}, \tag{8.36}$$

was calculated in [Sha86b, PS89],

$$C_\omega(r,r') \;=\; \overline{n_\omega(r)}\,\overline{n_\omega(r')}\,e^{-\Delta r/l_\omega}\,\begin{cases} \left(\frac{\sin(k_\omega\Delta r)}{k_\omega\Delta r}\right)^2 & , \quad d=3 \\ J_0^2(k_\omega\Delta r) & , \quad d=2 \end{cases}, \tag{8.37}$$

where $\overline{n_\omega(r)} = \overline{\left|\psi_\omega(r)\right|^2}$ is the average intensity of the wave.

The extension to the nonmonochromatic case of a BEC is quite straightforward. Let us start with the average density of the BEC, $\overline{n(r)}$. The BEC wave function at time t is given by

$$\Psi(r,t) \;=\; \int dR\, G^R(r,R,t)\,\Phi(R). \tag{8.38}$$

Using (A.39), one obtains in the large t (and large r) limit [SMTS08]

$$\begin{aligned} \overline{n(r)} \;&=\; \overline{|\,\Psi(r,t)\,|^2} \\ &=\; -\frac{1}{\pi}\int d\epsilon\, P_\epsilon\,(r,t)\int \frac{dk}{(2\pi)^d}\,\mathrm{Im}\overline{G_k^R}(\epsilon)\,|\tilde{\Phi}(k)|^2 \end{aligned} \tag{8.39}$$

where $\tilde{\Phi}(k)$ is the Fourier transform of the initial condition (8.35). The (equal time) field-field correlation function, $C_{\rm field}(\Delta r,t) \equiv \overline{\Psi^*(r,t)\Psi(r',t)}$, differs from Eq. (8.39) only by an extra factor, $f(\Delta r,\epsilon)$, defined in (8.27),

$$C_{\rm field}(\Delta r,t) \;=\; -\frac{1}{\pi}\int d\epsilon\, P_\epsilon\,(r,t)\int \frac{dk}{(2\pi)^d}\,f(\Delta r,\epsilon)\,\mathrm{Im}\bar{G}(k,\varepsilon)\,|\tilde{\Phi}(k)|^2\,. \tag{8.40}$$

Approximating, as above, $\mathrm{Im}\overline{G_k^R}(\epsilon) = -\pi\delta(\epsilon - \epsilon_k)$, we obtain the final expression for the field-field correlation function,

$$C_{\rm field}(\Delta r, t) \;=\; \int \frac{dk}{(2\pi)^d}\, P_{\epsilon_k}(r,t)\, f(\Delta r, \epsilon_k)\, |\tilde{\Phi}(k)|^2\,. \tag{8.41}$$

The short-range density-density correlation function is given by

$$\begin{aligned} C(\Delta r, t) &\equiv \overline{n(r)n(r')} - \overline{n(r)}\,\overline{n(r')} - \delta\,(r-r')\,\overline{n(r)} \\ &= |C_{\rm field}(\Delta r, t)|^2\,. \end{aligned} \tag{8.42}$$

Eqs. (8.41) and (8.42), supplemented by the expression Eq. (8.27) for the f-function, provide the general solution for the density correlations in a BEC diffusing in a weak random potential.

To get an estimate for the three-dimensional normalized correlation function,

$$I(\Delta r, t) \;=\; \frac{C(\Delta r, t)}{\overline{n(r',t)}\,\overline{n(r',t)}}, \tag{8.43}$$

we assume a Gaussian envelope,

$$\Phi(r) \;=\; \frac{1}{2\pi^{3/4} R_0^{3/2}}\, e^{-\frac{r^2}{2R_0^2} + \mathrm{i}\frac{r^2}{a_0^2}} \;\equiv\; A\, e^{-(r/r_0)^2}. \tag{8.44}$$

Then the Fourier transform of the BEC wave function takes the form

$$\tilde{\Phi}(k) \;=\; A\, r_0^3\, e^{-(kr_0/2)^2}, \tag{8.45}$$

such that

$$\left|\tilde{\Phi}(k)\right|^2 \;\approx\; \frac{2}{\pi^{3/2} k_0^3}\, e^{-(k/k_0)^2}, \tag{8.46}$$

where $k_0 = 2R_0/a_0^2 \simeq 1/\xi$, ξ being the healing length of the BEC [DGPS99].

The numerical evaluation of Eq. (8.43) (see Fig. 8.3) shows that, quite similar to the case of the Fermi gas, where $I(\Delta r, t)$ decayed on the length scale of the Fermi wavelength, $I(\Delta r, t)$ decays on a scale $\Delta r \sim \xi$, i.e., the relevant length scale of the system *in the trap*. This scale remains nearly constant in time. Since the "cutoff function", $|\tilde{\Phi}(k)|^2$, under the integral in Eq. (8.41) is not as sharp as the step function in Eq. (8.28), the oscillations of the normalized correlation function are even weaker than for the fermionic case. The short-range correlations, shown in Fig. 8.3, imply that the image of a condensate, diffusing in a weak random potential, should exhibit a random pattern of particle density (speckle). The

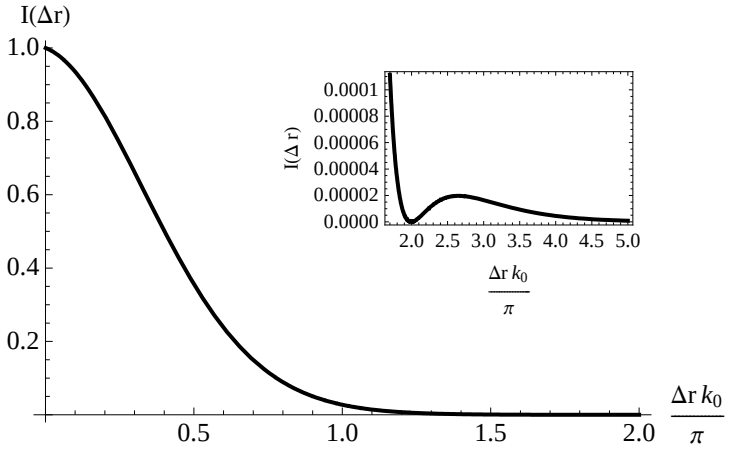

(a)

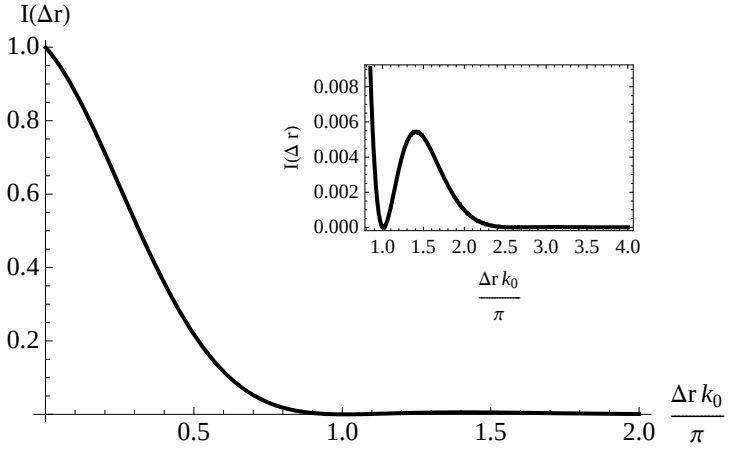

(b)

Figure 8.3: The normalized density-density correlation function $I(\Delta r, t)$ of a BEC for (a) $d = 3$ and (b) $d = 2$. As in Fig. 8.2 the parameters were set to $k_0 l_0 = 10$, $r = 50 l_0$, $t = 3r^2/(2dD_{k_0})$, $D_k = D_{k_0}(k/k_0)^{4-d}$, $l_k = l_0\,(k/k_0)^{3-d}$.

typical size of each speckle spot is of the order of a few healing lengths.

As in the case of the expanding Fermi gas, some fraction of the condensate will presumably get caught by disorder [Sha07]. However, for weak disorder, and, in 2D for length scales shorter than the localization length, and time scales shorter than the localization time [SMTS08], this fraction will be small and the corresponding corrections do not significantly alter the results from above. In addition, we assumed in both cases a Gaussian white noise disorder potential (cf. Appendix A). However, in experiments the disorder potential often possesses a finite correlation length, in particular, if speckle potentials are used [SPCL$^+$07]. Nevertheless, our results remain qualitatively correct, as long as the correlation length remains shorter than the de-Broglie wavelength of the atoms.

Chapter 9

Disordered Bose-Hubbard model

Collisions of atoms in a Fermi gas are strongly suppressed for atoms within the same spin state due to the Pauli exclusion principle. Therefore, thermalization is less efficient than for a Bose gas and the evaporative cooling-down of a Fermi gas to ultra low temperatures is a formidable task [Jin02, GPS08]. For that reason, most (time-of-flight) experiments on ultracold gases have been done for bosons yet, and experiments on (interacting) Fermions are less explored [KZ08]. In particular, the Bose-Hubbard model has been, and still is an active area of research, which has been shown [JBC$^+$98] to describe a bose gas in a deep optical potential. Thus, a natural and interesting question would be whether our analysis of the Anderson-Hubbard model for electrons (fermions) can also be applied to bosons.

9.1 Phase diagram of the disordered Bose-Hubbard model

In the context of bosons, the Anderson-Hubbard model is usually referred to as the *disordered Bose-Hubbard model*, and so we will do the same in the following. In complete analogy to Eq. (5.4) and (7.41), respectively, its Hamiltonian for spinless bosons reads

$$\hat{H}_{BH} \;=\; \sum_{i\sigma}(\varepsilon_i - \mu) b_i^\dagger b_i \;+\; \frac{U}{2}\sum_i \hat{n}_i(\hat{n}_i - 1) \;-\; t\sum_{<i,j>} b_i^\dagger b_j, \qquad (9.1)$$

where $b_i^\dagger, b_i$ are Bose creation and annihilation operators, and $\hat{n}_i = b_i^\dagger b_i$.

This bosonic version of the disordered Hubbard model was brought into the focus of research by the seminal works [GS88, FWGF89], and was originally discussed in the context of, e.g., superfluid ^{4}He in porous media and granular superconductors [FWGF89]. Since then it has attracted a lot of attention, not only because

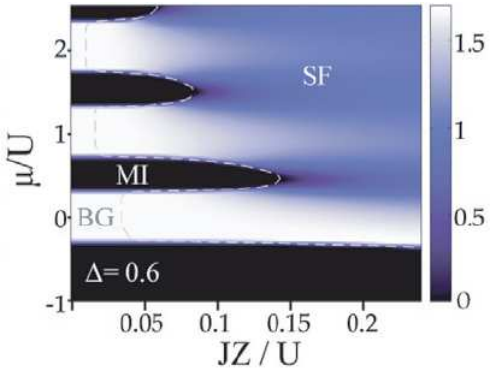

Figure 9.1: Phase diagram of the Bose-Hubbard model for fixed disorder strength, $\Delta/U = 0.6$, at zero temperature including a Mott-insulating (MI), a superfluid (SF) and a Bose glass (BG) phase. $J \equiv t$ is the hopping amplitude and Z denotes the coordination number ($Z = 2d$ for a hypercubic lattice in d dimensions). Plot taken from [BH09].

of its physical applications, but particularly also because of the theoretical challenge to understand its interesting, highly non-trivial physical properties. (For a recent reference with special emphasize on the application to atomic gases see, e.g., [LSA+07].)

Most significantly, the Bose-Hubbard model differs from its fermionic analog in undergoing a thermodynamic phase transition into a superfluid BEC below some critical temperature. Thus, even in dimensions $d \leq 2$ the system possesses three different ground states [GS88, FWGF89], which can be distinguished by their values for the compressibility $\kappa = dN/d\mu$ and the superfluid order parameter $\phi = \langle b_i \rangle$: the superfluid condensate ($\kappa > 0, \phi \neq 0$), the Mott insulator ($\kappa = 0, \phi = 0$) and the Bose glass ($\kappa > 0, \phi = 0$). Fig. 9.1 shows a phase diagram of the Bose-Hubbard model obtained within a stochastic mean-field approximation [BH09] for an intermediate disorder strength. While the details of the zero temperature phase diagram are still under debate, the general behavior and the three different phases can clearly be observed from the figure.
For stronger disorder, $\Delta > U$, the lobes of the Mott insulating phase would completely vanish and only the Bose glass and the superfluid phase would survive [FWGF89, FM96]. In contrast, for $\Delta = 0$, the lobes would become larger and the Bose glass phase would disappear.
For bosons, the noninteracting limit, $U \to 0$, is pathological, because it would inevitably yield a fragmented condensate [MHUB06], where all particles occupy the lowest (localized) single-particle Lifshitz states (cf. Sec. 3.2.4). Therefore, an almost noninteracting Bose glass is commonly called a Lifshitz glass.

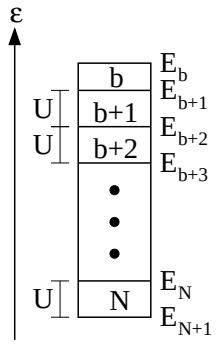

Figure 9.2: Ground state configuration of the disordered Bose-Hubbard model in the atomic-limit. $b(N)$ is the minimal(maximal) occupation number, i.e., the occupation number of the lattice sites with an on-site energy from the upper(lower) boundary of the disorder distribution.

9.2 Atomic-limit approximation for the disordered Bose-Hubbard model

From the discussion above and from the motivation of the atomic-limit approximation, we can immediately conclude that the applicability of our approach to the disordered Bose-Hubbard model is much more restricted than for the fermionic Anderson-Hubbard model. Generally, the atomic-limit (or strong coupling limit) can also act as a good starting point for the Bose-Hubbard model [FM96]. However, our single-particle description based on the occupation numbers of the atomic-limit can be meaningful only within the Bose glass phase. Therefore, we have to restrict our considerations to $\Delta \gg t$. To stay outside the Mott insulating phase we additionally require $\Delta > U$. But despite these restrictions it remains an interesting regime, because the total occupation number per lattice is unrestricted for bosons, and we can expect that this implies significant changes as compared to the fermionic case.

9.2.1 Ground state configuration

As in the previous chapters, we first need to determine the ground state configuration in the atomic-limit. For this purpose, we again assume (Δ, U, ρ) to be fixed, external parameters. In particular, with regard to the atomic gas experiments this seems to be more appropriate than fixing the chemical potential.
Denoting the highest site occupation number of the atomic-limit ground state configuration by $N \geq 1$ and the minimal one by $b \geq 0$, we can define a cascade of on-site energies $E_0, ..., E_{N+1}$, such that (cf. Fig. 9.2)

$$\langle \hat{n}_i \rangle \; = \; n \quad \Leftrightarrow \quad \varepsilon_i \in [E_n, E_{n+1}]. \tag{9.2}$$

Besides, we can read off from Fig. 9.2 that

$$E_0 = E_1 = \ldots = E_b = \Delta/2 \tag{9.3}$$
$$E_i = E_{i+1} + U \quad \forall i \in \{b, \ldots, N\} \tag{9.4}$$
$$E_{N+1} = -\Delta/2 \tag{9.5}$$
$$\mu = E_{b+1} + b \cdot U. \tag{9.6}$$

Therefore, we obtain the following two equations yielding the ground state configuration in the atomic-limit,

$$N - b = \left\lceil \frac{\mu - b \cdot U + \Delta/2}{U} \right\rceil \tag{9.7}$$
$$\rho - b = (N-b)\,\frac{\mu - (N-1)U + \Delta/2}{\Delta} + \frac{U}{\Delta}\,\frac{(N-b)(N-b-1)}{2}, \tag{9.8}$$

where $\lceil x \rceil$ denotes the ceiling function giving the smallest integer $\geq x$. Because of the integer-valued problem, no closed solution of this system of equations exists. However, for each parameter set it is an easy task to iteratively find the solution of Eqs. (9.7) and (9.8).

As for the fermionic problem, the transport properties of the interacting Bose glass are determined by the particles at the chemical potential μ. The effective disorder distribution for the single-particle propagation on top of the frozen interacting particle sea can be read off again from the retarded Green's function. For the case of the Bose-Hubbard model in the atomic-limit its calculation is in complete analogy to the fermion problem and the result is

$$G_i^{R,0}(E) = \frac{\langle \hat{n}_i \rangle + 1}{E - (\varepsilon - \mu + U\langle \hat{n}_i \rangle) + \mathrm{i}0^+} - \frac{\langle \hat{n}_i \rangle}{E - (\varepsilon - \mu + U(\langle \hat{n}_i \rangle - 1) + \mathrm{i}0^+}. \tag{9.9}$$

Thus, we see that the probability for particle-like transport, corresponding to an effective potential shift of $\varepsilon_i \mapsto \varepsilon_i + \langle \hat{n}_i \rangle U$, is $(\langle \hat{n}_i \rangle + 1)/(2\langle \hat{n}_i \rangle + 1)$. The probability for hole-like transport and an effective shift by $(\langle \hat{n}_i \rangle - 1)U$ is $(\langle \hat{n}_i \rangle)/(2\langle \hat{n}_i \rangle + 1)$.

For calculating disorder averages, for instance within the coherent potential approximation, it is again useful to avoid an explicit determination of $p_{\mathrm{A}}(\varepsilon)$, but to

use the identity (cf. Eq. (7.47)),

$$\begin{aligned}
&\int d\varepsilon\, p_{\rm A}(\varepsilon)\, f(\varepsilon) \\
&= \frac{1}{\Delta}\sum_{i=0}^{N}\left(\frac{i+1}{2i+1}\int\limits_{E_{i+1}}^{E_i} d\varepsilon\, f(\varepsilon+iU) + \frac{i}{2i+1}\int\limits_{E_{i+1}}^{E_i} d\varepsilon\, f(\varepsilon+(i-1)U)\right) \\
&= \frac{1}{\Delta}\left(\frac{b+1}{2b+1}\int\limits_{E_{b+1}+bU}^{\Delta/2+bU} d\varepsilon\, f(\varepsilon) + \frac{b}{2b+1}\int\limits_{E_{b+1}+(b-1)U}^{\Delta/2+(b-1)U} d\varepsilon\, f(\varepsilon)\right) \\
&\quad + \frac{1}{\Delta}\sum_{i=b+1}^{N-1}\left(\frac{i+1}{2i+1}\int\limits_{E_{i+1}+iU}^{E_i+iU} d\varepsilon\, f(\varepsilon) + \frac{i}{2i+1}\int\limits_{E_{i+1}+(i-1)U}^{E_i+(i-1)U} d\varepsilon\, f(\varepsilon)\right) \\
&\quad + \frac{1}{\Delta}\left(\frac{N+1}{2N+1}\int\limits_{-\Delta/2+NU}^{E_N+NU} d\varepsilon\, f(\varepsilon) + \frac{N}{2N+1}\int\limits_{-\Delta/2+(N-1)U}^{E_N+(N-1)U} d\varepsilon\, f(\varepsilon)\right), \quad (9.10)
\end{aligned}$$

which is valid for each function $f(\varepsilon)$. Using Eqs. (9.3)-(9.6) we can simplify Eq. (9.10) and finally obtain

$$\begin{aligned}
&\int d\varepsilon\, p_{\rm A}(\varepsilon)\, f(\varepsilon) \\
&= \frac{1}{\Delta}\left(\frac{b+1}{2b+1}\int\limits_{\mu}^{\Delta/2+bU} d\varepsilon\, f(\varepsilon) + \frac{b}{2b+1}\int\limits_{\mu-U}^{\Delta/2+(b-1)U} d\varepsilon\, f(\varepsilon)\right) \\
&\quad + \frac{B(N,b)}{\Delta}\int\limits_{\mu}^{\mu+U} d\varepsilon\, f(\varepsilon) + \frac{A(N,b)}{\Delta}\int\limits_{\mu-U}^{\mu} d\varepsilon\, f(\varepsilon) \\
&\quad + \frac{1}{\Delta}\left(\frac{N+1}{2N+1}\int\limits_{-\Delta/2+NU}^{\mu+U} d\varepsilon\, f(\varepsilon) + \frac{N}{2N+1}\int\limits_{-\Delta/2+(N-1)U}^{\mu} d\varepsilon\, f(\varepsilon)\right). \quad (9.11)
\end{aligned}$$

The coefficients $A(N,b)$ and $B(N,b)$ are given by

$$A(N,b) = 1 - B(N,b) = \frac{N-b+1}{2} - \frac{\psi(N+1/2)-\psi(b+3/2)}{4}, \quad (9.12)$$

where

$$\psi(n+1/2) = -\gamma - 2\log(2) + \sum_{k=1}^{n}\frac{2}{2k-1} \quad (9.13)$$

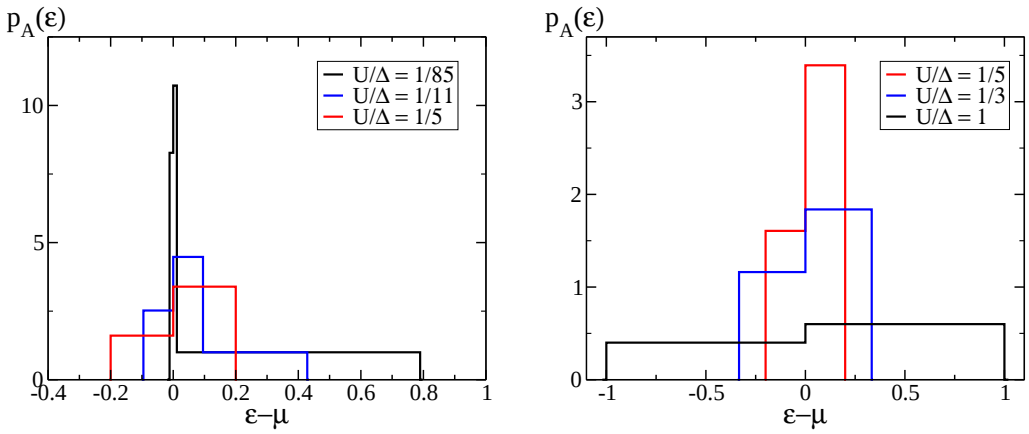

Figure 9.3: Effective probability distribution function of the disordered Bose-Hubbard model in atomic-limit approximation for $\rho = 2$. a) weak to intermediate interaction b) intermediate to strong interaction.

is the digamma function and γ is the Euler-Mascheroni constant [AS72].

9.2.2 Numerical results

Having derived Eq. (9.11), we are able to evaluate the effective single-particle Hubbard model in the atomic-limit approximation. The analysis can now be done in complete analogy with the fermion problem, because spin statistics do not matter for a single particle in a static potential. Therefore, we can again use the self-consistent theory for single-particle Anderson localization to study numerically localization of the strongly disordered system.

Fig. 9.3 shows the effective probability distribution function for various interaction strengths. The lattice filling was fixed at $\rho = 2$, which is a realistic experimental value [GME+02]. For extremely low interactions (black curve in Fig. 9.3(a)), only the sites at the lower boundary of the probability distribution are occupied. In this regime, we expect the formation of fragmented condensates in the deepest valleys of the energy landscape. For intermediate interaction strengths (red curves in Fig. 9.3), the particles starts to occupy a larger portion of lattice sites, and the width of the effective disorder distribution shrinks. For strong interactions (black curve in Fig. 9.3(b)), two disorder broadened Hubbard bands start to form, and an efficient screening of disorder is not possible anymore. The same observation can be made by considering the variance of the effective on-site energy distribution, Fig. 9.4.

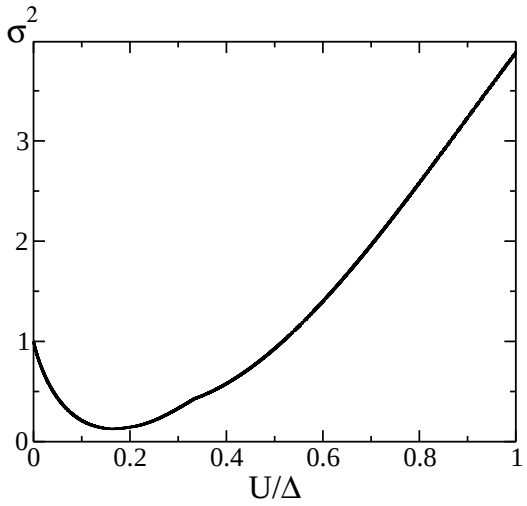

Figure 9.4: Variance of the effective probability distribution for $\rho = 2$, normalized to its noninteracting value of $\Delta^2/12$.

For the calculation of the localization length of a boson at the chemical potential μ, we apply Eq. (9.11) to the CPA equation, Eq. (7.9), to obtain the single-particle self energy. Afterwards, we are able to evaluate the transport equations, which are the same as in Ch. 7.
Fig. 9.5 shows the localization length as a function of U for fixed disorder strength and fixed lattice filling. From the discussion in the previous section, the atomic-limit approximation should be applicable in the regime $\Delta > U \gg t$. As we observe from the plot, in this regime ($4 \lesssim U \lesssim 10$) the localization length is a monotonous, slowly varying function of U. In particular, the nonmonotonic behavior of $\xi(U)$, observed for fermions (Ch. 7), is absent here. The reason is that the particle number per lattice site is unrestricted for bosons. Thus, at smaller interaction strengths the occupation numbers can be better adopted to the disorder potential. Consequentely, more and more spectral weight is accumulated at the chemical potential, and, hence, ξ increases for decreasing interaction strength. At small interaction strengths ($U < 4$), the maximal particle number N (cf. Sec. 9.2) quickly increases towards the condensate phase. Here, the atomic-limit becomes less applicable (and artificially predicts a step-like increase of ξ each time N is increased by 1).
Since our method is not able to describe the transition from the Bose glass to the superfluid phase, the derivation of a meaningful phase diagram is unfortunately not possible, in contrast to the Anderson-Hubbard model (for fermions). However, it seems likely that the system monotonically delocalizes until the superfluid phase is reached.

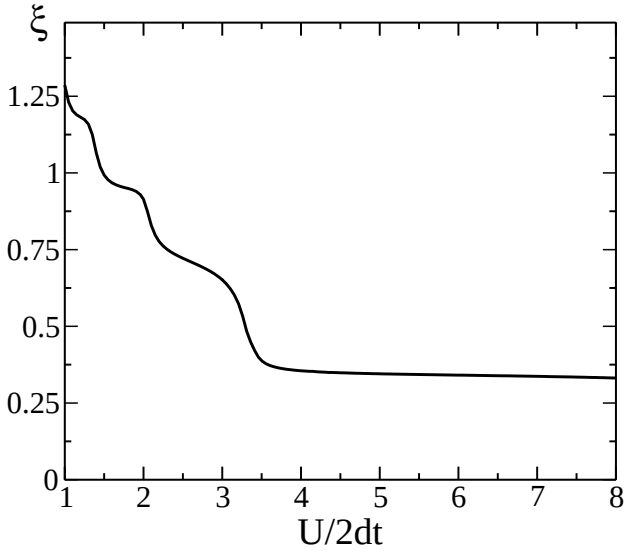

Figure 9.5: Localization length as a function of the interaction strength for $\Delta/2td = 10$ and $\rho = 2$ in 2D.

Chapter 10

Conclusion

In this thesis, we studied the interplay of repulsive two-particle interactions and disorder. On its own, either of these effects is known to yield metal-insulator transitions in real materials. After having given an overview of the disorder-induced Anderson metal-insulator transition and interaction-induced Mott transition, we turned to the question of their interplay. As we explained, in many systems not only one effect is relevant for the metal-insulator transition, but in general both. Therefore, a better general understanding of the interplay and competition, respectively, of interactions and disorder is needed.
In particular, we investigated the Anderson-Hubbard model, which is the minimal lattice model containing local interactions and disorder. We discussed that many numerical results for this model show a pronounced nonmonotonic interaction-disorder-dependence of transport and its relevant length scale. Based on a strong disorder ansatz, which we explained to be the relevant regime in the (Anderson) insulating phase, we developed an atomic-limit approximation, which allowed for a systematic and transparent analysis of the underlying physical mechanisms. The local Hubbard interaction was included statically by taking into account an interaction-induced shift of the local disorder potential. In particular, we did not treat the interaction effect on a disorder-averaged level. Instead, we respected the local changes of the potential due to the disorder-dependent electron occupation of lattice sites. In this way, we could derive a single-particle Anderson model with an interaction-dependent disorder distribution, which we explained to describe effectively the propagation of single-particle excitations on the background of the interacting Fermi sea.
Using this ansatz, we could reproduce very well many numerical results for the Anderson-Hubbard model published in recent years. Furthermore, we could show that the nonmonotonic behavior of the single-particle localization length, which defines the relevant transport length scale of the interacting problem, results from the competition of screening of the disorder by weak interactions and hopping suppression by strong interactions. Moreover, we showed that, in two dimensions, the screening effect can induce an exponential enlargement of the localiza-

tion length and derived the three-dimensional phase diagram of the Anderson-Hubbard model within our atomic-limit approximation. The former was particularly important, because it was claimed recently by different authors that within the Anderson-Hubbard model numerical indications for a two-dimensional metal-insulator transition were found. By comparison of our results with these findings, we could give strong arguments to the effect that the observed transition is most probably a numerical artefact due to finite-size effects in the numerics, induced by the exponential enhancement of the relevant length scale.

Motivated by rapid progress in experiments on cold atomic gases, we turned to the diffusion of a noninteracting atomic gas cloud in a disordered environment, released from an optical trap. After deriving the formulation of the expansion process in terms of disorder-averaged Green's functions, we calculate the averaged particle density and the short-ranged density-density correlations (atomic speckles) of the gas cloud as a function of the expansion time. As we could show, the presence of the static disorder potential yields interesting changes compared to the ballistic case. Scattering off inhomogeneities yields a randomization of the wave functions' phases. Consequently, no significant long-ranged correlations on the scale of the mean interparticle distance is built up, as is known from ballistic expansion, but only short-ranged correlations exist, which are of the order of the relevant length in the trap before the release.

As the great majority of experiments on cold gases has been done till now for Bose gases, we also discussed briefly the atomic-limit approximation for the disordered Bose-Hubbard model. After giving a short overview of the zero temperature phase diagram of the disordered Hubbard model, we derived the effective disorder distribution of the atomic-limit approximation and calculated the corresponding localization length. As we discussed, the approach was more restricted than for the fermion model, because of the existence of the superfluid Bose-Einstein condensate phase, which remained outside the applicability of our ansatz. In contrast to the fermion model, the particle occupation number per lattice site is unrestricted for bosons. As a consequence, the disorder screening effect becomes a monotonic function of the interaction strength, and we conjectured that the localization of the system decreases monotonously towards the superfluid phase.

The atomic-limit approximation neglects dynamic effects caused by particle number fluctuations, as well as spin-ordering. Although comparison of our and known numerical results seems to confirm that these effects, compared to screening, are less relevant, an useful extension of our method would be an inclusion of cluster effects, which, at least, would take into account short-ranged correlation effects and particle number fluctuations. A re-production of our results would be a strong confirmation of the validity of our work.

Appendix A

Single particle in a disordered potential: perturbation theory

If the disorder potential is weak or the length scale of the system is significantly smaller than the relevant localization length, the propagation of a single particle or the transport properties of the system can often be well described within perturbation theory. In this chapter, we will briefly present the disorder perturbation theory, because we will refer to its results at different points within this thesis. The notation will follow closely the one in [AM07], where a more detailed and comprehensive discussion of the subject can be found.

Starting from a basis of extended Bloch states, which diagonalizes the periodic part of the Hamiltonian, we consider the Hamiltonian

$$\hat{H} \;=\; \sum_k \epsilon_k c_k^\dagger c_k \;+\; \sum_{k,q} V_q \, c_{k+q}^\dagger c_k. \tag{A.1}$$

To keep things simple, we suppress the spin index of the electrons. Its inclusion is straightforward and does not alter any of the results apart from a trivial multiplicative factor.
For convenience, we will always assume in this thesis that the disorder potential is an isotropic Gaussian white noise potential with zero mean, i.e., it fulfills

$$\overline{V_q} \;=\; 0 \;, \qquad \overline{V_q \, V_k} \;=\; \gamma \, \delta(q+k) \;. \tag{A.2}$$

In position space that corresponds to

$$\overline{V(x)} \;=\; 0 \;, \qquad \overline{V(x)V(y)} \;=\; \gamma\delta(x-y) \;. \tag{A.3}$$

For example, for the Anderson model, Eq. (3.1), we can identify $\gamma = \Delta^2/12$.

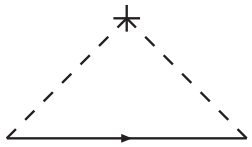

Figure A.1: Self-energy diagram of the Born approximation. Dashed lines denote the scattering potential, the solid line denotes the bare single-particle propagator and the cross denotes the disorder averaging.

A.1 Single-particle propagator

On the single-particle level, it is often sufficient to include the disorder effect within low orders of perturbation theory. For instance, the self-energy can often be treated within the Born approximation, i.e., lowest order perturbation theory, yielding (see Fig. A.1)

$$\Sigma_k^{R/A}(E) \;=\; \sum_q \overline{V_q\, V_{-q}}\, G_{k+q}^{R/A,0}(E), \tag{A.4}$$

where

$$G_k^{R/A,0}(E) \;=\; \frac{1}{E-\epsilon_k \pm \mathrm{i}0^+}. \tag{A.5}$$

The imaginary part of the self-energy defines the relevant elastic collision time τ, which is readily calculated to be

$$\frac{1}{2\tau} \;=\; -\mathrm{Im}\Sigma_k^R(E) \;=\; \pi\gamma N_0(E) \;\approx\; \pi\gamma N_0(\varepsilon_\mathrm{F}), \tag{A.6}$$

with the bare density of states

$$N_0(E) \;=\; -\frac{1}{\pi}\int \frac{dk}{(2\pi)^d}\,\mathrm{Im}G_k^{R,0}(E). \tag{A.7}$$

Consequently, the disorder-averaged single-particle propagator becomes (see Eq. (3.19))

$$\overline{G_k^{R/A}}(E) \;=\; \frac{1}{E-\epsilon_k \pm \mathrm{i}/2\tau}. \tag{A.8}$$

A.2 Vertex functions

Diffusion vertex

To calculate transport properties, we have to consider the disorder-averaged two-particle vertex functions. The first one is the diffusion vertex arising from the

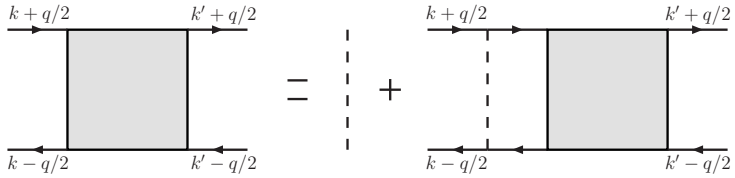

Figure A.2: Graphical representation of the two-particle diffusion propagator (grey box).

ladder diagrams (cf. Fig. 3.3(b)), defined by (see Fig. A.2)

$$\tilde{D}(\omega,q) \;=\; \gamma \,+\, \gamma \int \frac{dk}{(2\pi)^d}\, \overline{G^R_{k+q/2}}(E+\omega/2)\overline{G^A_{k-q/2}}(E-\omega/2)\tilde{D}(\omega,q). \quad \text{(A.9)}$$

Considering the static limit, where $\omega, q \to 0$, we get

$$\gamma \int \frac{dk}{(2\pi)^d}\, \overline{G^R_{k+q/2}}(E+\omega/2)\overline{G^A_{k-q/2}}(E-\omega/2) \quad \text{(A.10)}$$

$$= \;\gamma \int \frac{dk}{(2\pi)^d}\, \frac{1}{E+\omega/2-\epsilon_{k+q}+\mathrm{i}/2\tau}\, \frac{1}{E-\omega/2-\epsilon_k-\mathrm{i}/2\tau} \quad \text{(A.11)}$$

$$\approx \;\gamma \int \frac{dk}{(2\pi)^d}\, \frac{1}{E+\omega/2-\epsilon_k-v_k\cdot q+\mathrm{i}/2\tau}\, \frac{1}{E-\omega/2-\epsilon_k-\mathrm{i}/2\tau}, \quad \text{(A.12)}$$

where we defined $v_k = \nabla_k \epsilon_k$. The remaining integral can be estimated to yield

$$\gamma \int \frac{dk}{(2\pi)^d}\, \frac{1}{E+\omega/2-\epsilon_k-v_k\cdot q+\mathrm{i}/2\tau}\, \frac{1}{E-\omega/2-\epsilon_k-\mathrm{i}/2\tau} \quad \text{(A.13)}$$

$$\approx \;N(\varepsilon_{\mathrm{F}})\gamma \int\limits_{k=k_{\mathrm{F}}} \frac{dS}{A_d} \int d\epsilon\, \frac{1}{E+\omega/2-\epsilon-v_k\cdot q+\mathrm{i}/2\tau}\, \frac{1}{E-\omega/2-\epsilon-\mathrm{i}/2\tau} \quad \text{(A.14)}$$

$$= \;2\mathrm{i}\pi N(\varepsilon_{\mathrm{F}})\gamma \int\limits_{k=k_{\mathrm{F}}} \frac{dS}{A_d}\, \frac{1}{\omega - v_k\cdot q+\mathrm{i}/\tau} \quad \text{(A.15)}$$

$$= \int\limits_{k=k_{\mathrm{F}}} \frac{dS}{A_d}\, \frac{1}{1-\mathrm{i}\omega\tau+\mathrm{i}v_k\cdot q\tau} \quad \text{(A.16)}$$

$$= \int\limits_{k=k_{\mathrm{F}}} \frac{dS}{A_d}\, (1+\mathrm{i}\omega\tau-\mathrm{i}v_k\cdot q\tau-(v_k\cdot q)^2\tau^2) \,+\, \mathcal{O}(\omega^2,q^3) \quad \text{(A.17)}$$

$$= \;1+\mathrm{i}\omega\tau - D_0 q^2\tau \,+\, \mathcal{O}(\omega^2,q^3) \quad \text{(A.18)}$$

Here, $\int_k dS$ denotes integration over the surface of the sphere of radius k.
In the last step, we introduced the bare diffusion coefficient,

$$D_0 = v^2_{k_{\mathrm{F}}}\tau/d. \quad \text{(A.19)}$$

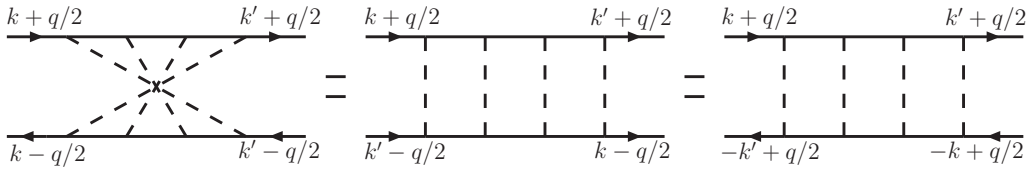

Figure A.3: Graphical representation of the cooperon propagator and its relation to the diffusion propagator by time reversal.

From Eqs. (A.9) and (A.18) we finally obtain

$$\tilde{D}(\omega, q) \;=\; \frac{\gamma}{\tau}\, D(\omega, q), \tag{A.20}$$

where

$$D(\omega, q) \;=\; \frac{1}{-\mathrm{i}\omega + D_0 q^2} \tag{A.21}$$

is the *diffusion propagator*, also called *diffuson*.

Cooperon vertex

In the presence of time reversal symmetry, the second important vertex function, the *cooperon (propagator)*, is directly read off from the diffuson by time-reversal (see Fig. A.3),

$$C(\omega, k, k') \;\equiv\; D(\omega, k + k') \;=\; \frac{1}{-\mathrm{i}\omega + D_0 (k + k')^2}. \tag{A.22}$$

A.3 Diffusive propagation in position space

In Ch. 8, we study the diffusive propagation in a disordered potential. For this, we need to find the corresponding expressions in the (r, t)-domain for the propagators from above. First we consider the single-particle propagator. For a free particle, $\epsilon_k = k^2/2m$, the Green's function in position can be calculated by Fourier transforming Eq. (A.5) [AM07],

$$G^{R,0}(r, \epsilon) \;=\; \begin{cases} -\mathrm{i}\pi N_0(\epsilon)\, e^{\mathrm{i}kr} & , \;\; d = 1 \\ -\mathrm{i}\pi N_0(\epsilon)\, H_0(kr) & , \;\; d = 2 \\ -\pi N_0(\epsilon)\, e^{\mathrm{i}k\cdot r}/(k\, r) & , \;\; d = 3 \end{cases}, \tag{A.23}$$

with $k = \sqrt{2m\epsilon}$ and $H_0(kr)$ being the Bessel function of the third kind.
Analogously, the disorder-averaged propagator can be calculated as [AM07]

$$\overline{G^R}(r, \epsilon) \;=\; G^{R,0}(r, \epsilon)\, e^{-r/2l_\epsilon}, \tag{A.24}$$

where $l_\epsilon = k\tau_\epsilon/m$ denotes the average mean free path.

Next, we need the diffusion propagator in the (r,t)-domain, which we will denote by $P_\varepsilon(r,t)$, and which is easily obtained from Eq. (A.21) by Fourier transformation [AM07],

$$\begin{aligned} P_\epsilon(r,t) &= \int \frac{dq}{(2\pi)^d} e^{-\mathrm{i}q\cdot r} \int \frac{d\omega}{2\pi} e^{-\mathrm{i}\omega t} \frac{1}{-\mathrm{i}\omega + D_\epsilon q^2} && \text{(A.25)} \\ &= \Theta(t) \int \frac{dq}{(2\pi)^d} e^{-\mathrm{i}q\cdot r - q^2 D_\epsilon t} && \text{(A.26)} \\ &= \Theta(t) \frac{e^{-r^2/(4D_\epsilon t)^{1/2}}}{(D_\epsilon t)^{d/2}} \int \frac{dq}{(2\pi)^d} e^{-(q+\mathrm{i}r/(4D_\epsilon t)^{1/2})^2} && \text{(A.27)} \\ &= \Theta(t) \frac{e^{-r^2/(4D_\epsilon t)^{1/2}}}{(4D_\epsilon t)^{d/2}}. && \text{(A.28)} \end{aligned}$$

Here, we explicitly included the (weak) energy dependence of the diffusion coefficient,

$$D_\epsilon = \frac{v_\epsilon^2 \tau_\epsilon}{d}, \qquad \text{(A.29)}$$

because for the analysis of the gas expansion we cannot restrict our considerations to particles at the Fermi level (see discussion in Sec. 8.1).

Now we can evaluate the product $\overline{G^R(r_1,R_1,t)\,G^A(r_2,R_2,t)}$. In the diffusive regime, where the vertex function is given by the diffusion propagator, we can transform this product according to (cf. Fig. A.2) [AM07, SMTS08]

$$\begin{aligned} &\overline{G^R(r_1,R_1,t)\,G^A(r_2,R_2,t)} \\ &= \int \frac{d\epsilon}{2\pi} \int \frac{d\omega}{2\pi} e^{-\mathrm{i}\omega t}\, \overline{G^R(r_1,R_1,\epsilon+\omega/2)\,G^A(r_2,R_2,\epsilon-\omega/2)} && \text{(A.30)} \\ &= \int dx \int dx' \int \frac{d\epsilon}{2\pi} \int \frac{d\omega}{2\pi} e^{-\mathrm{i}\omega t}\, \overline{G^R}(r_1-x,\epsilon+\omega/2)\,\overline{G^A}(r_2-x,\epsilon-\omega/2) \\ &\qquad \times \frac{\gamma}{\tau_\epsilon} P_\epsilon(x-x',\omega)\,\overline{G^R}(x'-R_1,\epsilon+\omega/2)\,\overline{G^A}(x'-R_2,\epsilon-\omega/2) && \text{(A.31)} \\ &\approx \int dx \int dx' \int \frac{d\epsilon}{2\pi}\, \overline{G^R}(r_1-x,\epsilon)\,\overline{G^A}(r_2-x,\epsilon)\,\frac{\gamma}{\tau_\epsilon} P_\epsilon(x-x',t) \\ &\qquad \times \overline{G^R}(x'-R_1,\epsilon)\,\overline{G^A}(x'-R_2,\epsilon), && \text{(A.32)} \end{aligned}$$

where we have neglected the weak ω-dependence of the average Green's functions in the last line.

While the diffusion propagator depends only weakly on $x - x'$, the disorder-averaged propagators decay on the scale of the mean free path (Eq. A.24). Thus, it is convenient to define

$$\Delta r \equiv r_1 - r_2, \quad r \equiv \frac{r_1 + r_2}{2}, \quad \Delta R \equiv R_1 - R_2, \quad R \equiv \frac{R_1 + R_2}{2}, \tag{A.33}$$

and to approximate

$$\begin{aligned} & \overline{G^R(r_1, R_1, t)\, G^A(r_2, R_2, t)} \\ \approx & \int \frac{d\epsilon}{2\pi} \frac{\gamma}{\tau_\epsilon} P_\epsilon(r - R, t) \int dx\, \overline{G^R}(x - \Delta r/2, \epsilon)\, \overline{G^A}(x + \Delta r/2, \epsilon) \\ & \times \int dx'\, \overline{G^R}(x' - \Delta R/2, \epsilon)\, \overline{G^A}(x' + \Delta R/2, \epsilon). \end{aligned} \tag{A.34}$$

The integrals over the space-variables can be rewritten by using the convolution theorem

$$\begin{aligned} & \int dx\, \overline{G^R}(x - \Delta r/2, \epsilon)\, \overline{G^A}(x + \Delta r/2, \epsilon) \\ = & \int \frac{dk}{(2\pi)^d}\, \overline{G^R}(k, \epsilon)\, \overline{G^A}(k, \epsilon)\, e^{-\mathrm{i}k\Delta r} && \text{(A.35)} \\ \overset{\text{(A.8)}}{=} & -2\tau_\epsilon \int \frac{dk}{(2\pi)^d}\, \mathrm{Im}\overline{G^R}(k, \epsilon)\, e^{-\mathrm{i}k\Delta r} && \text{(A.36)} \\ = & -2\tau_\epsilon\, \mathrm{Im}\overline{G^R}(\Delta r, \epsilon), && \text{(A.37)} \end{aligned}$$

which for $\Delta r = 0$ reduces to

$$\int dx\, \overline{G^R}(x - \Delta r/2, \epsilon)\, \overline{G^A}(x + \Delta r/2, \epsilon) \;=\; 2\pi\tau_\epsilon N_0(\epsilon) \;=\; \frac{1}{\gamma}. \tag{A.38}$$

Thus, we obtain

$$\overline{G^R(r, R_1, t)\, G^A(r, R_2, t)} \;\approx\; -\frac{1}{\pi} \int d\epsilon\; P_\epsilon(r - R, t)\, \mathrm{Im}\overline{G^R}(\Delta R, \epsilon). \tag{A.39}$$

Appendix B

Auxiliary-particle representation

Perturbative calculations for the (Anderson-)Hubbard model are difficult for two different reasons. First, the Mott-Hubbard phase transition at half-filling necessarily yields a breakdown of perturbation theory. But even away from the transition at half filling, a systematic perturbative calculation is non-trivial. The reason is that in many situations one is interested in the strong coupling limit, i.e. $U \gg t$, as it is relevant for many materials. Starting from the noninteracting electron gas and including the correlation effects perturbatively often yields incorrect results. Therefore, it would seem to be more convenient to start from the atomic limit ($t = 0$) and use an expansion in the hopping amplitude. Since the eigenbasis of the local interaction is $\{|i0\rangle, |i\uparrow\rangle, |i\downarrow\rangle, |i2\rangle\}$, where $|2\rangle \equiv |\uparrow\downarrow\rangle$, the interaction term gets diagonalized in terms of the *Hubbard operators* [Hub64a]

$$X^i_{\alpha\beta} \;=\; |i\alpha\rangle\langle\beta i|, \qquad \alpha, \beta \in \{0, \uparrow, \downarrow, 2\}. \tag{B.1}$$

However, these states are not free [BLS94]. Hence, the Hubbard operators do not obey the canonical (anti-)commutator relations [Hub64a], and Wick's theorem is not applicable. Therefore, a systematic perturbation expansion gets difficult. A convenient way to avoid these difficulties is to introduce auxiliary-particle operators and to express the Hubbard operators in terms of them [Col84, KR86], which is subject of the following section.

B.1 Anderson-Hubbard Hamiltonian in auxiliary-particle representation

In this section, we will derive the basic relations for the auxiliary-particle representation of the Anderson-Hubbard model. The derivation is a straightforward extension of the results of [Col84] and follows closely the notation used therein (see also [KW03]).

Our starting point is the Anderson-Hubbard Hamiltonian, Eq. (5.4),

$$\begin{aligned}\hat{H}_{AH} &\equiv \hat{H}_{dis} + \hat{H}_{kin} + \hat{H}_U \\ &= \sum_{i\sigma}(\varepsilon_i - \mu)c^\dagger_{i\sigma}c_{i\sigma} - t\sum_{<i,j>,\sigma} c^\dagger_{i\sigma}c_{j\sigma} + \frac{U}{2}\sum_{i\sigma}\hat{n}_{i,\sigma}\hat{n}_{i,-\sigma}. \qquad \text{(B.2)}\end{aligned}$$

The auxiliary-particle annihilation (creation) operators $a_i^{(\dagger)}$, $b_i^{(\dagger)}$, and $f_{i\sigma}^{(\dagger)}$, defined by their action on the vacuum state $|vac\rangle$

$$a_i^\dagger|vac\rangle = |i2\rangle, \qquad f_{i\sigma}^\dagger|vac\rangle = |i\sigma\rangle, \qquad b_i^\dagger|vac\rangle = |i0\rangle, \qquad \text{(B.3)}$$

are related to the single-particle operators via

$$c_{i\sigma} = b_i^\dagger f_{i\sigma} + \mathrm{sgn}(\sigma) f_{i-\sigma}^\dagger a_i \qquad \text{(B.4)}$$

$$c_{i\sigma}^\dagger = f_{i\sigma}^\dagger b_i + \mathrm{sgn}(\sigma) a_i^\dagger f_{i-\sigma}, \qquad \text{(B.5)}$$

where

$$\mathrm{sgn}(\sigma) = \begin{cases} 1 & , \ \sigma = \uparrow \\ -1 & , \ \sigma = \downarrow \end{cases}. \qquad \text{(B.6)}$$

Eqs. (B.4) and (B.5) can easily be proven by considering the action of the auxiliary-particle operators on the basis states $\{|i0\rangle, |i\uparrow\rangle, |i\downarrow\rangle, |i2\rangle\}$. Inserting Eqs. (B.4) and (B.5) into Eq. (B.2) yields immediately the auxiliary-particle representation of the Anderson-Hubbard model,

$$\begin{aligned}\hat{H}_{AH}^{(aux)} &= \sum_{i\sigma}(\varepsilon_i - \mu)f_{i\sigma}^\dagger f_{i\sigma} + \sum_i (2(\varepsilon_i - \mu) + U)a_i^\dagger a_i \qquad \text{(B.7)} \\ &\quad - t\sum_{<i,j>,\sigma}\Big(f_{i\sigma}^\dagger b_j^\dagger f_{j\sigma} b_i + \mathrm{sgn}(\sigma) f_{i\sigma}^\dagger f_{j-\sigma}^\dagger a_j b_i - \mathrm{sgn}(\sigma) a_i^\dagger b_j^\dagger f_{j\sigma} f_{i-\sigma} \\ &\qquad\qquad - a_i^\dagger f_{j\sigma}^\dagger a_j f_{i\sigma}\Big).\end{aligned}$$

The physical subspace, which we have to consider, is the space in which the total number of auxiliary-particles per site is always exactly one

$$\hat{Q}_i \equiv b_i^\dagger b_i + \sum_\sigma f_{i\sigma}^\dagger f_{i\sigma} + a_i^\dagger a_i \stackrel{!}{=} \mathbb{1}. \qquad \text{(B.8)}$$

However, in order to use the standard techniques of many-body perturbation theory we have to work within the grand-canonical ensemble, instead of the canonical one [AGD77]. Therefore, we introduce local chemical potentials λ_i and transform

the Hamiltonian to

$$\begin{aligned}\hat{H}^{(aux)}_{AH,gc} &\mapsto \hat{H}^{(aux)}_{AH} + \sum_i \lambda_i \hat{Q}_i \\ &= \sum_i \lambda_i b_i^\dagger b_i + \sum_{i\sigma}(\varepsilon_i - \mu + \lambda_i) f^\dagger_{i\sigma} f_{i\sigma} + \sum_i (2(\varepsilon_i - \mu) + U + \lambda_i) a_i^\dagger a_i \\ &\quad - t \sum_{<i,j>,\sigma} \Big(f^\dagger_{i\sigma} b^\dagger_j f_{j\sigma} b_i + \mathrm{sgn}(\sigma) f^\dagger_{i\sigma} f^\dagger_{j-\sigma} a_j b_i - \mathrm{sgn}(\sigma) a_i^\dagger b^\dagger_j f_{j\sigma} f_{i-\sigma} \\ &\qquad\qquad - a_i^\dagger f^\dagger_{j\sigma} a_j f_{i\sigma} \Big) . \end{aligned} \tag{B.9}$$

B.2 Calculation of physical expectation values

It is useful to note, that $\forall \omega \in \mathbb{R}$ the unitary transformation $\hat{U}(\omega)$, which maps

$$a_i \mapsto e^{\mathrm{i}\omega} a_i \ , \quad b_i \mapsto e^{\mathrm{i}\omega} b_i \ , \quad f_{i\sigma} \mapsto e^{\mathrm{i}\omega} f_{i\sigma} \ , \tag{B.10}$$

leaves the creation and annihilation operators unchanged, $U^\dagger(\omega) c^{(\dagger)}_{i\sigma} U(\omega) = c^{(\dagger)}_{i\sigma}$. Hence, any physical observable $\hat{A}$ commutes with $\hat{Q}_i$. In particular, the auxiliary-particle number per site is a conserved quantity, $[\hat{Q}_i, \hat{H}^{(aux)}_H] = 0$ [KW03]. Therefore, we can decompose the grand-canonical quantum expectation value of $\hat{A}$ according to

$$\langle \hat{A} \rangle_{gc} = \frac{\mathrm{tr}\left(e^{-\beta \hat{H}^{(aux)}_{AH,gc}} \hat{A} \right)}{\mathrm{tr}\left(e^{-\beta \hat{H}^{(aux)}_{AH,gc}} \right)} = \frac{1}{Z_{gc}} \prod_i \sum_{Q_i=0}^{\infty} e^{-\beta \lambda_i Q_i} \mathrm{tr}\left(e^{-\beta \hat{H}^{(aux)}_{AH}} \hat{A} \right)_{\{Q_i\}} . \tag{B.11}$$

Here, Z_{gc} denotes the grand-canonical partition sum and the trace on the right side has to be taken in the subspace of fixed $\{Q_i\}$. At the end, we have to project onto the physical subspace where $\{Q_i \equiv 1\}$. From Eq. (B.11) we see that the contributions of the different subspaces to the sum on the right side are of the order $\mathcal{O}(e^{-\beta \lambda_i Q_i})$. Thus, in the limit $\lambda_i \to \infty$ only the summand of the subspace of the lowest Q_i contributes. To ensure that this is the one with $\{Q_i \equiv 1\}$ we have to guarantee that the contributions from the subspaces vanish, where at least one $Q_i = 0$. For that purpose, we replace $\hat{A}$ by $\hat{A} \prod_i Q_i$ in Eq. (B.11) and

normalize,

$$\left(\prod_i \lim_{\lambda_i\to\infty}\right)\frac{\left\langle \hat{A}\prod_i \hat{Q}_i\right\rangle_{gc}}{\left\langle\prod_i \hat{Q}_i\right\rangle_{gc}} = \left(\prod_i \lim_{\lambda_i\to\infty}\right)\frac{\mathrm{tr}\left(e^{-\beta\hat{H}^{(aux)}_{AH}}\hat{A}\prod_i \hat{Q}_i\right)}{\mathrm{tr}\left(e^{-\beta\hat{H}^{(aux)}_{AH}}\prod_i \hat{Q}_i\right)} \tag{B.12}$$

$$= \left(\prod_i \lim_{\lambda_i\to\infty}\right)\frac{\prod_i\sum_{Q_i=1}^{\infty} e^{-\beta\lambda_i Q_i}\,\mathrm{tr}\left(e^{-\beta\hat{H}^{(aux)}_{AH}}\hat{A}\prod_i \hat{Q}_i\right)_{\{Q_i\}}}{\prod_i\sum_{Q_i=1}^{\infty} e^{-\beta\lambda_i Q_i}\,\mathrm{tr}\left(e^{-\beta\hat{H}^{(aux)}_{AH}}\prod_i \hat{Q}_i\right)_{\{Q_i\}}}$$

$$= \frac{\mathrm{tr}\left(e^{-\beta\hat{H}^{(aux)}_{AH}}\hat{A}\right)_{\{Q_i\equiv 1\}}}{\mathrm{tr}\left(e^{-\beta\hat{H}^{(aux)}_{AH}}\right)_{\{Q_i\equiv 1\}}}$$

$$= \langle\hat{A}\rangle.$$

Thus, Eq. (B.12) provides a possibility to calculate first the grand-canonical expectation value of any physical observable, e.g., by calculating many-body Feynman diagrams, and, afterwards, to transform the result into the physical expectation value by taking the limit $\{\lambda_i\}\to\infty$.

B.3 Single-particle propagator in lowest order perturbation theory

In Eqs. (6.38)-(6.41), $\mathcal{G}^R_{ij\sigma}(E)$, the single-particle propagator of the Anderson-Hubbard model, was used to establish the strong-disorder relation between the localization length and the effective disorder distribution $p_{\mathrm{A}}(\varepsilon)$. In the following, we will calculate perturbatively $\mathcal{G}^R_{ij\sigma}(E)$ by using the auxiliary-particle representation to prove Eq. (6.41). For this purpose, the standard rules for evaluating Feynman diagrams in the Matsubara representation will be used [AGD77].

We start our discussion with the local propagator $\mathcal{G}^R_{ii\sigma}(E)$. The corresponding propagator in imaginary (Matsubara) time representation is

$$\mathcal{G}_{ii\sigma}(\tau) = -\langle T_\tau\,(c_{i\sigma}(\tau)\,c^\dagger_{i\sigma}(0))\rangle. \tag{B.13}$$

The corresponding lowest order Feynman diagrams in auxiliary-particle representation are shown in Fig. B.1. After Fourier transformation into the frequency-domain we get

$$\Gamma_i(\mathrm{i}\omega) \equiv -\frac{1}{\beta}\sum_{\omega'}\left(\mathcal{G}^f_{i\sigma}(\mathrm{i}\omega')\,\mathcal{G}^b_i(\mathrm{i}\omega'-\mathrm{i}\omega) - \mathcal{G}^a_i(\mathrm{i}\omega'+\mathrm{i}\omega)\,\mathcal{G}^f_{i,-\sigma}(\mathrm{i}\omega')\right), \tag{B.14}$$

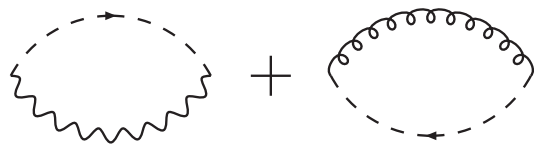

Figure B.1: Feynman diagrams of the lowest order contribution to the local propagator $\mathcal{G}_{ii\sigma}$. The dashed line denotes the bare fermion propagator $\mathcal{G}^f_{i\sigma}$, the wiggled line the bare bose operator $\mathcal{G}^b_i$ and the curled line denotes $\mathcal{G}^a_i$.

where the bare auxiliary-particle propagators are given by

$$\mathcal{G}^b_i(\mathrm{i}\omega) = \frac{1}{\mathrm{i}\omega - \lambda_i} \tag{B.15}$$

$$\mathcal{G}^f_{i\sigma}(\mathrm{i}\omega) = \frac{1}{\mathrm{i}\omega - (\varepsilon_i - \mu) - \lambda_i} \tag{B.16}$$

$$\mathcal{G}^a_i(\mathrm{i}\omega) = \frac{1}{\mathrm{i}\omega - 2(\varepsilon_i - \mu) - U - \lambda_i}. \tag{B.17}$$

Doing the Matsubara sum and performing the analytic continuation to real frequencies yields

$$\Gamma_i(\omega) = \frac{f(\varepsilon_i - \mu + \lambda_i) + b(\lambda_i)}{\omega - (\varepsilon_i - \mu) + \mathrm{i}0^+} + \frac{f(\varepsilon_i - \mu + \lambda_i) + b(2(\varepsilon_i - \mu) + U + \lambda_i)}{\omega - (\varepsilon_i - \mu + U) + \mathrm{i}0^+}, \tag{B.18}$$

where $f(x)$ and $b(x)$ are the Fermi and Bose distribution functions, respectively.

According to Sec. B.2, the physical propagator is obtained in lowest order perturbation theory by the projection

$$\mathcal{G}^R_{ii\sigma}(\omega) = \lim_{\lambda_i \to \infty} \frac{\Gamma_i(\omega)}{\langle Q_i \rangle_0} \tag{B.19}$$

$$= \lim_{\lambda_i \to \infty} \frac{\Gamma_i(\omega)}{b(2(\varepsilon_i - \mu) + U + \lambda_i) + 2f(\varepsilon_i - \mu + \lambda_i) + b(\lambda_i)} \tag{B.20}$$

$$= \frac{1}{\omega - (\varepsilon_i - \mu) + \mathrm{i}0^+} \frac{e^{-\beta(\varepsilon_i - \mu)} + 1}{e^{-\beta(2(\varepsilon_i - \mu) + U)} + 2e^{-\beta(\varepsilon_i - \mu)} + 1} \tag{B.21}$$

$$+ \frac{1}{\omega - (\varepsilon_i - \mu + U) + \mathrm{i}0^+} \frac{e^{-\beta(\varepsilon_i - \mu)} + e^{-\beta(2(\varepsilon_i - \mu) + U)}}{e^{-\beta(2(\varepsilon_i - \mu) + U)} + 2e^{-\beta(\varepsilon_i - \mu)} + 1}.$$

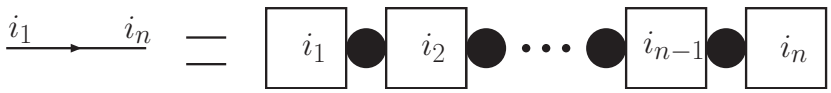

Figure B.2: Lowest order Feynman diagram of the propagator $\mathcal{G}_{i_1 i_n \sigma}$. The black dots correspond to a hopping amplitude t and the boxes represent the local propagators $\mathcal{G}_{ii\sigma}$ (see Fig. B.1).

At zero temperature, i.e., in the limit $\beta \to \infty$, we finally get

$$\begin{aligned} \mathcal{G}^R_{ii\sigma}(\omega) &= \frac{\Theta(\varepsilon_i - \mu)}{\omega - (\varepsilon_i - \mu) + \mathrm{i}0^+} + \frac{1}{2}\frac{\Theta(\varepsilon_i - (\mu - U))\,\Theta(\mu - \varepsilon_i)}{\omega - (\varepsilon_i - \mu) + \mathrm{i}0^+} \\ &\quad + \frac{1}{2}\frac{\Theta(\varepsilon_i - (\mu - U))\,\Theta(\mu - \varepsilon_i)}{\omega - (\varepsilon_i - \mu + U) + \mathrm{i}0^+} + \frac{\Theta((\mu - U) - \varepsilon_i)}{\omega - (\varepsilon_i - \mu + U) + \mathrm{i}0^+}, \end{aligned} \tag{B.22}$$

which is the correct expression for the local propagator in the atomic-limit, Eq. (6.27).

Next, we can proceed with the non-local propagator $\mathcal{G}^R_{ij\sigma}(\omega)$, which is needed to calculate the localization length, Eq. (6.40). Let's assume that the shortest path between site i and j, which is the only contribution entering in lowest order perturbation theory, is given by the sequence of sites $i_1, i_2, i_3, \ldots, i_{n-1}, i_n$, with $i = i_1$ and $j = i_n$. Then the perturbative expansion yields (cf. Fig. B.2)

$$\mathcal{G}^R_{ij\sigma}(\omega) = t^{n-1} \lim_{\lambda_{i_1}\to\infty} \ldots \lim_{\lambda_{i_n}\to\infty} \frac{\Gamma_{i_1}(\omega)\ldots\Gamma_{i_n}(\omega)}{\langle Q_{i_1}\ldots Q_{i_n}\rangle_0} \tag{B.23}$$

$$= \left(\lim_{\lambda_{i_1}\to\infty} \frac{\Gamma_{i_1}(\omega)}{\langle Q_{i_1}\rangle_0}\right) t \left(\lim_{\lambda_{i_2}\to\infty} \frac{\Gamma_{i_2}(\omega)}{\langle Q_{i_2}\rangle_0}\right) t \ldots t \left(\lim_{\lambda_{i_n}\to\infty} \frac{\Gamma_{i_n}(\omega)}{\langle Q_{i_n}\rangle_0}\right) \tag{B.24}$$

$$= \mathcal{G}^R_{i_1 i_1 \sigma}(\omega)\, t \ldots t\, \mathcal{G}^R_{i_n i_n \sigma}(\omega). \tag{B.25}$$

As the on-site energies are independent random variables, the disorder average has to be taken with respect to the original on-site energy distribution, whose joint probability function is $p(\varepsilon_{i_1}, \ldots, \varepsilon_{i_n}) \equiv p(\varepsilon_{i_1}) \ldots p(\varepsilon_{i_n})$, which yields

$$\overline{\mathcal{G}^R_{ij\sigma}(\omega)} = \overline{\mathcal{G}^R_{i_1 i_1 \sigma}(\omega)}\, t \ldots t\, \overline{\mathcal{G}^R_{i_n i_n \sigma}(\omega)} \tag{B.26}$$

Using Eq. (B.22) and identity (7.12), the right hand side of Eq. (B.26) can be transformed according to

$$\overline{\mathcal{G}^R_{ij\sigma}(\omega)} = \overline{G^{R,0}_{i_1 i_1 \sigma}(\omega)}\, t \ldots t\, \overline{G^{R,0}_{i_n i_n \sigma}(\omega)} \tag{B.27}$$

$$= \overline{G^R_{ij\sigma}(\omega)}, \tag{B.28}$$

where the disorder average of the non-interacting single-particle propagators has to be taken with respect to the effective distribution function $p_{\mathrm{A}}(\varepsilon)$.

Appendix C

Effective probability distributions of the atomic-limit approximation

In this chapter, we present a complete definition of the effective probability distribution function $p_{\mathrm{A}}(\varepsilon)$ as a function of (Δ, U, ρ) for spin $S = 1/2$ and $S = 3/2$. In the latter case, we restrict to the experimentally relevant regime $\rho < 1/2$.

C.1 Spin-1/2

Probability distribution function

1. case: $0 \le U \le \frac{1}{3}\Delta\rho\,, \quad 0 \le \rho \le 1 \qquad (\mu = \frac{1}{2}(\Delta\rho - \Delta + U))$

$$p_{\mathrm{A}}(\varepsilon) \;=\; \frac{1}{\Delta} \cdot \begin{cases} 1 \;, & -\Delta/2 + U \le \varepsilon \le \mu - U \\ 3/2 \;, & \mu - U \le \varepsilon \le \mu + U \\ 1 \;, & \mu + U \le \varepsilon \le \Delta/2 \\ 0 \;, & \text{elsewhere} \end{cases} \tag{C.1}$$

2. case: $\frac{1}{3}\Delta\rho < U \le \Delta\rho\,, \quad 0 \le \rho \le 1/2 \qquad (\mu = \frac{1}{2}(\Delta\rho - \Delta + U))$

$$p_{\mathrm{A}}(\varepsilon) \;=\; \frac{1}{\Delta} \cdot \begin{cases} 1/2 \;, & \mu - U \le \varepsilon \le -\Delta/2 + U \\ 3/2 \;, & -\Delta/2 + U \le \varepsilon \le \mu + U \\ 1 \;, & \mu + U \le \varepsilon \le \Delta/2 \\ 0 \;, & \text{elsewhere} \end{cases} \tag{C.2}$$

3. case: $\frac{1}{3}\Delta\rho < U \le \frac{1}{3}\Delta(2-\rho)\,, \quad 1/2 \le \rho \le 1 \qquad (\mu = \frac{1}{2}(\Delta\rho - \Delta + U))$

$$p_{\mathrm{A}}(\varepsilon) \;=\; \frac{1}{\Delta} \cdot \begin{cases} 1/2 \;, & \mu - U \le \varepsilon \le -\Delta/2 + U \\ 3/2 \;, & -\Delta/2 + U \le \varepsilon \le \mu + U \\ 1 \;, & \mu + U \le \varepsilon \le \Delta/2 \\ 0 \;, & \text{elsewhere} \end{cases} \tag{C.3}$$

4. case: $\frac{1}{3}\Delta(2-\rho) < U \leq \Delta\rho\,, \quad 1/2 \leq \rho \leq 1 \qquad (\mu = \frac{1}{2}(\Delta\rho - \Delta + U))$

$$p_{\rm A}(\varepsilon) \;=\; \frac{1}{\Delta}\cdot\begin{cases} 1/2 & , \quad \mu - U \leq \varepsilon \leq -\Delta/2 + U \\ 3/2 & , \quad -\Delta/2 + U \leq \varepsilon \leq \Delta/2 \\ 1/2 & , \quad \Delta/2 \leq \varepsilon \leq \mu + U \\ 0 & , \quad \text{elsewhere} \end{cases} \tag{C.4}$$

5. case: $\Delta\rho < U \leq \Delta(1-\rho)\,, \quad 0 \leq \rho \leq 1/2 \qquad (\mu = \Delta(\rho - \frac{1}{2}))$

$$p_{\rm A}(\varepsilon) \;=\; \frac{1}{\Delta}\cdot\begin{cases} 1/2 & , \quad -\Delta/2 \leq \varepsilon \leq \mu \\ 1 & , \quad \mu \leq \varepsilon \leq -\Delta/2 + U \\ 3/2 & , \quad -\Delta/2 + U \leq \varepsilon \leq \mu + U \\ 1 & , \quad \mu + U \leq \varepsilon \leq \Delta/2 \\ 0 & , \quad \text{elsewhere} \end{cases} \tag{C.5}$$

6. case: $\Delta(1-\rho) < U \leq \Delta\,, \quad 0 \leq \rho \leq 1/2 \qquad (\mu = \Delta(\rho - \frac{1}{2}))$

$$p_{\rm A}(\varepsilon) \;=\; \frac{1}{\Delta}\cdot\begin{cases} 1/2 & , \quad -\Delta/2 \leq \varepsilon \leq \mu \\ 1 & , \quad \mu \leq \varepsilon \leq -\Delta/2 + U \\ 3/2 & , \quad -\Delta/2 + U \leq \varepsilon \leq \Delta/2 \\ 1/2 & , \quad \Delta/2 \leq \varepsilon \leq \mu + U \\ 0 & , \quad \text{elsewhere} \end{cases} \tag{C.6}$$

7. case: $\Delta\rho < U \leq \Delta\,, \quad 1/2 \leq \rho \leq 1 \qquad (\mu = \Delta(\rho - \frac{1}{2}))$

$$p_{\rm A}(\varepsilon) \;=\; \frac{1}{\Delta}\cdot\begin{cases} 1/2 & , \quad -\Delta/2 \leq \varepsilon \leq \mu \\ 1 & , \quad \mu \leq \varepsilon \leq -\Delta/2 + U \\ 3/2 & , \quad -\Delta/2 + U \leq \varepsilon \leq \Delta/2 \\ 1/2 & , \quad \Delta/2 \leq \varepsilon \leq \mu + U \\ 0 & , \quad \text{elsewhere} \end{cases} \tag{C.7}$$

8. case: $\Delta < U, \quad 0 \leq \rho \leq 1 \qquad (\mu = \Delta(\rho - \frac{1}{2}))$

$$p_{\rm A}(\varepsilon) \;=\; \frac{1}{\Delta}\cdot\begin{cases} 1/2 & , \quad -\Delta/2 \leq \varepsilon \leq \mu \\ 1 & , \quad \mu \leq \varepsilon \leq \Delta/2 \\ 0 & , \quad \Delta/2 \leq \varepsilon \leq -\Delta/2 + U \\ 1/2 & , \quad -\Delta/2 + U \leq \varepsilon \leq \mu + U \\ 0 & , \quad \text{elsewhere} \end{cases} \tag{C.8}$$

9. case: $0 \le U \le \frac{1}{3}\Delta(2-\rho)\,, \quad 1 \le \rho \le 2 \qquad (\mu = \frac{1}{2}(\Delta\rho - \Delta + U))$

$$p_{\mathrm{A}}(\varepsilon) \;=\; \frac{1}{\Delta}\cdot\begin{cases} 1 \;, & -\Delta/2+U \le \varepsilon \le \mu - U \\ 3/2 \;, & \mu - U \le \varepsilon \le \mu + U \\ 1 \;, & \mu + U \le \varepsilon \le \Delta/2 \\ 0 \;, & \text{elsewhere} \end{cases} \tag{C.9}$$

10. case: $\frac{1}{3}\Delta(2-\rho) \le U \le \frac{1}{3}\Delta\rho\,, \quad 1 \le \rho \le 3/2 \qquad (\mu = \frac{1}{2}(\Delta\rho - \Delta + U))$

$$p_{\mathrm{A}}(\varepsilon) \;=\; \frac{1}{\Delta}\cdot\begin{cases} 1 \;, & -\Delta/2+U \le \varepsilon \le \mu - U \\ 3/2 \;, & \mu - U \le \varepsilon \le \Delta/2 \\ 1/2 \;, & \Delta/2 \le \varepsilon \le \mu + U \\ 0 \;, & \text{elsewhere} \end{cases} \tag{C.10}$$

11. case: $\frac{1}{3}\Delta\rho \le U \le \Delta(2-\rho)\,, \quad 1 \le \rho \le 3/2 \qquad (\mu = \frac{1}{2}(\Delta\rho - \Delta + U))$

$$p_{\mathrm{A}}(\varepsilon) \;=\; \frac{1}{\Delta}\cdot\begin{cases} 1/2 \;, & \mu - U \le \varepsilon \le -\Delta/2+U \\ 3/2 \;, & -\Delta/2+U \le \varepsilon \le \Delta/2 \\ 1/2 \;, & \Delta/2 \le \varepsilon \le \mu + U \\ 0 \;, & \text{elsewhere} \end{cases} \tag{C.11}$$

12. case: $\frac{1}{3}\Delta(2-\rho) \le U \le \Delta(2-\rho)\,, \quad 3/2 \le \rho \le 2 \qquad (\mu = \frac{1}{2}(\Delta\rho - \Delta + U))$

$$p_{\mathrm{A}}(\varepsilon) \;=\; \frac{1}{\Delta}\cdot\begin{cases} 1 \;, & -\Delta/2+U \le \varepsilon \le \mu - U \\ 3/2 \;, & \mu - U \le \varepsilon \le \Delta/2 \\ 1/2 \;, & \Delta/2 \le \varepsilon \le \mu + U \\ 0 \;, & \text{elsewhere} \end{cases} \tag{C.12}$$

13. case: $\Delta(2-\rho) \le U \le \Delta(\rho-1)\,, \quad 3/2 \le \rho \le 2 \qquad (\mu = \Delta(\rho - \frac{3}{2}) + U)$

$$p_{\mathrm{A}}(\varepsilon) \;=\; \frac{1}{\Delta}\cdot\begin{cases} 1 \;, & -\Delta/2+U \le \varepsilon \le E_2 \\ 3/2 \;, & E_2 \le \varepsilon \le \Delta/2 \\ 1 \;, & \Delta/2 \le \varepsilon \le E_2 + U \\ 1/2 \;, & E_2 + U \le \varepsilon \le \Delta/2 + U \\ 0 \;, & \text{elsewhere} \end{cases} \tag{C.13}$$

14. case: $\Delta(\rho-1) \le U \le \Delta\,, \quad 3/2 \le \rho \le 2 \quad (\mu = \Delta(\rho - \frac{3}{2}) + U)$

$$p_{\rm A}(\varepsilon) \;=\; \frac{1}{\Delta}\cdot\begin{cases} 1/2 & , \quad E_2 \le \varepsilon \le -\Delta/2+U \\ 3/2 & , \quad -\Delta/2+U \le \varepsilon \le \Delta/2 \\ 1 & , \quad \Delta/2 \le \varepsilon \le E_2+U \\ 1/2 & , \quad E_2+U \le \varepsilon \le \Delta/2+U \\ 0 & , \quad \text{elsewhere} \end{cases} \tag{C.14}$$

15. case: $\Delta(2-\rho) \le U \le \Delta\,, \quad 1 \le \rho \le 3/2 \quad (\mu = \Delta(\rho - \frac{3}{2}) + U)$

$$p_{\rm A}(\varepsilon) \;=\; \frac{1}{\Delta}\cdot\begin{cases} 1/2 & , \quad E_2 \le \varepsilon \le -\Delta/2+U \\ 3/2 & , \quad -\Delta/2+U \le \varepsilon \le \Delta/2 \\ 1 & , \quad \Delta/2 \le \varepsilon \le E_2+U \\ 1/2 & , \quad E_2+U \le \varepsilon \le \Delta/2+U \\ 0 & , \quad \text{elsewhere} \end{cases} \tag{C.15}$$

16. case: $\Delta \le U\,, \quad 1 \le \rho \le 2 \quad (\mu = \Delta(\rho - \frac{3}{2}) + U)$

$$p_{\rm A}(\varepsilon) \;=\; \frac{1}{\Delta}\cdot\begin{cases} 1/2 & , \quad E_2 \le \varepsilon \le \Delta/2 \\ 0 & , \quad \Delta/2 \le \varepsilon \le -\Delta/2+U \\ 1 & , \quad -\Delta/2+U \le \varepsilon \le E_2+U \\ 1/2 & , \quad E_2+U \le \varepsilon \le \Delta/2+U \\ 0 & , \quad \text{elsewhere} \end{cases} \tag{C.16}$$

Mean value and variance

$$\overline{\varepsilon} \;=\; \frac{1}{2}U\rho \tag{C.17}$$

$$\sigma^2 \;\equiv\; \mathrm{var}[\varepsilon] \;=\; \frac{\Delta^2}{12}\begin{cases} 1-\hat\rho\hat U+\hat\rho\hat U^2+3\hat U^3 & , \quad \rho<1\,,\,\hat U<\rho \\ 1-2\rho'\hat U+\hat\rho\hat U^2 & , \quad \rho<1\,,\,\hat U\ge\rho \\ 1-\hat\rho\hat U+\hat\rho\hat U^2+3\hat U^3 & , \quad \rho\ge1\,,\,\hat U<2-\rho \\ 1-2\tilde\rho\hat U+\hat\rho\hat U^2 & , \quad \rho\ge1\,,\,\hat U\ge2-\rho, \end{cases} \tag{C.18}$$

with

$$\hat U \;=\; U/\Delta\,, \quad \hat\rho \;=\; 3\rho(2-\rho)\,, \quad \rho' \;=\; 3\rho(1-\rho)\,, \quad \tilde\rho \;=\; 3\left(\tfrac{1}{4}-(\rho-\tfrac{3}{2})^2\right)$$

C.2 Spin-3/2

Only results for $\rho < 1/2$ were presented (see Sec. 7.5).

Probability distribution function

1. case: $0 \leq U \leq \frac{1}{10}\Delta\rho \qquad (\mu = \frac{1}{4}(\Delta\rho - 2\Delta + 6U))$

$$p_{\mathrm{A}}(\varepsilon) \;=\; \frac{1}{\Delta} \cdot \begin{cases} 1 \;, & -\Delta/2 + 3U \leq \varepsilon \leq \mu - U \\ 5/2 \;, & \mu - U \leq \varepsilon \leq \mu + U \\ 1 \;, & \mu + U \leq \varepsilon \leq \Delta/2 \\ 0 \;, & \text{elsewhere} \end{cases} \tag{C.19}$$

2. case: $\frac{1}{10}\Delta\rho \leq U \leq \frac{1}{6}\Delta\rho \qquad (\mu = \frac{1}{4}(\Delta\rho - 2\Delta + 6U))$

$$p_{\mathrm{A}}(\varepsilon) \;=\; \frac{1}{\Delta} \cdot \begin{cases} 3/2 \;, & \mu - U \leq \varepsilon \leq -\Delta/2 + 3U \\ 5/2 \;, & -\Delta/2 + 3U \leq \varepsilon \leq \mu + U \\ 1 \;, & \mu + U \leq \varepsilon \leq \Delta/2 \\ 0 \;, & \text{elsewhere} \end{cases} \tag{C.20}$$

3. case: $\frac{1}{6}\Delta\rho \leq U \leq \frac{1}{3}\Delta\rho \qquad (\mu = \frac{1}{3}(\Delta\rho - \frac{3}{2}\Delta + 3U))$

$$p_{\mathrm{A}}(\varepsilon) \;=\; \frac{1}{\Delta} \cdot \begin{cases} 3/4 \;, & \mu - U \leq \varepsilon \leq -\Delta/2 + 2U \\ 3/2 \;, & -\Delta/2 + 2U \leq \varepsilon \leq \mu \\ 9/4 \;, & \mu \leq \varepsilon \leq -\Delta/2 + 3U \\ 5/2 \;, & -\Delta/2 + 3U \leq \varepsilon \leq \mu + U \\ 1 \;, & \mu + U \leq \varepsilon \leq \Delta/2 \\ 0 \;, & \text{elsewhere} \end{cases} \tag{C.21}$$

4. case: $\frac{1}{3}\Delta\rho \leq U \leq \Delta\rho \qquad (\mu = \frac{1}{2}(\Delta\rho - \Delta + U))$

$$p_{\mathrm{A}}(\varepsilon) \;=\; \frac{1}{\Delta} \cdot \begin{cases} 1/4 \;, & \mu - U \leq \varepsilon \leq -\Delta/2 + U \\ 3/4 \;, & -\Delta/2 + U \leq \varepsilon \leq \mu \\ 7/4 \;, & \mu \leq \varepsilon \leq -\Delta/2 + 2U \\ 9/4 \;, & -\Delta/2 + 2U \leq \varepsilon \leq \mu + U \\ 1 \;, & \mu + U \leq \varepsilon \leq \Delta/2 \\ 0 \;, & \text{elsewhere} \end{cases} \tag{C.22}$$

5. case: $\Delta\rho \le U \le \Delta - \Delta\rho \qquad (\mu = \Delta(\rho - \frac{1}{2}))$

$$p_{\mathrm{A}}(\varepsilon) = \frac{1}{\Delta} \cdot \begin{cases} 1/4 & , \quad -\Delta/2 \le \varepsilon \le \mu \\ 1 & , \quad \mu \le \varepsilon \le -\Delta/2 + U \\ 7/4 & , \quad -\Delta/2 + U \le \varepsilon \le \mu + U \\ 1 & , \quad \mu + U \le \varepsilon \le \Delta/2 \\ 0 & , \quad \text{elsewhere} \end{cases} \tag{C.23}$$

6. case: $\Delta - \Delta\rho \le U \le \Delta \qquad (\mu = \Delta(\rho - \frac{1}{2}))$

$$p_{\mathrm{A}}(\varepsilon) = \frac{1}{\Delta} \cdot \begin{cases} 1/4 & , \quad -\Delta/2 \le \varepsilon \le \mu \\ 1 & , \quad \mu \le \varepsilon \le -\Delta/2 + U \\ 7/4 & , \quad -\Delta/2 + U \le \varepsilon \le \Delta/2 \\ 3/4 & , \quad \Delta/2 \le \varepsilon \le \mu + U \\ 0 & , \quad \text{elsewhere} \end{cases} \tag{C.24}$$

7. case: $\Delta \le U \qquad (\mu = \Delta(\rho - \frac{1}{2}))$

$$p_{\mathrm{A}}(\varepsilon) = \frac{1}{\Delta} \cdot \begin{cases} 1/4 & , \quad -\Delta/2 \le \varepsilon \le \mu \\ 1 & , \quad \mu \le \varepsilon \le \Delta/2 \\ 0 & , \quad \Delta/2 \le \varepsilon \le -\Delta/2 + U \\ 3/4 & , \quad -\Delta/2 + U \le \varepsilon \le \mu + U \\ 0 & , \quad \text{elsewhere} \end{cases} \tag{C.25}$$

Mean value and variance

$$\overline{\varepsilon} = \frac{3}{4} U\rho \tag{C.26}$$

$$\sigma^2 = \frac{\Delta^2}{12} \begin{cases} 1 + \frac{9}{4}\rho(\rho-4)\hat{U} - \frac{27}{4}\rho(\rho-4)\hat{U}^2 - 15\hat{U}^3 & , \quad 0 \le \hat{U} < \frac{1}{6}\rho \\ 1 + 3\rho(\rho-3)\hat{U} - \frac{27}{4}\rho(\rho-\frac{4}{9})\hat{U}^2 - 6\hat{U}^3 & , \quad \frac{1}{6}\rho \le \hat{U} < \frac{1}{3}\rho \\ 1 + \frac{9}{2}\rho(\rho-2)\hat{U} - \frac{27}{4}\rho(\rho-\frac{20}{9})\hat{U}^2 - \frac{3}{2}\hat{U}^3 & , \quad \frac{1}{3}\rho \le \hat{U} < \rho \\ 1 + 9\rho(\rho-1)\hat{U} - \frac{3}{4}\rho(\rho-12)\hat{U}^2 & , \quad \rho \le \hat{U} \end{cases} \tag{C.27}$$

with $\hat{U} = U/\Delta$

Appendix D

Herbert-Jones-Thouless formula

In this chapter, we will briefly present the main steps of the proof of the Herbert-Jones-Thouless formula used in Sec. (6.4). For that purpose, we consider the one-dimensional single-particle Anderson Hamiltonian with N lattice sites and periodic boundary conditions

$$\hat{H} \;=\; \sum_{i=1}^{N} \varepsilon_i c_i^\dagger c_i \;+\; t \sum_{i=1}^{N} (c_{i+1}^\dagger c_i + c_{i-1}^\dagger c_i). \tag{D.1}$$

The eigenvalues and eigenstates of $\hat{H}$ shall be denoted by $\{E_1, ..., E_N\}$ and $\{|\psi_1\rangle, ..., |\psi_N\rangle\}$, respectively. Furthermore, we set $t = 1$ and denote the eigenfunction amplitudes by $a_i^j \equiv \langle i|\psi_j\rangle$, which are assumed to be real.

Using the definition of the single-particle propagator as the resolvent (cf. Eq. (3.3)),

$$G(E) \;=\; (E - \hat{H})^{-1}, \tag{D.2}$$

we can express it as [HJ71]

$$G(E) \;=\; \frac{\mathrm{adj}(E - \hat{H})^{-1}}{\det(E - \hat{H})} \;=\; \frac{\mathrm{adj}(E - \hat{H})^{-1}}{\prod_{i=1}^{N} (E - E_i)}, \tag{D.3}$$

where $\mathrm{adj}(E - \hat{H})^{-1}$ denotes the adjugate matrix of $(E - \hat{H})^{-1}$. From Eq. (D.1) we obtain the matrix element

$$\langle 1|\mathrm{adj}(E - \hat{H})^{-1}|N\rangle \;=\; (-1)^{N+1} \det(A) \;=\; (-1)^{N+1}. \tag{D.4}$$

Here, A is the lower triangular matrix

$$A = \begin{pmatrix} 1 & & & & & \\ E-\varepsilon_2 & 1 & & & 0 & \\ 1 & E-\varepsilon_3 & 1 & & & \\ & 1 & E-\varepsilon_4 & 1 & & \\ & & \ddots & \ddots & \ddots & \\ 0 & & & 1 & E-\varepsilon_N & 1 \end{pmatrix}. \tag{D.5}$$

Thus, we get [HJ71]

$$G_{1N}(E) \equiv \langle 1|G(E)|N\rangle = \frac{\langle 1|\mathrm{adj}(E-\hat{H})^{-1}|N\rangle}{\prod_{i=1}^{N}(E-E_i)} = \frac{(-1)^{N+1}}{\prod_{i=1}^{N}(E-E_i)}. \tag{D.6}$$

At $E = E_j$, $G_{1N}(E)$ has a pole with residuum[1]

$$R(E_j) = \frac{(-1)^{N+1}}{\prod_{\substack{i=1 \\ i\neq j}}^{N}(E_j-E_i)}. \tag{D.7}$$

On the other hand, we can express the residuum in terms of the eigenfunction amplitudes [Tho72],

$$\begin{aligned} R(E_j) &= \lim_{E\to E_j}(E-E_j)G_{1N}(E) && \text{(D.8)}\\ &= \lim_{E\to E_j}(E-E_j)\,\langle 1|(E-\hat{H})^{-1}|N\rangle && \text{(D.9)}\\ &= \lim_{E\to E_j}(E-E_j)\sum_{i=1}^{N} a_1^i\, a_N^i\,(E-E_i)^{-1} && \text{(D.10)}\\ &= a_1^j\, a_N^j. && \text{(D.11)} \end{aligned}$$

Using the asymptotics of the localized wavefunctions, Eq. (3.5), we can estimate

$$|a_1^j\, a_N^j| = C\cdot e^{-(N-1)/\xi_j}. \tag{D.12}$$

[1]We can assume the eigenvalues to be non-degenerate, because in the infinite system, all eigenvalues of $\hat{H}$ are non-degenerate with probability 1.

Then, from Eqs. (D.7), (D.11) and (D.12) we obtain,

$$\frac{1}{\xi_j} = -\lim_{N\to\infty}\frac{1}{N-1}\log|a_1^j\, a_N^j| \tag{D.13}$$

$$= \lim_{N\to\infty}\frac{1}{N-1}\sum_{\substack{i=1\\ i\neq j}}^{N}\log|E_j - E_i| \tag{D.14}$$

$$= \int d\varepsilon\, N(\varepsilon)\,\log|E_j-\varepsilon|. \tag{D.15}$$

In the last line, we inserted the definition of the integrated (disorder-averaged) density of states,

$$N(\varepsilon) = \frac{1}{N}\sum_{i=1}^{N}\delta(E-E_i). \tag{D.16}$$

To finish the proof of the Herbert-Jones-Thouless formula, we have to consider the case $E \neq E_i\ \forall i \in \{1,...,N\}$. In this case, from Eq. (D.2) one can derive the recursion relation

$$G_{iN}(E) = (\varepsilon_i - E)G_{i-1,N}(E) - G_{i-2,N}(E) \tag{D.17}$$

$$\Leftrightarrow \quad \begin{pmatrix} G_{NN}(E)\\ G_{N-1,N}(E)\end{pmatrix} = \prod_{i=1}^{N} T^{(i)}(E)\begin{pmatrix} G_{10}(E)\\ 0\end{pmatrix}, \tag{D.18}$$

where we introduced the transfer matrix

$$T^{(i)}(E) = \begin{pmatrix} \varepsilon_i - E & -1\\ 1 & 0\end{pmatrix}. \tag{D.19}$$

The same recursion relation is achieved if we construct an iterative solution of $\hat{H}|\psi\rangle = E|\psi\rangle$,

$$\begin{pmatrix} a_N(E)\\ a_{N-1}(E)\end{pmatrix} = \prod_{i=1}^{N} T^{(i)}(E)\begin{pmatrix} a_1(E)\\ 0\end{pmatrix}, \quad a_i(E) = \langle i|\psi\rangle, \tag{D.20}$$

which yields

$$\frac{a_N(E)}{a_1(E)} = \frac{G_{NN}(E)}{G_{1N}(E)}. \tag{D.21}$$

Since E is not an eigenvalue of $\hat{H}$, the iterative solution grows exponentially [Tho72, Ish73, LGP88],

$$a_N(E) \sim e^{N/\xi(E)} a_1(E). \tag{D.22}$$

Thus, we get

$$\frac{1}{\xi(E)} = \lim_{N\to\infty}\frac{1}{N}\log\left|\frac{G_{NN}(E)}{G_{1N}(E)}\right| \tag{D.23}$$

$$= \lim_{N\to\infty}\frac{1}{N}\left\{\log\left|\sum_{i=1}^{N}\frac{|a_i^N|^2}{E-E_i}\right| + \sum_{i=1}^{N}\log|E-E_i|\right\}. \tag{D.24}$$

The first term contributes only, if $|E-E_j| < e^{-N}$ for some E_j. Otherwise it cancels completely in the limit $N\to\infty$. Therefore, if we denote the eigenvalue closest to E by E_j, we get

$$\lim_{N\to\infty}\frac{1}{N}\sum_{i=1}^{N}\log|E-E_i| \leq \frac{1}{\xi(E)} \leq \lim_{N\to\infty}\frac{1}{N}\sum_{\substack{i=1\\ i\neq j}}^{N}\log|E-E_i|. \tag{D.25}$$

Combining Eqs. (D.15) and (D.25) we finally arrive at the Herbert-Jones-Thouless formula,

$$\frac{1}{\xi(E)} = \int d\varepsilon\, N(\varepsilon)\,\log|E-\varepsilon|. \tag{D.26}$$

Appendix E

Coherent potential approximation

In the following, we will briefly derive the self-consistent equations of the coherent potential approximation (CPA). For extensive reviews on this method and applications to disordered systems see, e.g., [YM73, EKL74].

The CPA is the best single-site approximation for calculating the self-energy of a disordered, single-particle lattice model. For its derivation we again restrict our considerations to the Anderson Hamiltonian

$$\hat{H}_A \;=\; \sum_{i\sigma} \varepsilon_i c^\dagger_{i\sigma} c_{i\sigma} \;-\; t \sum_{<i,j>,\sigma} c^\dagger_{i\sigma} c_{j\sigma}. \tag{E.1}$$

The idea of the effective medium approximation is to introduce a complex, effective potential (the CPA self-energy) $\Sigma(E)$, which incorporates the effect of the disorder potential on a disorder-averaged level. For that purpose, we rewrite the Anderson Hamiltonian as

$$\begin{aligned} \hat{H}_A \;&\equiv\; \hat{H}_{dis} + \hat{H}_{kin} \equiv \hat{V} + \hat{H}_0 \\ &=\; \sum_{i\sigma} (\varepsilon_i - \Sigma(E)) c^\dagger_{i\sigma} c_{i\sigma} \;-\; \sum_{i,j,\sigma} (t_{ij} - \Sigma(E)\,\delta_{i,j}) c^\dagger_{i\sigma} c_{j\sigma}, \end{aligned} \tag{E.2}$$

with

$$t_{ij} \;:=\; \begin{cases} t & , \quad |i-j| = 1 \\ 0 & , \quad \text{otherwise} \end{cases} . \tag{E.3}$$

Treating the local disorder potential $\hat{V}$ as a perturbation to the kinetic term, the unperturbed propagator reads

$$\begin{aligned} \hat{g}(E) \;&=\; (E - \hat{H}_{kin})^{-1} \\ \Leftrightarrow \quad g_k(E) \;&=\; \langle k | (E - \hat{H}_{kin})^{-1} | k \rangle \;=\; \frac{1}{E - \epsilon_k - \Sigma(E)}, \end{aligned} \tag{E.4}$$

where ϵ_k is the Fourier transform of the kinetic tight-binding potential, Eq. (7.14). The full propagator of the Anderson Hamiltonian, Eq. (E.2), is then given by

$$\hat{G}(E) \;=\; (E - \hat{H}_A)^{-1} \;=\; \hat{g}(E) \,+\, \hat{g}(E)\hat{T}(E)\hat{g}(E), \tag{E.5}$$

where

$$\hat{T}(E) \;=\; \hat{V}(E) \,+\, \hat{V}(E)\hat{g}(E)\hat{T}(E) \tag{E.6}$$

is the single-particle scattering matrix.

By definition, the CPA self-energy shall include on average all scattering contributions. Therefore, it is required that the disorder-averaged scattering matrix vanishes,

$$\overline{\hat{T}} \;\stackrel{!}{=}\; 0. \tag{E.7}$$

Defining

$$\hat{t}_i(E) \;\equiv\; t_i(E)\,|i\rangle\langle i|, \tag{E.8}$$

$$t_i(E) \;\equiv\; V_i\,(E) \,+\, V_i\,(E) g_{ii}(E) t_i(E) \;=\; \frac{V_i\,(E)}{1 - V_i\,(E) g_{ii}(E)}, \tag{E.9}$$

where

$$V_i\,(E) \;=\; \langle i|\hat{V}(E)|i\rangle \;=\; \varepsilon_i - \Sigma, \tag{E.10}$$

$$g_{ii}(E) \;=\; \langle i|\hat{g}(E)|i\rangle \;=\; \int \frac{dk}{(2\pi)^d}\, g_k(E), \tag{E.11}$$

Eq. (E.6) can be rewritten as

$$\begin{aligned}\hat{T}(E) \;=\; & \sum_i \hat{t}_i(E) \,+\, \sum_{i\neq j} \hat{t}_i(E)\hat{g}(E)\hat{t}_j(E) \\ & +\, \sum_{i\neq j\neq k} \hat{t}_i(E)\hat{g}(E)\hat{t}_j(E)\hat{g}(E)\hat{t}_k(E) \,+\, \ldots\,.\end{aligned} \tag{E.12}$$

Therefore, the CPA condition, Eq. (E.7), becomes

$$\begin{aligned}0 \;\stackrel{!}{=}\; & \sum_i \overline{\hat{t}_i(E)} \,+\, \sum_{i\neq j} \overline{\hat{t}_i(E)\hat{g}(E)\hat{t}_j(E)} \\ & +\, \sum_{i\neq j\neq k} \overline{\hat{t}_i(E)\hat{g}(E)\hat{t}_j(E)\hat{g}(E)\hat{t}_k(E)} \,+\, \ldots\,.\end{aligned} \tag{E.13}$$

To take the average over disorder realizations, we apply a single-site approximation and assume that a particle never returns to a lattice site, i.e, we assume

that the restrictions on the sums, $i \neq j, i \neq j \neq k, \ldots$, can be replaced by the restriction that all indices are pairwise distinct. Then we finally obtain

$$\begin{aligned} 0 \stackrel{!}{=} & \sum_i \overline{\hat{t}_i(E)} + \sum_{i \neq j} \overline{\hat{t}_i(E)} \hat{g}(E) \overline{\hat{t}_j(E)} \\ & + \sum_{i \neq j \neq k \neq i} \overline{\hat{t}_i(E)} \hat{g}(E) \overline{\hat{t}_j(E)} \hat{g}(E) \overline{\hat{t}_k(E)} + \ldots . \end{aligned} \tag{E.14}$$

Since the system becomes translationally invariant after averaging over disorder realizations, i.e., $\overline{\hat{t}_i(E)} = \overline{\hat{t}_j(E)}$, $\forall i, j$, condition (E.14) yields

$$0 \stackrel{!}{=} \overline{\hat{t}_i(E)} = \int d\varepsilon \, p(\varepsilon) \frac{\varepsilon - \Sigma(E)}{1 - g_{ii}(E)(\varepsilon - \Sigma(E))}, \tag{E.15}$$

where $p(\varepsilon)$ is the probability density of the on-site energy distribution. Finally, we use Dyson's equation

$$\overline{\hat{G}}(E) = \left(E - \hat{H}_{kin} - \Sigma(E) \right)^{-1} \tag{E.16}$$

to make Eq. (E.15) self-consistent and end up with the CPA equation

$$0 = \int d\varepsilon \, p(\varepsilon) \frac{\varepsilon - \Sigma(E)}{1 - \overline{G}_0(E)(\varepsilon - \Sigma(E))}, \tag{E.17}$$

where

$$\overline{G}_0(E) = \int \frac{dk}{(2\pi)^d} \frac{1}{E - \epsilon_k - \Sigma(E)}. \tag{E.18}$$

(An alternative diagrammatical derivation of Eq. (E.17) is also possible and can be found in [EKL74].)

The CPA condition, Eq. (E.17), was derived under the assumption of weak disorder, where the local potential was taken as a perturbation of the extended states. Thus, the CPA becomes exact in the limit $\Delta/t \to 0$ [YM73]. However, the CPA becomes also exact in the limit of strong disorder, $t/\Delta \to 0$, because the CPA equation can also be derived within a locator expansion taking the kinetic term as a perturbation [EKL74, KKW90, Kro90]. Thus, the CPA is the best single-site approximation and, in addition, it interpolates between the limits of strong and weak disorder.

Finally, two more equivalent formulations of the CPA exist:

$$\Sigma(E) = \int d\varepsilon \, p(\varepsilon) \frac{\varepsilon}{1 - \overline{G}_0(E)(\varepsilon - \Sigma(E))} \tag{E.19}$$

and

$$1 = \int d\varepsilon\, p(\varepsilon) \frac{1}{1 - \overline{G}_0(E)(\varepsilon - \Sigma(E))}. \tag{E.20}$$

Proof.
E.17 $\Leftrightarrow$ E.19:
From Dyson's equation we get $\Sigma(E) \neq -(\overline{G}_0(E))^{-1}$ and can conclude

$$\begin{aligned}
\Sigma(E) &= \int d\varepsilon\, p(\varepsilon) \frac{\varepsilon}{1 - \overline{G}_0(E)(\varepsilon - \Sigma(E))} \\
\Leftrightarrow \quad 0 &= \int d\varepsilon\, p(\varepsilon) \frac{\varepsilon}{1 - \overline{G}_0(E)(\varepsilon - \Sigma(E))} - \Sigma(E) \\
\Leftrightarrow \quad 0 &= \int d\varepsilon\, p(\varepsilon) \frac{\varepsilon - \Sigma(E) + (\varepsilon - \Sigma(E))\overline{G}_0(E)\Sigma(E)}{1 - \overline{G}_0(E)(\varepsilon - \Sigma(E))} \\
\Leftrightarrow \quad 0 &= \int d\varepsilon\, p(\varepsilon) \frac{\varepsilon - \Sigma(E)}{1 - \overline{G}_0(E)(\varepsilon - \Sigma(E))} (1 + \overline{G}_0(E)\Sigma(E)) \\
\Leftrightarrow \quad 0 &= \int d\varepsilon\, p(\varepsilon) \frac{\varepsilon - \Sigma(E)}{1 - \overline{G}_0(E)(\varepsilon - \Sigma(E))}
\end{aligned}$$

E.17 $\Leftrightarrow$ E.20:
Here we use that $\overline{G}_0(E) \neq 0$ and conclude

$$\begin{aligned}
1 &= \int d\varepsilon\, p(\varepsilon) \frac{1}{1 - \overline{G}_0(E)(\varepsilon - \Sigma(E))} \\
\Leftrightarrow \quad 0 &= \int d\varepsilon\, p(\varepsilon) \frac{1}{1 - \overline{G}_0(E)(\varepsilon - \Sigma(E))} - 1 \\
\Leftrightarrow \quad 0 &= \int d\varepsilon\, p(\varepsilon) \frac{\varepsilon - \Sigma(E)}{1 - \overline{G}_0(E)(\varepsilon - \Sigma(E))} \overline{G}_0(E) \\
\Leftrightarrow \quad 0 &= \int d\varepsilon\, p(\varepsilon) \frac{\varepsilon - \Sigma(E)}{1 - \overline{G}_0(E)(\varepsilon - \Sigma(E))}
\end{aligned}$$

□

Appendix F

Self-consistent transport theory of Anderson localization

In this chapter, we will briefly sketch the derivation of the self-consistent transport theory of Anderson localization and discuss some analytical properties used in the analysis of the atomic-limit approximation. Originally, the self-consistent theory was derived for weak disorder and dimensions $d \leq 2$, starting from an extended state basis [VW80a, VW80b]. Later on, the theory was re-developed using a locator expansion [Kop84a, Kop84b] finally resulting in a formulation valid for arbitrary disorder strength [KKW90, Kro90]. A detailed review can be found in [VW92]. Our presentation will closely follow the argumentation of [Kro90].

F.1 Derivation of the self-consistent equation

To obtain the self-consistent equation for the dynamical diffusion coefficient, we start by considering the particle-hole Green's function (cf. Eq.(3.18))

$$\Phi_{kk'}(E,\omega,q) \;=\; \overline{G^R(E+\omega,k+q/2,k'+q/2)\,G^A(E,k'-q/2,k-q/2)}. \quad \text{(F.1)}$$

Denoting the irreducible two-particle vertex function by $U_{kk'}(E,\omega,q)$, the particle-hole Green's function can be expressed by the Bethe-Salpeter equation [Ram98]

$$\begin{aligned}\Phi_{kk'}(E,\omega,q) \;&=\; \overline{G^R_{k+q/2}(E+\omega)}\,\overline{G^A_{k-q/2}(E)} \\ &\quad\times\left(\delta(k-k') \;+\; \int \frac{dk''}{(2\pi)^d}\,U_{kk''}(E,\omega,q)\,\Phi_{k''k'}(E,\omega,q)\right). \quad \text{(F.2)}\end{aligned}$$

Eq. (F.2) can be simplified by using the identity

$$\overline{G^R}\,\overline{G^A} \;=\; -\frac{\overline{G^R}-\overline{G^A}}{\frac{1}{\overline{G^R}}-\frac{1}{\overline{G^A}}} \quad \text{(F.3)}$$

and the Ward identity

$$\Delta\Sigma_k(E,\omega,q) \;=\; \int \frac{dk'}{(2\pi)^d}\, U_{kk'}(E,\omega,q)\, \Delta G_{k'}(E,\omega,q), \tag{F.4}$$

where

$$\Delta\Sigma_k(E,\omega,q) \;\equiv\; \Sigma^R_{k+q/2}(E+\omega) \,-\, \Sigma^A_{k-q/2}(E) \tag{F.5}$$

$$\Delta G_k(E,\omega,q) \;\equiv\; \overline{G^R_{k+q/2}(E+\omega)} - \overline{G^A_{k-q/2}(E)}. \tag{F.6}$$

Thus, in ladder approximation (cf. Appendix A, Fig. A.2), where $U_{kk'}(E,\omega,q) \equiv U(\omega,q)$, the full two-particle vertex function becomes

$$\Gamma_{kk'}(E,\omega,q) \;=\; U_{kk'}(E,\omega,q) \,+\, \int \frac{dk''}{(2\pi)^d}\, U_{kk''}(E,\omega,q)\, \overline{G^R_{k+q/2}(E+\omega)} \times \overline{G^A_{k-q/2}(E)}\, \Gamma_{k''k'}(E,\omega,q) \tag{F.7}$$

$$= \;\frac{U(\omega,q)}{1 \,-\, U(\omega,q)\, \int \frac{dk''}{(2\pi)^d}\, \overline{G^R_{k''+q/2}(E+\omega)}\, \overline{G^A_{k''-q/2}(E)}} \tag{F.8}$$

$$\overset{\omega,q\to 0}{=} \; -\frac{2\mathrm{Im}\overline{G^R_0}(E) U(\omega,q)^2}{-\mathrm{i}\omega \,+\, D_0(E) q^2}, \tag{F.9}$$

with

$$D_0(E) \;=\; -\frac{1}{\mathrm{Im}\overline{G^R_0}(E)} \int \frac{dk}{(2\pi)^d} (v_k \cdot \hat{q})^2 [\mathrm{Im}\overline{G^R_k}(E)]^2. \tag{F.10}$$

The corresponding expression for the cooperon vertex then reads

$$\tilde{C}(E,\omega,k,k') \;=\; \frac{2\mathrm{Im}\overline{G^R_0}(E) U(\omega,q)^2}{-\mathrm{i}\omega \,+\, D_0(E)(k+k')^2} \tag{F.11}$$

In the limit of weak disorder, Eq. (F.9) becomes the well-known diffusion propagator, Eq. (A.20), and $D_0(E)$ becomes the bare diffusion constant, Eq. (A.19) (see Sec. F.3.1).

At the Anderson transition and within the localized phase, the diffusion coefficient vanishes. Therefore, a diagrammatic expansion for $D(E,\omega)$ is difficult, as one has to ensure that all contributions, taken into account, cancel each other exactly. Thus, even small contributions have to be included. In contrast, the self-consistent transport theory is based on a diagrammatic expansion of the density correlation function $\Phi_{kk'}(E,\omega,q)$, which is related to the *inverse* diffusion coefficient [VW80a, Ram98], which diverges in the limit $\omega \to 0$, $q \neq 0$. From Eqs. (F.3)

and (F.4) and using the hydrodynamic limit, the momentum-integrated density-density correlation function can be written as [Kro90]

$$\Phi(E,\omega,q) = \int \frac{dk}{(2\pi)^d} \int \frac{dk'}{(2\pi)^d}\, \Phi_{kk'}(E,\omega,q) \tag{F.12}$$

$$= \frac{-2\mathrm{Im}\overline{G_0^R}(E) + \frac{q\,R(E)}{-\mathrm{i}\omega + 1/\tau + M(E,\omega)}}{-\mathrm{i}\omega + q^2 D(E,\omega)}, \tag{F.13}$$

where the current-relaxation kernel is given by

$$M(E,\omega) = -\frac{2}{\mathrm{Im}\overline{G_0^R}(E)\, D_0(E)} \int \frac{dk}{(2\pi)^d} \int \frac{dk'}{(2\pi)^d} (v_k \cdot \hat{q})\, \mathrm{Im}\overline{G_k^R}(E) \times U_{kk'}(E,\omega)\, (\mathrm{Im}\overline{G_{k'}^R}(E))^2 (v_{k'} \cdot \hat{q}), \tag{F.14}$$

$$R(E) = \frac{1}{2} \int \frac{dk}{(2\pi)^d} (v_k \cdot \hat{q})^2\, (\overline{G_k^R}(E)^2 + \overline{G_k^A}(E)^2), \tag{F.15}$$

and the generalized, frequency-dependent diffusion coefficient is defined as

$$D(E,\omega) = \frac{D_0(E)}{1 - \mathrm{i}\omega\tau + \tau M(E,\omega)}. \tag{F.16}$$

This diffusion coefficient, which enters in Eq. (F.13), is the bare one, renormalized by the inverse current-relaxation kernel. As mentioned above, we can calculate the inverse current-relaxation kernel by approximating $U_{kk'}(E,\omega)$ by the most diverging class of diagrams. As it was shown in [VW80a, VW80b], this class is generated by the maximally crossed diagrams (see [Ram98] as well). With this identification, Eq. (F.16) finally becomes [Kro90]

$$D(E,\omega) = D_0(E) + \frac{2\mathrm{Im}\Sigma^R(E)}{[\mathrm{Im}\overline{G_0^R}(E)]^2\, D_0(E)} \int \frac{dk}{(2\pi)^d} \int \frac{dk'}{(2\pi)^d} (v_k \cdot \hat{q}) \times \frac{\mathrm{Im}\overline{G_k^R}(E)[\mathrm{Im}\overline{G_{k'}^R}(E)]^2}{(k+k')^2 - \mathrm{i}\omega/D(\omega,E)}\, (v_{k'} \cdot \hat{q}). \tag{F.17}$$

In the limit $\omega \to 0$, the dynamic diffusion coefficient vanishes in the localized regime as [VW80a, VW80b, Ram98]

$$D(E,\omega) = -\mathrm{i}\omega\tilde{\xi}^2(E) + \mathcal{O}(\omega^2). \tag{F.18}$$

Here, $\tilde{\xi}^2(E)$ is the decay (localization) length of the *two*-particle Green's function, Eq. (F.1), and the density correlations, respectively, [VW92, Ram98]

$$\phi(E,\omega,x-x') \overset{\omega\to 0}{\sim} e^{-x/\tilde{\xi}(E)}, \tag{F.19}$$

which differs from the single-particle localization length $\xi(E)$ by a factor of 2,

$$\xi(E) \;=\; 2\tilde{\xi}(E). \tag{F.20}$$

Thus, in the static limit, we can determine the localization length $\xi(E)$ from Eq. (F.17) via

$$\begin{aligned} 0 \;\stackrel{!}{=}\; D_0(E) + \frac{2\mathrm{Im}\Sigma^R(E)}{[\mathrm{Im}\overline{G_0^R}(E)]^2\, D_0(E)} \int \frac{dk}{(2\pi)^d} \int \frac{dk'}{(2\pi)^d} (v_k \cdot \hat{q}) \\ \times \frac{\mathrm{Im}\overline{G_k^R}(E)[\mathrm{Im}\overline{G_{k'}^R}(E)]^2}{(k+k')^2 + 4/\xi^2(E)}\, (v_{k'} \cdot \hat{q}). \end{aligned} \tag{F.21}$$

F.2 Particle-hole symmetry of the self-consistent transport theory

In Ch. 7, we discussed that for the lattice system we have to slightly modify the self-consistent equation, Eq. (F.17) by replacing $(k+k')^2$ by $(k+k')^2_{2\pi}$ in the denominator of the cooperon propagator. In the following, we will prove that this replacement is necessary to restore particle-hole symmetry, as mentioned in Ch. 7.

Particle-hole symmetry means, that the physical quantities are invariant under the transformation $(E-\mu) \mapsto -(E-\mu)$. (For simplicity, we will assume $\mu = 0$ in the following, which is always possible by choosing appropriate energy units.) From the dispersion relation of the d-dimensional square lattice, Eq. (7.14),

$$\epsilon_k \;=\; -2t \sum_{i=1}^{d} \cos k_i\,, \tag{F.22}$$

we obtain that $\epsilon_{k+\pi} = \epsilon_{k+\pi} = -\epsilon_k$. Besides, $v_{k+\pi} = v_{k-\pi} = -v_k$. Thus, we conclude that

$$\mathrm{Im}\overline{G_k^R}(-E) \;=\; \frac{\mathrm{Im}\Sigma^R(-E)}{(-E-\epsilon_k - \mathrm{Re}\Sigma^R(-E))^2 + (\mathrm{Im}\Sigma^R(-E))^2} \tag{F.23}$$

$$\;=\; \frac{\mathrm{Im}\Sigma^R(E)}{(E-\epsilon_{k+\pi} - \mathrm{Re}\Sigma^R(E))^2 + (\mathrm{Im}\Sigma^R(E))^2} \tag{F.24}$$

$$\;=\; \mathrm{Im}\overline{G_{k+\pi}^R}(E), \tag{F.25}$$

Here, we used $\mathrm{Im}\Sigma^R(-E) = \mathrm{Im}\Sigma^R(E)$ and $\mathrm{Re}\Sigma^R(-E) = -\mathrm{Re}\Sigma^R(E)$. The former follows from the symmetry of the spectrum, and then the latter is implied by causality, i.e., by the Kramers-Kronig relation [AGD77]. With the same argument, we can conclude that $\mathrm{Im}\overline{G_0^R}(-E) = \mathrm{Im}\overline{G_0^R}(E)$.

Denoting again the first Brillouin zone of the reciprocal lattice by Ω, we can analyze the transformation behavior of the bare diffusion constant, Eq. (F.10),

$$\begin{aligned} D_0(-E) &= -\frac{1}{\mathrm{Im}\overline{G_0^R}(-E)} \int_\Omega \frac{dk}{(2\pi)^d} (v_k \cdot \hat{q})^2 [\mathrm{Im}\overline{G_k^R}(-E)]^2 && \text{(F.26)} \\ &= -\frac{1}{\mathrm{Im}\overline{G_0^R}(E)} \int_\Omega \frac{dk}{(2\pi)^d} (v_k \cdot \hat{q})^2 [\mathrm{Im}\overline{G_{k+\pi}^R}(E)]^2 && \text{(F.27)} \\ &= -\frac{1}{\mathrm{Im}\overline{G_0^R}(E)} \int_\Omega \frac{dk}{(2\pi)^d} (v_{k-\pi} \cdot \hat{q})^2 [\mathrm{Im}\overline{G_k^R}(E)]^2 && \text{(F.28)} \\ &= -\frac{1}{\mathrm{Im}\overline{G_0^R}(E)} \int_\Omega \frac{dk}{(2\pi)^d} (v_k \cdot \hat{q})^2 [\mathrm{Im}\overline{G_k^R}(E)]^2 && \text{(F.29)} \\ &= D_0(E). && \text{(F.30)} \end{aligned}$$

For the dynamical diffusion constant the same calculation yields

$$\begin{aligned} D(-E,\omega) &= D_0(-E) + \frac{2\mathrm{Im}\Sigma^R(-E)}{[\mathrm{Im}\overline{G_0^R}(-E)]^2 D_0(-E)} \int_\Omega \frac{dk}{(2\pi)^d} \int_\Omega \frac{dk'}{(2\pi)^d} (v_k \cdot \hat{q}) \\ &\qquad \times \frac{\mathrm{Im}\overline{G_k^R}(-E)[\mathrm{Im}\overline{G_{k'}^R}(-E)]^2}{(k+k')^2 - \mathrm{i}\omega/D(\omega,-E)} (v_{k'} \cdot \hat{q}) && \text{(F.31)} \\ &= D_0(E) + \frac{2\mathrm{Im}\Sigma^R(E)}{[\mathrm{Im}\overline{G_0^R}(E)]^2 D_0(E)} \int_\Omega \frac{dk}{(2\pi)^d} \int_\Omega \frac{dk'}{(2\pi)^d} (v_k \cdot \hat{q}) \\ &\qquad \times \frac{\mathrm{Im}\overline{G_k^R}(E)[\mathrm{Im}\overline{G_{k'}^R}(E)]^2}{(k+k'-2\pi)^2 - \mathrm{i}\omega/D(\omega,-E)} (v_{k'} \cdot \hat{q}). && \text{(F.32)} \end{aligned}$$

Thus, only if $k+k'-2\pi \mapsto k+k'$ in the denominator of the cooperon propagator, i.e., if the correct replacement $(k+k')^2 \mapsto (k+k')^2_{2\pi}$ is made, does the diffusion coefficient respect the particle-hole symmetry of the system, $D(-E,\omega) = D(E,\omega)$.

F.3 Limits of strong and weak disorder

F.3.1 Weak disorder

In the limit of weak disorder and dimensions $d > 2$, the self-consistent equations from Sec. F.1 reproduce the result from weak localization perturbation calculation. To see this, we start with the definition of the bare diffusion constant, Eq. (F.10). Assuming that the single-particle propagator is given within Born

approximation, Eq. (A.8), we get

$$
\begin{aligned}
D_0(E) &= -\frac{1}{\mathrm{Im}\overline{G_0^R}(E)} \int_\Omega \frac{dk}{(2\pi)^d} (v_k \cdot \hat{q})^2 [\mathrm{Im}\overline{G_k^R}(E)]^2 && \text{(F.33)} \\
&\approx \frac{v_{k_\mathrm{F}}^2}{\pi N(E)} \int \frac{dS}{A_d} \cos^2\Theta \int d\epsilon\, N(\epsilon) [\mathrm{Im}\overline{G_k^R}(E)]^2 && \text{(F.34)} \\
&\approx \frac{v_{k_\mathrm{F}}^2}{d\pi} \int d\epsilon \left(\frac{1/2\tau}{\epsilon^2 + 1/4\tau^2} \right)^2 && \text{(F.35)} \\
&= 2\tau \frac{v_{k_\mathrm{F}}^2}{d\pi} \int d\epsilon \frac{1}{(\epsilon + \mathrm{i})^2 (\epsilon - \mathrm{i})^2} && \text{(F.36)} \\
&= \frac{v_{k_\mathrm{F}}^2}{d} \tau && \text{(F.37)} \\
&\overset{\text{(A.19)}}{=} D_0. && \text{(F.38)}
\end{aligned}
$$

Next, we have to check that the renormalized diffusion coefficient becomes the bare diffusion constant in the limit of weak disorder and $\omega \to 0$ in dimension $d > 2$. For that purpose, we have to prove that assuming $D(E,\omega) = D_0$ in the last term on the right hand side of Eq. (F.17) yields a vanishing contribution of this term to $D(E,\omega)$.

$$
\begin{aligned}
D(E,\omega) &\overset{\omega \to 0}{=} D_0 + \frac{2\mathrm{Im}\Sigma^R(E)}{[\mathrm{Im}\overline{G_0^R}(E)]^2 D_0} \int_\Omega \frac{dk}{(2\pi)^d} \int_\Omega \frac{dk'}{(2\pi)^d} (v_k \cdot \hat{q}) \\
&\qquad \times \frac{\mathrm{Im}\overline{G_k^R}(E) [\mathrm{Im}\overline{G_{k'}^R}(E)]^2}{(k+k')_{2\pi}^2} (v_{k'} \cdot \hat{q}) && \text{(F.39)} \\
&\approx D_0 - \frac{2\mathrm{Im}\Sigma^R(E)}{[\mathrm{Im}\overline{G_0^R}(E)]^2 D_0} \int_\Omega \frac{dk}{(2\pi)^d} (v_k \cdot \hat{q})^2 \, [\mathrm{Im}\overline{G_k^R}(E)]^3 \\
&\qquad \times \int_\Omega \frac{dQ}{(2\pi)^d} \frac{1}{Q^2} && \text{(F.40)} \\
&\approx D_0 - \frac{2\mathrm{Im}\Sigma^R(E)}{[\mathrm{Im}\overline{G_0^R}(E)]^2 D_0} \int_\Omega \frac{dk}{(2\pi)^d} (v_k \cdot \hat{q})^2 \, [\mathrm{Im}\overline{G_k^R}(E)]^3 \\
&\qquad \times \int_\Omega \frac{dQ}{(2\pi)^d} \frac{1}{Q^2} && \text{(F.41)} \\
&\approx D_0 - \frac{v_{k_\mathrm{F}}^2}{\pi^2 \tau d \, N(E) D_0} \int_\Omega \frac{dk}{(2\pi)^d} [\mathrm{Im}\overline{G_k^R}(E)]^3 \int_\Omega \frac{dQ}{(2\pi)^d} \frac{1}{Q^2} && \text{(F.42)}
\end{aligned}
$$

$$\approx \quad D_0 - \frac{4v_{k_F}^2 \tau}{\pi^2 d D_0} \int d\epsilon \frac{1}{(\epsilon - \mathrm{i})^3 (\epsilon + \mathrm{i})^3} \int_\Omega \frac{dQ}{(2\pi)^d} \frac{1}{Q^2} \tag{F.43}$$

$$= \quad D_0 \left(1 - \frac{6}{\pi D_0} \int \frac{dQ}{(2\pi)^d} \frac{1}{Q^2} \right) \tag{F.44}$$

$$\overset{d \geq 2}{=} \quad D_0 + \mathcal{O}(D_0^{-1}). \tag{F.45}$$

Thus, in the limit of weak disorder, $D(E, \omega \to 0) = D_0$ is indeed a solution of Eq. (F.17), and the self-consistent transport theory in the formulation of [KKW90, Kro90] reduces correctly to the weak localization limit.

F.3.2 Limit of strong disorder and Anderson transition

Having discussed the weak disorder regime, we focus now on the case of strong disorder. In Sec. 3.5, we mentioned that the self-consistent transport theory does not describe exactly the critical behavior of the Anderson model close to the metal-insulator transition in three dimensions. For instance, the critical exponents obtained from the self-consistent equation differ from the exact ones (see Sec. 3.5). Furthermore, the theory slightly overestimates the localizing effect of the disorder potential, yielding a smaller critical disorder strength than the correct one (see Sec. 7.4). Astonishingly, we can use a crude, strong-disorder approximation to estimate the critical disorder strength, predicted by the self-consistent theory for the Anderson transition of the lattice Anderson model. For large enough disorder strength Δ, we approximate

$$N(E) \quad \approx \quad \frac{1}{\Delta} \quad \approx \quad -\frac{1}{\pi} \mathrm{Im} \overline{G_0^R}(E) \tag{F.46}$$

$$\mathrm{Im} \overline{G_k^R}(E) \quad \approx \quad \frac{1}{\mathrm{Im} \Sigma_0^R(E)} \quad \approx \quad \mathrm{Im} \overline{G_0^R}(E) \quad \approx \quad -\frac{\pi}{\Delta}. \tag{F.47}$$

Using these relations we get

$$D_0(E) \quad = \quad -\frac{1}{\mathrm{Im} \overline{G_0^R}(E)} \int_\Omega \frac{dk}{(2\pi)^3} (v_k \cdot \hat{q})^2 [\mathrm{Im} \overline{G_k^R}(E)]^2 \tag{F.48}$$

$$\approx \quad \frac{4t^2 \pi}{\Delta} \int_{-\pi}^{\pi} \frac{dk}{2\pi} \sin(k)^2 \tag{F.49}$$

$$= \quad \frac{2t^2 \pi}{\Delta} \tag{F.50}$$

and

$$
\begin{aligned}
D(E,\omega\to 0) &= D_0 + \frac{2\mathrm{Im}\Sigma^R(E)}{[\mathrm{Im}\overline{G_0^R}(E)]^2 D_0}\int_\Omega \frac{dk}{(2\pi)^d}\int_\Omega \frac{dk'}{(2\pi)^3}(v_k\cdot\hat{q}) \\
&\qquad \times \frac{\mathrm{Im}\overline{G_k^R}(E)[\mathrm{Im}\overline{G_{k'}^R}(E)]^2}{(k+k')_{2\pi}^2}\,(v_{k'}\cdot\hat{q}) \qquad \text{(F.51)}\\
&\approx D_0 + \frac{8t^2}{D_0}\int_\Omega \frac{dk}{(2\pi)^3}\int_\Omega \frac{dk'}{(2\pi)^3}\frac{\sin(k_x)\,\sin(k'_x)}{(k+k')_{2\pi}^2} \qquad \text{(F.52)}\\
&= D_0 - \frac{4t^2}{D_0}\hat{C}_\infty(1,0,0) \qquad \text{(F.53)}\\
&\approx \frac{2t^2\pi}{\Delta} - \frac{2\Delta}{\pi}\hat{C}_\infty(1,0,0). \qquad \text{(F.54)}
\end{aligned}
$$

$\hat{C}_\infty(1,0,0)\approx 0.08$ is the first mode of the Fourier transform of the cooperon propagator (see Eq.(7.39)). The transition happens if $D(E,\omega)=0$. Thus, we obtain a critical disorder strength

$$
\frac{\Delta_c}{t} \approx \frac{\pi}{\sqrt{\hat{C}_\infty(1,0,0)}} \approx 11, \qquad \text{(F.55)}
$$

which has to be compared with the numerical result $\Delta_c/t\approx 11.7$. Thus, our calculation gives further support to our argument, given at the end of Sec. 6.1, that even close to the Anderson-Hubbard transition the system might be describable within a strong-disorder approximation like the atomic-limit approximation (see also discussion in [CG09]).

We note that in the self-consistent transport theory of Anderson localization yields incorrect results in the limit $\Delta\to\infty$ and the one-dimensional case. (Here, we have to note that both cases are essentially the same, as the dimension becomes unimportant for $\Delta\to\infty$.) From the Herbert-Jones-Thouless formula, Eq. (6.37), we obtain in the limit $\Delta\to\infty$,

$$
\frac{1}{\xi} \approx \frac{1}{\Delta}\int_{-\Delta/2}^{\Delta/2} dx\,\log|x| \sim \log\Delta. \qquad \text{(F.56)}
$$

However, using the same strong-disorder approximation as before, we estimate from Eq. (F.21) for the self-consistent transport theory

$$\begin{aligned} 0 &= D_0 + \frac{2\mathrm{Im}\Sigma^R(E)}{[\mathrm{Im}\overline{G_0^R}(E)]^2 D_0} \int_\Omega \frac{dk}{(2\pi)^d} \int_\Omega \frac{dk'}{(2\pi)^d} (v_k \cdot \hat{q}) \\ &\qquad \times \frac{\mathrm{Im}\overline{G_k^R}(E)[\mathrm{Im}\overline{G_{k'}^R}(E)]^2}{(k+k')_{2\pi}^2 + 1/\xi^2} (v_{k'} \cdot \hat{q}) \qquad \text{(F.57)} \\ &\approx D_0 + \frac{8t^2}{D_0} \xi^2 \int_\Omega \frac{dk}{(2\pi)^d} \int_\Omega \frac{dk'}{(2\pi)^d} \frac{\sin(k_x)\,\sin(k'_x)}{\xi^2\,(k+k')_{2\pi}^2 + 1} \qquad \text{(F.58)} \\ &\approx D_0 - \frac{8t^2}{D_0} \xi^4 \int_\Omega \frac{dk}{(2\pi)^d} \int_\Omega \frac{dk'}{(2\pi)^d} \sin(k_x)\,\sin(k'_x)\,(k+k')_{2\pi}^2 \qquad \text{(F.59)} \\ \Rightarrow \quad \xi^4 &\sim D_0^2 \sim \frac{1}{\Delta^2} \qquad \text{(F.60)} \\ \Rightarrow \quad \xi &\sim \frac{1}{\sqrt{\Delta}} \qquad \text{(F.61)} \end{aligned}$$

Thus, the localization length calculated within the self-consistent transport theory decreases faster than the exact one.

Despite these shortcomings, in [Kro90] it was shown that in the relevant physical regime of strong (but not too strong) disorder the self-consistent theory yields qualitatively and quantitatively reasonable results, which deviate from the exact ones within a well acceptable range.

Bibliography

[AA79] B. L. Altshuler and A. G. Aronov, Sov. Phys. JETP **50**, 968 (1979).

[AA85] B. L. Altshuler and A. G. Aronov, in *Electron-electron interactions in disordered systems*, edited by A. L. Efros and M. Pollak (Elsevier, Amsterdam, 1985), p. 1.

[AAL80] B. L. Altshuler, A. G. Aronov, and P. A. Lee, Phys. Rev. Lett. **44**, 1288 (1980).

[AALR79] E. Abrahams, P. W. Anderson, D. C. Licciardello, and T. V. Ramakrishnan, Phys. Rev. Lett. **42**, 673 (1979).

[ACP07] G. E. Astrakharchik, R. Combescot, and L. P. Pitaevskii, Phys. Rev. A **76**, 063616 (2007).

[ADL04] E. Altman, E. Demler, and M. D. Lukin, Phys. Rev. A **70**, 013603 (2004).

[AEM+95] M. H. Anderson, J. R. Ensher, M. R. Matthews, C. E. Wieman, and E. A. Cornell, Science **269**, 198 (1995).

[AGD77] A. A. Abrikosov, L. P. Gorkov, and I. E. Dzyaloshinski, *Methods of Quantum Field Theory in Statistical Physics* (Dover, New York, 1977).

[AKS01] E. Abrahams, S. V. Kravchenko, and M. P. Sarachik, Rev. Mod. Phys **73**, 251 (2001).

[AM76] N. W. Ashcroft and N. D. Mermin, *Solid State Physics* (Saunders College Publ., Fort Worth, 1976).

[AM93] M. Aizenman and S. Molchanov, Commun. Math. Phys. **157**, 245 (1993).

[AM07] E. Akkermans and G. Montambaux, *Mesoscopic Physics of Electrons and Photons* (Cambridge University Press, Cambridge, 2007).

[AMM+nt] B. L. Altshuler, G. W. Martin, D. L. Maslov, V. M. Pudalov, A. Prinz, G. Brunthaler, and G. Bauer, arXiv:0008005 (preprint).

[And58] P. W. Anderson, Phys. Rev. **109**, 1492 (1958).

[And97] P. W. Anderson, *The Theory of Superconductivity in the High-T_c Cuprates* (Princeton University Press, Princeton, 1997).

[AS72] M. Abramowitz and I. A. Stegun, *Handbook of Mathematical Functions* (Dover, New York, 1972).

[AZ97] A. Altland and M. Zirnbauer, Phys. Rev. B **55**, 1142 (1997).

[BAA06] D. M. Basko, I. L. Aleiner, and B. L. Altshuler, Ann. of Phys. **321**, 1126 (2006).

[BAA07] D. M. Basko, I. L. Aleiner, and B. L. Altshuler, Phys. Rev. B **76**, 052203 (2007).

[BAA08] D. M. Basko, I. L. Aleiner, and B. L. Altshuler, in *Problems of Condensed Matter Physics: Quantum Coherence Phenomena in Electron-hole and Coupled Matter-light Systems*, edited by A. L. Ivanov and S. G. Tikhodeev (Oxford University Press, 2008), p. 50.

[BDZ08] I. Bloch, J. Dalibard, and W. Zwerger, Rev. Mod. Phys. **80**, 885 (2008).

[Ber84] G. Bergmann, Phys. Rep. **107**, 1 (1984).

[BH09] U. Bissbort and W. Hofstetter, Eur. Phys. Lett. **86**, 50007 (2009).

[BHV05] K. Byczuk, W. Hofstetter, and D. Vollhardt, Phys. Rev. Lett. **94**, 056404 (2005).

[BJZ+08] J. Billy, V. Josse, Z. Zuo, A. Bernard, B. Hambrecht, P. Lugan, D. Clement, L. Sanchez-Palencia, P. Bouyer, and A. Aspect, Nature **453**, 891 (2008).

[BK93] D. Belitz and T. R. Kirkpatrick, Rev. Mod. Phys. **66**, 261 (1993).

[BLS94] V. Bach, E. H. Lieb, and J. P. Solovej, J. Stat. Phys. **76**, 3 (1994).

[BPVB07] P. Buonsante, V. Penna, A. Vezzani, and P. B. Blakie, Phys. Rev. A **76**, 011602 (2007).

[BSTH95] C. C. Bradley, C. A. Sackett, J. J. Tollett, and R. G. Hulet, Phys. Rev. Lett. **75**, 1687 (1995).

[BZ92] A. Brezini and N. Zekri, Phys. Stat. Sol. (b) **169**, 253 (1992).

[CA09] M. W. Cho and S.-A. Ahn, Comp. Phys. Comm. **180**, 549 (2009).

[Cas08] Y. Castin, in *Ultra-Cold Fermi Gases (Proceedings of the International School of Physics "Enrico Fermi")*, vol. 164, edited by M. Inguscio, W. Ketterle, and C. Salomon (IOS Press, Amsterdam, 2008), p. 289.

[CCL+84] C. Castellani, C. D. Castro, P. A. Lee, M. Ma, S. Sorella, and E. Tabet, Phys. Rev. B **30**, 1596 (1984).

[CCL98] C. Castellani, C. D. Castro, and P. A. Lee, Phys. Rev. B **57**, R9381 (1998).

[CCLM84] C. Castellani, C. D. Castro, P. A. Lee, and M. Ma, Phys. Rev. B **30**, 527 (1984).

[CCPS08] S. Chiesa, P. B. Chakraborty, W. E. Pickett, and R. T. Scalettar, Phys. Rev. Lett. **101**, 086401 (2008).

[CDS07] P. B. Chakraborty, P. J. H. Denteneer, and R. T. Scalettar, Phys. Rev. B **75**, 125117 (2007).

[CFKS87] H. L. Cycon, R. G. Froese, W. Kirsch, and B. Simon, *Schrödinger Operators* (Springer, Berlin, 1987).

[CFO69] M. H. Cohen, H. Fritzsche, and S. R. Ovshinsky, Phys. Rev. Lett. **22**, 1065 (1969).

[CG09] X. Chen and R. J. Gooding, Phys. Rev. B **80**, 115125 (2009).

[CGJTnt] C. Chin, R. Grimm, P. Julienne, and E. Tiesinga, arXiv:0812.1496 (preprint).

[CL90] R. Carmona and J. Lacroix, *Spectral Theory of Random Schrödinger Operators* (Birkhäuser, Boston, 1990).

[Cla67] A. H. Clark, Phys. Rev. **154**, 750 (1967).

[CLN99] C. Chamon, A. W. W. Ludwig, and C. Nayak, Phys. Rev. B **60**, 2239 (1999).

[Col84] P. Coleman, Phys. Rev. B **29**, 3035 (1984).

[CS08] N. Cherroret and S. E. Skipetrov, Phys. Rev. Lett. **101**, 190406 (2008).

[CS09] N. Cherroret and S. E. Skipetrov, Phys. Rev. A **79**, 063604 (2009).

[Dag94] E. Dagotto, Mod Rev. Phys. **66**, 763 (1994).

[Dat95] S. Datta, *Electronic Transport in Mesoscopic Systems* (Cambridge University Press, Cambridge, 1995).

[DGPS99] F. Dalfovo, S. Giorgini, L. P. Pitaevskii, and S. Stringari, Rev. Mod. Phys. **71**, 463 (1999).

[DJ98] I. H. Deutsch and P. S. Jessen, Phys. Rev. A **57**, 1972 (1998).

[DK89] H. von Dreifus and A. Klein, Commun. Math. Phys. **124**, 285 (1989).

[DMA+95] K. B. Davis, M.-O. Mewes, M. R. Andrews, N. J. van Druten, D. S. Durfee, D. M. Kurn, and W. Ketterle, Phys. Rev. Lett. **75**, 3969 (1995).

[DMA07] Y. Dubi, Y. Meir, and Y. Avishai, Nature **449**, 876 (2007).

[DS03] P. J. H. Denteneer and R. T. Scalettar, Phys. Rev. Lett. **90**, 246401 (2003).

[DST99] P. J. H. Denteneer, R. T. Scalettar, and N. Trivedi, Phys. Rev. Lett. **83**, 4610 (1999).

[Eco06] E. N. Economou, *Green's Functions in Quantum Physics* (Springer, Berlin Heidelberg, 2006).

[EFG+05] F. H. L. Essler, H. Frahm, F. Göhmann, A. Klümper, and V. E. Korepin, *The One-Dimensional Hubbard Model* (Cambridge Univ. Press, Cambridge, 2005).

[EFR08] A. Eilmes, A. M. Fischer, and R. A. Römer, Phys. Rev. B **77**, 245117 (2008).

[EKL74] R. J. Elliott, J. A. Krumhansl, and P. L. Leath, Rev. Mod. Phys. **46**, 465 (1974).

[Elg09] A. Elgart, Duke Math. J. **146**, 331 (2009).

[EM08] F. Evers and A. D. Mirlin, Rev. Mod. Phys. **80**, 1355 (2008).

[EMM+99] U. Elsner, V. Mehrmann, F. Milde, R. A. Römer, and M. Schreiber, SIAM J. Sci. Comput. **20**, 2089 (1999).

[EP85] A. L. Efros and M. Pollak, *Electron-electron interactions in disordered systems* (Elsevier, Amsterdam, 1985).

[ER95] P. P. Edwards and C. N. R. Rao, *Metal-Insulator Transitions Revisited* (Taylor & Francis, London, 1995).

[ES75] A. L. Efros and B. I. Shklovskii, J. Phys. C **8**, L49 (1975).

[ES85] A. L. Efros and B. I. Shklovskii, in *Electron-electron interactions in disordered systems*, edited by A. L. Efros and M. Pollak (Elsevier, Amsterdam, 1985), p. 409.

[ET72] J. T. Edwards and D. J. Thouless, J. Phys. C **5**, 807 (1972).

[FA80] L. Fleishman and P. W. Anderson, Phys. Rev. B **21**, 2366 (1980).

[FAL78] L. Fleishman, P. W. Anderson, and D. C. Licciardello, Phys. Rev. Lett. **40**, 1340 (1978).

[FGW+05] S. Fölling, F. Gerbier, A. Widera, O. Mandel, T. Gericke, and I. Bloch, Nature **434**, 481 (2005).

[Fin83] A. M. Finkel'stein, Sov. Phys. JETP **57**, 97 (1983).

[Fin84] A. M. Finkel'stein, Z. Phys. B **56**, 189 (1984).

[FKS08] S. Fishman, Y. Krivolapov, and A. Soffer, J. Stat. Phys. **131**, 843 (2008).

[FKS09a] S. Fishman, Y. Krivolapov, and A. Soffer, Nonlinearity **22**, 2861 (2009).

[FKS09b] S. Flach, D. O. Krimer, and C. Skokos, Phys. Rev. Lett. **102**, 024101 (2009).

[Fle] G. Fleury, private communication.

[FLG+07] L. Fallani, J. E. Lye, V. Guarrera, C. Fort, and M. Inguscio, Phys. Rev. Lett. **98**, 130404 (2007).

[FM96] J. K. Freericks and H. Monien, Phys. Rev. B **53**, 2691 (1996).

[FS83] J. Fröhlich and T. Spencer, Comm. Math. Phys. **88**, 151 (1983).

[FW71] A. L. Fetter and J. D. Walecka, *Quantum Theory of Many-Particle Physics* (McGraw-Hill, Boston, 1971).

[FW08a] G. Fleury and X. Waintal, Phys. Rev. Lett. **100**, 076602 (2008).

[FW08b] G. Fleury and X. Waintal, Phys. Rev. Lett. **101**, 226803 (2008).

[FWGF89] M. P. A. Fisher, P. B. Weichman, G. Grinstein, and D. S. Fisher, Phys. Rev. B **40**, 546 (1989).

[FWnt] G. Fleury and X. Waintal, arXiv:0902.3171 (preprint).

[Geb97] F. Gebhard, *The Mott metal insulator transition* (Springer, Berlin, 1997).

[GK92] A. Georges and G. Kotliar, Phys. Rev. B **45**, 6479 (1992).

[GK04] F. Germinet and A. Klein, Duke Math. J. **124**, 309 (2004).

[GKKR96] A. Georges, G. Kotliar, W. Krauth, and M. J. Rozenberg, Rev. Mod. Phys. **68**, 13 (1996).

[GLK79] L. P. Gorkov, A. I. Larkin, and D. E. Khmel'nitskii, JETP Lett. **30**, 228 (1979).

[GME+02] M. Greiner, O. Mandel, T. Esslinger, T. W. Hänsch, and I. Bloch, Nature **415**, 39 (2002).

[GMP77] I. Y. Goĺdshtein, S. A. Molchanov, and L. A. Pastur, Functs. Anal. y. Prilozhen **11**, 1 (1977).

[GMP05] I. V. Gornyi, A. D. Mirlin, and D. G. Polyakov, Phys. Rev. Lett. **95**, 206603 (2005).

[GPS08] S. Giorgini, L. P. Pitaevskii, and S. Stringari, Rev. Mod. Phys. **80**, 1215 (2008).

[GS87] T. Giamarchi and H. J. Schulz, Europhys. Lett. **12**, 1287 (1987).

[GS88] T. Giamarchi and H. J. Schulz, Phys. Rev. B **37**, 325 (1988).

[GSL] `http://www.gnu.org/software/gsl/`.

[GWO99] R. Grimm, M. Weidemüller, and Y. B. Ovchinnikov, in *Advances in Atomic, Molecular and Optical Physics*, vol. 42, edited by B. Bederson and H. Walther (Academic Press, 1999), p. 95.

[Her01] I. F. Herbut, Phys. Rev. B **63**, 113102 (2001).

[Hir85] J. E. Hirsch, Phys. Rev. B **31**, 4403 (1985).

[HJ71] D. C. Herbert and R. Jones, J. Phys. C **4**, 1145 (1971).

[HLN80] S. Hikami, A. I. Larkin, and Y. Nagaoka, Prog. Theor. Phys. **63**, 707 (1980).

[Hoc92] P. Hoch, in *Out of the Crystal Maze (Chapters from the History of Solid-State Physics)*, edited by L. Hoddeson, E. Braun, J. Teichmann, and S. Weart (University Pres, Oxford, 1992), p. 182.

[HT04] D. Heidarian and N. Trivedi, Phys. Rev. Lett. **93**, 126401 (2004).

[Hub63] J. Hubbard, Proc. Roy. Soc. A **276**, 238 (1963).

[Hub64a] J. Hubbard, Proc. Roy. Soc. A **277**, 237 (1964).

[Hub64b] J. Hubbard, Proc. Roy. Soc. A **281**, 401 (1964).

[HXT+07] J. Huang, J. S. Xia, D. C. Tsui, L. N. Pfeiffer, and K. W. West, Phys. Rev. Lett. **98**, 226801 (2007).

[IFT98] M. Imada, A. Fujimori, and Y. Tokura, Rev. Mod. Phys. **70**, 1039 (1998).

[Imr02] Y. Imry, *Introduction to mesoscopic physics* (Oxford University Press, Oxford, 2002).

[Ish73] K. Ishii, Prog. Theor. Phys. Suppl. **53**, 73 (1973).

[Jan98] M. Janssen, Phys. Rep. **295**, 1 (1998).

[JBC+98] D. Jaksch, C. Bruder, J. I. Cirac, C. W. Gardiner, and P. Zoller, Phys. Rev. Lett. **81**, 3108 (1998).

[Jin02] D. Jin, Physics World, April (2002).

[KBMS90] B. Kramer, K. Broderix, A. MacKinnon, and M. Schreiber, Physica A **167**, 163 (1990).

[KKF+94] S. V. Kravchenko, G. V. Kravchenko, J. E. Furneaux, V. M. Pudalov, and M. D'Iorio, Phys. Rev. B **50**, 8039 (1994).

[KKFA08] G. Kopidakis, S. Komineas, S. Flach, and S. Aubry, Phys. Rev. Lett. **100**, 084103 (2008).

[KKNSnt] E. Z. Kuchinskii, N. A. Kuleeva, I. A. Nekrasov, and M. V. Sadovskii, arXiv:0908.3747 (preprint).

[KKW90] J. Kroha, T. Kopp, and P. Wölfle, Phys. Rev. B **41**, 888 (1990).

[KM93] B. Kramer and A. MacKinnon, Rep. Prog. Phys. **56**, 1469 (1993).

[KNS08] E. Z. Kuchinskii, I. A. Nekrasov, and M. V. Sadovskii, JETP **106**, 581 (2008).

[Kop84a] T. Kopp, J. Phys. C **17**, 1897 (1984).

[Kop84b] T. Kopp, J. Phys. C **17**, 1919 (1984).

[KR86] G. Kotliar and A. E. Ruckenstein, Phys. Rev. Lett. **57**, 1362 (1986).

[Kro90] J. Kroha, Physica A **167**, 231 (1990).

[KS04] S. V. Kravchenko and M. P. Sarachik, Rep. Prog. Phys. **67**, 1 (2004).

[KSS96] Y. Kagan, E. L. Surkov, and G. V. Shlyapnikov, Phys. Rev. A **54**, R1753 (1996).

[KV04] G. Kotliar and D. Vollhardt, Adv. Phys. **57**, 53 (2004).

[KW03] J. Kroha and P. Wölfle, in *Theoretical Methods for Strongly Correlated Electrons*, edited by D. Senechal, A. Tremblay, and C. Bourbonnais (Springer, Berlin, 2003), p. 297.

[KZ08] W. Ketterle and M. W. Zwierlein, in *Ultra-Cold Fermi Gases (Proceedings of the International School of Physics "Enrico Fermi")*, vol. 164, edited by M. Inguscio, W. Ketterle, and C. Salomon (IOS Press, Amsterdam, 2008), p. 95.

[Lan56] L. D. Landau, Sov. Phys. JETP **3**, 920 (1956).

[Lan57] R. Landauer, IBM J. Res. Dev. **1**, 223 (1957).

[Lan59] L. D. Landau, Sov. Phys. JETP **8**, 70 (1959).

[Lan70] R. Landauer, Phil. Mag. **21**, 863 (1970).

[Lan91] R. Lang, *Spectral Theory of Random Schrödinger Operators* (Springer, Berlin, 1991).

[Leg01] A. J. Leggett, Rev. Mod. Phys. **73**, 307 (2001).

[LFM+05] J. E. Lye, L. Fallani, M. Modugno, D. S. Wiersma, C. Fort, and M. Inguscio, Phys. Rev. Lett. **95**, 070401 (2005).

[LGP88] I. M. Lifshits, S. A. Gredeskul, and L. A. Pastur, *Introduction to the Theory of Disordered Systems* (Wiley, New York, 1988).

[Lie95] E. H. Lieb, in *Proceedings of the XI International Congress of Mathematical Physics*, edited by D. Iagolnitzer (Int. Press Inc., Boston, 1995), p. 392.

[Lif64] I. M. Lifshitz, Adv. Phys. **13**, 483 (1964).

[LL80] L. D. Landau and E. M. Lifshitz, *Statistical Physics, Part I* (Butterworth Heinemann, Oxford, 1980).

[LM62] E. H. Lieb and D. C. Mattis, Phys. Rev. **125**, 164 (1962).

[LN66] J. S. Langer and T. Neal, Phys. Rev. Lett. **16**, 984 (1966).

[LNW06] P. A. Lee, N. Nagaosa, and X.-G. Wen, Rev. Mod. Phys. **78**, 17 (2006).

[Löh98] H. von Löhneysen, Phil. Trans. R. Soc. Lond. A **356**, 139 (1998).

[LR85] P. A. Lee and T. V. Ramakrishnan, Rev. Mod. Phys. **57**, 287 (1985).

[LSA+07] M. Lewenstein, A. Sanpera, V. Ahufinger, B. Damski, A. Sen, and U. Sen, Adv. Phys. **56**, 243 (2007).

[LT75a] D. C. Licciardello and D. J. Thouless, J. Phys. C **8**, 4157 (1975).

[LT75b] D. C. Licciardello and D. J. Thouless, Phys. Rev. Lett. **35**, 1475 (1975).

[LW68] E. H. Lieb and F. Y. Wu, Phys. Rev. Lett. **20**, 1445 (1968).

[LW03] E. H. Lieb and F. Y. Wu, Physica A **321**, 1 (2003).

[MD79] N. F. Mott and E. A. Davis, *Electron processes in non-crystalline materials* (Clarendon Press, Oxford, 1979).

[MHUB06] E. J. Müller, T.-L. Ho, M. Ueda, and G. Baym, Phys. Rev. A **74**, 033612 (2006).

[MK92] E. Medina and M. Kardar, Phys. Rev. B **46**, 9984 (1992).

[Mot61] N. F. Mott, Philos. Mag. **6**, 287 (1961).

[Mot67] N. F. Mott, Adv. Phys. **16**, 49 (1967).

[Mot69] N. F. Mott, Philos. Mag. **19**, 835 (1969).

[Mot90] N. F. Mott, *Metal-Insulator Transitions* (Taylor & Francis, London, 1990).

[MSB89] M. Milovanovic, S. Sachdev, and R. N. Bhatt, Phys. Rev. Lett. **63**, 82 (1989).

[MT61] N. F. Mott and W. D. Twose, Phys. Adv. **10**, 107 (1961).

[MV89] W. Metzner and D. Vollhardt, Phys. Rev. Lett. **62**, 324 (1989).

[MW71] M. Morgan and P. A. Walley, Philos. Mag. **23**, 661 (1971).

[MW04] W. Magnus and S. Winkler, *Hill's Equation* (Dover, New York, 2004).

[NG07] P. Nagornykh and V. Galitski, Phys. Rev. A **75**, 065601 (2007).

[OH07] V. Oganesyan and D. Huse, Phys. Rev. B **75**, 155111 (2007).

[OPH09] V. Oganesyan, A. Pal, and D. Huse, Phys. Rev. B **80**, 115104 (2009).

[OYTM08] M. Okumura, S. Yamada, N. Taniguchi, and M. Machida, Phys. Rev. Lett. **101**, 016407 (2008).

[OYTM09] M. Okumura, S. Yamada, N. Taniguchi, and M. Machida, Phys. Rev. B **79**, 184417 (2009).

[PBPB97] V. M. Pudalov, G. Brunthaler, A. Prinz, and G. Bauer, JETP Lett. **65**, 932 (1997).

[PF92] L. A. Pastur and A. Figotin, *Spectra of Random and Almost-Periodic Operators* (Springer, Berlin, 1992).

[PF02] A. Punnoose and A. M. Finkel'stein, Phys. Rev. Lett. **88**, 016802 (2002).

[PF05] A. Punnoose and A. M. Finkel'stein, Science **310**, 289 (2005).

[Phi93] P. Phillips, Annu. Rev. Phys. Chem. **44**, 115 (1993).

[PN66] D. Pines and P. Nozieres, *The Theory of Quantum Liquids* (Benjamin, New York, 1966).

[PPJ+01] F. Pierre, H. Pothier, P. Joyez, N. O. Birge, D. Esteve, and M. H. Devoret, Phys. Rev. Lett. **86**, 1590 (2001).

[PPST09] L. Pollet, N. Prokof'ev, B. V. Svistunov, and M. Troyer, Phys. Rev. Lett. **103**, 140402 (2009).

[PS89] R. Pnini and B. Shapiro, Phys. Rev. B **39**, 6986 (1989).

[PS03] L. Pitaevskii and S. Stringari, *Bose-Einstein Condensation* (Clarendon, Oxford, 2003).

[PS08] A. S. Pikovsky and D. L. Shepelyansky, Phys. Rev. Lett. **100**, 094101 (2008).

[PSO09] J. Prior, A. M. Somoza, and M. Ortuño, Eur. Phys. J. B **70**, 513 (2009).

[Ram98] J. Rammer, *Quantum Transport Theory* (Perseus Books, Reading (MA), 1998).

[RBO+07] T. Rom, T. Best, D. van Oosten, U. Schneider, S. Fölling, B. Paredes, and I. Bloch, Nature **444**, 733 (2007).

[RDF+08] G. Roati, C. D'Errico, L. Fallani, M. Fattori, C. Fort, M. Zaccanti, G. Modugno, M. Modugno, and M. Inguscio, Nature **453**, 895 (2008).

[RJLS95] R. del Rio, S. Jitomirskaya, Y. Last, and B. Simon, Phys. Rev. Lett. **75**, 117 (1995).

[RMP+83] T. F. Rosenbaum, R. F. Milligan, M. A. Paalanen, G. A. Thomas, R. N. Bhatt, and W. Lin, Phys. Rev. B **27**, 7509 (1983).

[SA01] B. D. Simons and A. Altland, in *Theoretical Physics at the End of the Twentieth Century*, edited by Y. Saint-Aubin and L. Vinet (Springer, Berlin, 2001), p. 451.

[Sar95] M. P. Sarachik, *Metal-Insulator Transitions Revisited* (Taylor & Francis, London, 1995).

[SBS03] B. Srinivasan, G. Benenti, and D. L. Shepelyansky, Phys. Rev. B **67**, 205112 (2003).

[SBWA09] Y. Song, S. Bulut, R. Wortis, and W. A. Atkinson, J. Phys. Cond. Mat. **21**, 385601 (2009).

[SCK09] E. Sasioglu, S. Caliskan, and M. Kumru, Phys. Rev. B **79**, 035123 (2009).

[Sha82] B. Shapiro, Phys. Rev. B **25**, 4266 (1982).

[Sha86a] B. Shapiro, Phys. Rev. B **34**, 4394 (1986).

[Sha86b] B. Shapiro, Phys. Rev. Lett. **57**, 2168 (1986).

[Sha88] B. S. Shastry, J. Stat. Phys. **50**, 57 (1988).

[Sha07] B. Shapiro, Phys. Rev. Lett. **99**, 060602 (2007).

[Sha08] R. Shankar, *Principles of quantum mechanics* (Springer, New York, 2008).

[She93] D. L. Shepelyansky, Phys. Rev. Lett. **70**, 1787 (1993).

[SI] H. Shinaoka and M. Imada, private communication.

[SI95] A. Shalgi and Y. Imry, in *Mesoscopic Quantum Physics: Proceedings of the Les Houches Summer School, Session LXI*, edited by E. Akkermans, J. L. Pichard, and G. Montambaux (Elsevier Science Ltd., Amsterdam, 1995), p. 229.

[SI09a] H. Shinaoka and M. Imada, Phys. Rev. Lett. **102**, 016404 (2009).

[SI09b] H. Shinaoka and M. Imada, J. Phys. Soc. Jpn. **78**, 094708 (2009).

[SInt] H. Shinaoka and M. Imada, arXiv:0906.4386 (preprint).

[SKSP97] D. Simonian, S. V. Kravchenko, M. P. Sarachik, and V. M. Pudalov, Phys. Rev. Lett. **79**, 2304 (1997).

[SMTS08] S. E. Skipetrov, A. Minguzzi, B. A. van Tiggelen, and B. Shapiro, Phys. Rev. Lett. **100**, 165301 (2008).

[SPCL+07] L. Sanchez-Palencia, D. Clement, P. Lugan, P. Bouyer, G. V. Shlyapnikov, and A. Aspect, Phys. Rev. Lett. **98**, 210401 (2007).

[SS82] D. Y. Sharvin and Y. V. Sharvin, JETP Lett. **34**, 272 (1982).

[Sto01] P. Stollmann, *Caught by Disorder* (Birkhäuser, Boston, 2001).

[SWA08] Y. Song, R. Wortis, and W. A. Atkinson, Phys. Rev. B **77**, 054202 (2008).

[TDAK03] D. Tanaskovic, V. Dobrosavljevic, E. Abrahams, and G. Kotliar, Phys. Rev. Lett. **91**, 066603 (2003).

[Tho72] D. J. Thouless, J. Phys. C **5**, 77 (1972).

[Tho74] D. J. Thouless, Phys. Rep. **13**, 93 (1974).

[Tho76] D. J. Thouless, J. Phys. Colloques **37**, C4 (1976).

[TL93] M. A. Tusch and D. E. Logan, Phys. Rev. B **48**, 843 (1993).

[TVS93] E. Tiesinga, B. J. Verhaar, and H. T. C. Stoof, Phys. Rev. A **47**, 4114 (1993).

[VKE68] B. Velicky, S. Kirkpatrick, and H. Ehrenreich, Phys. Rev. **175**, 747 (1968).

[VKF09] H. Veksler, Y. Krivolapov, and S. Fishman, Phys. Rev. E **80**, 037201 (2009).

[Vol94] D. Vollhardt, in *Perspectives in Many-Particle Physics (Proceedings of the International School of Physics "Enrico Fermi")*, vol. 121, edited by R. A. Broglia, J. R. Schrieffer, and P. F. Bortignon (North Holland, Amsterdam, 1994), p. 31.

[VW80a] D. Vollhardt and P. Wölfle, Phys. Rev. Lett. **45**, 842 (1980).

[VW80b] D. Vollhardt and P. Wölfle, Phys. Rev. B **22**, 4666 (1980).

[VW82] D. Vollhardt and P. Wölfle, Phys. Rev. Lett **48**, 699 (1982).

[VW92] D. Vollhardt and P. Wölfle, in *Electronic Phase Transitions*, edited by W. Hanke and Y. V. Kopaev (Elsevier Science, Amsterdam, 1992), p. 1.

[Weg76] F. Wegner, Z. Phys. B **25**, 327 (1976).

[Weg79] F. Wegner, Z. Phys. B **35**, 207 (1979).

[Weg80] F. Wegner, Z. Phys. B **36**, 209 (1980).

[WPL99] S. Waffenschmidt, C. Pfleiderer, and H. v. Löhneysen, Phys. Rev. Lett. **83**, 3005 (1999).

[WZ09] W.-M. Wang and Z. Zhang, J. Stat. Phys. **134**, 953 (2009).

[YM73] F. Yonezawa and K. Morigaki, Prog. Theor. Phys. Suppl. **53**, 1 (1973).

[Zim79] J. M. Ziman, *Models of disorder* (Cambridge University Press, Cambridge, 1979).

Publications

- *Static screening and delocalization effects in the Hubbard-Anderson model*, Peter Henseler, Johann Kroha, and Boris Shapiro, Phys. Rev. B. **77**, 075101 (2008).
- *Density correlations in cold atomic gases: Atomic speckles in the presence of disorder*,
  Peter Henseler and Boris Shapiro, Phys. Rev. A **77**, 033624 (2008).
- *Self-consistent study of Anderson localization in the Anderson-Hubbard model in two and three dimensions*,
  Peter Henseler, Johann Kroha, and Boris Shapiro, Phys. Rev. B. **78**, 235116 (2008).

Deutsche Zusammenfassung

Es ist bekannt, dass sowohl starke Unordnung als auch starke Zweiteilchenwechselwirkung in Materialien mit teilweise gefülltem Leitungsband Metall-Isolator-Übergänge erzeugen können. Während beide Effekte separat betrachtet inzwischen recht gut verstanden werden, trifft dieses für das Wechselspiel zwischen Unordung und (repulsiver) Wechselwirkung nicht zu. Da in vielen Materialien allerdings weder ein rein unordnungsinduzierter Anderson-Übergang noch ein rein wechselwirkungsinduzierter Mott-Übergang auftritt, ist es von fundamentaler Bedeutung, einen besseren Einblick in die Physik ungeordneter, wechselwirkender Systeme zu gewinnen.
In der vorliegenden Arbeit haben wir deshalb das Anderson-Hubbard-Modell untersucht, welches das minimale Gittermodell darstellt, das Unordnungs- und Korrelationsphysik beinhaltet. Letztere wird dabei in Form eines lokalen Hubbard-Wechselwirkungspotentials berücksichtigt. Nach einer Einführung des Modells und einem Überblick über die wesentlichen Merkmale des Anderson- und des Mott-Hubbard-Übergangs wurde die *atomic-limit approximation* für das Anderson-Hubbard Modell entwickelt und hergeleitet. Ausgehend vom Grenzwert starker Unordnung, in dem Einteilchenanregungen gemäß der Theorie der Anderson-Lokalisierung räumlich stark lokalisiert sind, nahmen wir in unserer Näherung an, dass der Hauptbeitrag der Wechselwirkung unter den Teilchen die Erzeugung einer effektiven Renormierung des Unordnungspotentials ist. Aufgrund der lokalen Abstoßung der Teilchen untereinander gibt es bei besetzten Gitterplätzen einen weiteren, additiven Beitrag zum lokalen Gitterplatzpotential, was eine effektive Anhebung des lokalen Unordnungspotentials der besetzten Gitterplätze verursacht. Aufgrund dieser Überlegung haben wir, ausgehend vom atomaren Limes, in welchem der Grundzustand des Systems einfach bestimmt werden kann, ein effektives Einteilchen-Anderson-Modell abgeleitet, welches die Physik der Einteilchenanregungen an der Fermikante beschreiben soll.
In mehreren Veröffentlichungen der letzten Jahre wurde berichtet, dass numerische Untersuchungen des Anderson-Hubbard-Modells eine nicht-monotone, komplexe Abhängigkeit der Transporteigenschaften des Systems bzw. dessen zugehöriger relevanter Längenskala ergeben hätten. Unser Ansatz erlaubte nun eine systematische und teilweise sogar analytische Untersuchung des Modells. Um quantitativ aussagekräftige Ergebnisse zu gewinnen, verwendeten wir die Selbstkon-

sistenztheorie der Anderson-Lokalisierung. Durch unsere Analyse konnten wir zeigen, dass eine relativ schwache Wechselwirkung zu einer effektiven Abschirmung des Unordnungspotentials führt. Starke Wechselwirkung besitzt hingegen einen gegenteiligen Effekt, da die Ausbildung der beiden Mott-Hubbard-Bänder eine Transportunterdrückung zur Folge hat. Der Vergleich mit den bekannten numerischen Ergebnissen zeigte, dass die Resultate unseres stark vereinfachten Modells sehr gut mit diesen übereinstimmten. Auf diese Weise gelang es uns, eine schlüssige Erklärung des physikalischen Ursprungs der numerischen Beobachtungen zu liefern. Darüberhinaus konnten wir die Bedeutung der Raumdimension auf die Auswirkungen der Unordnungsabschirmung für schwache Wechselwirkung herausarbeiten. In mehreren unabhängigen Veröffentlichungen der letzten Jahre wurde berichtet, dass Hinweise auf einen Metall-Isolator-Übergang im Anderson-Hubbard-Modell in zwei Dimensionen gefunden wurden. Aus der Theorie der Anderson-Lokalisierung ist allerdings bekannt, dass in zwei Dimensionen die Lokalisierungslänge exponentiell von der Unordnungsstärke abhängt. Da sich die Stärke des Abschirmungseffekts als proportional zur Unordnungsstärke herausstellte, kommt es deshalb in zwei Dimensionen zu einem exponentiellen Anwachsen der für den Transport relevanten Längenskala. Wie unsere Untersuchungen zeigten, ist es deshalb äußerst wahrscheinlich, dass die Beobachtung einer metallischen Phase ein *finite-size effect* war und auf einer Fehlinterpretation der numerischen Daten beruhte. Innerhalb unseres Zugangs konnten wir außerdem ein Phasendiagramm für das dreidimensionale Anderson-Hubbard-Modell bestimmen.

In den letzten Jahren gab es in der Quantenoptik große experimentelle Fortschritte. Insbesondere ist es u.a. möglich, optische Potentiale so präzise zu justieren, dass theoretische Modelle, welche wie das Anderson-Hubbard-Modell ursprünglich zur vereinfachten Beschreibung von Materialien entwickelt wurden, nun experimentell direkt zugänglich werden. Da die meisten Experimente bisher für Bosegase durchgeführt wurden, haben wir unsere *atomic-limit approximation* auch auf das ungeordnete Bose-Hubbard-Modell angewendet. Aufgrund der unterschiedlichen Spin-Statistik kann es in diesem Modell bei relativ schwacher Wechselwirkung zur Bildung eines Bose-Einstein-Kondensats kommen. Da der Einteilchenansatz in dieser superfluiden Phase keine sinnvolle Beschreibung liefern kann, ist unser Zugang hier nur sehr viel stärker eingeschränkt anwendbar als im Anderson-Hubbard-Modell für Fermionen und nur zur Beschreibung der Bose-Glasphase verwendbar. Aufgrund der prinzipiell unbeschränkten Teilchenzahl pro Gitterplatz beobachteten wir eine monotone Abnahme der Lokalisierungslänge mit steigender Wechselwirkung. Obwohl unser Ansatz die Bestimmung des Phasenübergangs von der lokalisierten zur superfluiden Phase nicht zuließ, legten unsere Ergebnisse nahe, dass bei abnehmender Wechselwirkung eine monotone Delokalisierung des Systems mit abschließendem Übergang zur superfluiden Phase erfolgt.

Experimentelle Messungen an ultrakalten Quantengasen finden üblicherweise unter Verwendung der *time-of-flight*-Technik statt. Deshalb betrachteten wir die diffusive Expansion eines atomaren Gases in einem ungeordneten statischen Potential. Im Zentrum unserer Betrachtungen standen dabei insbesondere die Ausbildung kurzreichweitiger Dichte-Dichte-Korrelationen (Speckle). Wie wir zeigen konnten, hatte die Streuung der Atome am Unordnungspotential überraschende Konsequenzen. Während aus Arbeiten zur ballistischen Expansion bekannt war, dass die Korrelationslänge der Dichte-Dichte-Korrelation mit der Expansionszeit des Gases anwächst, und auf diese Weise immer in der Größenordnung des mittleren Teilchenabstands bleibt, war im ungeordneten Fall kein solches Anwachsen der Korrelationslänge festzustellen. Aufgrund der Ausbildung einer zufälligen Phase der Wellenfunktion durch die Streuprozesse blieben die Korrelationen auch während der Expansion stets sehr kurzreichweitig, und die zugehörige Korrelationslänge blieb in der Größenordnung des ursprünglichen mittleren Teilchenabstands vor Beginn des Expansionsprozesses.